

July 2020

Characterization of a Natural Clayey Silt and the Effects of Sample Disturbance on Soil Behavior and Engineering Properties

Øyvind Blaker

Follow this and additional works at: https://scholarworks.umass.edu/dissertations_2



Part of the [Geotechnical Engineering Commons](#)

Recommended Citation

Blaker, Øyvind, "Characterization of a Natural Clayey Silt and the Effects of Sample Disturbance on Soil Behavior and Engineering Properties" (2020). *Doctoral Dissertations*. 1904.
https://scholarworks.umass.edu/dissertations_2/1904

This Open Access Dissertation is brought to you for free and open access by the Dissertations and Theses at ScholarWorks@UMass Amherst. It has been accepted for inclusion in Doctoral Dissertations by an authorized administrator of ScholarWorks@UMass Amherst. For more information, please contact scholarworks@library.umass.edu.

**CHARACTERIZATION OF A NATURAL CLAYEY SILT AND THE EFFECTS
OF SAMPLE DISTURBANCE ON SOIL BEHAVIOR AND ENGINEERING
PROPERTIES**

A Dissertation Presented

by

ØYVIND BLAKER

Submitted to the Graduate School of the
University of Massachusetts Amherst in partial fulfillment
of the requirements for the degree of

DOCTOR OF PHILOSOPHY

May 2020

Civil and Environmental Engineering

© Copyright by Øyvind Blaker 2020

All Rights Reserved

**CHARACTERIZATION OF A NATURAL CLAYEY SILT AND THE EFFECTS
OF SAMPLE DISTURBANCE ON SOIL BEHAVIOR AND ENGINEERING
PROPERTIES**

A Dissertation Presented

by

ØYVIND BLAKER

Approved as to style and content by:

Don J. DeGroot, Chair

Guoping Zhang, Member

Julie Brigham-Grette, Member

Jason T. DeJong, Member

John E. Tobiason, Department Head
Department of Civil and Environmental Engineering

DEDICATION

To my family

ACKNOWLEDGEMENTS

This research was primarily supported by the Norwegian Geotechnical Institute (NGI) and the Research Council of Norway (RCN) under grant No. 245650/F50. The field vane tests and GUS sampling were conducted with support from the US National Science Foundation (NSF) under Grant Nos. CMMI-1436793 and CMMI-1436617. NGI and the Norway-America Association (NORAM) provided support allowing the author to fulfill the required one academic year residency at the University of Massachusetts (UMass) Amherst. Any opinions, findings, conclusions, and recommendations expressed in this thesis are those of the author and do not necessarily reflect the views of the NGI, RCN, NSF or NORAM.

I would also like to thank my academic advisor and committee chair Professor Don J. DeGroot for your guidance, support and for improving my skills as a researcher; Professor Jason T. DeJong at UC Davis, Professors Guoping Zhang and Julie Brigham - Grette at UMass Amherst for serving as committee members for this research; and Dr. William G. Lukas for valuable discussions and for paving the way for ISA testing on intermediate soils at UMass Amherst. I extend my sincere gratitude to my NGI colleagues, in particular: Morten Sjørnsen, Dr. Rune Dyvik, Dr. Yusuke Suzuki, James Michael Oloka, Pasquale Carotenuto, Jan Gundersen, Dr. Roselyn Carroll, Tom Lunne, Dr. Priscilla Paniagua, Dr. Jean-Sébastien L'Heureux, Thomas Langford, Victor Bjørn Smith and Kristoffer Kåsin for facilitating the research activities described herein.

Finally, I want to thank my family: my parents and parents in law for all your assistance in the last few months; my sister and brother for the much-needed weekend retreats in the mountains; my daughter Ylva Helene for your unconditional love; and last but not least, my amazing wife Maritha for your encouragement and patience.

ABSTRACT

CHARACTERIZATION OF A NATURAL CLAYEY SILT AND THE EFFECTS OF SAMPLE DISTURBANCE ON SOIL BEHAVIOR AND ENGINEERING PROPERTIES

MAY 2020

ØYVIND BLAKER

M.S., NORWEGIAN UNIVERSITY OF SCIENCE AND TECHNOLOGY

Ph.D., UNIVERSITY OF MASSACHUSETTS AMHERST

Directed by: Professor Don J. DeGroot

Silts are considered a challenging material to deal with in geotechnical engineering design practice and there has been limited research on determining the engineering parameters of silts either by in situ or laboratory testing. This thesis presents results of an extensive research program that investigated the in situ and laboratory behavior of a low plasticity silt deposit at the Norwegian National Geotechnical Test Site at Halden, Norway. Results from multiple in situ tests including: piezocone, pore pressure dissipation, in situ pore pressure measurements, field vane, self-boring pressuremeter and screw plate load tests were synthesized to characterize the Halden silt. Soil sampling using a suite of different samplers of varying sampler geometry and sampling methods were conducted. Laboratory tests performed on the collected samples included: index and soil classification, oedometer, consolidated undrained and drained triaxial, bender element and constant volume direct simple shear. The laboratory tests provided data for interpretation of geological setting, depositional history, deformation, strength, stiffness and hydraulic flow properties of the different soil units at the site. Moreover, simulated tube sampling performed on block sample and reconstituted

specimens of silt using the ideal sampling approach complemented data provided by the different soil samplers. These results advanced the understanding of the effects of tube sample disturbance on engineering parameters in this soil type. Results revealed two soil units of low plasticity clayey silt (ML) over silty clay (CL). Geology and the normally consolidated stress state of the underlying clay unit indicates that the silt is near normally consolidated as well. Interpretation of the undrained shear strength of the silt specimens was complex as the in situ tests were potentially influenced by partial drainage while conventional undrained triaxial tests displayed dilative type behavior with no unique (peak) undrained shear strength. Significant alteration of the intact or reconstituted soil state occurred during field sampling using a poor geometry sampler and likewise during laboratory simulation of poor geometry tube sampling. Yet, the clay-based sample quality assessment methods using recompression strains did not track sample quality well for the Halden silt nor did shear wave velocity. The effects of sample disturbance were very pronounced in undrained triaxial shear with generally increasing undrained shear strength with increasing disturbance but with little to no change in the effective stress friction angle. Based on a collective evaluation of the laboratory and in situ screw plate load tests practical recommendations on selection of undrained shear strength for design and associated foundation performance are provided.

TABLES OF CONTENTS

	Page
ACKNOWLEDGEMENTS	v
ABSTRACT	vi
LIST OF TABLES	xii
LIST OF FIGURES	xiv
CHAPTER	
1 INTRODUCTION	1
2 HALDEN RESEARCH SITE: GEOTECHNICAL CHARACTERIZATION OF A POST GLACIAL SILT	4
2.1 Introduction	5
2.2 Regional setting and methods	6
2.3 Engineering geology	6
2.3.1 Deglaciation history and depositional environment	6
2.3.2 Source of material	7
2.3.3 Stress history	8
2.3.4 Stratigraphy	10
2.4 Soil composition	11
2.4.1 Grain size distribution	11
2.4.2 Grain shape and mineralogy	12
2.4.3 Carbon content	12
2.4.4 Salinity	13
2.4.5 Soil fabric	14
2.5 State and index properties	15
2.5.1 Water content and Atterberg limits	15
2.5.2 Total unit weight and void ratio	16
2.5.3 Unit weight of solid particles	16
2.6 Engineering properties	17
2.6.1 In situ testing - measurements	17
2.6.2 Overconsolidation ratio, OCR	21
2.6.3 Coefficient of earth pressure at rest, K_0	23
2.6.4 Small strain shear modulus	24

2.6.5	Constrained modulus	25
2.6.6	Coefficients of consolidation	26
2.6.7	Hydraulic conductivity.....	27
2.6.8	In situ undrained shear strength – field vane testing.....	28
2.6.9	In situ undrained shear strength – pressuremeter testing.....	29
2.6.10	In situ undrained shear strength – flat dilatometer testing.....	30
2.6.11	In situ strength – cone penetration testing	31
2.6.12	Undrained strength from laboratory testing.....	32
2.6.13	Remolded undrained shear strength and sensitivity.....	34
2.6.14	Effective stress strength parameters.....	35
2.6.15	Sample quality	37
2.7	Engineering problems	38
2.7.1	Soil sampling	39
2.7.2	Stress history.....	40
2.7.3	Partial drainage	41
2.7.4	Case history: Remmen wastewater treatment facility.....	42
2.8	Summary and conclusions	45
2.9	Acknowledgments.....	46
3	INTACT, DISTURBED AND RECONSTITUTED UNDRAINED SHEAR BEHAVIOR OF LOW PLASTICITY NATURAL CLAYEY SILT	77
3.1	Introduction.....	78
3.2	Current practice in sampling of silts and assessment of undrained shear strength	80
3.2.1	Tube and block sampling.....	80
3.2.2	Laboratory simulation of tube sampling - Ideal Sampling Approach (ISA).....	81
3.2.3	Selection of undrained shear strength for design.....	83
3.3	Methods of investigation.....	85
3.3.1	Soil sampling	85
3.3.2	Specimen preparation.....	85
3.3.3	Triaxial testing	87
3.3.4	Incremental loading oedometer testing.....	88
3.3.5	Bender element testing.....	88
3.4	Results – block samples and reconstituted specimens	89
3.4.1	1-D compression behavior	89
3.4.2	Block and reconstituted undrained stress-strain behavior	90
3.4.3	ISA strain cycling behavior	93

3.4.4	Post-ISA reconsolidation and disturbed undrained shear behavior.....	94
3.4.5	Influence of tube sampling.....	95
3.5	Discussion of results	96
3.6	Summary and conclusions	99
3.7	Data availability statement.....	100
3.8	Acknowledgements.....	100
4	EFFECTS OF SAMPLING TECHNIQUES ON MATERIAL BEHAVIOUR AND ENGINEERING PROPERTIES OF LOW-PLASTICITY NATURAL SILT	113
4.1	Introduction.....	113
4.2	In situ and laboratory test techniques.....	118
4.3	Results.....	121
4.3.1	CRS behavior	122
4.3.2	Triaxial shear behaviour	124
4.3.3	Shear wave velocity	127
4.4	Discussion.....	129
4.5	Conclusions.....	134
4.6	Data Availability Statement.....	137
4.7	Acknowledgements.....	138
4.8	Supplemental section	138
4.8.1	Sampler geometry	138
4.8.2	Driller's log from borehole HALB04.....	141
4.8.3	CRS specimen data	141
4.8.4	CAUC specimen data.....	141
4.8.5	CADC specimen data.....	141
4.8.6	V_s analysis of in situ results	141
5	IN SITU STRENGTH AND STIFFNESS PROPERTIES FROM SCREW PLATE LOAD TESTING IN SILT	161
5.1	Introduction.....	162
5.2	Background and analysis	164
5.2.1	Previous work	164
5.2.2	Bearing capacity.....	165
5.2.3	Soil parameters from SPLT	167
5.3	Materials and methods	170
5.3.1	Soil sampling and laboratory testing.....	170
5.3.2	Screw plate load testing	171

5.3.3	Finite element modelling	173
5.4	Results.....	174
5.4.1	Drained and undrained triaxial shear behavior	175
5.4.2	SANISAND model calibration	176
5.4.3	Screw plate load – displacement behavior.....	177
5.4.4	Measured and predicted bearing capacity.....	179
5.5	Interpretation of results	181
5.5.1	Coefficient of horizontal consolidation	181
5.5.2	Stiffness.....	182
5.5.3	Shear strength.....	183
5.6	Summary and conclusions	186
5.7	Acknowledgements.....	188
6	SUMMARY AND CONCLUSIONS	204
APPENDICES		
A:	CONFERENCE PUBLICATION.....	208
B:	CONFERENCE PUBLICATION.....	215
	REFERENCES	225

LIST OF TABLES

Table	Page
Table 2–1 Summary of geophysical, in situ and laboratory tests conducted at Halden research site, with general test procedure references and key parameters.	48
Table 2–2 Summary of Halden stratigraphy, with X-ray images at 0°, 45° and 90° degree axial orientation, and split core images at 20 ms and 40 ms exposure time.	50
Table 2–3 Results of X-ray diffraction analyses on 3 specimens from Halden research site.	52
Table 3–1 Key initial, after consolidation and post-ISA data from IL oedometer and CAUC tests on block, disturbed and reconstituted Halden silt.	101
Table 3–2 Undrained shear strength of Halden silt Block 10 (11.5m) tests using Brandon et al. (2006) failure criteria for dilating soils.	102
Table 3–3 Undrained shear strength of Halden silt MT and SD (11.5m) tests using Brandon et al. (2006) failure criteria for dilating soils.	103
Table 4–1 Summary of average classification properties at Halden.	144
Table 4–2 Summary of dimensions and derived properties of samplers used in this study.	145
Table 4–3 Driller's log from borehole HALB04 (Sherbrooke block sampling) at Halden.	146
Table 4–4 Summary initial and after consolidation data from Halden CRS oedometer test specimens and associated qualitative sample quality assessments.	147
Table 4–5 Summary initial and after consolidation data from Halden CAUC test specimens and associated qualitative sample quality assessments.	148
Table 4–6 Summary initial and after consolidation data from Halden CADC test specimens and associated qualitative sample quality assessments.	149
Table 4–7 Seismic cone geometry for the different equipment.	150
Table 5–1 Average classification properties of Halden silt and clay (Blaker et al. 2019).	189

Table 5–2 Summary of classification and consolidation metrics for triaxial tests at Halden research site.	190
Table 5–3 Summary of s_{uC} and s_{uE} at different failure criteria for dilating soils. Undrained triaxial tests at Halden research site.	191
Table 5–4 Best fit SANISAND input parameters for Halden silt at 11.5 m depth.	192
Table 5–5 Measured and predicted bearing capacities from SPLTs at Halden research site.	193

LIST OF FIGURES

Figure	Page
Figure 2.1 (a) Site location, and (b) site layout. Investigated locations include resistivity and geophysical investigation tools (ERT, MASW), ground water and temperature monitoring, soil sampling using various samplers and in situ testing (CPTU, SCPT, RCPTU, SDMT, FVT, SBP and SPLT).....	53
Figure 2.2 Shoreline reconstruction curves from Halden region (Northern and Southern Østfold), after Klemsdal (2002). The research site most likely emerged from the marine environment c. 5,000 years ago.....	54
Figure 2.3 Quaternary map of the Halden area, Southeast Norway, with the research site circled in red. The colors reflect the geological processes and general properties of the deposits. Shades of blue indicate that the soils have been transported by and deposited in a marine environment. These deposits dominate the Halden area. Shades of green indicate soils that were deposited by the ice. Shades of yellow indicate fluvial deposits, and pink shows exposed bedrock. After Olsen and Sørensen (1993).....	54
Figure 2.4 (a) Pore pressure from in-situ piezometers (locations HALP01- HALP04) and u_2 from CPTU (locations HALC11, HALC12 and HALC19). The dotted line indicates the theoretical hydrostatic pore pressure acting from 2 m depth. (b) In-situ pore pressure measured by four electric piezometers installed at 5 m, 10 m, 15 m and 20 m depth, and rainfall in the area, October 2016 to October 2018.....	55
Figure 2.5 Thermistor string temperature log in location HALB05; (a) with depth at selected dates, and (b) with time since October 2017.....	55
Figure 2.6 In-situ stress conditions (u_0 , σ_{v0} and σ'_{v0}).	56
Figure 2.7 Classification and CPTU data; (a) Soil units, (b) natural water content and Atterberg limits, (c) total unit weight, (d) clay particle and fines content, (e) corrected cone resistance, q_t , (f) pore pressure, u_2 , and (g) sleeve friction, f_s	57
Figure 2.8 Approximate depth to bedrock across the research site.	58
Figure 2.9 Classification data; (a) typical grain size distribution curves for Unit I, and Units II and III. (b) Soil classification triangle (Norwegian Geotechnical Society 2011), which suggests 14 soil classes based on the percentage of clay, silt and sand particles.....	59
Figure 2.10 SEM from 6.4 m depth.	60

Figure 2.11 SEM from 8.6 m depth.	60
Figure 2.12 (a) Soil units, (b) unit weight of solid particles, (c) TC and TOC, and (d) resistivity from laboratory and field measurements.	61
Figure 2.13 Casagrande plasticity chart with results of Atterberg limits on soil Unit II and III.	61
Figure 2.14 CPTU data from six locations; (a) cone resistance, q_c , (b) shoulder pore pressure, u_2 , (c) sleeve friction, f_s , and derived parameters (d) normalized cone resistance, Q_t , (e) pore pressure ratio, B_q , and (f) soil behavior type index, I_c	62
Figure 2.15 Soil behavior type charts (Robertson 1990) from location HALC11 by means of (a) normalized cone resistance, Q_t , versus pore pressure parameter, B_q , and (b) normalized cone resistance, Q_t , versus normalized friction ratio, F_r	63
Figure 2.16 In-situ shear wave velocity (V_{vh} , V_s) from SCPT and SDMT, and Multichannel Analyses of Surface Waves (MASW).	64
Figure 2.17 Results of DMT testing with (a) corrected first reading, (b) corrected second reading, and intermediate DMT parameters (c) material index, I_D , (d) horizontal stress index K_D , and (e) dilatometer modulus, E_D	65
Figure 2.18 Typical self-boring pressure meter results. Interpretation of σ_{h0} and $s_{u,SBP}$ based on Marsland and Randolph (1977) methodology.	66
Figure 2.19 Stress history data from field and laboratory testing. (a) yield stress, σ'_p , (b) overconsolidation ratio, OCR, and (c) coefficient of earth pressure at rest, K_0	66
Figure 2.20 Small strain shear modulus, G_{max} , from field and laboratory measurements of V_{vh} and V_s (SCPT, SDMT, MASW and bender elements).	67
Figure 2.21 Three typical results from CRS testing on specimens from Halden block samples. (a) Void ratio versus log vertical stress, (b) void ratio versus vertical stress, (c) coefficient of consolidation, c_v , versus vertical stress, and (d) constrained modulus, M versus vertical stress.	68
Figure 2.22 (a) Constrained modulus at the in situ effective vertical stress, M_0 and (b) vertical and (c) horizontal coefficient of consolidation with depth, with DeJong et al. (2013) clay-silt transition indicated.	69
Figure 2.23 Hydraulic conductivity (k_v , k_h) from laboratory testing.	69

Figure 2.24 Undrained shear strength from (a) field vane tests, self-boring pressuremeter tests and CPTU, (b) DMT and CPTU, (c) fall cone tests.	70
Figure 2.25 Typical CAUC test results from Halden block samples (HALB04) by means of (a) shear stress versus vertical strain, (b) shear-induced pore pressure versus vertical strain, and (c) stress-path plots. A strong tendency for dilative behavior develops negative shear induced pore pressure in the specimens and results in strain hardening upon shearing. As observed in other silts and intermediate soils no unique (peak) undrained shear strength is identified.	71
Figure 2.26 Results of CAUC and constant volume DSS tests on block samples of Halden silt. Undrained shear strength is interpreted as the shear stress at (a) maximum pore pressure, u_{max} , (b) $A=0$, and (c) a limiting shear strain of 5 % in DSS and 5% axial strain in CAUC.	72
Figure 2.27 Results of (a) remolded undrained shear strength, and (b) sensitivity from fall cone and field vane tests.	72
Figure 2.28 Interpretation of effective stress friction angle from DMT, CPTU, and laboratory CAUC tests on block samples.	73
Figure 2.29 Evaluation of $\Delta e/e_0$ from (a) oedometer, (b) triaxial and (c) DSS testing on silt specimens from block samples.	73
Figure 2.30 Sherbrooke block sampling of Halden silt (borehole HALB04); (a) Apparently good quality block from 11.5 m depth, (b) Damaged lower part of block from 12.4 m depth. Damage was caused by the retracting knives at the base of the block.	74
Figure 2.31 Location plan showing the Remmen wastewater treatment facility (RWTF) relative to the Halden research site, the slope in question and the neighboring houses (No. 8 and 10). Borehole locations 1, 2, 4 and 5 include cone penetration tests. 54 mm Geonor fixed piston sampling was conducted at location 5.	74
Figure 2.32 Cross-section showing original slope and post-failure slope profiles from North-West.	75
Figure 2.33 LiDAR results shows elevation contours of (a) Pre-failure conditions, and (b) post-failure conditions.	76
Figure 3.1 Ideal sampling approach (ISA, Baligh et al. 1987) concept illustrated by (a) shear stress versus vertical strain, and (b) stress path plots. – data for block sample specimen of Halden silt.	104

Figure 3.2 1D consolidation of Sherbrooke block and reconstituted (slurry) Halden silt. Vertical effective stress versus vertical strain on (a) linear and (b) semi - log axis, and (c) void ratio versus log stress.....	105
Figure 3.3 Undrained shear behavior of (a to c) Sherbrooke block and (d to f) reconstituted Halden silt.	106
Figure 3.4 "Aging" effect on undrained triaxial compression shear behavior of reconstituted (slurry) Halden silt. (a) Stress - strain, (b) stress - path, and (c) shear modulus reduction with shear strain.....	107
Figure 3.5 ISA strain cycling behavior from triaxial tests on (a to c) block, and (d to f) reconstituted (slurry) Halden silt.....	108
Figure 3.6 Post-ISA undrained shear behavior from triaxial tests on (a to c) block, and (d to f) reconstituted (slurry) Halden silt.....	109
Figure 3.7 Effect of simulated (ISA, Baligh et al., 1987) and true sample disturbance on undrained shear behavior of Halden silt. (a) Stress - strain, (b) pore pressure - strain, and (c) stress - path.	110
Figure 3.8 Undrained shear strength criteria (Brandon et al.2006) illustrated for CAUC tests on three types of Halden silt samples (NGI 54, GP-S and Sherbrooke block). (a) Stress – strain, (b) pore pressure - strain, and (c) stress - path.	111
Figure 3.9 Effects of simulated sampling disturbance (ISA, Baligh et al., 1987) on selection of undrained shear strength from CAUC tests on Sherbrooke block samples of Halden silt for various criteria (data in Table 3–2).	112
Figure 4.1 Classification properties with depth based on sampler and advanced test type. Halden research site.....	151
Figure 4.2 1-D consolidation behaviour of Halden silt specimens from different samplers and depth intervals. (a – c) Vertical effective stress with vertical strain, and (d – f) constrained modulus with vertical effective stress.....	152
Figure 4.3 Undrained shear behaviour of Halden silt specimens from different samplers and depth intervals (a-d) 5.3m, (e-h) 7.5 - 9.5m and (i-l) 12.6 - 14.5m. Normalised shear stress and pore pressure with strain and stress path.....	153
Figure 4.4 Drained shear behaviour of Halden silt specimens from depth interval 8 -13m with (a) normalised shear stress, (b) volumetric strain with axial strain, and (c) normalised stress path.	154

Figure 4.5 Measured and normalized shear wave velocities with depth at Halden, with (a) $V_{vh \text{ in situ}}$ with depth, (b) $V_{vh-\sigma_{vo}} / V_{vh \text{ in situ avg}}$ from triaxial test specimens, (c) $V_{vh-\sigma_{vo}}^* / V_{vh \text{ in situ avg}}^*$ from triaxial test specimens, and Halden V_s data with sample quality criteria for clays proposed by (d) Landon et al. (2007) and (e) Donohue and Long (2010). With annotation of acceptable or disturbed quality assessment based on material behaviour.	155
Figure 4.6 Derived CRS oedometer properties of Halden silt specimens from different samplers and depths, with (a) w_i versus m , (b) m versus depth, and (c) $C_{rw,i} / C_{cw}$ with depth and sample quality criteria for intermediate soils proposed DeJong et al. (2018).	156
Figure 4.7 Normalised undrained shear strengths from triaxial tests on Halden silt specimens from different samplers at various criteria: (a) u_{max} , (b) Skempton $A_f = 0$ and (c) 10% axial strain.	157
Figure 4.8 (a) Geometry of generic sampler and terms used in sampler geometry equations, and (b) Classification of Sherbrooke block samples of Halden silt from qualitative review.	158
Figure 4.9 Strain energy versus vertical effective stress from CRS oedometer tests on Halden silt specimens from different samplers and depth intervals (a) 4.0 - 5.5m, (b) 7.0 -10.5m and (c) 12.5 - 14.5m.	159
Figure 4.10 Strain energy - based compression ratio, $C_{rw,i} / C_{cw}$, versus $\Delta e / e_0$ from CRS oedometer tests on Halden silt specimens from different samplers.	160
Figure 5.1 Halden research site layout. Investigated locations include electrical piezometers, cone penetration testing, field vane testing, self-boring pressuremeter testing, soil sampling and screw plate load testing.	194
Figure 5.2 The screw plate load test (SPLT) equipment.	195
Figure 5.3 Simplified 2D axisymmetric Plaxis model of SPLTs using 309 15-noded triangular elements with refined mesh around the screw plate.	196
Figure 5.4 Classification and CPTU parameters with depth at the Halden research site: (a) soil units; (b) water content and Atterberg limits; (c) total unit weight; (d) percentage clay (< 0.002 mm) and fines (< 0.063 mm) particles; (e) CPTU corrected cone resistance; (f) pore pressure ratio, and; (g) soil behavior type index.	197
Figure 5.5 Undrained and drained triaxial test (CAUC, CAUE and CADC) results at Halden research site. (a) Shear stress and (b) excess pore pressure versus vertical strain, and (c) stress – path. Results from the	

SANISAND numerical model calibration for 11.5 m depth are plotted with experimental data.....	198
Figure 5.6 Screw plate load test results from (a) 5.3 m, (b) 7.3 m to 9.3 m, and (c) 11.3 m to 17.8 m depth, with values of interpreted bearing capacities q_{TI} , $q_{0.1D}$, and $q_{0.15D}$ indicated on each curve. q_{HYP} were extrapolated from the stress – displacement results to the asymptotic value.	199
Figure 5.7 Interpreted bearing capacities, q_{ult} , with depth from the (a) tangent intersect (q_{TI}), (b) 0.1D ($q_{0.1D}$), and (c) hyperbolic (q_{HYP}) methods.	200
Figure 5.8 Numerical simulation of SPLTs from 11.3 m depth using the SANISAND soil model. Development of excess pore pressures, Δu , at 16 mm vertical displacement in (a) $t = 1$ min ($v = 16$ mm/min), and (c) $t = 12$ min ($v = 1.3$ mm/min), with (c-d) showing zoomed view of the refined mesh around the plate.	201
Figure 5.9 Drained elastic modulus, E_d , interpreted from SPLTs, laboratory oedometer (CRS and IL) tests and self-boring pressuremeter tests.	202
Figure 5.10 I Interpreted soil strength parameters from SPLTs compared to laboratory triaxial and DSS tests, with: (a) Undrained shear strength from q_{TI} relative to s_{uC} and s_{uD} interpreted at the u_{max} criterion; (b) Undrained and drained shear strength from $q_{0.15D}$ relative to s_{uC} and s_{uD} interpreted at the $A_f = 0$ criterion, and q_f from drained triaxial compression tests; and (c) Undrained shear strength from q_{HYP} relative to s_{uC} and s_{uD} interpreted at the $\gamma_{lim} = \gamma_f = 15$ % criterion.	203

CHAPTER 1

INTRODUCTION

Reliable soil parameters are paramount in detailed design of structures or evaluation of geotechnical stability problems. While conservatism resulting from insufficient or lack of geotechnical data can lead to over design and cost ineffectiveness, adequate but poor-quality laboratory or in situ data may, if used in design, lead to unsatisfactory and in-compliant foundation performance as one of the limit states are violated. The probability of foundation failure is reduced by applying an adequate global factor of safety (FS), material and load factors, or by reliability-based design. However, understanding soil behavior and identifying disturbed or acceptable quality, i.e. reliable and unreliable laboratory soil data and true in situ properties are still of fundamental importance for the integrity of any design analyses and predicting foundation performance after installation.

Significant research efforts have been made to establish recommendations for conducting geotechnical site investigations, soil characterization to obtain design parameters, and the effects of sampling disturbance on these properties in clays (Lefebvre and Poulin 1979; LaRochelle et al. 1981; Wroth 1984; Tanaka et al. 1996; Lunne et al. 1997; Hight and Leroueil 2003; Lunne et al. 2006; DeGroot and Ladd 2012) and sands (Ladd 1978; Robertson and Campanella 1983; Vaid et al. 1999; Jamiolkowski et al. 2003; Wood et al. 2008; Andersen and Schjetne 2013). Silts, however, represent a soil category typically labelled challenging by geotechnical engineers and information on high quality sampling procedures, sample quality assessment methods, and determination of accurate engineering properties of this soil type is limited. Silts and other intermediate soils can complicate the design and construction phases of infrastructure projects both onshore and

offshore, e.g., in the North Sea as described by Senneset et al. (1988) and Solhjell et al. (2017) and can lead to severe building damage during earthquakes, e.g., the 1999 Kocaeli earthquake in Turkey as described by Bray et al. (2004). Geotechnical engineering practice needs better guidance on evaluation of the quality of obtained field and laboratory data for silts and selection of appropriate strength and deformation parameters for use in design.

The goals of this research were to: characterize the natural, low plasticity silt at the Norwegian Geo-Test Site (NGTS) at Halden, Norway, using a suite of in situ tools and soil samplers; develop a better understanding of the response of this soil to the sampling process by comparison of laboratory data on specimens from the different sample types, and by way of laboratory simulation of sampling disturbance of initially high quality samples. Field loading using the screw plate load test provided direct measurement of in situ stress–displacement data, from which in situ bearing capacity and soil parameters could be interpreted.

Chapter 2 presents the results of an extensive geotechnical characterization study of the research site at Halden, Norway including a suite of in situ testing techniques and laboratory tests for strength, deformation and hydraulic flow properties. The author is the lead author, responsible for writing and organizing the paper, conducting parts of the testing, and supervising and interpreting the experimental results with Dr. Roselyn Carroll and Dr. Priscilla Paniagua of the Norwegian Geotechnical Institute (NGI). This paper has been published in *AIMS Geosciences*, Volume 5, Issue 2, 2019. Coauthoring the paper are Carroll, R. Paniagua, P., DeGroot, D.J. and L'Heureux, J-S.

Chapter 3 presents the results of an investigation into the effects of simulated and true tube sampling disturbance on the recompression strain, shear wave velocity and undrained shear behavior and of a natural, low plasticity silt at the research site at Halden, Norway. The author is the lead author, responsible for writing and organizing the paper, testing, and evaluating experimental results. This paper has been accepted for *ASCE Journal of Geotechnical and Geoenvironmental Engineering*. Coauthoring this paper is DeGroot, D.J.

Chapter 4 presents a study of effects of sampler type on stress–strain behavior and engineering properties with depth of the low plasticity silt at Halden, Norway. This paper is submitted to *ASCE Journal of Geotechnical and Geoenvironmental Engineering*. The author is the second author and was responsible for conducting parts of the testing, supervising, interpreting the experimental results and writing the manuscript with Dr. Roselyn Carroll (lead author) of NGI.

Chapter 5 presents the results of an experimental and numerical investigating of the in situ stress–displacement behavior, bearing capacity and engineering parameters of the Halden silt using the screw-plate load test. This paper will be submitted to the *Canadian Geotechnical Journal*. Coauthoring this paper is DeGroot, D.J. and DeJong, J.T.

Appendices A and B contain two papers; one published in the proceedings of the *5th International Conference on Geotechnical and Geophysical Site Characterisation* (ISC'5), and one approved for ISC'6 - organized September 2020.

CHAPTER 2

HALDEN RESEARCH SITE: GEOTECHNICAL CHARACTERIZATION OF A POST GLACIAL SILT

This paper describes the geology and geotechnical engineering properties of the Halden silt; a 10–12 m thick deposit of fjord-marine, low plasticity clayey silt. Over the last six years, the test site has been well characterized by combining the results from a number of geophysical and in situ tools, including; electrical resistivity tomography, multi-channel analysis of surface wave surveys, cone penetration testing, dissipation testing, in situ pore pressure measurements, seismic flat dilatometer testing, field vane testing, self-boring pressure meter testing, screw plate load testing and hydraulic fracture testing. The results from these investigations assist the interpretation of layering and in situ soil properties. Soil sampling and advanced laboratory testing have provided data for interpretation of geological setting and depositional history, soil fabric, strength, stiffness and hydraulic properties. However, interpretation of the stress history, based on oedometer tests and clay-based correlations to the cone penetration test, are unreliable. They contradict the depositional history, which suggests that the soil units at the site are near normally consolidated, except for some surface weathering and desiccation. Further, undrained shear strength interpretations are complex as the in situ tests are potentially influenced by partial drainage, and conventional undrained triaxial tests do not provide a unique (peak) undrained shear strength. Despite certain interpretation challenges the paper presents important reference data to assist in the interpretation and assessment of similar silts, and provide some guidance on important geotechnical properties for projects where limited design parameters are available.

2.1 Introduction

Permanent geotechnical test sites provide valuable references for industry, public authorities, research organizations and academia. Some established and historic geotechnical tests sites include Onsøy (Lacasse et al. 1985; Lunne et al. 2003; Berre et al. 2007; Berre 2013), Bothkennar (Hight et al. 1992), Venice lagoon (Ricceri and Butterfield 1974; Cola and Simonini 2002), Burswood (Low et al. 2011), Balina (Pineda et al. 2016; Kelly et al. 2017), UMass Amherst (Lutenegger and Miller 1994; DeGroot and Lutenegger 2003), and Texas A&M (Briaud and Gibbens 1999). This paper presents the results of an extensive study of a silt site in Halden, Norway. The soil at the site was first investigated in 2011 after a local landslide nearby, following a period with significant rainfall. It was found to consist of a homogeneous, low plasticity clayey silt over soft marine clay. Silts, similar to the deposit found in Halden, but also other intermediate soils like silty sands, silty clays etc. are frequently encountered in Norwegian infrastructure projects onshore and on the Norwegian continental shelf. There is a general perception that they represent a category of challenging soils as it is difficult to obtain samples of high quality, to evaluate sample disturbance and quality, and little guidance is available on the selection of appropriate engineering properties for practical use. A widely accepted particle size classification defines silt as particles in the range of 0.002 mm and 0.063 mm (ISO 2002) and these particles are typically transported by moving currents (e.g. rivers and creeks) and settle in still water. As such, silt deposits are often found all over the world in conjunction with fjords, estuaries and lakes. Therefore, the knowledge acquired at the Halden research site is of national and international importance.

2.2 Regional setting and methods

Halden is located in Southeastern Norway, approximately 120 km south of Oslo, see Figure 2.1a. The research site is one of five National Geo Test Sites (NGTS) and located west of the city center, in what is currently a public park (Rødsparken) belonging to the Halden municipality. It covers about 6000 m² and its topography is almost flat. Elevation above mean sea level varies from +27 m to +34 m (NN2000 datum) from the southwest to northeast. Towards the north and west, the site borders a ridge which ascends to +55 m. Another ridge varying between +35 m to +44 m borders the site to the east. A residential area is found along the road Bøkerveien to the south.

The site has been characterized by combining the results of a number of geological, geophysical and geotechnical site investigation tools. A complete list of all geophysical, in situ and laboratory tests conducted at the site, with general test procedure references and key parameters are presented in Table 2-1. All test locations are presented on the map in Figure 2.1b.

2.3 Engineering geology

2.3.1 Deglaciation history and depositional environment

Deglaciation of Southeastern Norway started at c. 16-15,000 years ago. It was interrupted at around 12,000 and 11,300 years ago by colder periods that led to re-advance of glaciers and formation of frontal moraines in the region (e.g. the "Ra" moraine). As the ice melted the land was subjected to intense isostatic uplift and relative fall of sea-level. The highest post-glacial sea level in the region (marine limit) is about

190 m above the present sea level and was formed 10,700 years ago (Sørensen 1999). The early Holocene period was characterized by rapid sedimentation of marine clays and silts at the site as a consequence of the rapid fall in sea-level. This was followed by more placid deposition in an estuarine/distal deltaic environment associated with the prograding Tista River delta. The shoreline reconstruction curves from the region, proposed by Klemsdal (Klemsdal 2002), show that the site most likely emerged from the marine environment c. 5,000 years ago (Figure 2.2). Two radiocarbon (^{14}C) datings of marine shell fragments are available from the research site (Table 2-2); one from the clay at about 16.3 m depth (elevation about 12 m.a.s.l), and a second from the clayey, silt at 6.4 m depth (22 m.a.s.l). The results indicate $11,820 \pm 25$ years before present (BP) and $6,455 \pm 25$ years BP, respectively. This corresponds well with earlier carbon dating results from the area (Olsen and Sørensen 1993) and the deglaciation history. The average rate of sedimentation corresponds to about 1.0 - 1.4 mm/year.

2.3.2 Source of material

Figure 2.3 presents the location of the research site within the regional geological setting. The Halden municipality lies within the Norwegian southeast basement area. The dominating bedrock is gneiss in the northeast and granite in the northwest and southeast (Olsen and Sørensen 1993). Glacial striations are generally north-south and northeast-southwest and topographical characteristics such as small valleys and hills are typically oriented in that direction. The most prominent geological feature in the area is the "Ra", an end moraine complex deposited about 11,300-10,700 years ago during the Early Younger Dryas. It traverses the region from northwest to southeast and retains the water

in lakes Tvetervatn, Rokkevatnet and Korsevatnet. Earlier the moraine also retained the larger lake Femsjøen. A second zone of marginal moraine, parallel to the Ra is located south of Halden, namely the "Outer Ra", or the Onsøy-Borge moraine. Between and outside these two features is a large veneer of clay deposits, interrupted in certain areas by silt and sand deposits, e.g. south of Halden. Areas northeast of the Ra are dominated by exposed bedrock, with clay only in local depressions. The Glomma River, Norway's longest and largest river, runs into the Oslo fjord in the city of Fredrikstad, about 25 km northwest of the Halden research site. East of the site flows a system of lakes and rivers called "Haldenvassdraget". This system is the second largest in Norway and runs into the Idde fjord in Halden through the Tista River (Figure 2.1a). During higher sea levels, the test site was likely highly influenced by both of these river systems, as Halden was inundated by the sea (Sørensen 1979). Thus the source of material supplied has an important contribution from the whole of southeastern Norway and has primarily been produced by glacial erosion, with secondary fluvial transport.

2.3.3 Stress history

From the geological history of the site no known loading events have occurred. Relative to the sea level the Oslo area has been rising steadily, and soil units were deposited during a single period of submergence (Kenney 1964). The depositional history hence suggests that the soil at the site is likely to be geologically normally consolidated, except perhaps for some surface weathering, desiccation and aging. Substantial erosion is unlikely to have occurred, but seasonal ground water and temperature fluctuations may cause some apparent preconsolidation. Data from one standpipe and four electrical

piezometers installed at 5 m, 10 m, 15 m and 20 m depth reveal that the ground water table is located at about 2 m depth and that the in situ pore pressure, u_0 (two year average - October 2016 to October 2018), is close to hydrostatic in the silt units and sub-hydrostatic in the clay layer below (Figure 2.4a). Sub-hydrostatic pore pressures can occur at sites located on a hill where vertical recharge into a low permeability clay layer is less than discharge occurring away (radially) from the site in an underlying higher permeability soil unit (Ostendorf et al. 2004). At Halden no such permeable material has been identified below the clay. However, fractured bedrock or a thin layer of gravel could facilitate radial drainage away from the site. The piezometer logs, presented in Figure 2.4b, demonstrate how the fluctuating ground water table causes peak pore pressures during winter and after the spring snow melt (February to May), and pore pressure lows at the end of the summer (August). These fluctuations cause seasonal changes in the mean effective stresses in the order of 5 - 10 kPa. Temperature fluctuations in the order of 20° Celsius are observed in the top soil throughout the year. However, below about 6 m depth the fluctuations are negligible, and the temperature is fairly constant with depth at about 8 degrees Celsius (Figure 2.5).

From the total unit weights (γ ; Section 2.5.2) and the in situ pore pressure depicted in Figure 2.4a the total and effective vertical stress conditions (σ_{v0} , σ'_{v0}) are derived and plotted in Figure 2.6. The total stress profile is approximated by using $\gamma = 19$ kN/m³ in Units I and II, and $\gamma = 20$ kN/m³ in Units III and IV. Interpretation of the apparent preconsolidation stress, or yield stress σ'_p (p'_c), from oedometer tests on silt is challenging. This is discussed in Section 2.6.2.

2.3.4 Stratigraphy

Soil layering across the site has been assessed by combining the results of a number of site investigation tools. Table 2-2 presents the Halden site stratigraphy, unit description with images of selected samples from the X-ray inspection (XRI) and split core imaging performed by the Geological Survey of Norway (NGU). The XRI system consists of an X-ray tube, an image intensifier and a high quality digital camera. The resulting images can be used to assess e.g. (i) soil type; (ii) soil macro fabric; (iii) the presence of inclusions such as stones, shells, sandy zones and root holes etc.; (iv) the presence of fissures, shear planes, discontinuities etc.; (v) degree of bioturbation; and (vi) indications of sample disturbance. The soil sample is placed between the X-ray tube and the image intensifier and different sections can be inspected by rotating the tube and sliding the assembled XRI configuration horizontally along the sample. Repeated runs produced three 16-bit greyscale images with 0, 45, and 90 degree axial orientation. X-ray transparency of a sediment is strongly influenced by the grain-size and the images are generally light grey for the fine-grained soils and dark grey for coarse-grained soils. The two split core images per sample were captured directly after opening using 20 ms and 40 ms exposure time.

Based on an overall interpretation of the geophysical, in situ testing and laboratory testing results the site stratigraphy is divided into four main soil units numbered Units I to IV, as depicted in Figure 2.7a to Figure 2.7g. The stratigraphy presented in the following describes the soil units as they have been identified in the southernmost part of the test site, i.e. beneath the main cluster of investigated locations shown in Figure 2.1b: A silty, clayey sand constitutes the top soil and extends down to

about 4.5 to 5 m depth (Unit I). It is generally loose to medium dense with some organic material (0.25% - 0.5% total organic carbon). Unit I rests above a clayey silt which extend down to about 15 - 16 m depth. This clayey silt is separated into two soil units (Unit II and III) based on the results of in situ and index tests but is regarded as the same material with the same geologic origin. Index and in situ tests reveal that the silt becomes sandier closer to the lowermost soil unit, Unit IV, which consists of a low to medium strength clay. This soil unit has a slightly laminated structure, with occasional shell fragments and drop stones. Depth to bedrock dips sharply from the northeast to southwest but is typically identified at 21 m depth in the southern part of the site (see Figure 2.8).

2.4 Soil composition

2.4.1 Grain size distribution

Figure 2.9a presents two grain size distribution curves from Unit I and a typical range of grain size distributions in the silt from Units II and III. All results below 5 m depth were determined using the hydrometer method (ISO 2016) or the falling drop method (Moum 1965). A summary of the clay size particle content ($d < 0.002$ mm) and fines content ($d < 0.063$ mm) with depth are presented with other classification parameters in Figure 2.7. The upper soil Unit I mainly consists of a silty, clayey sand. The fines content in the two silt units (Units II and III) is generally higher than 80%, slightly decreasing towards the interface with the clay in Unit IV. The clay content ($d < 0.002$ mm) is fairly constant at around 8% in Units II and III, classifying this as a clayey silt according to ISO 14688-1 (ISO 2002) and the Norwegian Geotechnical Society

(NGF) soil classification triangle (Norwegian Geotechnical Society 2011) in Figure 2.9b. However, based on the plasticity properties of the soil (see Section 2.5.1) the Unified Soil Classification System (USCS) classifies these soils as silty clay with sand to lean clay with sand. No grain size data has yet been acquired in the clay layer Unit IV.

2.4.2 Grain shape and mineralogy

Scanning electron microscope (SEM) images in Figure 2.10 and Figure 2.11, from 6.4 m and 8.6 m depth respectively, demonstrate that the silt particles are largely angular (Pettijohn 1949). Table 2-3 presents the results of three X-ray diffraction (XRD) analyses performed by the Geological Survey of Norway (NGU) on particles from Unit II and III. The results reveal very similar mineralogical content with depth. Both Units II and III contain similar amounts of quartz, plagioclase, clay minerals and mafic minerals (amphibole). These results are consistent with mineralogical analyses of the sand and silt fractions of the glacial tills examined in the region west of the Oslo fjord (Rosenqvist 1975). The clay minerals are illite and chlorite, and the presence of expanding clay minerals are low or absent.

2.4.3 Carbon content

Total carbon (TC) and Total Organic Carbon (TOC) were determined by dry combustion at NGUs laboratory using a LECO SC-632 analyzer with an infrared (IR) detector (Leco Corp., St. Joseph, MI). The carbon content in the silt units is generally low. Figure 2.12 shows that in Unit II the average TC was 0.49% with a range from 0.43% - 0.54%. In Unit III the average TC is 0.24%, ranging from 0.19% - 0.28%.

Meanwhile the TOC in Unit II average is 0.46% while the average is lower in Unit III at a value of 0.22%.

2.4.4 Salinity

Nine salinity tests were performed in the laboratory by means of electrical conductivity (κ) to determine the NaCl equivalents of the pore water according to ISO 11265 (ISO 1994). Electrical resistivity tomography (ERT) profiles were conducted at the site by injecting a current into the subsurface through steel electrodes, installed 10 - 20 cm into the ground, and the apparent resistivity distribution along a profile or area was measured. Direct measurements of resistivity were also made during cone penetration testing at locations HALC06 and HALC10, using a resistivity add-on module with the original cone (RCPTU). The adapter consisted of an array of four ring electrodes in a Wenner configuration with equal (0.25 m) spacing between the electrodes. The RCPTU depth was corrected for the distance between the electrodes and the cone tip.

The laboratory salinity tests indicate electric conductivity (inverse of resistivity) in the range of 119 $\mu\text{S}/\text{cm}$ to 485 $\mu\text{S}/\text{cm}$, which corresponds to NaCl equivalents of 1.1 to 4.6 g NaCl/L. These results are converted to resistivity and plotted with results of measurements conducted on selected triaxial test specimens in Figure 2.12d. Indications from the RCPTUs at locations HALC6 and HALC10, as also presented in Figure 2.12d, are that the laboratory measurements are on the low side of the in situ measurements. The in situ resistivity decreases from about 300-1000 Ωm in the top soil to a fairly constant value of 100-150 Ωm in the silt. There is fair agreement between the RCPTU and ERT profiles, indicating that the in situ resistivity measurements can be considered more

reliable than the laboratory measurements. The change in resistivity is linked to the reduction in salt content, and considering the fact that the soil at the site was deposited in a post glacial fjord-marine environment, leaching of the silt is likely to have occurred due to rainfall and snow melting in the Halden region. It has been suggested for Norwegian clays, that unleached marine clays have resistivities in the range of 1 - 10 Ωm while fully leached, potentially quick clay deposits, clayey moraine and silty sediments typically have resistivities in the range of 10-100 Ωm (Solberg et al. 2008; Solberg et al. 2012).

2.4.5 Soil fabric

Soil Units II and III are generally homogeneous, structureless to mottled, with primary bedding and laminations almost absent due to bioturbation. Such structureless soils are common in fjord-marine environments subjected to hemipelagic sedimentation and seafloor biological activity (Hansen et al. 2011). The XRI images (see Table 2-2) appear to confirm that that mottling is associated with internal reworking of the sediments and consequently with the partial or complete loss of any primary sedimentary bedding structures. In contrast, Unit IV shows some weak laminations and the occasional presence of drop stones (sand/gravel particles) interpreted as ice rafted debris (IRD). There is some evidence of shell fragments and iron sulphide spots, resulting from decomposition of organic matter. No evidence of cementation or fissures has been found in either of the soil units.

2.5 State and index properties

2.5.1 Water content and Atterberg limits

The measured natural water contents (w) are somewhat scattered, but generally decrease with depth from about 31% at 4 m depth to about 26% at 16 m (Figure 2.7b). The scatter is thought to be due to different sampling techniques, and the fact that different measurements have been made over several years, i.e. certain samples may have experienced some loss of moisture during storage. Results from measurements made the same day on samples from HALB02 all show a consistent trend decreasing with depth. While in Unit II the results generally fall between 26% and 32%, the water content in Unit III decreases with depth from about 26% at 12 m depth to about 21% at 15 m. The decreasing water content with depth in Units II and III coincides with a decreasing organic content (TOC) and increasing total unit weight of the soil (See Sections 2.4.3 and 2.5.2, respectively).

The liquid limit (w_L), as measured using the fall cone, and plastic limit (w_P) were conducted in accordance with ISO 17892-12 (ISO 2018). In Unit II w_L and w_P varies between 28% and 37%, and 22% and 25%, respectively. Average plasticity index (I_P) in this soil unit is 9.3%. In Unit III w_L varies between 25% and 29%, w_P ranges from 20% to 23% and average plasticity index is 6.6%. Figure 2.13 shows that the results generally plot on and above the A-line in a Casagrande plasticity chart, just on the division between the inorganic low plasticity clay (CL) and inorganic silts (ML). The known differences in liquid limit, as determined by means of the fall cone and Casagrande cup for low I_P soils would likely have shifted the Halden silt data points down and left in the plasticity chart,

if the Casagrande cup was used (Norwegian Geotechnical Institute 2002). As such, a data point from the fall cone that plots on or just above the A-line could shift to below the A-line if the liquid limit was measured using a Casagrande cup.

2.5.2 Total unit weight and void ratio

Total unit weights (γ_t) are estimated from the Multi Sensor Core Logger (MSCL), from direct measurement of advanced laboratory test specimens and from measured specimen water contents. The MSCL measures soil density based on emitted gamma ray attenuation using a ^{137}Cs radioactive source and a sodium iodide, NaI (TI) radiation detector. Figure 2.7c shows that the total unit weight in Unit II generally falls between 18.9 kN/m^3 and 19.2 kN/m^3 . In Unit III the total unit weight increases with depth from about 19.5 kN/m^3 at 12 m to about 20.5 kN/m^3 at 15 m, with an average value of 19.9 kN/m^3 . Results from the MSCL show an increase in total unit weight in Unit II. The trend is similar to that obtained from laboratory results based on direct measurements and water contents. However, the MSCL results are slightly higher. This may be due to whole core measurements where total density measurements integrate the entire sample thickness.

From a constant specific gravity of 2.69 (see section 2.5.3) the calculated in situ void ratio (e_0) decreases from about 0.82 at 5 m depth, to 0.6 at 15 m.

2.5.3 Unit weight of solid particles

Measured unit weight of solid particles (γ_s) ranges between 26.1 kN/m^3 and 26.5 kN/m^3 , with an average value of 26.3 kN/m^3 (specific gravity, $G_s=2.69$), see Figure 2.12.

2.6 Engineering properties

A number of in situ and advanced laboratory tests were performed to determine the engineering properties of the silt units at Halden (see Table 2-1 for the general test procedures). In this section the measured in situ data are first presented, followed by a comparison of engineering properties from laboratory test results and the derived parameters from in situ test results. The results focus on the silt units (i.e. Units II and III).

2.6.1 In situ testing - measurements

2.6.1.1 Field vane testing

Field vane testing (FVT) was performed using a Geotech AB 130×65 mm vane with a tapered lower end in general accordance with the Norwegian guidelines (Norwegian Geotechnical Society 1989). After pre-drilling down to about 4.5 m the vane was advanced to the target depth from the ground level encased in a protective housing. The vane was then pushed out of the housing and rotated using electric heads and the torque was measured on the drill rig. Both intact and remolded tests were conducted at a rate of shearing of about 0.1 °/s. Remolded tests were performed after 10 full revolutions of the vane. The intact and remolded FVT results are presented in subsequent Sections 2.6.8 and 2.6.13, respectively.

2.6.1.2 Cone penetration testing

A number of different manufacturers' piezocones were tested at Halden, including Geomil, A.P.van den Berg, Pagani, Environmental Mechanics (Envi) and Geotech AB cones. They were all 10 cm² compression cones with 150 cm² friction sleeves and the pore pressure transducer located in the u₂ position. The CPTU tests were performed in general accordance with Norwegian guidelines (Norwegian Geotechnical Society 2010) and ISO 22476-1 (ISO 2012). Figure 2.14a to Figure 2.14f present selected measured (corrected cone resistance, q_t, pore pressure, u₂, and sleeve friction, f_s) and derived (normalized cone resistance, Q_t, pore pressure ratio, B_q, and soil behavior type index, I_c) CPTU parameters from a number of tests conducted across the test site. In the silt units, Units II and III, q_t typically plots around 1 MPa, similar to that of the clay unit below. In the deeper parts of the silt deposit q_t increases from 1 MPa at 12 m depth to about 2 MPa at around 16 m depth. Normalized cone resistance ($Q_t = [q_t - \sigma_{v0}]/\sigma'_{v0}$) is generally high in the top soil, but decreases to about 7.5 in the depth range 5 - 16 m. Excess pore pressures are generated behind the cones in the silt and clay units, and the pore pressure ratio, $B_q = (u_2 - u_0)/(q_t - \sigma_{v0})$, is generally around 0.1 - 0.3 in the silt units and 0.8 - 1.0 in the deeper clay. Previous experience on different soils (Lunne et al. 2018) has shown there is some variability in the measured sleeve friction, f_s between the different cones tested at the site. The soil behavior type index, $I_c = [(3.47 - \log Q_t)^2 + (\log F_r + 1.22)^2]^{0.5}$, generally plots between 2.6 and 2.95 (Silt mixtures - clayey silt to silty clay). Normalized friction ratio, $F_r = 100\% \times f_s/(q_t - \sigma_{v0})$, ranges from 1% to 3% depending on cone manufacturer. As shown in Figure 2.15, normalized soil behavior type (SBT_N) charts (Robertson 1990) based on Q_t, F_r and B_q from CPTU location HALC11 typically indicate

SBT zones 4 (Silt mixtures - clayey silt to silty clay) and 5 (Sand mixtures - silty sand to sandy silt).

2.6.1.3 Shear wave velocity

Direct measurements of shear wave velocity were made during a number of seismic cone penetration and seismic dilatometer tests at the site using a seismic add-on module with the original cone/dilatometer. Two multi-channel analyses of surface waves (MASW) profiles were also acquired. The SCPTU/SDMT configurations had a source at ground level and two geophones mounted behind the cone or dilatometer with a 0.5 or 1.0 m spacing thus giving a measure of shear wave velocity for a vertically propagating horizontally polarized shear wave, V_{vh} . In order to increase the signal-to-noise ratio and reduce the uncoherent noise the seismic traces were typically stacked and filtered through a Butterworth bandpass filter. The velocity was computed from the time lag corresponding to the maximum of the cross-correlation between the two geophone signals. The MASW data acquisition was conducted using a linear array of 24 vertical geophones with a natural frequency of 4.5 Hz, and the inversion of the dispersion curves provided a 1D shear wave velocity, V_s , profile averaging the subsurface properties below the geophone array. Figure 2.16 demonstrates a clear trend of increasing shear wave velocity from about 110 m/s at 2 m depth to about 200 m/s at 16 m. The higher shear wave velocities at location HALC13 compared to the general trend from the other locations are likely associated with a higher uncertainty in the velocity estimates at this location (greater error estimates). There is generally a very good agreement between the SDMT and the SCPTU results. However, the MASW results (HALM01 and HALM02)

are somewhat higher than the general trend from the other test methods. The inversion data fit was of limited quality, and as a result of the decreasing depth to bedrock along the geophone array the velocities below 8 m to 12 m depth likely integrate bedrock velocities and are removed. A MASW survey conducted by the University of Iceland demonstrated increased resolution compared to the tests at HALM01 and HALM02, and the results coincide better with the SCPT data below 8 m depth (see Figure 2.16).

2.6.1.4 Flat dilatometer testing

Measured flat dilatometer data from location HALD01 is presented in Figure 2.17a to Figure 2.17e. Testing was conducted in general accordance with ISO 22476-11 (ISO 2017). The corrected pressure readings, P_0 and P_1 , are presented along with the three intermediate DMT parameters I_D (material index), K_D (horizontal stress index), and E_D (dilatometer modulus), e.g. (Marchetti 1980; Marchetti et al. 2006). There is some scatter above 5 m. The data is more consistent in the silt and clay units below. Soil classification charts based on I_D and E_D (Marchetti et al. 2006) typically classify the silts in Units II and III as mud, mud and/or peat or clay. Based primarily on I_D (Marchetti et al. 2006) the silts are identified as clays, but it is noted that; " *I_D sometimes misdescribes silt as clay and vice versa, and of course a mixture of clay-sand would generally be described by I_D as silt*". Assessment of OCR and K_0 using the Marchetti equations (Marchetti 1980) are presented in Sections 2.6.2 and 2.6.3.

2.6.1.5 Self- boring pressuremeter testing

Four self-boring pressuremeter tests were conducted in location HALP01 in general accordance with ISO 22476-5 (ISO 2012) using the Cambridge InSitu Ltd. six-arm pressuremeter probe. The borehole HALP01 was drilled using an auger bit with a nominal size of 120 mm using water flush. The SBPT was self-bored to the required depth with the cutter positions optimized and at a rate such that a minimum of disturbance was introduced in the soil. After the first three tests a steel casing was advanced to 11.5 m to stabilize the borehole. The probe was calibrated prior to and after testing and corrections for membrane stiffness were made upon data reduction. The four test results from 6.1 m, 8.0 m, 10.0 m and 12.0 m depth, plotted in Figure 2.18, are average data for each tier of strain arms. Three to four unload-reload loops were conducted at each depth.

2.6.2 Overconsolidation ratio, OCR

An evaluation of the overconsolidation ratio (OCR) profile is dependent on reliable interpretation of the preconsolidation stress or yield stress, σ'_p , from laboratory oedometer tests or an appropriate correlation of yield stress to cone resistance, none of which yet exist for silts. As will be discussed in Section 2.6 the Halden silt 1D compression curves of log effective vertical stress with void ratio are generally very flat, and interpretation of σ'_p from these oedometer tests have proved very challenging. Both the conventional Casagrande interpretation (Casagrande 1936), Janbu (Janbu 1963) and Pacheco Silva (Pacheco Silva 1970) methods resulted in unreliable values of σ'_p . However, the geological history of the area (see Section 2.3) is well understood and no

loading or large erosion events are likely to have caused overconsolidation of the soil units at the research site. The well-established correlations of yield stress to CPTU cone resistance valid for natural clays (Lunne et al. 1997), $\sigma'_p = k \times (q_t - \sigma_{v0})$ suggests a normally consolidated stress history for the clay (Unit IV) below the silt Units II and III (see Figure 2.19a and Figure 2.19b). In this equation, k is a constant and in this case taken as 0.3, which is a typical value used for clays (Mayne 2007). Normally consolidated or lightly overconsolidated clay (OCR= 1.0 - 1.3) at this depth is confirmed by the FVTs conducted at the site using the Chandler methodology (Chandler 1988), where $\sigma'_p = \sigma'_{v0} \times [(s_{u,FVT}/\sigma'_{v0})/S_{FVT}]^{1.05}$ and S_{FVT} is estimated as a function of plasticity index (in this case taken as 0.15 and 0.2 in the silt and clay units, respectively, based on an assumed plasticity index, $I_p = 10\%$ and 20%). From the geological history and evidence of the near normally consolidated stress state of the lower clay one can thus infer that the uniform silt Units II and III above this clay unit, are also normally consolidated. This implies that the CPTU and FVT correlations discussed above, which suggest OCR in the range of 2 to 5 in the silt Units II and III, are unreliable and inappropriate for this soil type. Any light overconsolidation is likely an effect of aging and fluctuating ground water table. Yield stress and OCR interpreted from DMTs (Figure 2.19a and Figure 2.19b) using the horizontal stress index, K_D (Marchetti 1980) (valid for clays with $I_D < 1.2$) suggest $OCR \leq 1$ and $OCR = 1.5$ in the silt and clay units, respectively. Dilatometer tests were used to confirm a low to medium overconsolidation ratio ($OCR = 1.2 - 3.7$) in the silt layers of the Malamocco test site, near Venice, Italy (Cola and Simonini 2002). Based on the above discussion an OCR in the range of 1.0 to

1.3 at Halden is considered reasonable. Following from this OCR assessment a k-factor of 0.15 - 0.2 would be more appropriate in the Halden silt, i.e. $\sigma'_p = 0.2 \times (q_t - \sigma_{v0})$.

2.6.3 Coefficient of earth pressure at rest, K_0

Coefficient of earth pressure at rest, $K_0 = \sigma'_{h0}/\sigma'_{v0}$ (Figure 2.19c.), was derived from DMT results using the clay correlation to K_D (Marchetti 1980), and from nine anisotropically consolidated drained and undrained triaxial tests in compression loading (CADC, CAUC) using the expression (Mesri and Hayat 1993):

$$K_0 = (1 - \sin \phi'_{cv})OCR^{\sin \phi'_{cv}} \quad (2.1)$$

where, ϕ'_{cv} is the constant-volume effective stress friction angle for triaxial compression (Mesri and Hayat 1993), in this case assumed to be equal to ϕ'_{mo} obtained in the CADC and CAUC tests at maximum obliquity, $(\sigma'_1/\sigma'_3)_{max}$. In this expression an OCR of 1.3 has been assumed (see Section 2.6.2).

Moreover, in situ horizontal total stresses were assessed from the four SBPTs plotted in Figure 2.18 based on a methodology proposed for London clay by Marsland and Randolph (1977). In this approach, the total horizontal stress and undrained shear strength of the soil adjacent to the probe are estimated by iteration. Once a first qualified value of σ_{h0} is assumed, the apparent mobilized cavity shear stress at the pressuremeter boundary can be derived from the measured expansion curve following the Palmer analyses (Palmer 1972). The peak shear strength of the soil is estimated from the maximum slope of the P-ln ($\Delta V/V$) curve, where P is the measured pressure, ΔV is the increase in volume from the reference state, and V is the current volume of the measuring cell at the measured pressure. The point at which the pressure-deformation curve

becomes significantly non-linear should correspond the in situ horizontal total stress plus the undrained shear strength in clays ($\sigma_{h0} + s_{u,SBP}$). The methodology assumes fully undrained conditions. However, as noted by Wroth (1984), the stress and strain fields surrounding the pressuremeter do not remain homogeneous during membrane expansion, and partial drainage will occur even in clays. As such, interpretation of SBPTs in silts is challenging and somewhat uncertain. K_0 interpreted from the four tests at Halden (Figure 2.19c) are consistently higher than the values interpreted from laboratory triaxial tests. This could indicate an over prediction of the effective horizontal stress resulting from partial drainage effects.

Despite uncertainties associated with the clay-based interpretation of the SBPT and DMT data there is fair agreement between the in situ and laboratory test results, and K_0 generally ranges between 0.6 and 0.45.

2.6.4 Small strain shear modulus

Small strain shear modulus, G_{max} , is interpreted from a number of SCPTs, one SDMT and two MASW profiles. Figure 2.20 presents G_{max} computed from in situ shear wave velocity measurements depicted in the previous Figure 2.16. Generally, the SCPT and SDMT G_{max} results increase linearly from about 30 MPa at 5 m depth to about 75 MPa at 16 m depth. Two SCPT results from location HALC13 plot outside the scale and are indicated in the figure ($G_{max} = 287$ mPa and 354 MPa). However, the results from this location are generally high, and likely a result of greater uncertainty in the shear wave velocity estimates (see Section 2.6.1.3). The linear increase in V_{vh} in the silt units is very consistent with the Rix and Stokoe correlation of G_{max} to cone resistance for sands (Rix

and Stoke 1991), presented in the figure. G_{\max} computed from the Mayne and Rix correlation of shear wave velocity to corrected cone resistance (Mayne and Rix 1995), valid for natural clays, plot below the in situ and MASW results. Bender element (BE) tests (Dyvik and Madshus 1985), performed on triaxial specimens (at $\sigma'_{vc} = \sigma'_{v0}$, $\sigma'_{hc} = \sigma'_{h0}$) and DSS specimens (at $\sigma'_{vc} = \sigma'_{v0}$), indicate that the small strain shear modulus measured in the laboratory is generally lower than the in situ test results.

2.6.5 Constrained modulus

For soft clays, primary consolidation properties are normally interpreted from oedometer curves of log effective stress (σ'_v) with strain (ϵ_v) or void ratio (e). Creep properties from plots of ϵ_v or void ratio with log time. This approach may be inappropriate for silts and other intermediate soils leading to unreliable interpretations, while, Janbu's theory for primary and secondary settlements (Janbu 1985) may be more suitable. In Janbu's framework the stress induced primary consolidation is calculated with an effective stress dependent constrained modulus ($M = \Delta\sigma'_v/\Delta\epsilon_v$). As observed in oedometer tests on other silts, e.g. Cola and Simonini (2002); Carroll and Long (2017), the three typical Halden CRS oedometer curves (rate of strain 5%/hr) of log effective stress with void ratio are generally quite flat (see Figure 2.21a). The compression curves are presented in linear scale in Figure 2.21b, which show no distinct yield as typically displayed by structured clays. As such interpretation of σ'_p from these curves is considered misleading. This 1D compression behavior seems to be characteristic of some intermediate soils (Martins et al. 2001; Long 2007; Long et al. 2010; Carroll and Long 2017). Janbu's modulus framework for silts ($M = 1/m_v = m \times p_a \times [\sigma'_v/p_a]^{1-a}$, where m_v is the

volume compressibility $\Delta\varepsilon_v/\Delta\sigma_v$, m is the modulus number, p_a is the reference stress = 100 kPa, and a is a stress exponent) gives a reasonable fit, as demonstrated in Figure 2.21d when the modulus number $m = 75$ and stress exponent $a = 0.25$ are taken. The Janbu modulus framework for clays ($M = m \times \sigma'_v$) is presented in the same figure using $m = 30$, but does not provide a good fit. Janbu's silt model has also been applied on Icelandic silts (Skúlason 1996), on Irish silts (Long 2007) and on another Norwegian silt from Os (Long et al. 2010).

Values of the constrained modulus at the in situ effective vertical stress, M_0 , from CRS and IL tests on specimens from block samples (HALB04) are plotted with depth in Figure 2.22a. With one exception at about 15 m depth, M_0 ranges from 5 to 10 MPa. This is consistent with the CPTU results from locations HALC11 and HALC12 using the correlation $M_0 = \alpha_i \times q_{net}$ with $\alpha_i = 10$ (Lunne et al. 1997) and Janbu's modulus framework for silts using $m = 70-80$, also presented in the figure.

2.6.6 Coefficients of consolidation

Coefficient of vertical consolidation (c_v) with log effective stress from three typical Halden CRS oedometer tests are presented in Figure 2.21c. c_v at the in situ vertical effective stress is determined from the base pore pressure (u_b) in CRS oedometer tests (Sandbækken et al. 1986), and from IL oedometer tests using the root time fitting method (Taylor 1948). The results are consistent with the values of c_v computed from the direct measurement of vertical hydraulic conductivity (k_v , see Section 2.6.7 and Sandbækken et al. (1986)) using the relationship $c_v = k_v / (m_v \times \gamma_w)$. In this equation m_v is the volume compressibility and γ_w is the unit weight of water at 20°C. The results plotted

in Figure 2.22b suggests an average coefficient of vertical consolidation of 1.3×10^{-5} m²/s, or about 400 m²/year. Results from other silts are typically in the order of 10 to 350 m²/year (Ladd et al. 1985; Sandven 2003; Long 2007).

Coefficient of horizontal consolidation (c_h) is interpreted from a number of CPTU dissipation tests (Carroll and Paniagua López 2018), where t_{50} is determined from the square root method (Sully et al. 1999), and determined in the laboratory on a block sample test specimen mounted horizontally in the CRS oedometer cell. All dissipation tests were conducted after penetrating the piezocones to target depth using standard CPTU penetration rate of 20 mm/s. Figure 2.22c shows that the in situ results indicate slightly lower c_h compared to the c_v determined in CRS and IL oedometers. However, the differences are not significant and the c_h result determined in the laboratory confirms this. Further, during dissipation testing, Halden silt exhibited a non-standard (dilatory type) behavior which introduces uncertainties in the interpretation of t_{50} and c_h , since the applied methods were generally developed for clays, and do not consider partial drainage.

2.6.7 Hydraulic conductivity

Constant-head hydraulic conductivity tests were conducted at different stress levels during a selected number of oedometer tests and during the consolidation stage of a number of triaxial tests. Hydraulic conductivity was determined by flowing de-aired water through the specimens, from bottom to top, by a 100 mm mercury column in a U-shaped saran tubing. The amount of water flowing in and out of the specimen was measured separately, and the tests were continued until the water inflow and outflow were approximately equal (Sandbækken et al. 1986). Both vertical and horizontal

hydraulic conductivity (k_v , k_h) are presented in Figure 2.23. Values from oedometer test specimens represent the hydraulic conductivity at zero axial strain (back-extrapolated along the linear $e - \log k$ line (Sandbækken et al. 1986), i.e. at a void ratio near in situ conditions. Values from triaxial test specimens represent the hydraulic conductivity near the in situ effective stress state (σ'_{vc} , σ'_{hc}), i.e. after consolidation and some subsequent change in void ratio (Δe) has occurred. Due to the larger volume of soil and the greater height of the triaxial test specimen the hydraulic conductivity measurements made on these specimens are generally considered more reliable. The average k_v of the triaxial test specimens is 9.8×10^{-9} m/s.

2.6.8 In situ undrained shear strength – field vane testing

Drainage conditions in silts during shear depend on a number of factors, including but not limited to loading regime, drainage path, clay content etc. An effective stress approach may in some cases be a more valid approach for silts and silty soils, but the total stress approach is often used in engineering practice and when an evaluation of the undrained shear strength is required. The field vane test results plotted in Figure 2.24a show that the interpreted peak intact undrained shear strength in the silt units is fairly constant with depth at around 40 - 45 kPa, except for some higher values close to the silt-clay interface around 14 - 16 m depth. No empirical correction factors have been applied. As will be discussed in subsequent sections, the results are very consistent with the derived undrained shear strength from location HALC12 using an undrained CPTU interpretation with $N_{kt} = 18$, and generally plot between the $s_u = 0.3\sigma'_{v0}$ and $0.5\sigma'_{v0}$ lines, indicated in the figure. As observed in the Norwegian Os silt (Long et al. 2010) and the

Swedish Borlänge silt (Larsson 1997) field vane test results in silt are typically significantly lower than the results from undrained triaxial tests on the same material, when s_{uC} is interpreted at simple peak or 10% axial strain like for clays. The reason for the high triaxial strength is the strong tendency for dilatant behavior during undrained shear (see Section 2.6.12). It should be noted, however, that field vane testing in silt may be subject to drained or partially drained conditions. As noted by Chandler (1988), if the coefficient of consolidation is not sufficiently low with respect to the rate of vane rotation, consolidation may occur. Moreover, Blight (1968) developed an approximate theory, supported by experimental tests in a silt (tailings, 5 - 15% clay content, $c_v = 370$ m²/year), by which one may determine the rate of vane rotation required to ensure undrained conditions. Based on these theoretical drainage curves for the vane test (Chandler 1988), indications are that the conventional rate of rotation (6 - 12°/min) does not provide shearing under fully undrained conditions in the silt units at Halden. Thus, the vane results between 5 m and 16 m depth in Figure 2.24a may not be an accurate measure of the undrained shear strength.

2.6.9 In situ undrained shear strength – pressuremeter testing

Figure 2.24a presents undrained shear strengths from the four self-boring pressuremeter tests interpreted using the Marsland and Randolph (1977) approach, see also Section 2.6.3. In this approach, undrained conditions are assumed, and the total horizontal stress (σ_{h0}) and peak cavity shear stress ($s_{u,SBP}$) at the pressuremeter boundary are estimated by iteration. The point at which the pressure-deformation curve becomes significantly non-linear should correspond to the in situ horizontal total stress plus the

undrained shear strength in clays. The undrained shear strengths estimated from this approach are consistent with field vane results, and $s_{u,SBP}$ ranges from 38 kPa to 51 kPa. Assessment of undrained shear strength using the limit pressure (p_L) (Marsland and Randolph 1977) yields values in the range of 31 kPa to 68 kPa but are associated with very large strains. A third interpretation approach, the Gibson and Anderson (1961) approach, is based on the assumption of an elastic-perfectly plastic material and yields significantly larger $s_{u,SBP}$ values. In clays, over predictions of undrained shear strength from SBPTs compared to laboratory tests on undisturbed soil have been observed (Wroth 1984; Aubeny et al. 2000). This is typically explained by partial consolidation during expansion (high gradients of pore pressure in the radial direction) and strain rate effects (increased 'viscosity' – shearing at strain rates much faster than conventional laboratory tests yields larger undrained shear strength). Noting that the SBPT is a rather slow test compared to other in situ techniques, e.g. the CPTU, partial drainage may have prevailed during membrane expansion at Halden. As a result, there is some uncertainty associated with the $s_{u,SBP}$ results in Figure 2.24a. The fact that the interpreted undrained shear strength values show fair agreement with the field vane test results and the CPTU correlation to q_t could be a result of compensating effects in the measurements and interpretation, and as such, somewhat fortuitous.

2.6.10 In situ undrained shear strength – flat dilatometer testing

DMT results in Figure 2.24b show that the Marchetti correlation for undrained shear strength from DMT (Marchetti 1980), $s_{u,DMT} = 0.22 \times \sigma'_{v0} \times (0.5K_D)^{1.25}$ has been found to fall somewhere close to the average undrained shear strength profile in some

clays. It appears that at Halden the correlation provides estimates on the low side of both field vane, pressuremeter and CPTU results evaluated with $N_{kt} = 15 - 18$. This is explained by the fact that the horizontal stress index, K_D is about 2 in the silt layers, and this corresponds to an interpreted OCR of 1. As a result, between 5 m and 13 m the undrained shear strength interpreted from DMT fall close to the normally consolidated line ($0.22\sigma'_{v0}$), also indicated on the plot. For Halden silt, $s_{u,DMT} = 0.45 \times \sigma'_{v0} \times (0.5K_D)^{1.25}$ would provide a better fit with the FVT data.

2.6.11 In situ strength – cone penetration testing

Undrained shear strength from the Halden CPTU data was estimated using $s_u = (q_t - \sigma_{v0})/N_{kt}$, with cone factors N_{kt} of 15 - 18 (see Figure 2.24a and Figure 2.24b). While the N_{kt} for assessment of shear strength from undrained triaxial tests in compression (s_{uC} interpreted at the maximum excess pore pressure, u_{max}) is about 15, the N_{kt} factor for field vane strength is closer to 18. These differences are attributed to the different mode of shear between the two test methods, strain rate differences, choice of failure criteria and possible partial drainage in the field vane tests. As will be discussed in more detail in Section 2.6.12, the triaxial test specimens exhibit dilative behavior during undrained shear and, unlike the field vane results, do not exhibit a unique (peak) undrained shear strength. The derived $N_{kt} = 15$ for triaxial tests is fairly consistent with the $B_q - N_{kt}$ relationship suggested by Lunne et al. (1997) for several Norwegian clays, although the Halden N_{kt} values are somewhat on the low side of what could be expected from a soil with such low B_q values (typically, $B_q = 0.1 - 0.25$) (Carroll and Paniagua López 2018). But again, this is based on the reference CAUC s_{uC} taken at u_{max} which is the lowest

derived value of s_u as discussed further in Section 2.6.12. Norwegian silts from the Brage offshore oil field (6% – 15% clay size particles, $I_p = 8\% - 9\%$) and an onshore site in Stjørdal (0% – 24% clay size particles) show N_{kt} values ranging from 15 to 30, according to Senneset et al. (1988). However, they point out that for soils with $B_q < 0.4$ a correlation between s_u and CPTU testing may be inappropriate due to partial drainage during penetration. Further, N_{kt} factors of 18 and 11 have been suggested for two Irish silts (5% – 6% clay size particles, $I_p = 3\% - 17\%$) (Long 2007), and the Norwegian Os silt (3% - 12% clay size particles, $I_p = 12\%$) (Long et al. 2010), respectively. In sum, when calibrated in reference to CAUC test results that exhibit dilative behavior, the resulting N_{kt} values depend significantly on what criterion is used to select s_{uC} as discussed below.

2.6.12 Undrained strength from laboratory testing

Index undrained shear strength by means of the fall cone tests (FC) were conducted in general accordance with the Norwegian standard (NS 1988), using a 100 g fall cone and in some cases a 400 g cone with both having a 30° cone angle. Results from a selected number of tests on block samples are presented in Figure 2.24c. Results from other boreholes are not presented to reduce factors related to; (i) variation in sampling technique, e.g. (Long et al. 2010; Carroll and Long 2017) while factors relating to (ii) fall cone operator dependency, (iii) scale effects, and (iv) local pockets of silt, sand or clay are other possible effects on the results. Three of the four shallow fall cone results in Figure 2.24c were obtained using a 400g cone and all four tests yield strengths significantly higher than the triaxial (CAUC) test results determined at the u_{max} criterion, discussed below.

Anisotropically consolidated undrained triaxial tests (CAUC) and direct simple shear (DSS) tests were performed to investigate the behavior of the Halden silt under static undrained loading. Triaxial test specimens were trimmed from block samples, consolidated to the best estimate in situ stress conditions ($\sigma'_{vc} = \sigma'_{v0}$, $\sigma'_{hc} = \sigma'_{h0}$, with an assumed $K_0 = 0.5$; Section 2.6.3). Specimens were sheared at a nominal axial strain rate of 1.4 %/hour (Berre 1982). The DSS tests were conducted as constant volume tests in a Geonor DSS device using 35 cm² specimen area and wire reinforced membranes. Specimens were loaded directly to the best estimate in situ vertical effective stress ($\sigma'_{vc} = \sigma'_{v0}$) and sheared at a nominal shear strain rate of 5 %/hour (Bjerrum and Landva 1966). The three selected triaxial test results in Figure 2.25a to Figure 2.25c show that, except for an initial contraction, the specimens show a strong tendency towards dilative behavior (i.e. strain hardening) upon shearing. Due to this behavior the interpretation of the undrained shear strength is complex and test results provide no unique (peak) undrained shear strength. The undrained shear strength from CAUC and DSS tests, depicted with an interpretation of CPTU HALC12 using $N_{kt} = 15$ and 18 in Figure 2.26a to Figure 2.26c, are determined using three different strength criteria (Brandon et al. 2006);

- (a) $s_u = q_f$ at the maximum pore pressure, u_{max} ,
- (b) $s_u = q_f$ at the point of which the pore pressure parameter $A = (\Delta u - \Delta \sigma_3)/(\Delta \sigma_1 - \Delta \sigma_3) = 0$, i.e., equal to the drained shear strength for a CADC loading stress path,
- (c) $s_u = q_f$ at a limiting strain, γ_{lim} (an axial strain $\epsilon_f = 5\%$, or $\gamma_f = 7.5\%$ in triaxial tests and at a shear strain $\gamma_{h,f} = 5\%$ in DSS).

Criterion (a) provides the lowest estimate undrained shear strength as the shear stress at this point is below the failure envelope and has not been fully mobilized, but together with criterion (b) is the most consistent interpretation procedure. While criterion (a) plots between the $s_{uC} = 0.3$ to $0.5\sigma'_{v0}$ lines, criteria (b) and (c) provide undrained shear strengths that plot much higher, and more scattered in the case of criterion (c). Two CAUC results from criterion (c) plot outside the scale in Figure 2.26c and are indicated in the figure ($s_{uC} = 131$ kPa and 177 kPa).

Typical DSS strength anisotropy ratios, $(s_{uD}/\sigma'_{v0}) / (s_{uC}/\sigma'_{v0})$ assessed at u_{max} , range from $0.70 - 0.78$, with an average value of 0.74 .

2.6.13 Remolded undrained shear strength and sensitivity

Remolded undrained shear strengths were determined from laboratory fall cone tests on block samples and field vane tests (Figure 2.27a). The remolded FVTs were conducted after 10 full revolutions of the vane and show that the remolded undrained shear strength is generally around 8 kPa. Fall cone results are somewhat more scattered, particularly in Unit II. Compared to the sleeve friction from two typical CPTU locations (HALC11 and HALC19) the field vane results agree very well. However, as discussed in Section 2.6.1.2 there is some variability in the measured sleeve friction between the different cones tested at the site. It should be noted that in Unit II and III the cone sleeve in location HALC12 recorded friction values twice the values recorded in HALC11 and HALC19.

Generally, soil sensitivity measurements from fall cone and field vane tests range between 2 and 7 (Figure 2.27b). The FVT results are somewhat more consistent with

depth than the fall cone, and typically decrease from about $S_t = 7$ at 5 m depth to about $S_t = 5$ at 15 m. The sensitivity of the clay unit below 16 m depth plots around $S_t = 3$. Some studies have suggested that the field vane data should be used with caution as measured strength, particularly remolded values, may be high (Long et al. 2010). Furthermore, remolding can change the coefficient of consolidation of the soil and thus potential partial drainage effects may differ between the intact and remolded tests.

2.6.14 Effective stress strength parameters

All soils are characterized by an effective stress friction envelope. This envelope is fundamental and referred to as the effective stress friction angle (ϕ' , ϕ'_{mo}), ideally obtained from drained triaxial tests in compression (CADC) but may also be assessed from undrained tests. The effective cohesion intercept (c') is not fundamental, but depends upon the yield surface, stress conditions, strain rate etc. Effective stress strength parameters are required for long term stability analyses. Figure 2.25c demonstrates that Halden silt has a consistent effective stress friction angle, ϕ'_{mo} , at maximum obliquity of about 36° in CAUC tests on block sample specimens with $c' = 0$. This friction angle is similar to results from drained tests. Friction angle values may also be assessed from CPTU data using e.g.:

- (i) The relationship between normalized cone resistance, Q_t and friction angle for uncemented, unaged, moderately compressible, predominately quartz sands (Robertson and Campanella 1983). The database was later corrected for calibration chamber boundary effects (Kulhawy and Mayne 1990), and an alternative relationship presented as:

$$\varphi' = 17.7^\circ + 11.0^\circ \times \log \left[\left(\frac{q_t / \sigma_{atm}}{\sigma'_{v0} / \sigma_{atm}} \right)^{0.5} \right] \quad (2.2)$$

- (ii) The NTH (now NTNU – Norwegian University of Science and Technology) limit plasticity approach (Janbu and Senneset 1974; Senneset et al. 1989), providing a relationship between normalized cone resistance number, N_m , the pore pressure ratio, B_q , and effective stress friction angle. For the simplified case, where the angle of plastification, β , and c' is taken as zero, an approximate expression for $B_q > 0.1$ becomes (Mayne 2007):

$$\varphi' = 29.5^\circ \times B_q^{0.121} \times (0.256 + 0.336 \cdot B_q + \log Q_t) \quad (2.3)$$

The two CPTU approaches are plotted with the laboratory data and DMT results in Figure 2.28. The DMT and CPTU correlations provide values that are significantly lower than the undrained triaxial test results. The DMT correlation of horizontal stress index, K_D to a friction angle, $\phi'_{safe,DMT}$ provides a lower bound estimate according to Marchetti et al. (2006); in this case the value is typically in the range of 22° and 25°. The CPTU and DMT interpretations seem inappropriate, and the laboratory data is considered more reliable as they are broadly consistent with data reported by other researchers. $\phi' = 37^\circ - 40^\circ$ are reported for Swedish silts (Börgesson 1981; Høeg et al. 2000), 32°-35° for Norwegian silts (Sandven 2003; Long et al. 2010), 28° - 39° for the American Mississippi Valley silt (Brandon et al. 2006), and $\phi' = 40^\circ$ and greater for Irish silts (Long 2007; Carroll and Long 2017).

2.6.15 Sample quality

An evaluation of sample quality should always be made while interpreting data from advanced geotechnical laboratory tests. Poor quality testing and sampling can adversely affect the interpreted engineering soil parameters, leading to poor geotechnical project performance and over or unsafe design. Methods developed to assess the quality of clay samples have existed for more than two decades, but there is still no established framework to quantify the degree of sampling disturbance in silts. The two conventional sample quality assessment frameworks using vertical strain, ε_{v0} (Terzaghi et al. 1996) and the normalized change in void ratio, $\Delta e/e_0$ (Lunne et al. 1997) (where Δe is the change in void ratio upon reloading back to the in situ vertical effective stress, and e_0 is the initial void ratio.), with both evaluated during laboratory recompression to the estimated in situ effective stresses, must be treated with caution in silts for two reasons:

- (i) they were developed for clays, and in particular, the $\Delta e/e_0$ method for normally consolidated to medium overconsolidated marine clays. These frameworks may therefore not be valid for silts. In particular the $\Delta e/e_0$ criteria were developed based on results from laboratory tests performed on marine clays collected from depths below the seafloor of 0 m to 25 m and range in properties of 6% to 43% for plasticity index, 20% to 67% for water content, and 1 to 4 for OCR (Lunne et al. 1997).
- (ii) loose silts may, if sheared drained or partially drained during tube sampling, densify and exhibit an artificially low change in void ratio upon recompression to in situ stresses (Hight and Leroueil 2003; Sandven 2003;

Carroll and Long 2017). As such, certain samples may appear of high quality when they have in fact been significantly altered.

$\Delta e/e_0$ values for the CRS/IL oedometer, DSS and CAUC triaxial test on specimens from block samples collected at the Halden are presented in Figure 2.29a to Figure 2.29c. Essentially all values fall within the "very good to excellent" (1), or "good to fair" (2) categories. As described in Table 2-1 soil sampling using several other techniques (Geonor 54 mm fixed piston composite sampler, 72 mm fixed piston sampler and Gel-Push sampler) have been conducted at the site and interpretation of the results from these are in progress and will be reported in a subsequent paper.

2.7 Engineering problems

A discrepancy between in situ and laboratory results, and the lack of established correlations to important engineering parameters, are a few examples of the challenges faced during investigations of silts. While silts and other intermediate soils can complicate the design and construction phases of infrastructure projects both onshore and offshore, like in the North Sea (Senneset et al. 1988; Solhjell et al. 2017), they lead to severe building damage during the 1999 Kocaeli earthquake in Turkey (Bray et al. 2004). Knowledge of soil behavior and engineering properties in these materials is paramount, and research sites like Halden will assist the geotechnical profession to advance the state of the art. Some practical engineering problems related to soil sampling, in situ and laboratory testing at the Halden silt site are discussed below, including a slope failure case history from the neighboring wastewater treatment facility.

2.7.1 Soil sampling

Six sampling boreholes were drilled at the Halden site and sixty five samples collected. While the two Geonor fixed piston samplers collected 54 mm and 72 mm samples down to 16.5 m depth without any reported issues, the gel-push sampler equipment needed certain modifications to ensure compatibility with the NGI drill rig. When the appropriate modifications were made gel-push samples were successfully collected down to 13.4 m depth. After sampling the tube was left in the ground for several minutes to improve equalization of pore water pressure and reduce possible effects such as loss of part of the sample on retrieval from the base of the borehole. Full recovery was achieved in most cases during tube sampling. Some authors (Hight and Leroueil 2003; Sandven 2003; Long 2007; Long et al. 2010) report that conventional tube sampling in intermediate silty soils tend to compress or dilate the soil depending on the initial void ratio and prevailing drainage conditions upon shear. Dense silts may dilate upon tube sampling with a resulting increase in void ratio while looser silts may compress during sampling (decrease in the sample void ratio). At Halden, a study of the effects of sampler type on engineering parameters and laboratory behavior of silt is ongoing, but visual inspection of a number of samples revealed no obvious bending of soil strata or laminations in the peripheral zone near the tube sampler wall. This may also be due to the fact that the Halden silt shows little to no primary bedding and laminations due to bioturbation. Although limited research has been published on experience with block samples of silt some studies report hand carved blocks (Bradshaw and Baxter 2007; Sau et al. 2014; Arroyo et al. 2015; Carroll and Long 2017). Sherbrooke block sampling has been conducted at Refneveien in Halden earlier (Carroll and Long 2017), this site is

approximately 500 m distance and 15 m lower in elevation from the Halden research site at Rødsparken described in this paper. Block sampling was successfully conducted at the Halden research site down to 15.2 m depth (see Figure 2.30a). On occasion, however, one or more of the spring-mounted blades were prevented from releasing by silt particles jamming the knives. As a result, the base of the block could not be properly separated from the bottom of the borehole and multiple attempts lead to disturbance of a few of the blocks. A second issue occurred as the blades retracted; in a few cases the friction between the knives and the silt at the base of the block would cause a wedge of soil to detach from the sample (Figure 2.30b). Similar issues were encountered at Skibbereen in Ireland during tube sampling as a result of fines collection behind the piston head during sampling (Carroll and Long 2017).

The lack of a reliable sample quality assessment framework for silts hinders determining which sampler could consistently provide a superior quality sample and hence better quality advanced laboratory test specimens. In the last few decades large diameter samples, e.g. Sherbrooke blocks (Lefebvre and Poulin 1979) and Laval samples (LaRochelle et al. 1981), have generally been considered superior to tube samples in clay. For silts further research on the efficacy of sampler type and sample sizes is needed.

2.7.2 Stress history

As demonstrated by the data presented herein, conducting oedometer tests on Halden silt specimens to assess stress history (σ'_p and OCR) serve limited purpose as the soil in this study was strain hardening immediately upon 1D loading in the CRS or IL cell. Thus determining if any preloading event occurred at the site was solely based on

the geological background of the site, which in this case is well understood and documented. While a classical Casagrande interpretation of yield stress from Halden oedometer test specimens results in an apparent overconsolidation ratio in the range of 2 to 5, it has been concluded herein that the true OCR is closer to 1, and except for some potential desiccation in the uppermost part of the soil profile, only aging and fluctuating ground water levels will have caused a yield stress slightly higher than the in situ vertical effective stress. Furthermore, classical CPTU correlations using factors established and validated for clays are inappropriate, misleading and in conflict with the depositional history of the site. For other silt sites, with limited knowledge of the geological background and no clay layers to assess, normally consolidated silts could be misinterpreted as overconsolidated if clay-based interpretation strategies are applied. Until more data on other silts worldwide are published, experiences from test sites such as Halden or Malamocco (Cola and Simonini 2002) may provide valuable information.

2.7.3 Partial drainage

Assessment of the prevailing drainage conditions in silts and other intermediate soils are particularly challenging. While for a certain foundation geometry and loading regime the soil response may be undrained, other combinations may act under partially-drained or fully drained conditions. This is also the case for in situ tests; depending on the rate of penetration, pore pressure dissipation may occur during testing. The influence of penetration rate and soil drainage properties (specifically the coefficient of consolidation) on the consolidation conditions in these soils are typically of great importance in design and can be captured by the normalized penetration velocity, $V = v \times d/c_h$, where v is the

cone penetration rate, d is the penetrometer diameter and c_h is the horizontal coefficient of consolidation. Fully undrained penetration typically occurs when V is larger than about 30 to 100 and if less is typically associated with partially drained penetration. Fully drained penetration occurs when V is less than about 0.03 (DeJong and Randolph 2012). A CPTU penetration rate study conducted at Halden (Carroll and Paniagua López 2018) demonstrated a clear increase in V with increased penetration rate as expected. While a reduced CPTU penetration rate (2 mm/s) resulted in V values in the region of 14–27, the conventional penetration rate of 20 mm/s yielded V values typically in the range of 95–273 in silt Units II and III. As such, undrained conditions are likely to prevail during standard cone penetration rate. It should be noted, however, that the suggested transition from undrained to partially drained conditions based on V or B_q at Halden are not in agreement. Excess pore pressures generated behind the cones in Halden are low ($B_q = 0.1 - 0.24$; Figure 2.14) and other researchers (Senne set et al. 1989) have suggested that partially drained conditions prevail when $B_q < 0.4$. Further investigation of this topic is required for validation. As noted in Sections 2.6.3 and 2.6.9 the self-boring pressuremeter test, but also the dilatometer test, are rather slow in situ techniques compared to the CPTU. Thus, drainage or partial drainage could become a major factor and introduces uncertainty in the engineering parameters (e.g. K_0 and s_u) interpreted from these tests.

2.7.4 Case history: Remmen wastewater treatment facility

Slopes on silts are typically susceptible to landslides and local liquefaction under certain unfavorable conditions. Saturation may be high even above the free ground water

table and the soils are quickly fully saturated if the water table increases (Sandven 2003). This typically occurs during or after periods with significant rainfall or during spring when snow is melting. The ground water table rises and quickly saturates the overlying soils and breaks the matrix suction. This consequently reduces the effective stresses and strength of the soils. However, on slopes where negative pore pressures (suction) dominate, failures may not necessarily occur very often. Evaluations of the stability of these slopes, typically using overly conservative values of soil strength and in situ pore pressure, may underestimate the factor of safety against failure. Between 2009 and 2012 the Swedish Geotechnical Institute, SGI, performed monitoring of negative pore pressures on two silt slopes in Sweden (Westerberg et al. 2014; Vesterberg et al. 2017). The stability analyses of one of these slopes showed that by including suction in the calculations, the factor of safety increased by 5% - 13%.

In the evening December 14th, 2011 a local landslide was triggered up-slope from the Remmen wastewater treatment facility (RWTF), immediately west of the Halden research site (see Figure 31). For safety of the neighboring residents, the nearby properties (No. 8 and 10) were immediately evacuated. A broken water supply pipeline combined with a period of significant rainfall may have caused instabilities in the slope.

The topography slopes from an elevation of about 28 m above sea level at the crown of the slope to about 6 m at the toe (Figure 32). The width and depth of the slide was about 30 m and 3-4 m, respectively. The debris, estimated to a volume somewhere in the range of 1000-2000 m³ stopped just short of the treatment facility, about 80 m from the main scarp. NGI subsequently carried out the following soil investigation; 8 Norwegian total soundings, 3 CPTUs, installation of two piezometers and one sampling

borehole on the slide crown using the Geonor 54 mm piston sampler. The field and laboratory testing revealed a clayey silt down to about 8 m depth, and 2 meters of silty clay over bedrock. Light detection and ranging (LiDAR) data from the site is also available from both pre- and post-failure. The elevation contours in Figure 2.33 shows that the debris have reached the access road and if only marginally greater, the landslide might have hit the exterior of the wastewater treatment facility and caused harm to infrastructure and people.

Effective stress slope stability calculations to assess the site conditions prior to failure were performed using the computer program BEAST (Clausen 2003) with 30 slices. In these analyses the silt was considered a granular material using an effective stress friction angle. For a circular failure surface similar to the one observed in the field, and by applying $\phi' = 34^\circ$ ($c' = 0$ kPa) and $\phi' = 26^\circ$ ($c' = 5$ kPa) in the top sand and underlying silt, respectively, a factor of safety (FS) equal to 1.0 was obtained. At failure (FS=1.0) the shear stresses (τ_{ff}) along the slip surface were generally in the range of 20 to 25 kPa.

Post-failure slope stability was still considered unacceptable and the probability of new slides considered high. To mitigate the risk of future hazards a dense grid of individual soilcrete columns were installed by means of deep soil mixing in the lower section of the slope. Deep soil mixing improves the strength characteristics by mechanically mixing the soil with a cementitious binder slurry, and as such the ground improvement stabilized the slope. Further, the soilcrete columns provided a foundation for the 1500-2000 m³ rock backfill now supporting the main scarp. The backfill is

resistant to erosion and acts as counterweight. The FS after these measures was calculated to about 2.0.

2.8 Summary and conclusions

Silts and similar intermediate soils represent a category of soils that are typically labelled challenging by geotechnical engineers. These soils can be difficult to sample, especially for very low plasticity to non-plastic silts, and there is no well-established framework to assess sample quality. Furthermore, little guidance is available on the selection of appropriate engineering properties for practical use. The Halden research site, located in Southeastern Norway, has been studied over a period of six years by combining the results of a number of geological, geophysical and geotechnical site investigation tools. The site emerged from the marine environment c. 5,000 years ago as a result of intense isostatic uplift and relative fall of sea-level. A silty, clayey sand constitutes the top soil and extends down to about 4.5 to 5 m depth. The clayey silt below is separated into two soil units based on the results of in situ and index tests, but is regarded as the same material with the same geologic origin and history. These extend down to about 15 - 16 m depth. Piezocone data reveals that the corrected cone resistance plots around 1 MPa, similar to that of the clay unit below, and excess pore pressures are generated behind the cones in the silt units. The pore pressure ratio is generally low, ranging between 0.1 - 0.3, and the soil behavior type index typically ranges between 2.6 and 2.95. The seismic cone results indicate a clear trend of increasing shear wave velocity with depth ranging from about 110 m/s at 2 m depth to 200 m/s at 16 m. Advanced CRS, CAUC and DSS laboratory testing revealed a number of challenges and limitations; (i)

Methods developed to assess the quality of clay samples may not necessarily apply to these soils and there is no established framework to quantify the degree of sample disturbance in silts. (ii) Interpretation of the stress history based on both oedometer test results and clay-based correlations to CPTU cone resistance are problematic and unreliable as they are in conflict the geological history in the area. Geology, and evidence of a normally consolidated stress state of the lower clay, suggests that also the silt is near normally consolidated. (iii) Undrained shear strengths, as interpreted from e.g. field vane tests, are consistent with the CPTU interpretations using $N_{kt} = 18$, but plot significantly lower than the results from undrained triaxial tests on block samples interpreted at large strain. The undrained triaxial tests exhibit a strong tendency for dilative behavior and provide no unique (peak) undrained shear strength. As a result, different strength criteria provide different results. Despite certain interpretation challenges the paper presents important reference data to assist in the interpretation and assessment of similar silts, and provide some guidance on important geotechnical properties for projects where limited design parameters are available.

2.9 Acknowledgments

The authors would like to thank The Research Council of Norway for their generous infrastructure grant to establish the five Norwegian GeoTest Sites for research (Grant No. 245650/F50). The field vane tests were conducted with support from the US National Science Foundation under Grant Nos. CMMI-1436793 and CMMI-1436617. The Norway-America Association (NORAM) have provided support to the first author to undertake certain research activities described herein. The authors would also like to

extend our gratitude to Halden Municipality, especially Egil Hult and Jan-Erik Hansen for providing access to the test site and supplying permanent water and electricity. Contributions from Pagani, Geomil Equipment, In Situ Site Investigation, Geological Survey of Norway and colleagues at NGI Field Investigations (Kristoffer Kåsin, Pål Kristian Karstensen, Rolf Ove Karlsen and Håvard Saur) and NGI Geosurveys (Helge Smebye and Sara Bazin) are also highly appreciated.

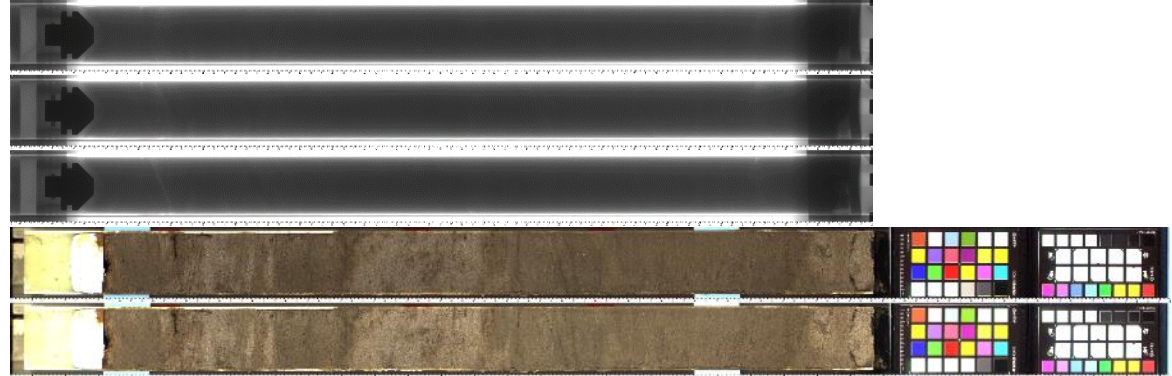
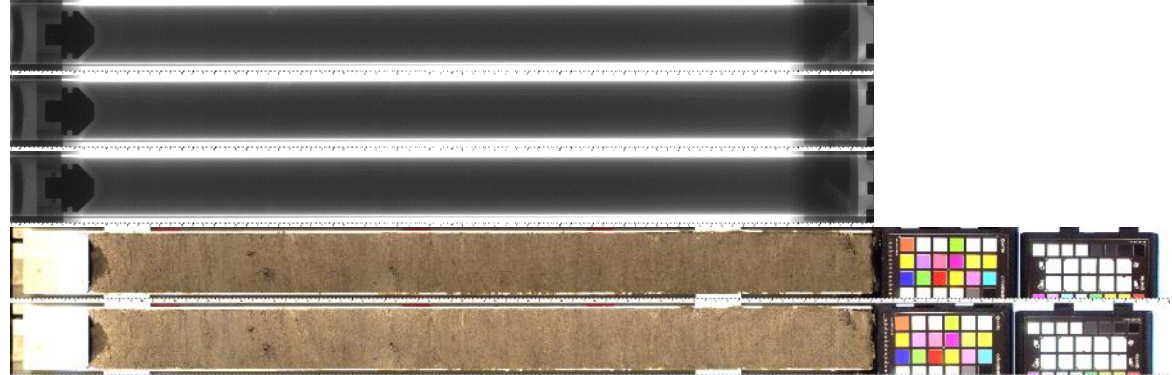
Table 2–1 Summary of geophysical, in situ and laboratory tests conducted at Halden research site, with general test procedure references and key parameters.

Test	Measured	Interpreted	Reference/Comment
<i>Geophysical / non-intrusive</i>			
Electrical resistivity tomography (ERT)	Resistivity	$z_{bedrock}$, soil type	
Multi-channel analysis of surface waves (MASW)	v_p, ω	v_s, G_{max}	
<i>In situ</i>			
Rotary pressure sounding (RPS)	F_{DT}	$z_{bedrock}$	Norwegian Geotechnical Society (1989)
Cone penetration test (CPTU, SCPT, RCPT)	$q_c, f_s, u_2, v_{vh}, \kappa$	$\sigma'_p, M, G_{max}, s_u, \phi', c_h$	ISO (2012)
Seismic flat dilatometer (SDMT)	$P_0, P_1, I_D, K_D, E_D, v_{vh}$	$s_{u,DMT}, K_0, \sigma'_p, \phi'$	ISO (2017)
Self-boring pressuremeter test (SBPT)	$P_0, P_f, P_L, \varepsilon_c$	$\sigma_h, K_0, s_{u,SBP}, G_{max}$	ISO (2012)
Pore pressure	u, t	u_0	Norwegian Geotechnical Society (2017), Piezometers
Field vane test (FVT)	Torque	$s_u, s_{u,rem}$	Norwegian Geotechnical Society (1989)
Ground temperature monitoring	T, t		Thermistor string
Hydraulic fracture test (HFT)	$\Delta V, P, t$		Bjerrum and Andersen (1972)
Screw plate load test (SPLT)	δ, q_{ult}		
<i>Sampling</i>			
Geonor (ϕ 72 mm) fixed piston			Norwegian Geotechnical Society (2013)
Geonor (ϕ 54 mm) fixed piston (composite)			Norwegian Geotechnical Society (2013)
Sherbrooke block (ϕ 250 mm)			Lefebvre and Poulin (1979); Norwegian Geotechnical Society (2013)
Mini-block (ϕ 150 mm)			Emdal et al. (2016)
Gel Push (ϕ 72 mm)			Tani and Kaneko (2006); Huang et al. (2008)

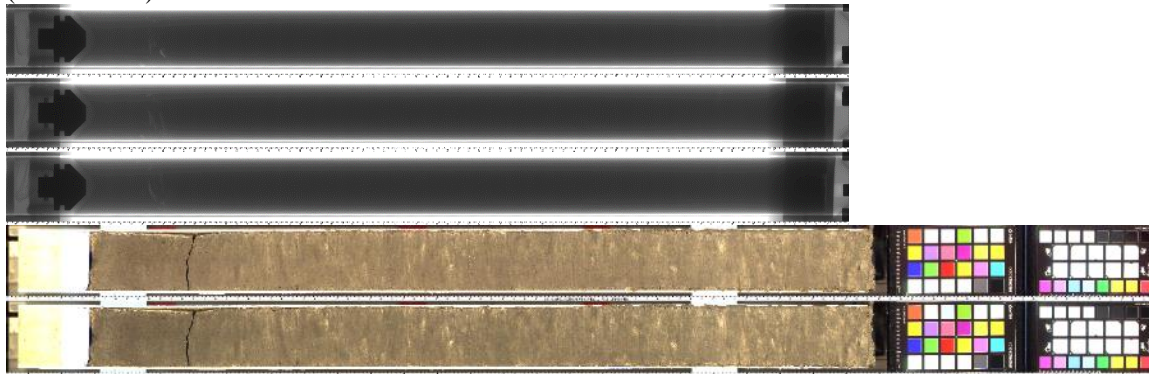
Laboratory

Water content	w	$\gamma_t (\rho_t)$	ISO (2014)
Unit weight (density)	$\gamma_d, \gamma_t (\rho_d, \rho_t)$		ISO (2014)
Unit weight of solid particles	$\gamma_s (\rho_s)$		ISO (2015)
Atterberg limits	w_L (LL), w_P (PL)	I_p (PI), I_L (LI)	ISO (2018)
Grain size distribution		% sand, silt, clay	Moum (1965); ISO (2016)
Fall cone test	Penetration	$s_u, s_{u,rem}$	NS (1988)
Carbon content	% TC, TOC		NGU in-house
Salinity	κ	gNaCl	ISO (1994)
X-ray diffraction (XRD)		% minerals	NGU in-house
X-ray inspection (XRI)			NGU in-house
Scanning Electron Microscopy (SEM)			
Multi sensor core logging (MSCL)	ρ_t , MS	n	NGU in-house
Split core imaging			NGU in-house
Incremental loading oedometer (IL)	$t, \sigma'_v, \varepsilon$	$\sigma'_p, c_c, c_v, c_\alpha, k_v$	ISO (2017)
Constant rate of strain oedometer (CRS)	$t, \sigma'_v, \varepsilon$	σ'_p, c_c, c_v, k_v	Sandbækken et al. (1986); NS (1993)
Hydraulic conductivity	k_h, k_v	r_k	Sandbækken et al. (1986); ISO (2004)
Electrical resistivity	Resistivity	κ	Wang et al. (2009)
Triaxial test: CAUC, CAUE, CK ₀ UC, CADC	ε, q, p, u	$c', \phi, s_{uC}, s_{uE}, E$	Berre (1982); ISO (2018)
Direct simple shear (DSS)	τ_h, σ'_v	s_{uD}, G	Bjerrum and Landva (1966); ASTM (2015)
Bender element test (BE)	V_{vh}	G_{max}	Dyvik and Madshus (1985)

Table 2–2 Summary of Halden stratigraphy, with X-ray images at 0°, 45° and 90° degree axial orientation, and split core images at 20 ms and 40 ms exposure time.

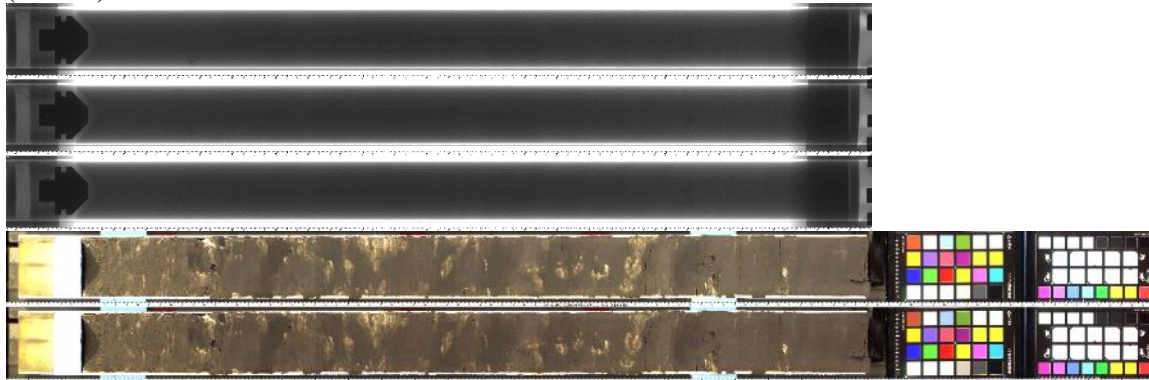
Depth range [m]	Soil description and imaging [-]	Comment [-]
0.0 - 4.5	<p data-bbox="357 487 1291 560">SAND, clayey, silty, fine, loose to medium dense, with organic material, brownish grey (Soil Unit I)</p> 	<p data-bbox="1543 682 1890 747">X-ray and split core imaging depth: 3.0 – 3.9 m</p>
4.5 – 12.1	<p data-bbox="357 966 1501 1039">SILT, sandy, clayey, low to medium strength, homogeneous, mottled, occ. shell fragments, brownish grey (Soil Unit II)</p> 	<p data-bbox="1543 966 1764 1031">¹⁴C age @ 6.4m: 6455 ± 25 years BP</p> <p data-bbox="1543 1193 1890 1258">X-ray and split core imaging depth: 4.8 – 5.6 m</p>

12.1 – 16.0 SILT, sandy, medium to high strength, homogeneous, highly bioturbated, mottled, occ. shell fragments, occ. black organic material, brownish grey
(Soil Unit III)



X-ray and split core imaging
depth: 12.0 – 12.8 m

16.0 – 21.3 CLAY, silty, low to medium strength, slightly laminated, occ. shell fragments, occ. drop stones
(Unit IV)



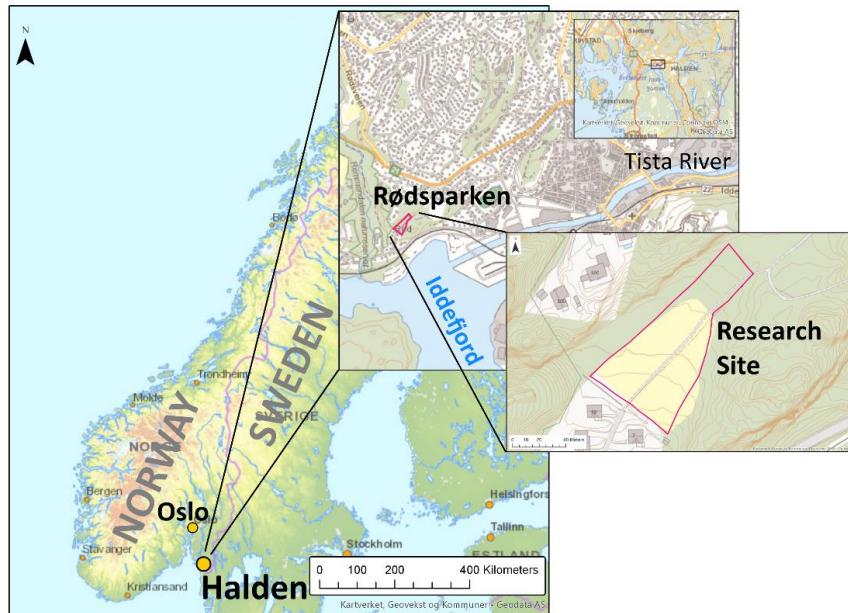
¹⁴C age @ 16.3m:
11820 ± 25 years BP

X-ray and split core imaging
depth: 15.6 – 16.4

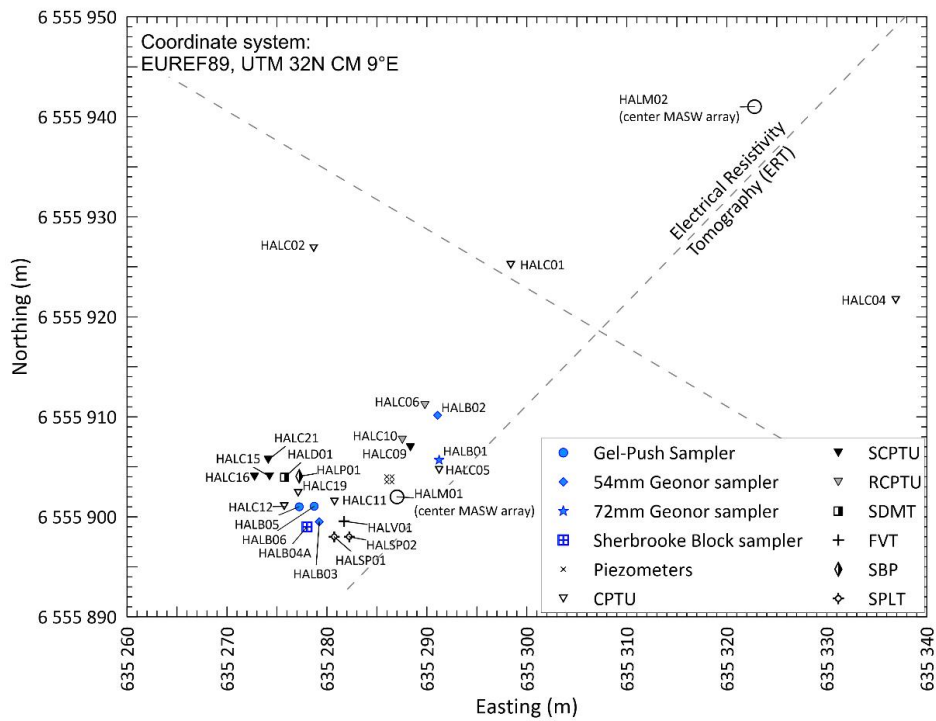
21.3 BEDROCK

Table 2–3 Results of X-ray diffraction analyses on 3 specimens from Halden research site.

Unit	Depth	Quartz	Potassium Feldspar	Plagioclase	Muscovite/Illite	Chlorite	Amphibole	Pyrite
-	m	%	%	%	%	%	%	%
II	6.2	41	12	30	8	3	6	trace
II	9.5	40	13	29	8	4	6	trace
III	13.5	44	12	30	7	2	5	trace



(a)



(b)

Figure 2.1 (a) Site location, and (b) site layout. Investigated locations include resistivity and geophysical investigation tools (ERT, MASW), ground water and temperature monitoring, soil sampling using various samplers and in situ testing (CPTU, SCPT, RCPTU, SDMT, FVT, SBP and SPLT).

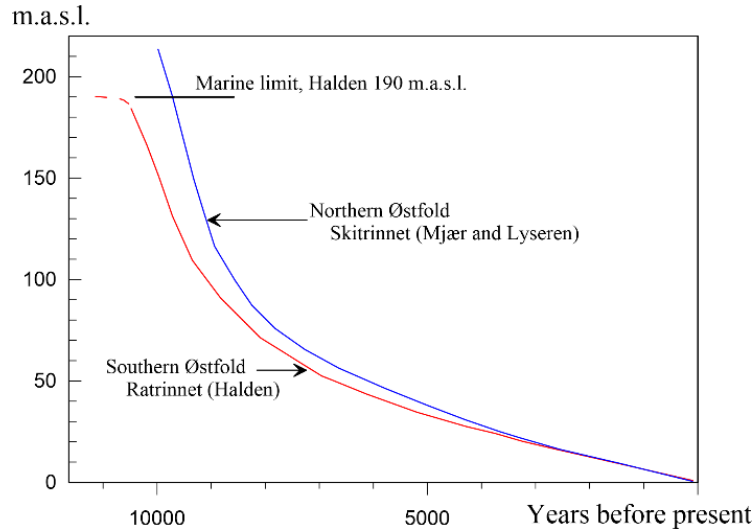


Figure 2.2 Shoreline reconstruction curves from Halden region (Northern and Southern Østfold), after Klemsdal (2002). The research site most likely emerged from the marine environment c. 5,000 years ago.



Figure 2.3 Quaternary map of the Halden area, Southeast Norway, with the research site circled in red. The colors reflect the geological processes and general properties of the deposits. Shades of blue indicate that the soils have been transported by and deposited in a marine environment. These deposits dominate the Halden area. Shades of green indicate soils that were deposited by the ice. Shades of yellow indicate fluvial deposits, and pink shows exposed bedrock. After Olsen and Sørensen (1993).

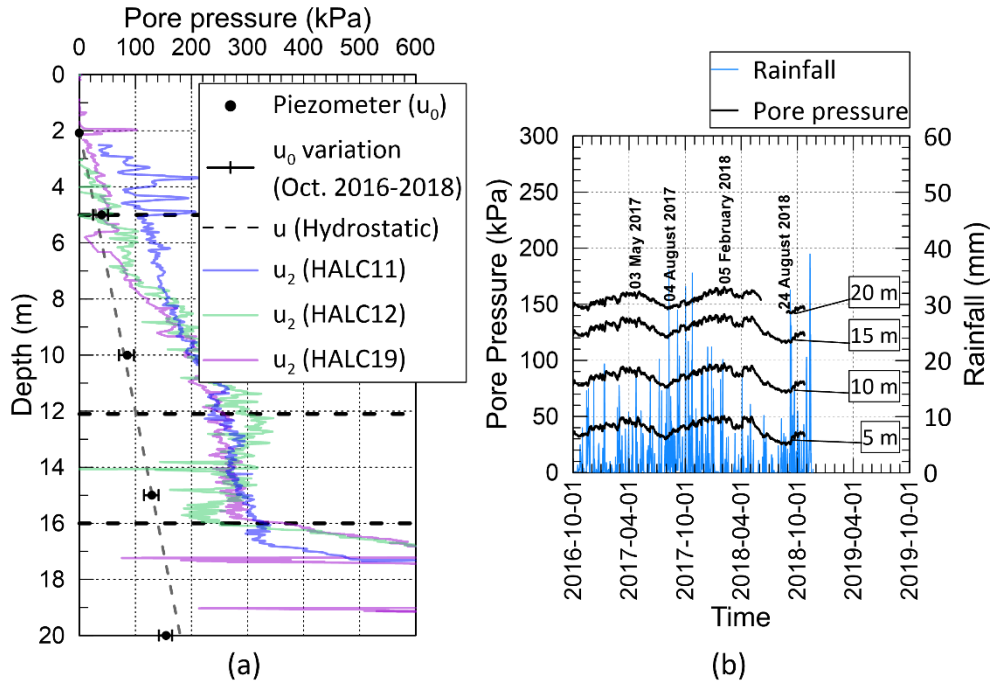


Figure 2.4 (a) Pore pressure from in-situ piezometers (locations HALP01-HALP04) and u_2 from CPTU (locations HALC11, HALC12 and HALC19). The dotted line indicates the theoretical hydrostatic pore pressure acting from 2 m depth. (b) In-situ pore pressure measured by four electric piezometers installed at 5 m, 10 m, 15 m and 20 m depth, and rainfall in the area, October 2016 to October 2018.

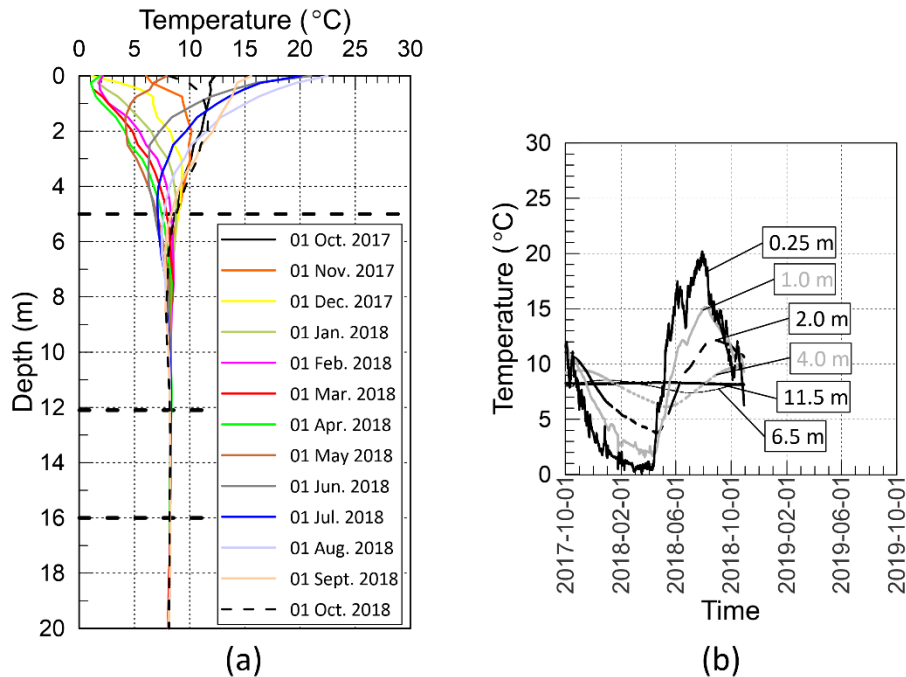


Figure 2.5 Thermistor string temperature log in location HALB05; (a) with depth at selected dates, and (b) with time since October 2017.

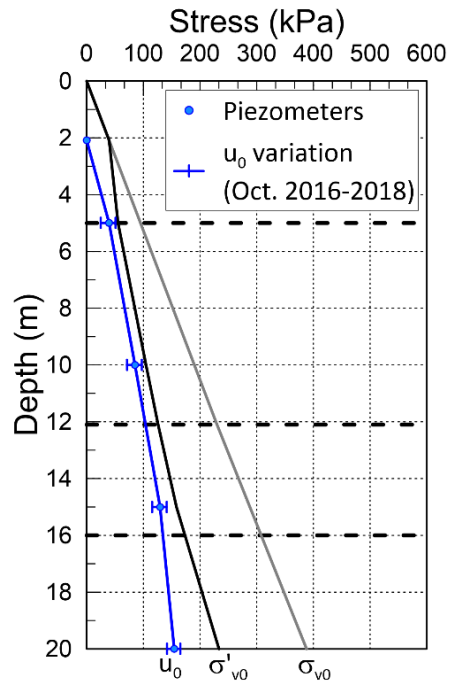


Figure 2.6 In-situ stress conditions (u_0 , σ_{v0} and σ'_{v0}).

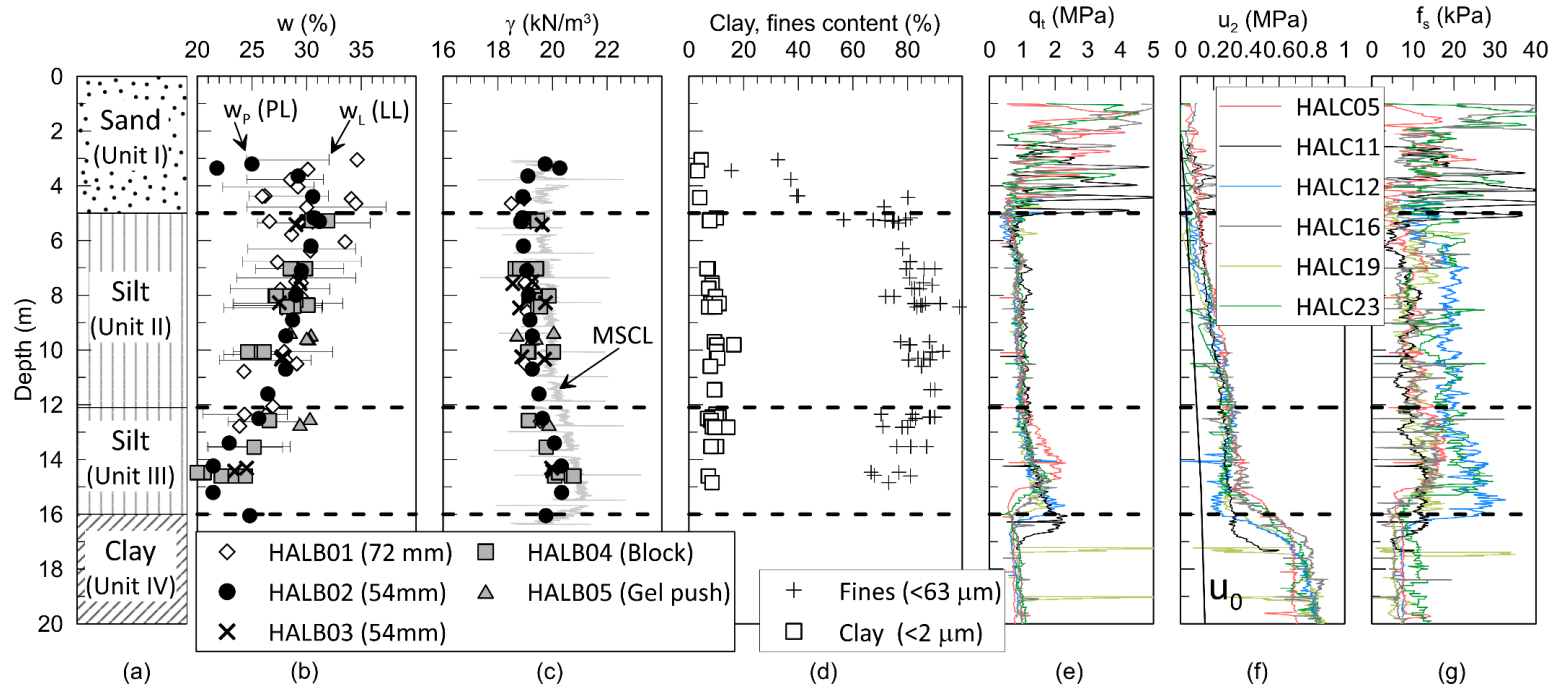


Figure 2.7 Classification and CPTU data; (a) Soil units, (b) natural water content and Atterberg limits, (c) total unit weight, (d) clay particle and fines content, (e) corrected cone resistance, q_t , (f) pore pressure, u_2 , and (g) sleeve friction, f_s .

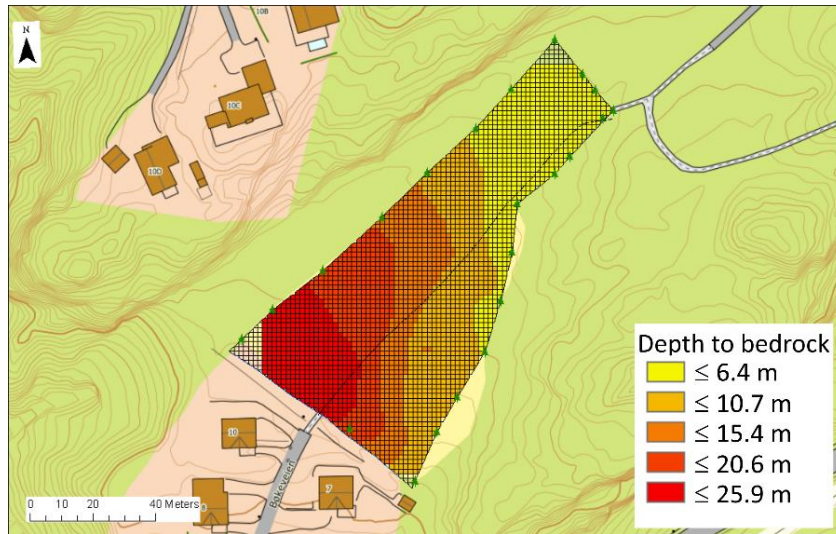


Figure 2.8 Approximate depth to bedrock across the research site.

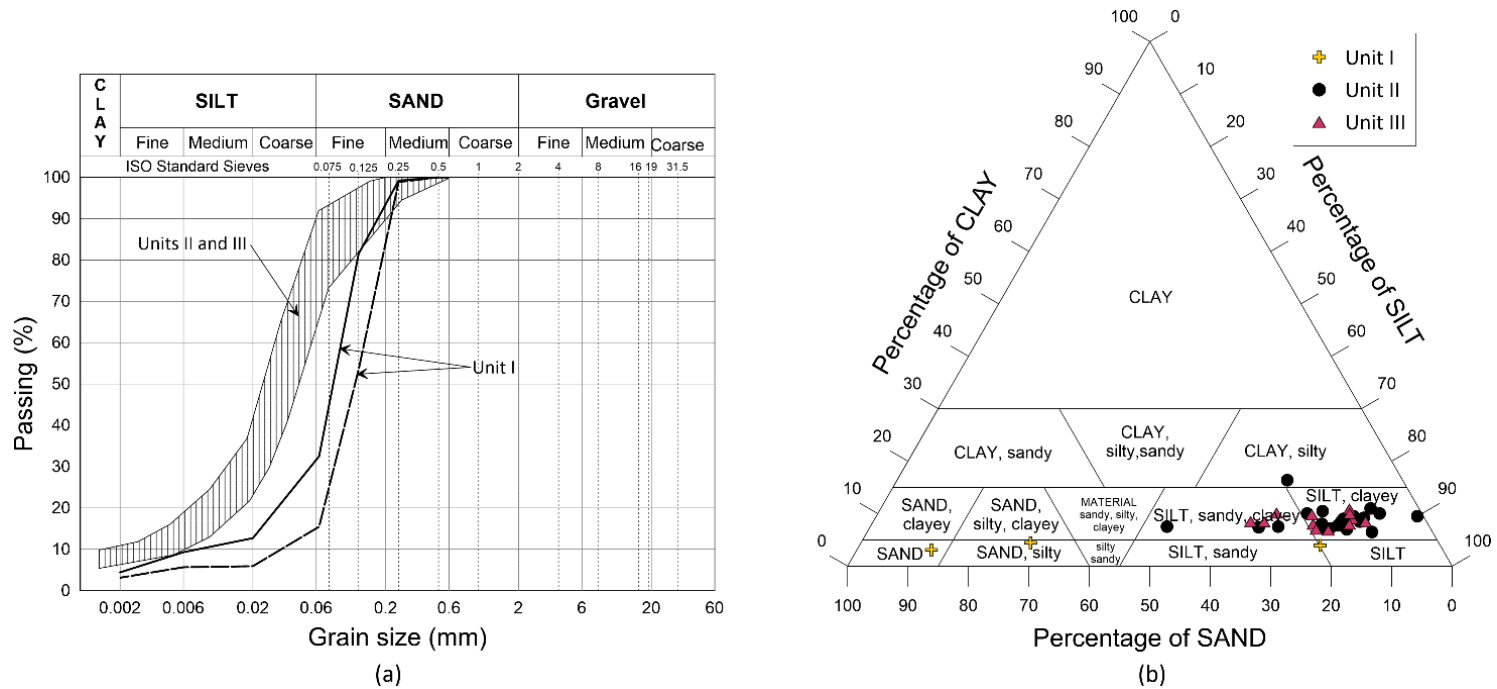


Figure 2.9 Classification data; (a) typical grain size distribution curves for Unit I, and Units II and III. (b) Soil classification triangle (Norwegian Geotechnical Society 2011), which suggests 14 soil classes based on the percentage of clay, silt and sand particles.

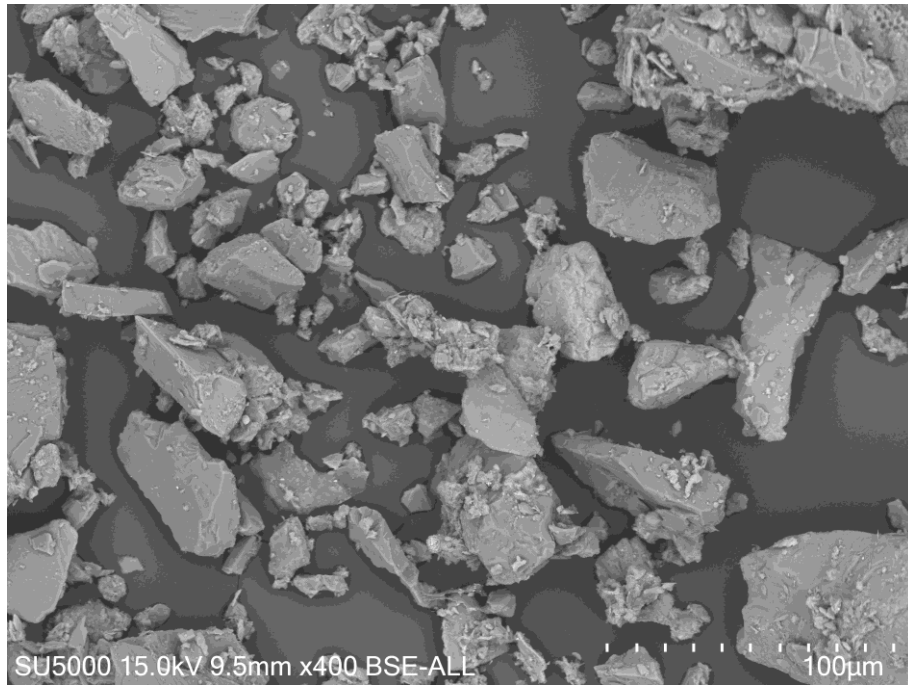


Figure 2.10 SEM from 6.4 m depth.

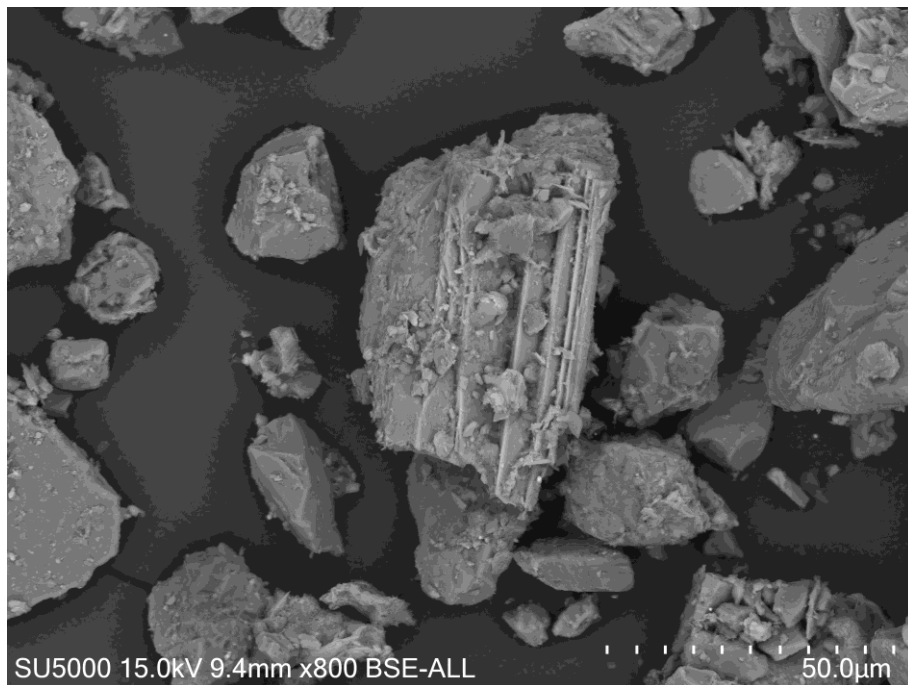


Figure 2.11 SEM from 8.6 m depth.

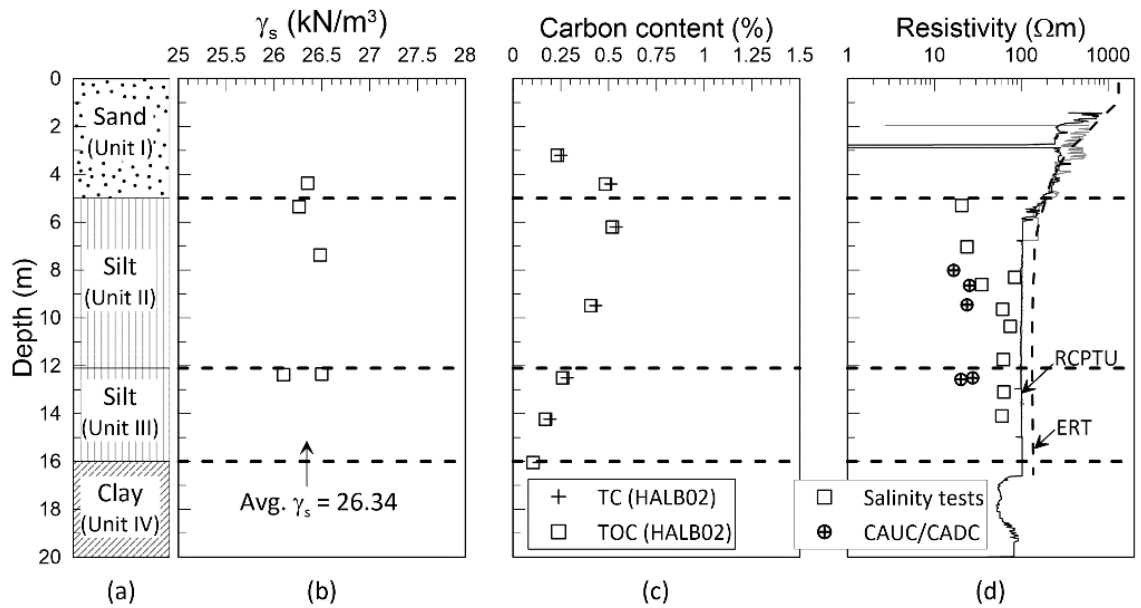


Figure 2.12 (a) Soil units, (b) unit weight of solid particles, (c) TC and TOC, and (d) resistivity from laboratory and field measurements.

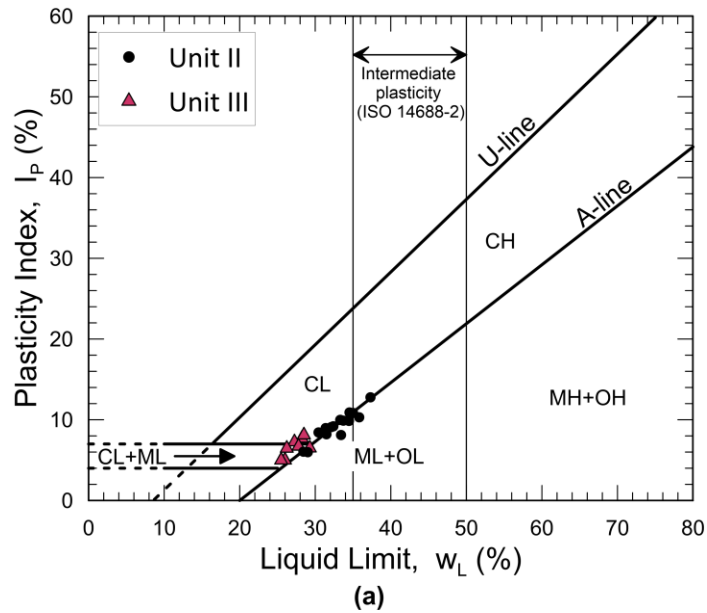


Figure 2.13 Casagrande plasticity chart with results of Atterberg limits on soil Unit II and III.

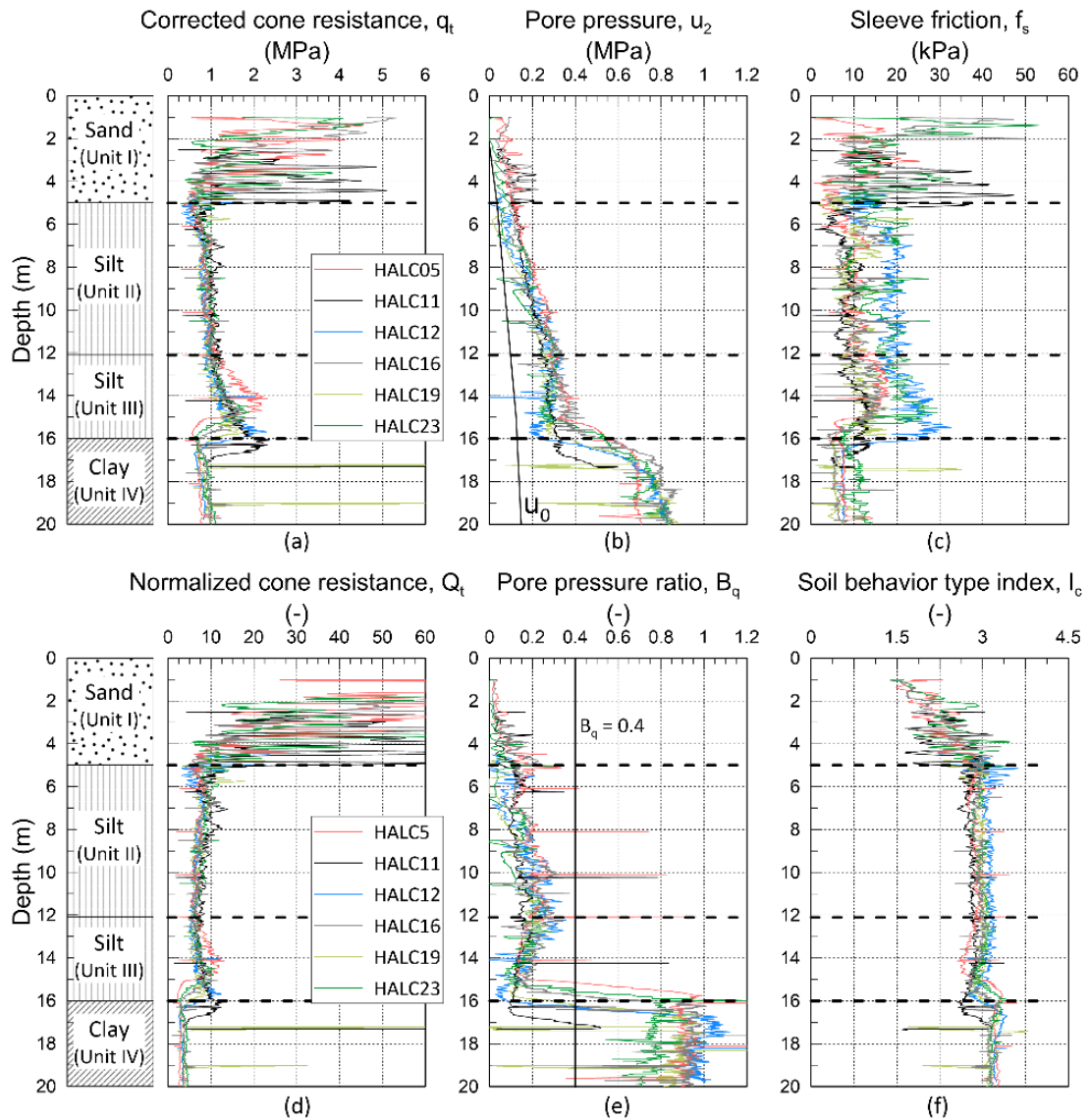


Figure 2.14 CPTU data from six locations; (a) cone resistance, q_c , (b) shoulder pore pressure, u_2 , (c) sleeve friction, f_s , and derived parameters (d) normalized cone resistance, Q_t , (e) pore pressure ratio, B_q , and (f) soil behavior type index, I_c .

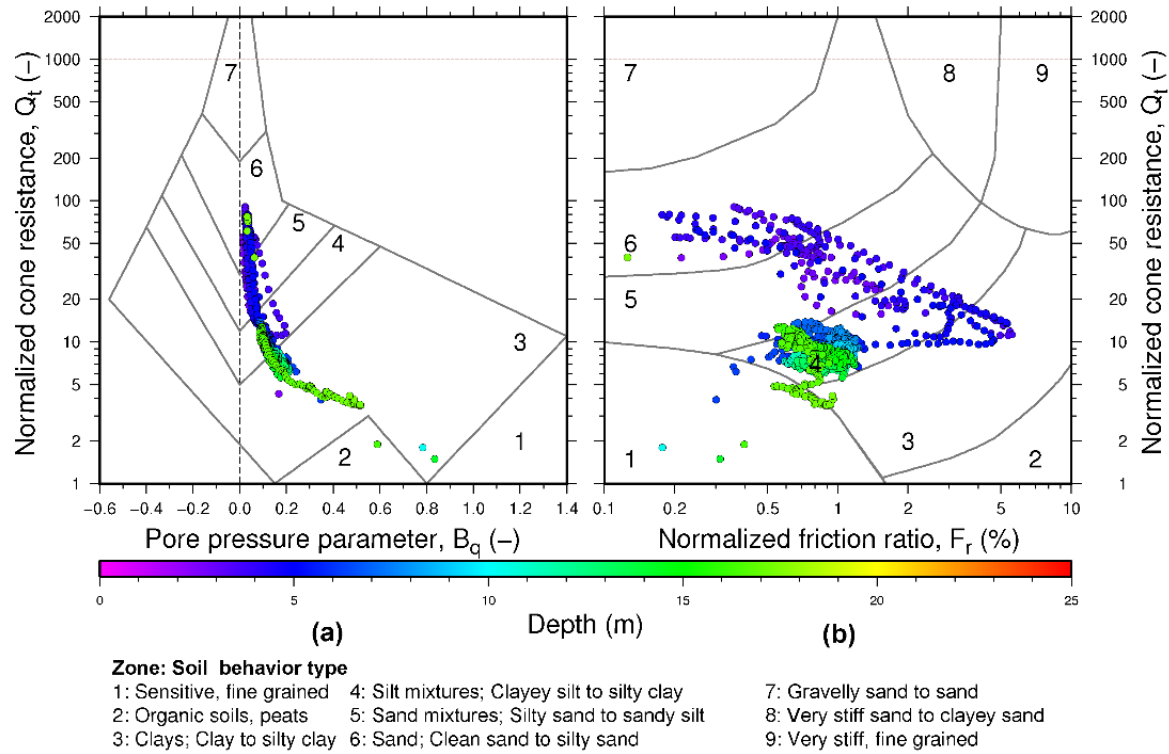


Figure 2.15 Soil behavior type charts (Robertson 1990) from location HALC11 by means of (a) normalized cone resistance, Q_t , versus pore pressure parameter, B_q , and (b) normalized cone resistance, Q_t , versus normalized friction ratio, F_r .

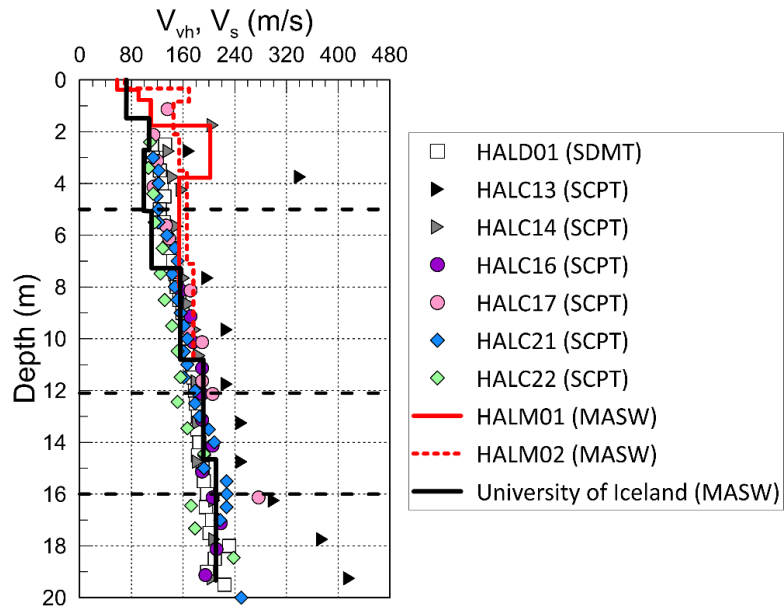


Figure 2.16 In-situ shear wave velocity (V_{vh} , V_s) from SCPT and SDMT, and Multichannel Analyses of Surface Waves (MASW).

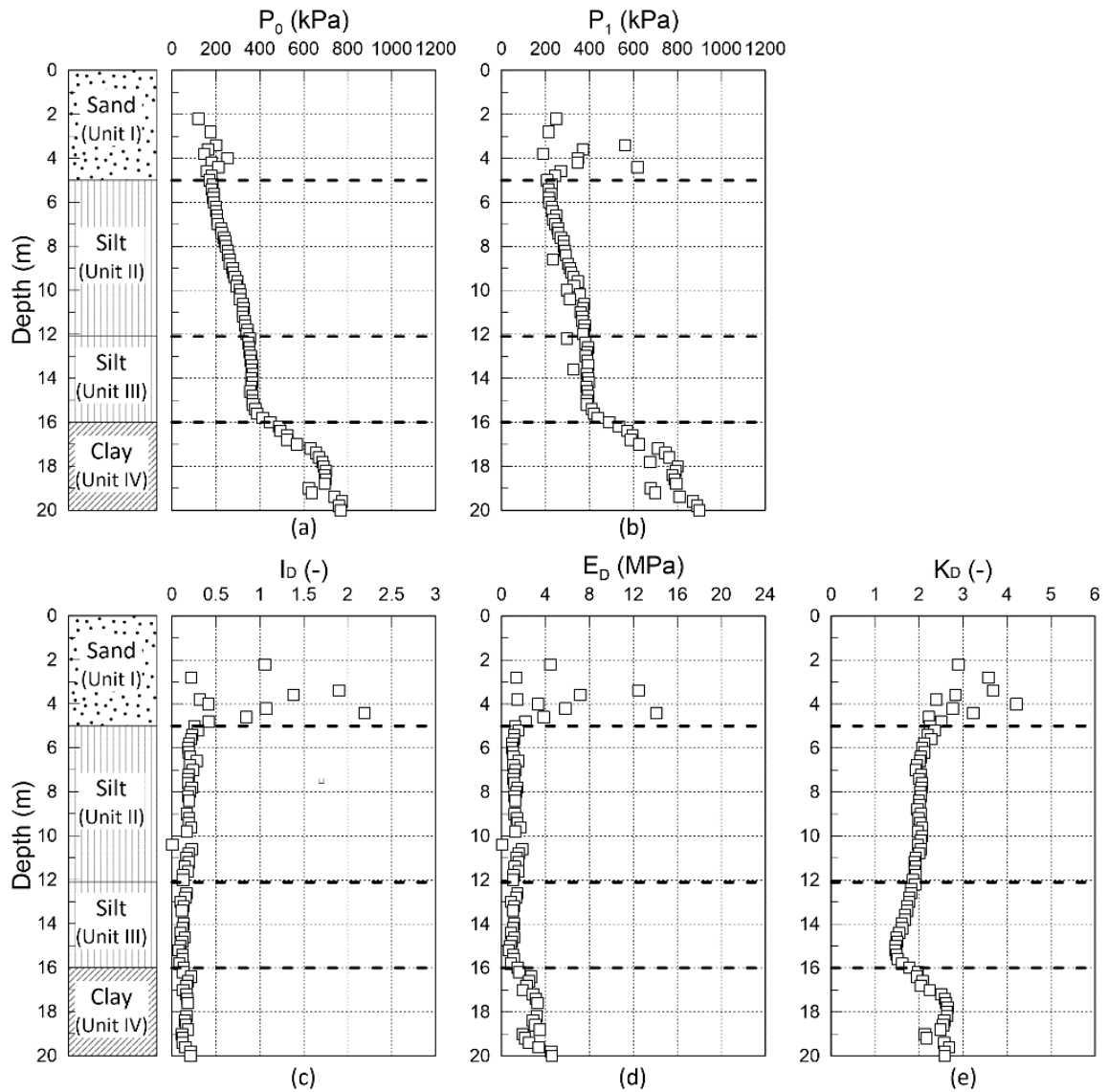


Figure 2.17 Results of DMT testing with (a) corrected first reading, (b) corrected second reading, and intermediate DMT parameters (c) material index, I_D , (d) horizontal stress index K_D , and (e) dilatometer modulus, E_D .

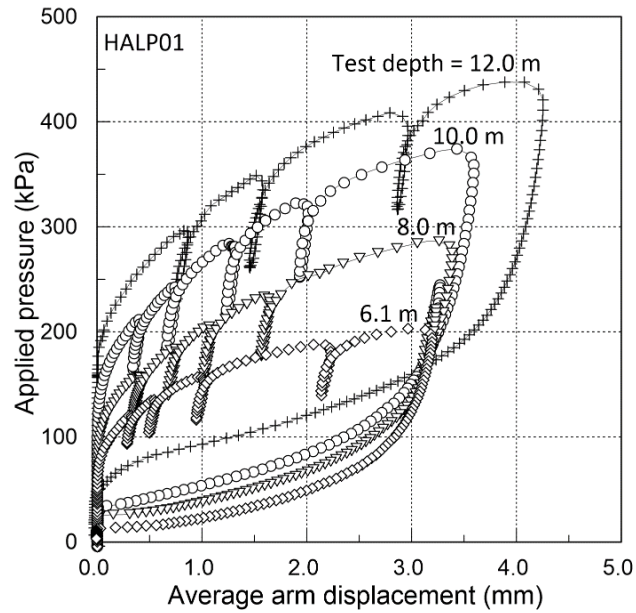


Figure 2.18 Typical self-boring pressure meter results. Interpretation of σ_{h0} and $s_{u,SBP}$ based on Marsland and Randolph (1977) methodology.

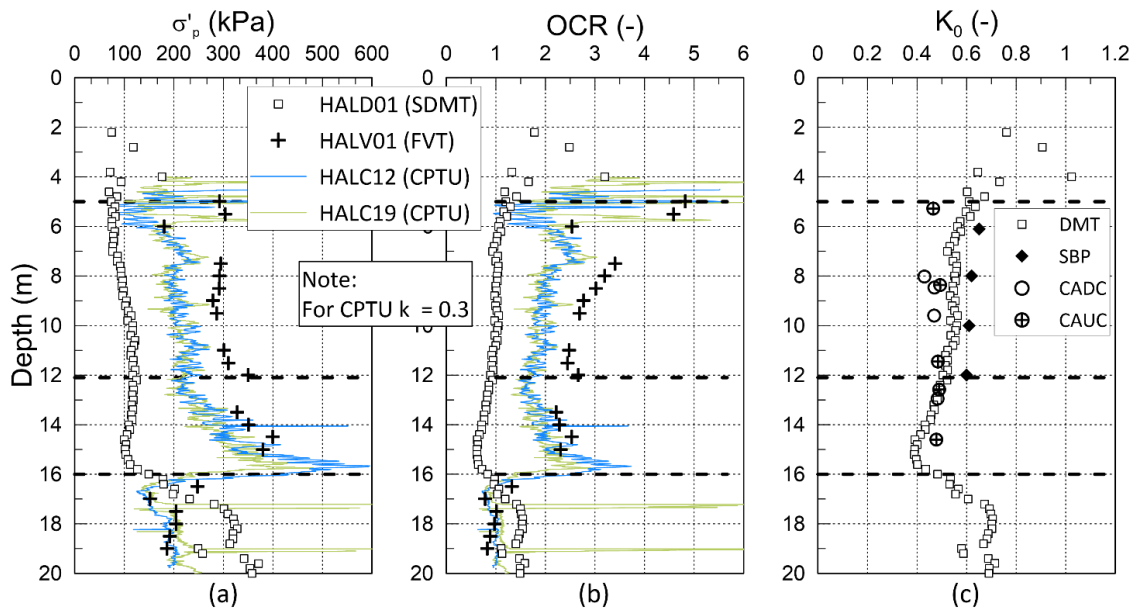


Figure 2.19 Stress history data from field and laboratory testing. (a) yield stress, σ'_p , (b) overconsolidation ratio, OCR, and (c) coefficient of earth pressure at rest, K_0 .

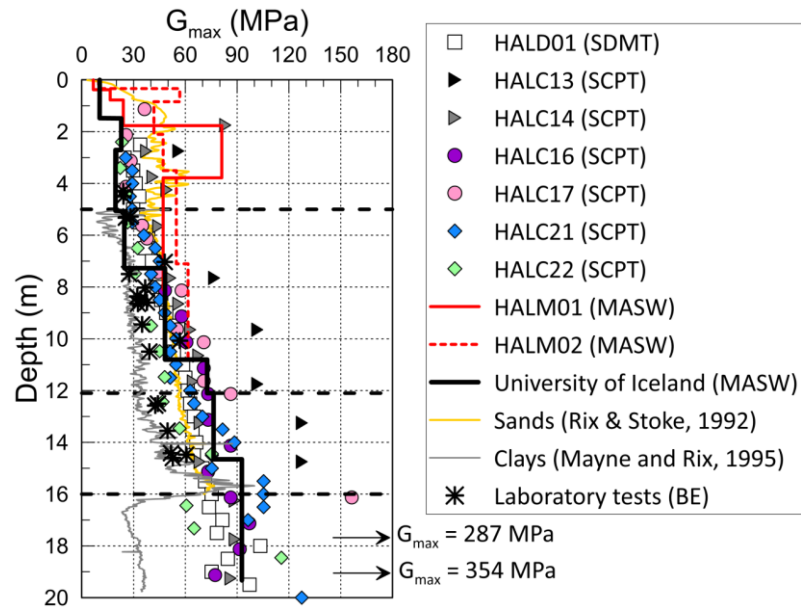


Figure 2.20 Small strain shear modulus, G_{max} , from field and laboratory measurements of V_{vh} and V_s (SCPT, SDMT, MASW and bender elements).

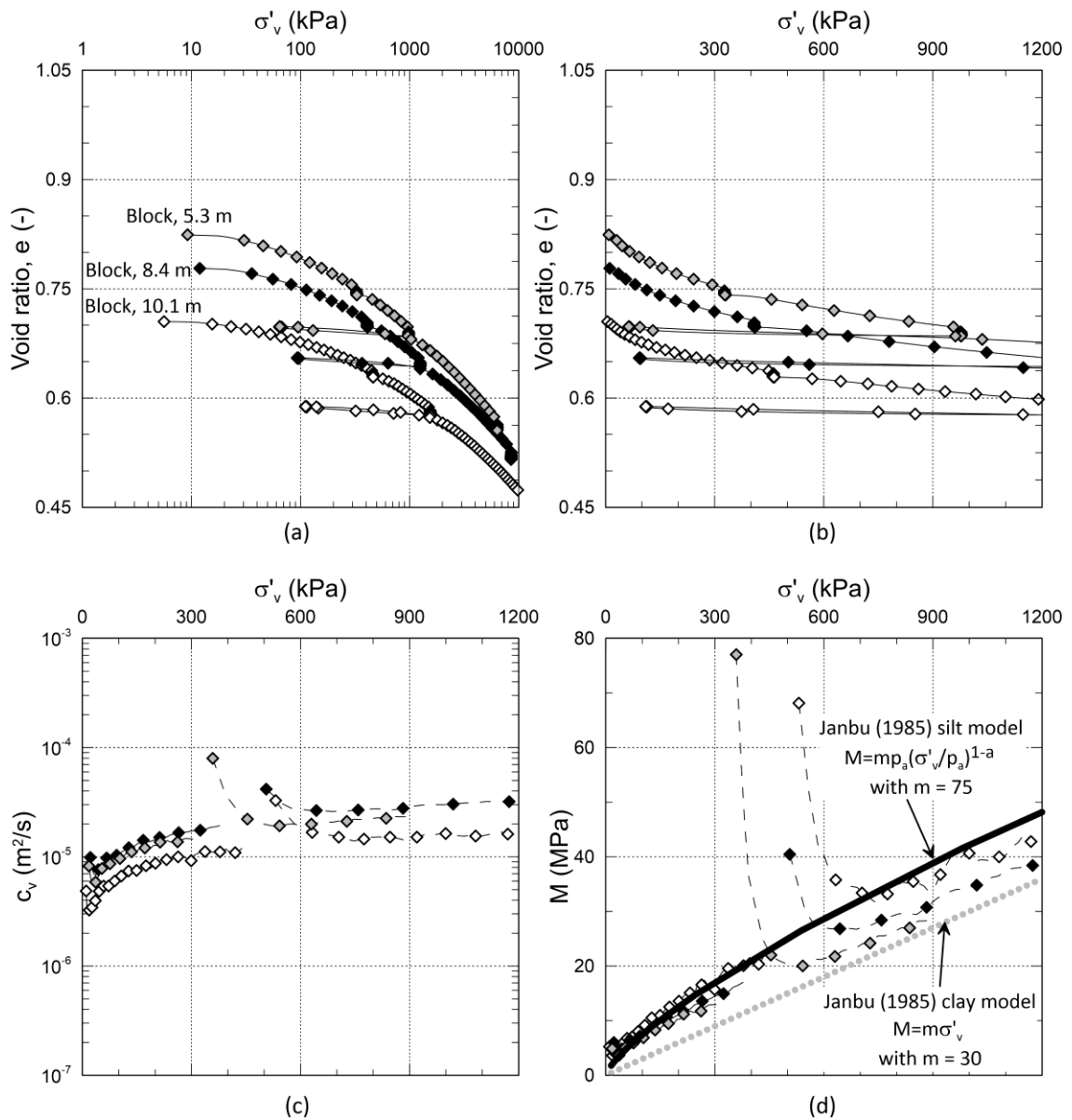


Figure 2.21 Three typical results from CRS testing on specimens from Halden block samples. (a) Void ratio versus log vertical stress, (b) void ratio versus vertical stress, (c) coefficient of consolidation, c_v , versus vertical stress, and (d) constrained modulus, M versus vertical stress.

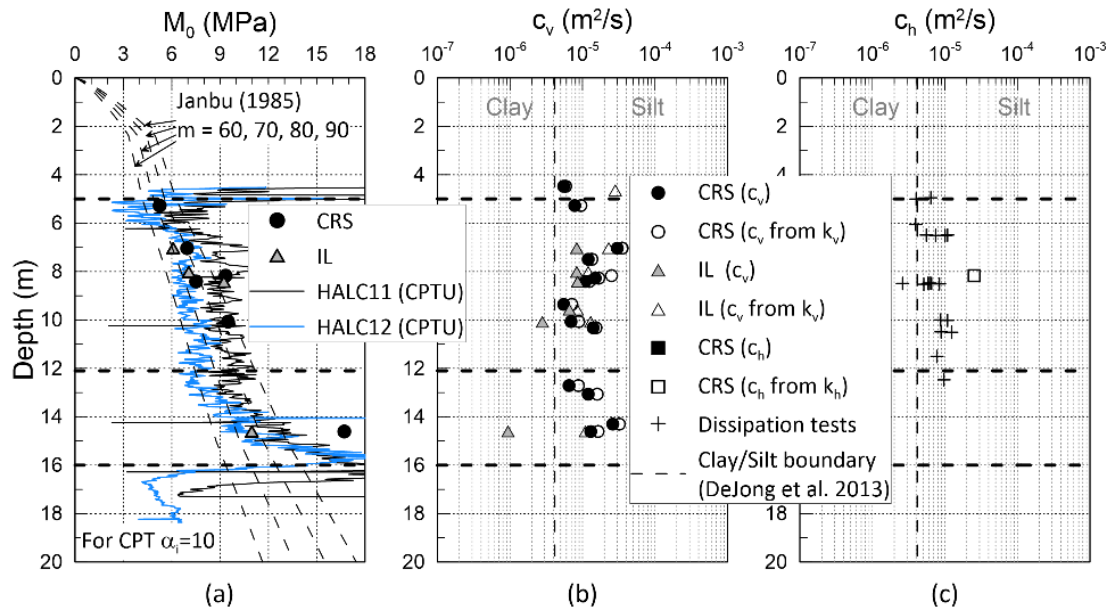


Figure 2.22 (a) Constrained modulus at the in situ effective vertical stress, M_0 and (b) vertical and (c) horizontal coefficient of consolidation with depth, with DeJong et al. (2013) clay-silt transition indicated.

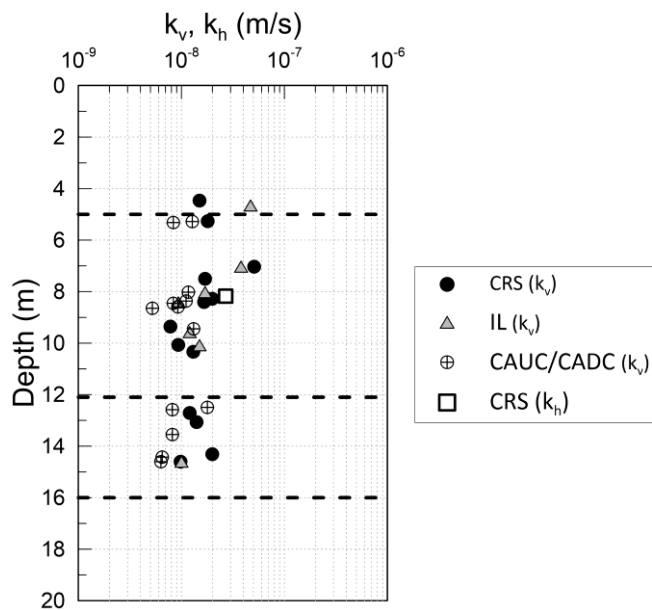


Figure 2.23 Hydraulic conductivity (k_v , k_h) from laboratory testing.

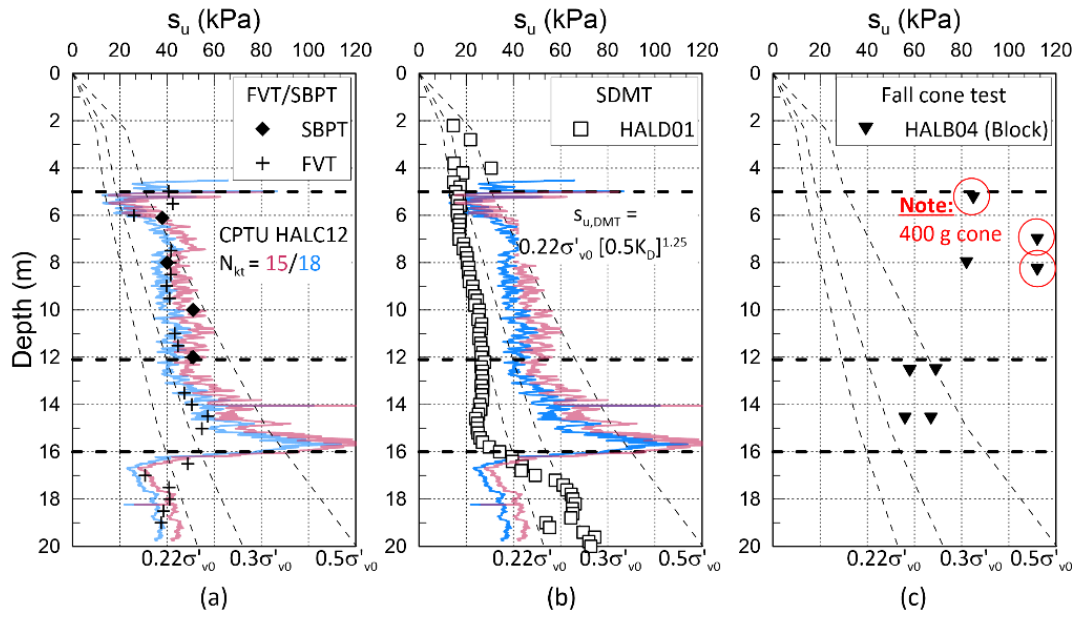


Figure 2.24 Undrained shear strength from (a) field vane tests, self-boring pressuremeter tests and CPTU, (b) DMT and CPTU, (c) fall cone tests.

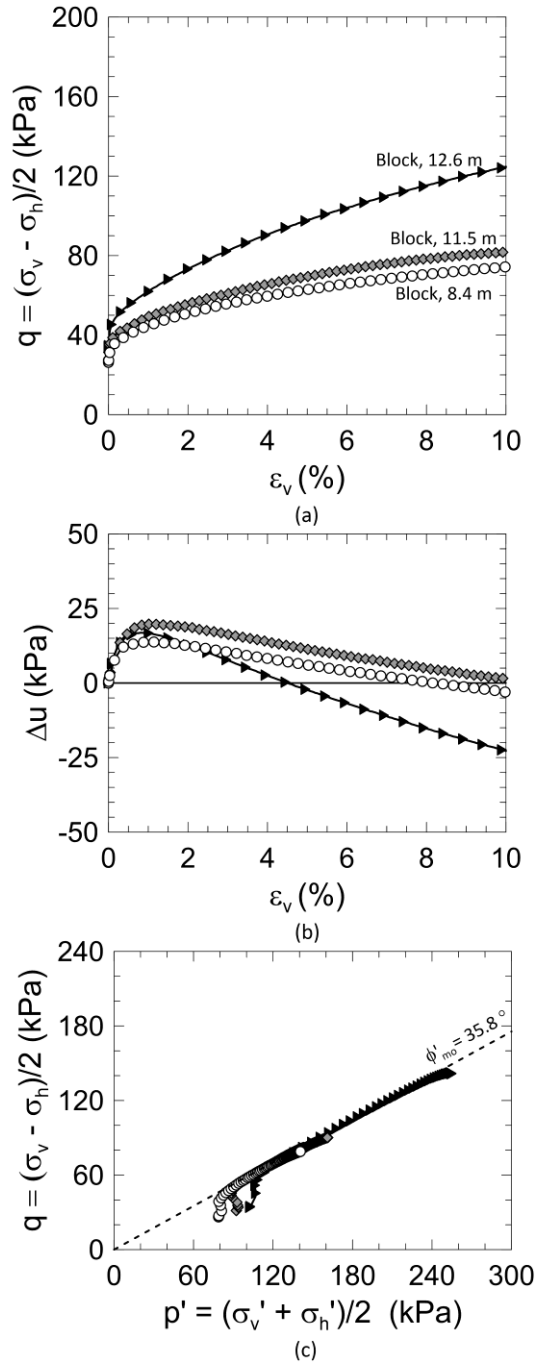


Figure 2.25 Typical CAUC test results from Halden block samples (HALB04) by means of (a) shear stress versus vertical strain, (b) shear-induced pore pressure versus vertical strain, and (c) stress-path plots. A strong tendency for dilative behavior develops negative shear induced pore pressure in the specimens and results in strain hardening upon shearing. As observed in other silts and intermediate soils no unique (peak) undrained shear strength is identified.

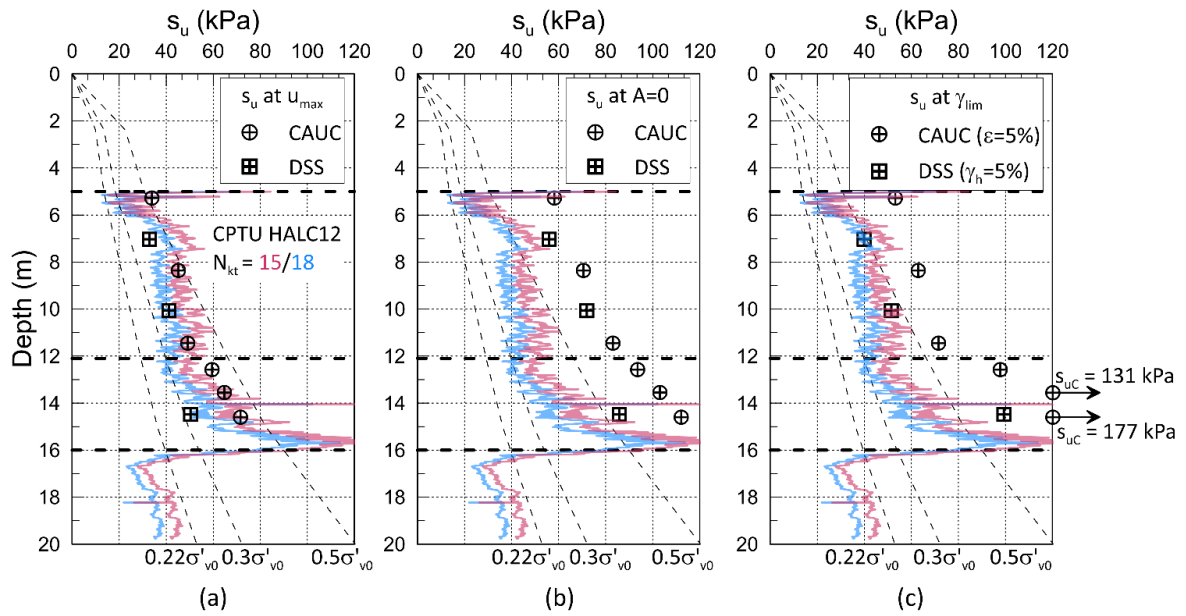


Figure 2.26 Results of CAUC and constant volume DSS tests on block samples of Halden silt. Undrained shear strength is interpreted as the shear stress at (a) maximum pore pressure, u_{max} , (b) $A=0$, and (c) a limiting shear strain of 5% in DSS and 5% axial strain in CAUC.

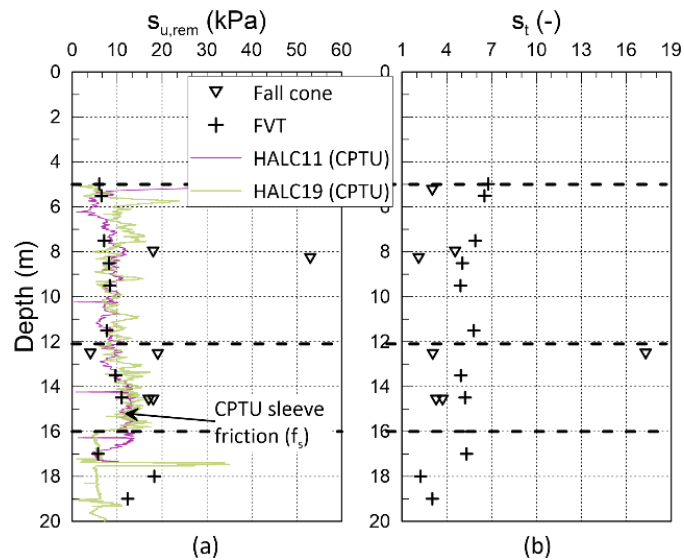


Figure 2.27 Results of (a) remolded undrained shear strength, and (b) sensitivity from fall cone and field vane tests.

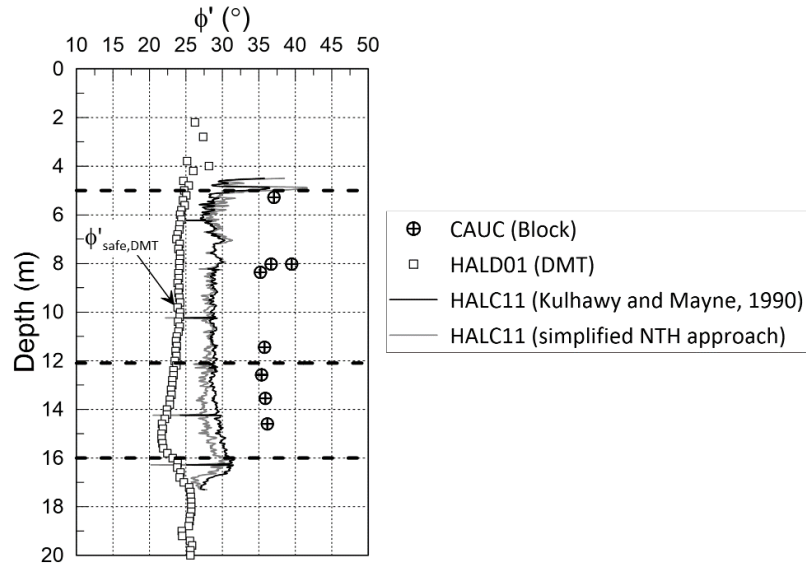


Figure 2.28 Interpretation of effective stress friction angle from DMT, CPTU, and laboratory CAUC tests on block samples.

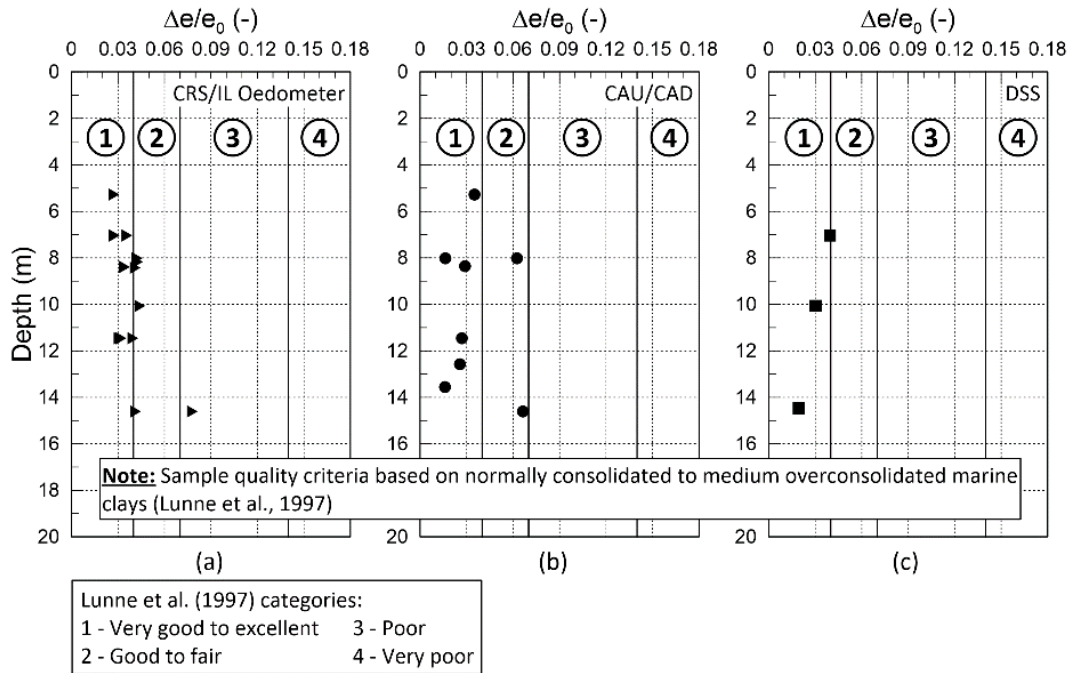


Figure 2.29 Evaluation of $\Delta e/e_0$ from (a) oedometer, (b) triaxial and (c) DSS testing on silt specimens from block samples.

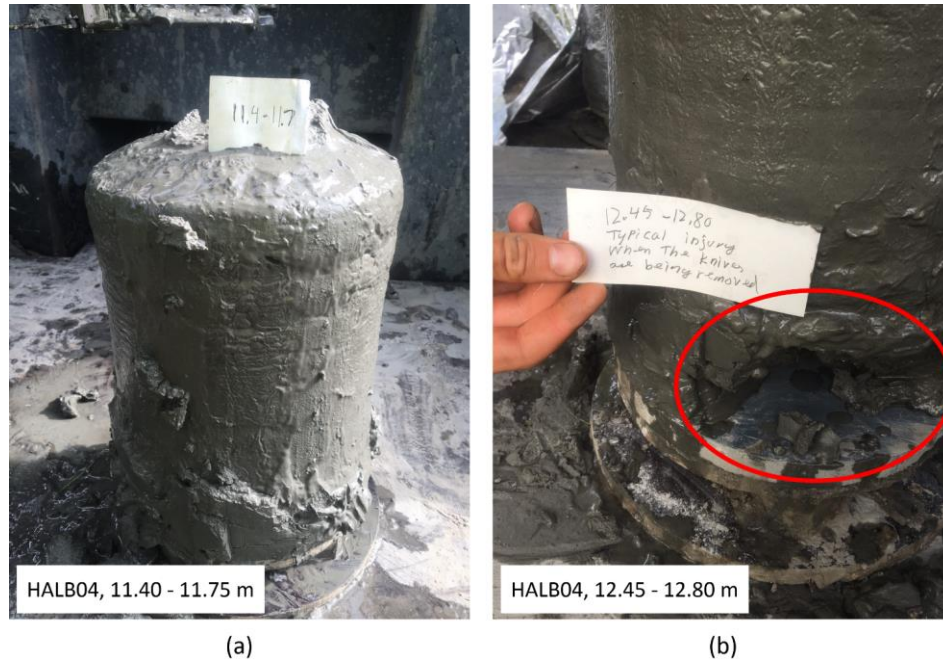


Figure 2.30 Sherbrooke block sampling of Halden silt (borehole HALB04); (a) Apparently good quality block from 11.5 m depth, (b) Damaged lower part of block from 12.4 m depth. Damage was caused by the retracting knives at the base of the block.

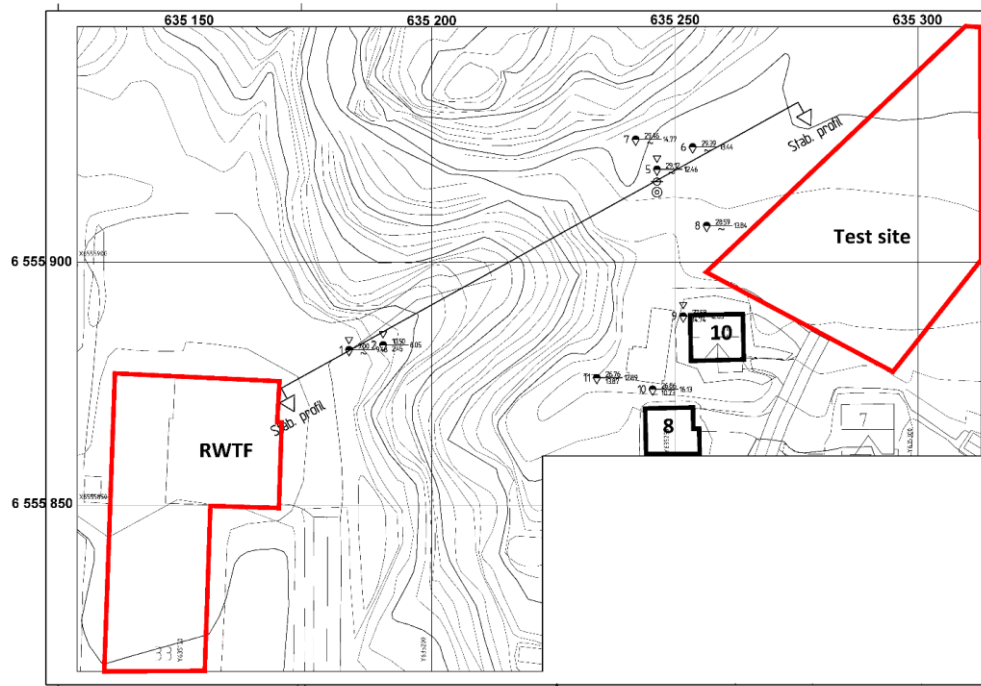


Figure 2.31 Location plan showing the Remmen wastewater treatment facility (RWTF) relative to the Halden research site, the slope in question and the neighboring houses (No. 8 and 10). Borehole locations 1, 2, 4 and 5 include cone penetration tests. 54 mm Geonor fixed piston sampling was conducted at location 5.

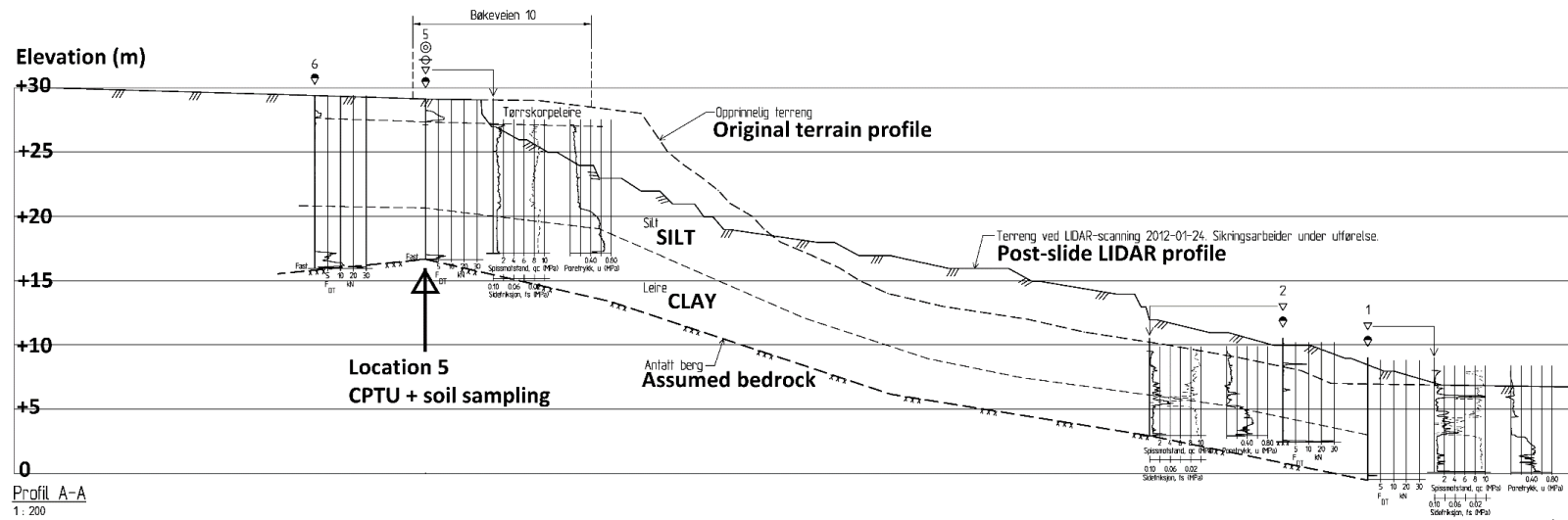


Figure 2.32 Cross-section showing original slope and post-failure slope profiles from North-West.

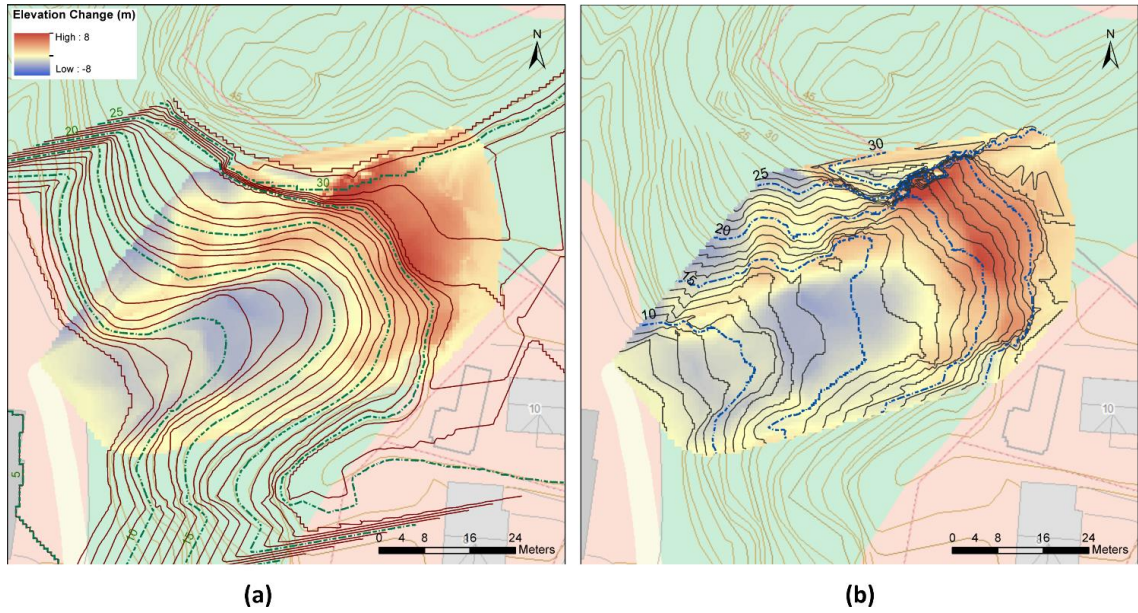


Figure 2.33 LiDAR results shows elevation contours of (a) Pre-failure conditions, and (b) post-failure conditions.

CHAPTER 3

INTACT, DISTURBED AND RECONSTITUTED UNDRAINED SHEAR BEHAVIOR OF LOW PLASTICITY NATURAL CLAYEY SILT

This paper presents a laboratory investigation of undrained triaxial shear behavior of a natural low plasticity silt from Halden, Norway in the intact, disturbed and reconstituted states. Sherbrooke block sample and reconstituted specimens were subjected to simulated tube sampling in a triaxial stress path cell system prior to reconsolidation and undrained shear to assess the effects of disturbance on undrained shear behavior, undrained shear strength and effective stress friction angle. Shear stress and pore pressure development were evaluated relative to that measured for the undisturbed reference state taken as that measured on specimens from the intact block sample. Furthermore, specimens trimmed from fixed piston tube samples collected from the field site were also tested for comparative purposes. Collectively, the results demonstrate that neither the volumetric method of evaluating sample quality for clays nor shear wave velocity track sample disturbance well for this low plasticity silt. Relative to the reference intact block sample tests simulated tube sampling results in an increasingly pronounced dilative type behavior during post-disturbance undrained shear and a general increase in undrained shear strength. Specimens from the block sample that were subjected to simulated tube sample disturbance showed similar stress-strain behavior to that from conventional anisotropically consolidated triaxial compression tests conducted on specimens from the tube samples, suggesting that significant alteration of the intact soil state occurred during tube sampling. Practical suggestions for selection of undrained

shear strength for intact low plasticity silts that exhibit dilative behavior such as the Halden silt are proposed.

3.1 Introduction

While effects of sampling and sample disturbance on undrained shear behavior of clays have been subject to extensive research for decades (La Rochelle and Lefebvre 1971; Lacasse et al. 1985; Hight et al. 1992; Tanaka et al. 1996; Lunne et al. 1997; Santagata and Germaine 2002; Lunne et al. 2006), few studies have investigated how tube sampling of low plasticity silts affects selection of engineering properties compared to those interpreted from companion high quality block samples. Indications are that tube sampling can densify loose silts and sands (e.g. Hight and Leroueil 2003) due to drained or partially drained conditions during sampling. As a result advanced laboratory testing (e.g. direct simple shear or triaxial compression) of these samples can lead to opposite effects of those often observed in naturally occurring structured clays, i.e., higher strength and stiffness properties than in situ values (Carroll and Long 2017; Lukas et al. 2019). The dilative nature of many silts and other intermediate soils (silty sand, sandy silt, clayey silt, silty clay, etc.) also results in strain hardening during undrained shear, and oftentimes, no unique undrained shear strength (peak) is observed (e.g. Fleming and Duncan 1990; Høeg et al. 2000; Sandven 2003; Brandon et al. 2006; Long 2007; Carroll and Long 2017). Consequently, significant uncertainties are associated with predicting the in situ undrained shear strength of silts using laboratory tests on apparently intact, so-called undisturbed samples. Furthermore, only one quantitative framework for assessment of sample quality has been proposed for low plasticity soils (DeJong et al.

2018). This method was developed for 1-D consolidation tests and is based on synthetic soil mixtures that do not exhibit the same sensitivity and structure as many naturally occurring soils. The lack of such practical recommendations has led to use of the clay-based volumetric sample quality assessment indices, e.g., normalized void ratio change, $\Delta e/e_0$, (Lunne et al. 1997) the recompression volumetric strain, ε_{vol} or Sample Quality Designation (SQD, Terzaghi et al. (1996)). While all soils are subject to strains during tube sampling, in clays the shearing can be considered undrained and thus under constant volume conditions (although there can be local redistribution of water content after tube sampling). Silts, however, may be undrained, partially drained, or drained during tube sampling depending on sampling rate, soil composition, type of sampler etc., and any potential volume changes occurring during and after sampling are unknown. The use of clay-based frameworks for silts has recently been shown to be misleading (Long et al. 2010; Carroll and Long 2017; DeJong et al. 2018; Lukas et al. 2019) even though its use has been presented in the literature.

This paper presents an assessment of the undrained triaxial shear behavior of a natural silt in the intact, reconstituted and disturbed states, where the Sherbrooke block sample is considered the best representation of intact soil. It investigates differences observed between tests on material from the block sample and specimens reconstituted using moist tamping and slurry deposition and compares the behavior of block sample material and specimens subjected to experimental sample disturbance simulation (Baligh et al. 1987). Furthermore, the undrained triaxial stress-strain behavior and interpreted undrained shear strength of the block sample and experimentally disturbed specimens are compared with results on specimens from the NGI 54 mm composite fixed piston

sampler (Andresen and Kolstad 1979) and Japanese Gel-Push Static fixed piston sampler (Tani and Kaneko 2006; Mori and Sakai 2016).

3.2 Current practice in sampling of silts and assessment of undrained shear strength

3.2.1 Tube and block sampling

Sample disturbance results from stress relief during drilling and straining during tube sampling. Other sources of post sampling disturbance include sample extrusion, transportation, sample storage and specimen trimming (Ladd and DeGroot 2003). The magnitude and effect of these factors are functions of soil type, drilling and sampling equipment, operator experience, transportation method, and storage time. For example, Baligh et al. (1987) and Clayton et al. (1998) investigated the effect of tube dimensions and cutting shoe geometry on sample quality and found that increasing area ratio (AR = ratio of the cross-sectional area of the sampler that is solid to that of the inside of the cutting shoe) resulted in a significant increase in the compressive centerline strains ahead of the sampler. Best practice recommendations from such research and that of others (e.g. Hight and Leroueil 2003; Ladd and DeGroot 2003) are that: 1) the area ratio should not exceed 10%, 2) the inside diameter should be greater than around 72 mm, 3) the cutting shoe should be sharp (e.g., around 5° to 10°), 4) the sample tube should have zero inside clearance, and 5) a fixed piston should be used.

Silts and intermediate low plasticity soils have traditionally been sampled using: (i) open drive U100 or split spoon samplers (Bray et al. 2004; Long 2007), both of which

have a poor geometry with a large area ratio and cutting angle; (ii) thin-walled samplers with a better geometry including Shelby tubes of various diameters (Brandon et al. 2006; Nocilla et al. 2006) and; (iii) different fixed piston samplers with thin-walled tubes (Høeg et al. 2000; Bray and Sancio 2006; Long et al. 2010; Solhjell et al. 2017). Although large diameter block type samplers, e.g. Sherbrooke (Lefebvre and Poulin 1979) and Laval samplers (LaRochelle et al. 1981) typically provide high quality samples of clays, there is limited experience with these sampling techniques for low plasticity silts. Examples of collection of hand-carved and downhole Sherbrooke block samples in this material include Bradshaw and Baxter (2007), Carroll and Long (2017) and Blaker et al. (2019).

Because of the challenge in collecting good quality samples of silts, some laboratories prepare advanced test specimens (e.g., triaxial) using reconstitution methods, including: moist and dry tamping (Ladd 1978), and slurry deposition (Wang et al. 2011; Lukas et al. 2019). Under controlled laboratory environments the effects of different variables can be studied, but due to particle reorientation, particle segregation, impact energy, and loss of structure and/or cementation effects, reconstituted soil may not necessarily be an attractive alternative for silts, nor be representative of the in-situ soil state and structure.

3.2.2 Laboratory simulation of tube sampling - Ideal Sampling Approach (ISA)

Tube sample disturbance can be simulated in the laboratory to study the effects on undrained shear behavior and engineering parameters. Baligh et al. (1987) and Clayton et al. (1998) used the Baligh (1985) strain path method to investigate the effects of undrained tube sampling in saturated clays. The result of this work demonstrated that a

tube sampler takes a centerline element of soil initially beneath the sampler into a strain cycle including both compression and extension strains during sampler penetration. This can be simulated in the laboratory using the Ideal Sampling Approach (ISA; illustrated for a silt in Figure 3.1) in which a specimen is consolidated to the estimated in situ stress condition, σ'_{v0} and σ'_{h0} (Step 1) of interest. In Step 2 tube sampling is simulated by shearing the specimen first in undrained compression to a predefined strain level, $+\varepsilon_{zz,max}$ (shown for +1% vertical strain in Figure 3.1; which is considered a representative value for a standard 76 mm outside diameter US Shelby tube), reversing the direction of loading and bringing the specimen into extension, i.e. to a strain level equal to $-\varepsilon_{zz,max}$, before returning to 0% vertical strain and removing the shear stress $q = 0.5(\sigma_v - \sigma_h)$, under undrained conditions. In Step 3 the "tube-sampled" specimen is reconsolidated back to σ'_{v0} and σ'_{h0} followed by the final Step 4 of undrained compression shearing the soil to failure. In the results section of this paper the final undrained shear results are compared to behavior of a companion test specimen that has not been subjected to the ISA strain cycle.

Clayton et al. (1992), Santagata and Germaine (2002) and Clayton et al. (1992); Santagata and Germaine (2002); Santagata et al. (2006) found that simulated tube sampling of clays results in a reduction in the mean effective stress $p' = 0.5(\sigma'_v + \sigma'_h)$, during ISA cycling, an increase in ε_{vol} or $\Delta e/e_0$ during post-ISA reconsolidation, and decreases in the small strain stiffness, undrained shear strength $s_u = q_f$ (where q_f is the shear stress at failure), and post-peak strain softening. ISA testing on silts have seen limited research efforts until recently but these soils have shown contrasting behavioral effects of disturbance relative to that of clays. For the Irish intermediate plasticity

Letterkenny silt Carroll and Long (2017) demonstrated that increasing the level of ISA strain damage resulted in an increase s_u and stiffness by almost 20%. Greater damage also resulted in an increase in the rate of negative shear induced pore pressure generation of the specimens. Lukas et al. (2019) tested various synthetic intermediate soils and found a decrease in the initial pre-peak stiffness, a decrease in strain-softening response and increases in s_u and vertical strain at failure $\varepsilon_{v,f}$ with increasing ISA strain. Also, the magnitude of these changes increased with decreasing plasticity index. These results are opposite of that found for the effect of tube sample disturbance on the behavior of low to moderately overconsolidated clays.

3.2.3 Selection of undrained shear strength for design

Due to sample disturbance effects, limitations in reconstitution methods, and the strain hardening nature of many silts, there are significant uncertainties associated with estimating the in situ s_u of silts for design purposes from laboratory tests (Wang et al. 1982; Fleming and Duncan 1990; Høeg et al. 2000; Carroll and Long 2017). Brandon et al. (2006) reviewed six criteria for interpretation of s_u of two natural silts from the Mississippi River Valley. For specimens sheared in triaxial compression, the criteria include: 1) maximum deviator stress, $(\sigma_1 - \sigma_3)_{max}$; 2) an assigned limiting vertical strain, $\varepsilon_{v,f}$; 3) state of zero excess shear induced pore pressure at failure $\Delta u_f = 0$, which is equivalent to Skempton's A parameter at failure equal to zero, $A_f = 0$ for $B = 1$; 4) point at which the effective stress path first reaches the failure envelope, defined by the K_f line; 5) maximum obliquity, $(\sigma'_1/\sigma'_3)_{max}$; and 6) maximum shear induced pore pressure, u_{max} . Note that with zero cohesion intercept, $c' = 0$, criteria 4 and 5 provide the same undrained

shear strength. Long et al. (2010) and Long (2007) found that the use of criterion (1) for anisotropically consolidated undrained triaxial compression (CAUC) tests on the Norwegian Os, and the Irish Sligo and Dunkettle silts gave unusually high s_u values and that other criteria (e.g., criteria 3 and 6) could more effectively reduce the scatter. Long et al. (2010) and Long (2007) concluded that due to the dilative nature of silty soils interpretation of s_u from CAUC tests using criterion (1), which is the traditional approach for clays, gives unrealistically high s_u values and advocated use of criterion (2) with $\varepsilon_{v,f} = 2\%$. Whereas Börgesson (1981), Wang et al. (1982) and Fleming and Duncan (1990) used $\varepsilon_{v,f}$ ranging from 5% to 15%. Criterion (6) typically provides the lowest value of s_u as u_{max} often occurs at small strain and thus before full mobilization of the in situ s_u has taken place. While Stark et al. (1994) used both criteria (1) and (6), Brandon et al. (2006) recommended criterion (3). Solhjell et al. (2017) evaluated s_u for a North Sea offshore silty, sandy, clayey soil unit for which the project design basis required both lower and upper bound estimates of s_u . The Authors selected s_u at the onset of dilative behavior (i.e., $\Delta u - \Delta\sigma_{oct} = 0$, where $\Delta\sigma_{oct} = 2\Delta q/3$ and $q = (\sigma_v - \sigma_h)/2$) in CAUC and direct simple shear (DSS) tests as the lower bound while the upper bound was estimated as the lesser value of the conventional peak shear stress (criterion 1) and s_u at $\varepsilon_{v,f} = 10\%$ for CAUC tests or 15% shear strain in DSS tests (criterion 2). Depending on the design conditions, it is evident that s_u for silts exhibiting dilative behavior can be significantly underestimated or overestimated. In summary, limited research is available on how sample disturbance influences the various s_u selection criterion and furthermore how laboratory s_u values for silts defined by the above-mentioned criteria relates to the in-situ s_u for specific design applications.

3.3 Methods of investigation

3.3.1 Soil sampling

Samples were collected at the Halden, Norway research site using the Sherbrooke block sampler (Lefebvre and Poulin 1979), the NGI 54 mm inner diameter (ID) composite piston (NGI 54) sampler (Andresen and Kolstad 1979) and the 71 mm ID Japanese Gel-Push Static (GP-S) sampler (Tani and Kaneko 2006). The latter injects a water-soluble polymeric lubricant (gel) from the sampler shoe to lubricate and reduce friction between the cut sample and sampler wall. The NGI 54 and GP-S samplers have outside diameter to thickness ratios (D_w/t) of 12 and 8, respectively, giving AR of about 44% and 78%. The former sampler has about 0.6% inside clearance and the latter about 1.5%. The Sherbrooke block samples are considered in this paper the best representation of intact soil and used as the reference laboratory behavior for the Halden silt.

3.3.2 Specimen preparation

Both consolidated triaxial and incremental load oedometer test specimens were prepared in the laboratory. Three specimen preparation methods were used: trimming of block and tube samples and two variations of soil reconstitution. Reconstituted specimens were prepared from a batch of air-dried untested material from the same depth as the collected samples and had essentially identical grain size distributions as the block sample. The individual reconstituted specimens were prepared either by moist tamping (MT) or slurry deposition (SD). In the MT method the amount of dry silt that provided the desired density for the specimens was mixed with about 3% (by mass) de-aired water.

The specimens were prepared on the triaxial pedestal in six separate equal-volume lifts using a split mold. The lower layers were under compacted (Ladd 1978) such that the energy applied to the successive layers would produce a specimen of approximately uniform density throughout when the preparation was finished. The top cap and membrane were sealed using O-rings and an internal under pressure of 20 - 30 kPa applied. The SD method was similar to the approach described by Wang et al. (2011) and Lukas et al. (2019) for which 200 - 400 g of air dried silt was thoroughly mixed with de-aired water at 1.5 - 2.0 times the liquid limit, and left overnight to hydrate. Then the slurry was mixed further and poured into an oedometer ring or, in the case of triaxial specimens, a split mold with an extension collar (ID = 54 mm) and the membrane already in place. All slurry specimens were left 4 - 10 hours to self-weight consolidate before free water was removed. Oedometer specimens were incrementally loaded to the estimated in situ vertical effective stress for the block sample $\sigma'_{v0} = 125$ kPa using dead weights, left overnight to consolidate, then unloaded and mounted in the oedometer load frame. Triaxial specimens were incrementally loaded to 50 kPa while still in the split mold, also using dead weights. The specimens were unloaded, the top cap and membrane sealed using O-rings and an internal underpressure of 30 kPa was applied for about 30 minutes prior to removal of the split mold. For both the MT and SD methods the specimen dimensions were measured while still under vacuum which was not released until the triaxial cell was filled with water and oil, and a cell pressure of about 30 kPa was applied. Both MT and SD specimens produced specimens with almost identical void ratio after consolidation as specimens prepared from the Sherbrooke block sample (Table 3-1).

Furthermore, replicate specimens prepared using the same method demonstrated repeatable undrained triaxial compression behavior, as presented in the results section.

3.3.3 Triaxial testing

The triaxial specimens were prepared to diameter, $d = 54$ mm and height, $h = 108$ mm and tested using the procedures described by Lacasse and Berre (1988). During the saturation process the test specimens were first subjected to an isotropic effective stress (cell pressure) equal to the estimated value of the initial negative pore pressure (suction) within the specimen. The porous filter stones were initially dry except for the SD specimens. At the initial isotropic stress, de-aired water was flushed through the porous stones and any tendency for volume change was prevented by adjusting the cell pressure until a stable condition was reached. Following this stage, backpressure was applied using a pressure volume controller and all B values, which were measured at the end of the consolidation phase, were $\geq 97\%$ except for one MT reconstituted specimen with a measured B value of 91%. All specimens were anisotropically consolidated to the best estimate σ'_{v0} and horizontal effective stress σ'_{h0} using an assumed $K_0 = 0.5$ (Blaker et al. 2019). All specimens were allowed to creep for 12 to 24 hours prior to undrained shear. ISA triaxial tests were performed with peak ISA vertical strains of $\pm 0.5\%$, $\pm 1.0\%$, and $\pm 3.0\%$ except for one test which was performed inadvertently with asymmetric vertical strains of $+1\%/-0.5\%$. The ISA strain cycles were followed by undrained removal of the deviator stress (reducing σ_v to $\sigma_v \approx \sigma_h$), the back pressure was re-set to the end-of-ISA pore pressure, and the specimen was reconsolidated back to σ'_{v0} and σ'_{h0} as shown for example in Figure 3.1. All monotonic and ISA undrained shear tests were strain-

controlled at a strain rate of 0.5 %/hr. The total radial stress was kept constant while the total axial stress was increased in compression (CAUC) and decreased in extension (CAUE). All stress measurements were corrected for membrane resistance and changes in specimen area (Berre 1982).

3.3.4 Incremental loading oedometer testing

Incremental loading (IL) oedometer tests were performed as per Sandbækken et al. (1986) using specimens trimmed from the block sample with a cross-sectional area of 20 cm² and height 20 mm and mounted with dry porous filter stones. Slurry specimens were prepared in a 50 cm² oedometer ring to a specimen height of 26 mm. Each load increment was maintained for 60 min, except for one test on the block sample specimen, on which a 24 hour increment duration was used. A load increment ratio of approximately one was used in all tests.

3.3.5 Bender element testing

Piezo ceramic bender elements (Dyvik and Madshus 1985) were used to measure the shear wave velocity of the triaxial specimens. The bender element at one end of the specimen was used to transmit a vertically (*v*) propagating horizontally (*h*) polarized sinusoidal shear wave. The receiver bender element detected the arrival of this shear wave at the opposite end of the specimen, and the velocity of the shear wave (V_{vh}) was determined. The transmitting signal was generated by a Wavetek model 29 10 MHz Direct Digital Synthesis (DDS) Function Generator, exciting the transmitting bender with a single ± 10 V amplitude sine wave triggered at a 10 Hz delay. The transmitted and

received signals were both recorded using a LDS-Nicolet Sigma 30 digital oscilloscope with 12-bit resolution and up to 10 Ms/s sampling rate.

3.4 Results – block samples and reconstituted specimens

The block and tube samples were collected in separate boreholes but all from the depth interval of 11.0 to 11.8 m below grade, and maximum horizontal distance of 3.3 m apart. Typical index and classification properties were: water content $w = 27\%$, fall cone liquid limit $w_L = 29\%$, plastic limit $w_P = 21\%$, plasticity index $I_P = 8\%$, liquidity index $I_L = 0.7$, silt fraction ($\% > 2\ \mu\text{m}$ and $< 63\ \mu\text{m}$) = 89 %, and clay fraction ($\% < 2\ \mu\text{m}$) = 9 % (Blaker et al. 2019). As noted above the liquid limit of 29 % was determined using the fall cone method (ISO 2018) but was also determined using the Casagrande Cup (ASTM 2017) which gave, as expected (e.g. DeGroot et al. 2019), a much lower liquid limit $w_{L,CC} = 23\%$ resulting in an $I_{P,CC} = 2\%$. These Casagrande values classify the Halden silt as ML in the Unified Soil Classification System (ASTM 2017).

3.4.1 1-D compression behavior

Figure 3.2 presents the 1-D IL results for two Sherbrook block sample specimens and one slurry consolidated specimen. Volumetric strains of 1.3% and 1.4% were measured for the two block specimens at σ'_{v0} corresponding to $\Delta e/e_0$ of 0.031 and 0.032. The strain energy based compression ratio, $C_{rw,i}/C_{cw}$ (DeJong et al. 2018) for the two block specimens was in the range of 0.16 - 0.20. Interpretation of the initial portion of the time-deformation curves using conventional root-time and log-time methods was not possible but it was evident that end of primary was reached well within 4 minutes and all

data points in Figure 3.2 are plotted at $t_c = 4$ minutes. Figure 3.2a shows no evidence of a yield or preconsolidation stress (σ'_p) and even if plotted in semi-log space the rounded nature of the compression curves are such that any Casagrande (1936) or Becker et al. (1987) interpretation of σ'_p is considered unreliable. Based on the geologic history of the site, as summarized by Blaker et al. (2019), the deposit is believed to be geologically normally consolidated but likely exists in a lightly overconsolidated state due to aging. The recompression ratio ($C_{re} = \Delta\varepsilon/\Delta\log\sigma'_v$) and maximum compression ratio ($C_{c\varepsilon,max}$) for the block specimens were 0.006 and 0.075, respectively, and the Janbu (1963) constrained modulus (M) at the in situ effective stress (σ'_{v0}) was about 11 MPa. The average unload-reload constrained modulus (M_{ur}) was about 130 MPa. Secondary consolidation effects were rather small, with $C_{\alpha\varepsilon}/C_{c\varepsilon}$ approximately equal to 0.035, and thus, consistent with the range suggested by Terzaghi et al. (1996) for inorganic clays and silts. The slurry consolidated specimen started at the same initial void ratio as the block samples but exhibited much greater compressibility, as anticipated, and the $e - \log\sigma'_v$ curve did not converge with that of the block samples within the maximum σ'_v values applied (Figure 3.2c).

3.4.2 Block and reconstituted undrained stress-strain behavior

Volumetric strain at σ'_{v0} for the consolidation phase of all the CAUC/E tests ranged from 0.8% to 1.3% and the corresponding $\Delta e/e_0$ values ranged from 0.014 to 0.031 (Table 3-1). The shear wave velocity values normalized by the in situ value, as measured downhole using a seismic flat dilatometer, SDMT (Blaker et al. 2019),

$V_{vh,0}/V_{vh,SDMT}$, ranged from 0.83 to 0.87 (Table 3-1). Overall, the measures of ε_{vol} , $\Delta e/e_0$ and $V_{vh,0}/V_{vh,SDMT}$ were uniform for the seven specimens trimmed from the block sample.

Figures 3a and 3b show that for CAUC testing the block sample specimens exhibited initial contractive behavior up to 1 - 2% vertical strain but thereafter switched to dilative behavior and strain hardening response. This behavior is clearly observed in Figure 3.3c which shows the effective stress paths turn towards and eventually run along the K_f line. All tests, including the CAUC test exhibited an effective stress friction angle at maximum obliquity of $\phi'_{mo} = 36^\circ$. This friction angle, which is the same as that measured for the SD and MT specimens, implies a normally consolidated $K_0 = (1 - \sin\phi')\text{OCR}^{\sin\phi'}$ (Mesri and Hayat 1993) of 0.41. With the Halden deposit considered to be lightly overconsolidated suggests an estimated in situ K_0 value somewhat greater than 0.41 and thus the value of 0.50 assumed at the start of the test program seems reasonable.

The reconstituted specimens prepared either by MT or SD had essentially the same initial and end of consolidation void ratios as the block sample specimens (Table 3-1) but exhibited significantly different undrained stress-strain behavior. Peak shear stresses of about 35 kPa occurred at around $\varepsilon_v = 0.1\%$ and the specimens developed u_{max} values of around 40 kPa as depicted in Figure 3.3d and Figure 3.3e. Both MT and SD specimens showed post-peak strain softening behavior but from about $\varepsilon_v = 3\%$ the stress-strain characteristics switch towards dilative behavior and strain hardening as the stress path reaches the K_f line at essentially the same maximum obliquity friction angle of 36° as the block sample specimens (Figure 3.3f).

The significant difference in the block and reconstituted undrained shear behavior is believed to be due to differences in structure. The reconstitution procedure most likely

does not replicate the depositional environment of the natural soil. Furthermore, the in situ soil had undergone significant aging, i.e., multiple log cycles of secondary compression (Blaker et al. 2019). In contrast, reconstituted laboratory specimens were aged for only a short period after end of primary consolidation. While physical handling and trimming of the block sample was possible without support, the SD specimens (with essentially the same void ratio and silt and clay content) had to be supported during preparation and even after dead-weight consolidation to 50 kPa. As no evidence of cementation has been found for the Halden silt (Blaker et al. 2019) this implies that an inherent structure of the block sample prevented collapse of the unconfined soil matrix and was likely also responsible for the stiffer strain hardening observed in CAUC tests and likewise for the 1D consolidation behavior. This intact structure could not be replicated by reconstitution in the laboratory by either of the two reconstitution methods without any form of aging of the soil. Figures 4a to 4c show how the stress-strain, stress-path and secant shear modulus ($G_u = \Delta(\sigma'_v - \sigma'_h)/3\Delta\varepsilon_v$) of reconstituted Halden silt (SD) changes after only 7 days (10^4 minutes) of drained creep in the triaxial cell. The lower void ratio after consolidation ($e_c = 0.67$ for 7 days creep versus 0.71 for 2 hours creep) cannot alone explain the 15% increase in peak shear stress of the "aged" SD specimen. The secant shear modulus at small shear strains of the unaged SD specimen was also lower for all levels of shear strain compared to the SD specimen subjected to 7 days of drained creep. Mesri et al. (1990) and Schmertmann (1991) hypothesized that drained creep is the dominant mechanism of aging of granular soils on an engineering timescale and that the increase in stiffness and strength during drained creep results from both increased density and continued particle rearrangement creating an increase in

macrointerlocking of particles and microinterlocking of surface roughness. Furthermore, angular particles, like those present in the Halden silt (Blaker et al. 2019), can result in a greater aging effect since they have a larger range of stable contacts and more particle interlocking (Mitchell and Soga 2005).

3.4.3 ISA strain cycling behavior

Positive shear induced pore pressure continuously developed during ISA shearing of the block sample specimens, which caused a significant reduction in p' as shown in Figure 3.5. For the $\pm 3.0\%$ ISA test, the effective stress path towards the end of the ISA strain cycle eventually tracked the CAUC/E K_f lines. The change in mean effective stress, $\Delta p'_c$, expressed as percentage of the pre-ISA mean effective stress after consolidation p'_c (Santagata and Germaine 2002), ranged from 74% and 98% (Figure 3.5c.). ISA shearing of the SD specimens with strain cycles of $\pm 1\%$ and $\pm 3\%$ also caused a significant decrease in p' with $\Delta p'/p'_c$ equal to 95% and 98% (Figure 3.5f) with the effective stress path towards the end of the ISA cycle also tracking the same K_f line as the block sample specimens. These effective stress path excursions for both the block and SD specimens towards very low p' values are consistent with that reported by Lukas et al. (2019) for synthetic silt mixtures. However, this significant loss of p' during ISA simulation of tube sampling is much greater than that measured for clays (e.g., Santagata and Germaine 2002).

3.4.4 Post-ISA reconsolidation and disturbed undrained shear behavior

The post-ISA recompression ε_{vol} and $\Delta e/e_0$ values required to bring the disturbed silt specimens back to the pre-ISA effective stress state increased with increasing magnitude of the ISA strain cycle (Table 3-1). For all post-ISA tests, e_0 was taken as the pre-ISA void ratio e_c . $\Delta e/e_0$ and ε_{vol} were both higher for the reconstituted specimens than the companion tests on block samples. Lunne et al. (2006) cautioned that the $\Delta e/e_0$ method may not be applicable for low plasticity silts. This appears to be the case here as the $\Delta e/e_0$ values in Table 3-1 show that even after being subjected to significant strain induced disturbance, the samples still rated within the "Very good to excellent" and "Good to fair" clay-based sample quality ratings (Lunne et al. 1997) or quality A or B using the SQD system (Terzaghi et al. 1996). It also confirms recently published findings of Carroll and Long (2017), DeJong et al. (2018) and Lukas et al. (2019). Furthermore, bender element tests demonstrated a significant decrease in V_{vh} during ISA (from $V_{vh,0}$ to $V_{vh,ISA}$) corresponding to large decrease in p' . $V_{vh,ISA}$, however, showed complete recovery to $V_{vh,0}$ upon post-ISA reconsolidation (Table 3-1). Yet, post-ISA undrained shear behavior was very different for ISA disturbed specimens compared to the reference block sample specimens, indicating that in this case V_{vh} does not track sample disturbance well.

Increasing ISA-imposed strain damage from $\pm 0.5\%$ to $\pm 3.0\%$ increased the rate of shear stress development with strain in the block sample specimens as shown in Figure 3.6a, especially for the $\pm 3.0\%$ test. This corresponds to an increasing rate of negative shear induced pore pressure with an increase in ISA strain (Figure 3.6b). However, as strain continues both the undisturbed specimen and the ISA disturbed specimens, all converged to the same failure envelope (Figure 3.6c). Figures 6d to 6f present results of

the post-ISA undrained shear behavior of the SD specimen and show similar trends to that of the block sample specimens though with more dramatic effect. At an ISA strain of $\pm 3.0\%$, the strain softening observed in the reference undisturbed SD specimen is completely removed, a much lower Δu is developed, and the effective stress path significantly shifts to the right (Figure 3.6f). Indeed, an interesting outcome of these tests is that with an increase in ISA disturbance strain level the behavior of the reconstituted soil progressively migrates towards that of the block sample.

3.4.5 Influence of tube sampling

Figure 3.7 presents results from two CAUC tests conducted on samples collected using the NGI 54 and GP-S fixed piston samplers. The values of ε_{vol} and $\Delta e/e_0$ during reconsolidation were 1.1 % and 0.024 for the NGI 54 and 1.1 % and 0.026 for the GP-S samples, which is essentially the same as that of the two CAUC block sample specimens (Table 3-1). These values suggest similar sample quality for the tube samples as that of the block samples and yet the undrained shear behavior is markedly different. The specimens from the tube samples have a much a greater rate of shear stress and negative pore pressure development with increasing vertical strain. Although at large strains all the tests converge to the same failure envelope at about $\phi'_{mo} = 36^\circ$. Results from the $\pm 1\%$ and 3% ISA tests performed on the block sample specimens are also plotted for reference in Figure 3.7. These results indicate a similarity in the effect on undrained shear behavior of actual tube sampling disturbance (NGI 54 and GP-S) and simulated tube sampling disturbance (ISA tests on the block sample). Both tube samplers have a poor area ratio with the GP-S sampler being the worse of the two and yet the results in Figure 3.7

indicate greater disturbance for the NGI 54 sampler. It is hypothesized that some compensation occurred due to the reduction in friction between the sampler wall and soil by the polymer gel.

3.5 Discussion of results

The field work described by Blaker et al. (2019) and the results presented above demonstrate that, although challenging, an intact Sherbrooke block sample in this case was successfully collected in a $I_p = 2\%$ soil with 89% silt and 9% clay. Recompression metrics, ε_{vol} and $\Delta e/e_0$, for the block and tube samples were low and similar, yet the undrained stress-strain behavior of the tube samples was markedly different, reaching much higher shear stress at lower strains. The post-ISA reconsolidation phase suggested that for Halden silt neither ε_{vol} , $\Delta e/e_0$, nor V_{vh} track sample disturbance for the ISA specimens; even after significant ISA induced disturbance post-ISA $\Delta e/e_0$ values were very low and $V_{vh,ISA}$ completely recovered to $V_{vh,0}$.

The low compressibility and dilative type behavior during undrained shear of the block sample specimens, and high compressibility and contractive type undrained shear behavior of the reconstituted specimens, are consistent with the differences observed by Høeg et al. (2000) for the Swedish Börlange silt. It appears that the natural soil structure and undrained response to triaxial compression loading of Halden silt cannot be replicated using reconstitution methods even when prepared to the same void ratio as the block sample specimens (Figure 3.3). One test did show that aging during 7 days of laboratory drained creep stiffened a slurry reconstituted specimen, but it still did not behave close to that of the block sample (Figure 3.4). At a minimum, a significantly

greater duration of drained creep would be required. Furthermore, natural seismic ground motion over the years could have also resulted in stiffening and strengthening of the natural silt deposit.

The significant effects of simulated tube sampling (ISA) were confirmed by the observed stress-strain behavior of collected NGI 54 and GP-S tube samples. Increasing degree of disturbance generally resulted in increasingly pronounced dilative type behavior and consequently higher mobilized shear stresses at almost all strength criteria (Table 3-2 and Table 3-3). The effective stress friction angle, however, was essentially the same for all tests, independent of sampling or preparation method (block, tube or reconstitution) and degree of disturbance. If undrained shear strength is required for design, selection of a representative value is highly dependent on the state of the laboratory test specimens, strength criterion and the design application, i.e. whether lower bound or higher bound values are required. Figure 3.8 illustrates how the combination of the Brandon et al. (2006) 1 to 6 undrained shear strength criteria and sampler type can have a significant effect on the selected undrained shear strength. The block sample is considered to be a more accurate representation of the intact soil than the tube samples, given difference in the stress-strain behavior. For a silt that exhibits dilative type behavior criterion 6 (u_{max}) gives close to the same s_u value for all three samplers. At this point, the soil is not dilating yet and the differences in measured behavior are small. Furthermore, selection of a representative design value of A_f (e.g. 0.0 or 0.25) will give near the same s_u for all tests as the Halden silt converges onto the same K_f line, independent of sample type, and at the same time typically limit $\varepsilon_{vf} < 10\%$. It is noted, however, that in Figure 3.8c the starting point (end of consolidation stress, i.e. p'_c and q_c) of the three tests show

small differences and values of s_u at $A_f = 0$ and 0.25 are thus somewhat different. For the other criteria, s_u of the tube sample specimens were generally well above that of the block sample, by up to 159% (Table 3-2). In the extreme case, a selected representative value of s_u from 11.5 m depth at Halden can range from about 50 kPa (block sample at criterion 6 - u_{max}) to 120 kPa (NGI 54 at criterion 2 - $\varepsilon_{vf} = 10\%$), a factor of 2.4. Figure 3.9 shows that, except for the u_{max} and $A_f = 0$ criteria, the undrained shear strength estimates increase with increasing magnitude of ISA induced strain for all other criteria. Relative to the reference monotonic block sample results (plotted at $\varepsilon_{zz} = 0\%$), the increase in s_u , is the largest for q_{max} and $\varepsilon_{vf} = 10\%$ criteria. These findings imply that undrained triaxial testing of tube sampled silt specimens can lead to selection of an unrealistically high undrained shear strength for design. These effects are opposite of that observed for low to moderate overconsolidation clays, where disturbance typically results in a softer stress-strain response and lower peak undrained shear strength.

The selection of undrained shear strength is an important issue for design of structures in silt where loading regime, structure geometry or drainage properties of the soil are such that undrained, or partially drained conditions prevail. From CAUC results for the Halden silt it appears that the shear stress at u_{max} represents the lower bound and at $\varepsilon_{vf} = 10\%$ the upper bound undrained shear strengths, respectively. Selection of the relevant s_u for design will need to consider if the field application will be undrained, fully drained, or partially drained. Applying A_f in the range of 0.0 to 0.25 as upper bound strength criterion; (i) reduces the range between the upper and lower bound undrained shear strength; (ii) allows the design to rely on dilative type behavior, but not on the shear induced pore pressure actually going negative or excessive values of strain; and (iii)

minimizes the adverse effect of sample disturbance on design parameter selection. At a minimum $A_f = 0$ provides a valuable reference undrained shear strength equal to the drained shear strength. For strongly dilative soils like the Halden silt any strength criterion yielding $A_f < 0$ needs careful consideration unless higher values of undrained shear strength are conservative, e.g. for extraction assessments, skirt penetration, pile driving etc. For stability problems, lower values of s_u are more conservative and consideration should be given to estimated strain levels and pore pressure dissipation in the field.

3.6 Summary and conclusions

This paper presents a laboratory investigation of the undrained shear behavior of a natural low plasticity silt from Halden, Norway in the intact, disturbed and reconstituted states. Specimens trimmed from a Sherbrooke block and reconstituted specimens were tested using the ideal sampling approach (ISA) framework in a triaxial stress path cell system. Three levels of ISA vertical strain cycles, $\pm 0.5\%$, $\pm 1\%$ and $\pm 3\%$, were applied to simulate different degrees of tube sampling disturbance. The sample quality recompression metrics, demonstrated that neither $\Delta e/e_0$, ε_{vol} , nor shear wave velocity, V_{vh} , track sample disturbance well for this low plasticity silt unlike that for moderate to low OCR clays. Relative to the reference block sample specimens ISA strain cycles, and subsequent reconsolidation to the best estimate in situ effective stress conditions, resulted in an increasingly pronounced dilative type behavior during post-ISA undrained triaxial shear, and a general increase in s_u . The ISA disturbed block sample specimens also showed similar stress-strain behavior as that measured in conventional CAUC tests

conducted on specimens from the NGI 54 mm composite and GP-S fixed piston tube samplers. These results indicate that tube sampling can cause significant alteration of the intact soil state. However, in all cases the intact, disturbed and reconstituted specimens reached the same effective stress failure envelope. For design applications an assessment of whether the field application will involve drainage is an important consideration. Applying undrained shear strength criteria for soils that exhibit dilative behavior the u_{max} and $0.25 \geq A_f \geq 0$ as lower and upper bound strength criteria reduces the range in characteristic undrained shear strength; ensures that s_u does not rely on net negative pore pressures or excessive strains; and mitigates the adverse effect of sample disturbance on design parameter selection.

3.7 Data availability statement

Some or all data, models, or code that support the findings of this study are available from the corresponding author upon reasonable request.

3.8 Acknowledgements

This study has primarily been financed by the Norwegian Geotechnical Institute (NGI), the Research Council of Norway (RCN) through project Norwegian GeoTest Sites (NGTS) Grant No. 245650, and Norway-America Association's (NORAM) Graduate Study and Research Scholarship Program. Any opinions, findings, and conclusions or recommendations expressed in this material are those of the author(s) and do not necessarily reflect the views of the NGI, RCN, NORAM. The support is gratefully acknowledged.

Table 3–1 Key initial, after consolidation and post-ISA data from IL oedometer and CAUC tests on block, disturbed and reconstituted Halden silt.

Test	Depth	Test type	Sample ₁₎	w_i	γ_t	$e_i^{2)}$	$e_c^{2)}$	$\varepsilon_{vc}^{2)}$	$\varepsilon_{vol}^{2)}$	$\Delta e/e_0$	$V_{vh,0}/V_{vh,SDMT}^{3)}$	$V_{vh,ISA}/V_{vh,0}^{3)}$	$V_{vh,p-ISA}/V_{vh,0}^{3)}$	$\Delta e/e_0^{4)}$ p-ISA
(-)	(m)	(-)	(-)	(%)	(kN/m ³)	(-)	(-)	(%)	(%)	(-)	(-)	(-)	(-)	(-)
HALB04-10-2-A1	11.5	IL	SB	27.8	19.25	0.76	0.74	1.38	1.38	0.032				
HALB04-10-2-A2	11.5	IL	SB	25.3	19.22	0.73	0.71	1.29	1.29	0.031				
HALB04-Batch3-1	-	IL	SD	30.1	19.53	0.77	0.68	5.18	5.18	0.119				
HALB04-10-1-A2	11.5	CAUC	SB	28.0	19.37	0.74	0.72	0.72	0.99	0.024	0.83			
HALB04-10-1-B1	11.5	CAUC	SB	27.3	19.39	0.73	0.71	0.78	1.10	0.026	0.83			
HALB04-10-1-D2	11.5	CAUC	SB	26.8	19.47	0.72	0.71	0.54	0.56	0.014	0.85			
HALB04-10-1-C2	11.5	ISA±0.5%	SB	25.9	19.32	0.72	0.70	0.65	1.12	0.026	0.86	0.70	1.01	0.010
HALB04-10-1-B2	11.5	ISA±1%	SB	27.7	19.39	0.73	0.71	0.70	1.15	0.027	0.84		1.03	0.017
HALB04-10-1-C1	11.5	ISA±1%	SB	26.5	19.44	0.71	0.69	0.86	1.29	0.031	0.87	0.56	1.01	0.017
HALB04-10-1-D1	11.5	ISA±3%	SB	27.4	19.47	0.72	0.71	0.55	0.79	0.018	0.85	0.41	0.99	0.039
HALB03-9-A1	11.6	CAUC	NGI54	27.9	19.55	0.72	0.71	0.90	1.08	0.026	0.83			
HALB06-4-D1	11.4	CAUC	GP-S	28.2	20.34	0.65	0.65	1.11	1.06	0.024	0.84			
HALB04-Batch1-1	-	CAUC	MT	28.0	19.32	0.75	0.70	2.08	2.40	0.056				
HALB04-Batch1-2	-	CAUC	MT	28.1	19.30	0.75	0.73	2.00	1.33	0.031				
HALB04-Batch1-3	-	CAUC	SD	28.1	19.30	0.75	0.71	2.55	2.14	0.049				
HALB04-Batch1-4	-	CAUC	SD	27.2	19.43	0.73	0.70	1.77	1.33	0.032				
HALB04-Batch1-5	-	ISA±1%	SD	27.5	19.40	0.73	0.70	2.65	2.02	0.048				0.026
HALB04-Batch1-6	-	ISA±3%	SD	28.0	19.31	0.75	0.70	3.28	2.52	0.059				0.066
HALB04-Batch2-1	-	CAUC (w/creep)	SD	26.6	19.51	0.71	0.67	3.02	2.36	0.056				

Note: ¹⁾ SB = Sherbrooke Block, NGI54 = NGI 54mm composite piston sampler, GP-S = Gel Push sampler, MT= Reconstituted, Moist Tamping, SD = Reconstituted, Slurry Deposition; ²⁾ Void ratio after preparation (e_i) and after consolidation to best estimate in situ stress conditions (e_c), vertical (ε_{vc}) and volumetric (ε_{vol}) strains after consolidation; ³⁾ Shear wave velocity from bender elements after consolidation ($V_{vh,0}$), after ISA imposed strain ($V_{vh,ISA}$), post-ISA reconsolidation ($V_{vh,p-ISA}$) and in situ shear wave velocity from seismic flat dilatometer, SDMT ($V_{vh,SDMT} = 178$ m/s), (Blaker et al. 2019). $V_{vh,0}$ averaged 151.3 m/s for all bender element tests on block sample specimens ($n = 8$, $SD = 2.56$ m/s); ⁴⁾ e_0 was taken as the pre-ISA void ratio, e_c .

Table 3–2 Undrained shear strength of Halden silt Block 10 (11.5m) tests using Brandon et al. (2006) failure criteria for dilating soils.

Sample or Test Type	$A_f = 0$		$A_f = 0.25$		$(\sigma'_1/\sigma'_3)_{\max}$		u_{\max}		K_f line		$\varepsilon_{v,f} = 5.0\%$	$\varepsilon_{v,f} = 10\%$	$(\sigma'_1 - \sigma'_3)_{\max}$
	q_f (kPa)	ε_f (%)	q_f (kPa)	ε_f (%)	q_f (kPa)	ε_f (%)	q_f (kPa)	ε_f (%)	q_f (kPa)	ε_f (%)	q_f (kPa)	q_f (kPa)	q_f (kPa)
<i>Sherbrooke block and tube samples</i>													
Sherbrooke Block	83.7	10.4	61.6	2.9	69.6	4.8	50.3	0.9	69.8	4.8	69.7	83.8	93.6
Sherbrooke Block	83.1	11.0	62.3	3.3	76.9	7.2	49.1	1.0	76.4	7.1	71.5	82.3	90.0
Tube (NGI 54)	89.6	5.2	62.8	2.0	85.9	4.7	52.1	1.0	84.7	4.7	88.0	120.8	148.7
Tube (GP-S)	94.1	8.1	67.9	3.5	67.0	3.4	53.5	1.6	66.7	3.4	77.4	102.1	118.5
<i>Ideal Sampling Approach (ISA)</i>													
± 0.5% ISA	87.2	6.8	57.8	1.0	87.8	7.0	56.1	0.8	85.6	6.9	79.8	93.0	98.6*
± ~1.0% ISA	85.9	5.5	52.1	0.5	89.6	6.0	59.7	1.0	88.7	6.0	83.5	98.9	111.8
± 1.0% ISA	86.8	5.1	54.4	0.4	94.5	6.9	57.2	0.6	90.9	5.9	85.2	101.4	110.9*
± 3.0% ISA	88.6	3.3	59.5	1.2	105.8	5.2	48.4	0.6	106.2	5.2	105.0	131.3	153.0

Note: $(\sigma'_1 - \sigma'_3)_{\max}$ at end of test, i.e. at about 20% vertical strain. * Specimen did not reach 20% vertical strain but stopped at about 15%.

Table 3–3 Undrained shear strength of Halden silt MT and SD (11.5m) tests using Brandon et al. (2006) failure criteria for dilating soils.

Sample or Test Type	$A_f = 0$		$(\sigma'_1/\sigma'_3)_{\max}$		u_{\max}		K_f line		$\varepsilon_{v,f} = 5.0\%$	$(\sigma'_1 - \sigma'_3)_{\max}$		
	q_f (kPa)	ε_f (%)	q_f (kPa)	ε_f (%)	q_f (kPa)	ε_f (%)	q_f (kPa)	ε_f (%)	q_f (kPa)	q_f (kPa)	ε_f (%)	
<i>Reconstituted specimens</i>												
MT, Undisturbed	-	-	33.0	7.5	31.4	5.7	33.0	7.5	30.8	40.5 (36.1)*	15.4 (0.1)*	
MT, Undisturbed	-	-	23.2	6.5	23.2	6.8	23.3	6.7	23.5	36.0*	0.1*	
SD, Undisturbed	-	-	30.4	9.3	26.4	5.0	31.2	9.9	26.4	41.5 (34.2)*	19.9 (0.1)*	
SD, Undisturbed	-	-	27.7	8.8	25.4	5.5	27.8	8.9	25.3	36.5 (34.6)*	19.5 (0.04)*	
<i>Ideal Sampling Approach (ISA)</i>												
SD, $\pm 0.5\%$ ISA	-	-	39.5	8.4	37.1	5.1	39.6	8.4	37.0	49.5 (38.7)*	19.9 (0.4)*	
SD, $\pm 3.0\%$ ISA	78.1	13.8	59.0	6.9	44.1	2.1	59.2	6.9	53.3	88.5	19.9	

Note: * Low strain peak shear stresses, i.e. peak shear stress prior to strain hardening behavior.

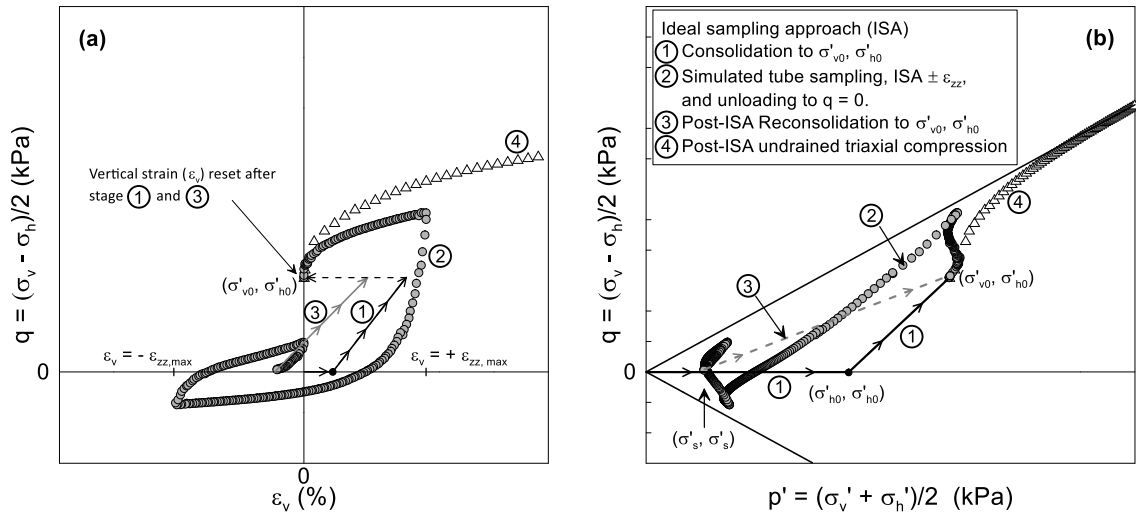


Figure 3.1 Ideal sampling approach (ISA, Baligh et al. 1987) concept illustrated by (a) shear stress versus vertical strain, and (b) stress path plots. – data for block sample specimen of Halden silt.

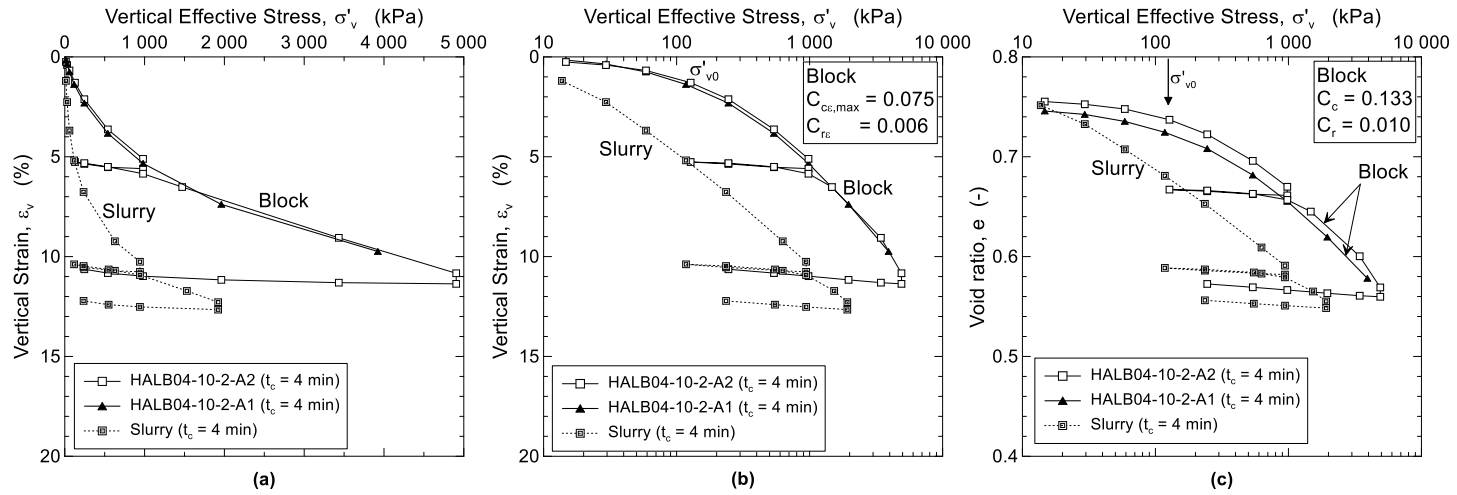


Figure 3.2 1D consolidation of Sherbrooke block and reconstituted (slurry) Halden silt. Vertical effective stress versus vertical strain on (a) linear and (b) semi - log axis, and (c) void ratio versus log stress.

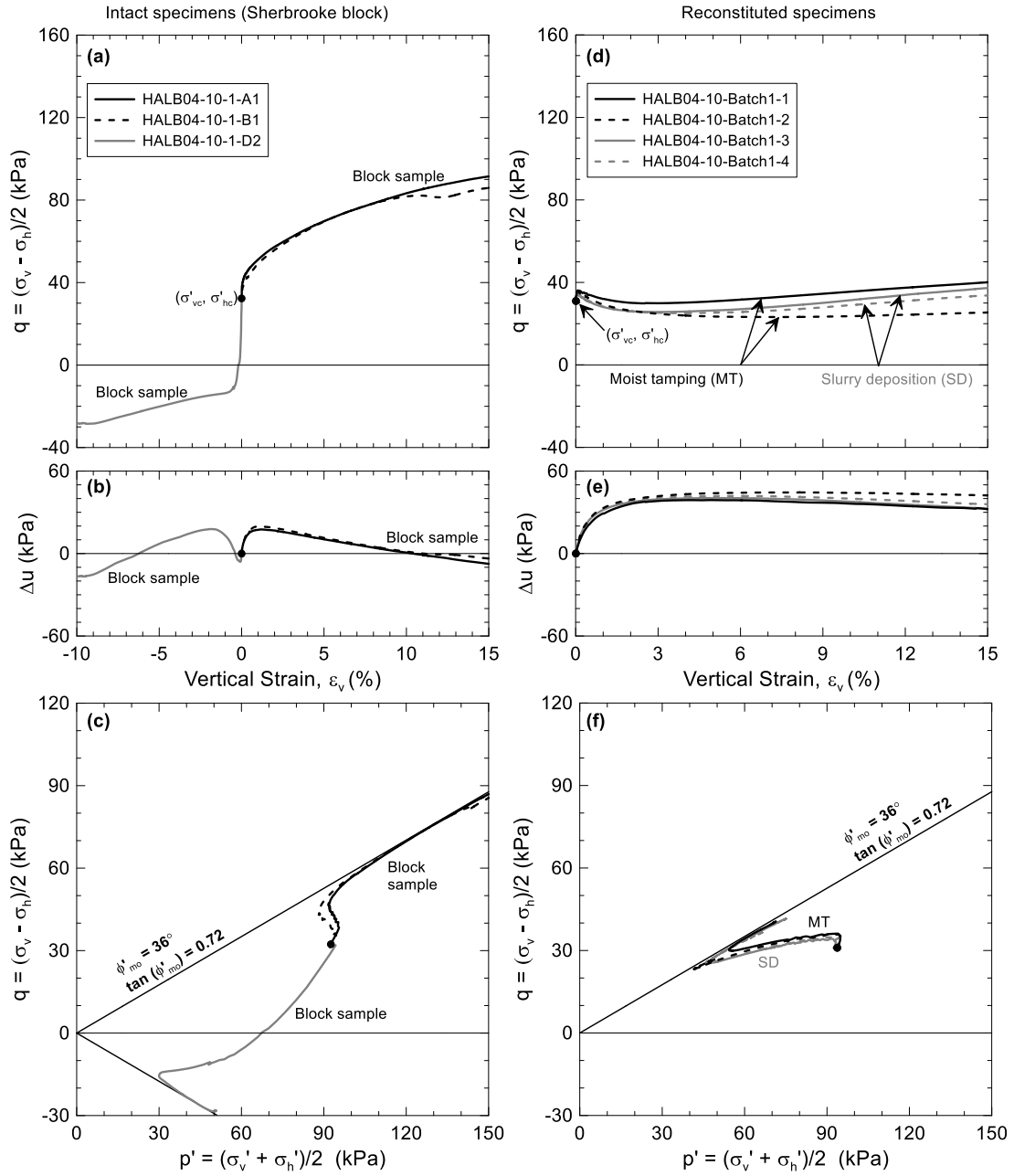


Figure 3.3 Undrained shear behavior of (a to c) Sherbrooke block and (d to f) reconstituted Halden silt.

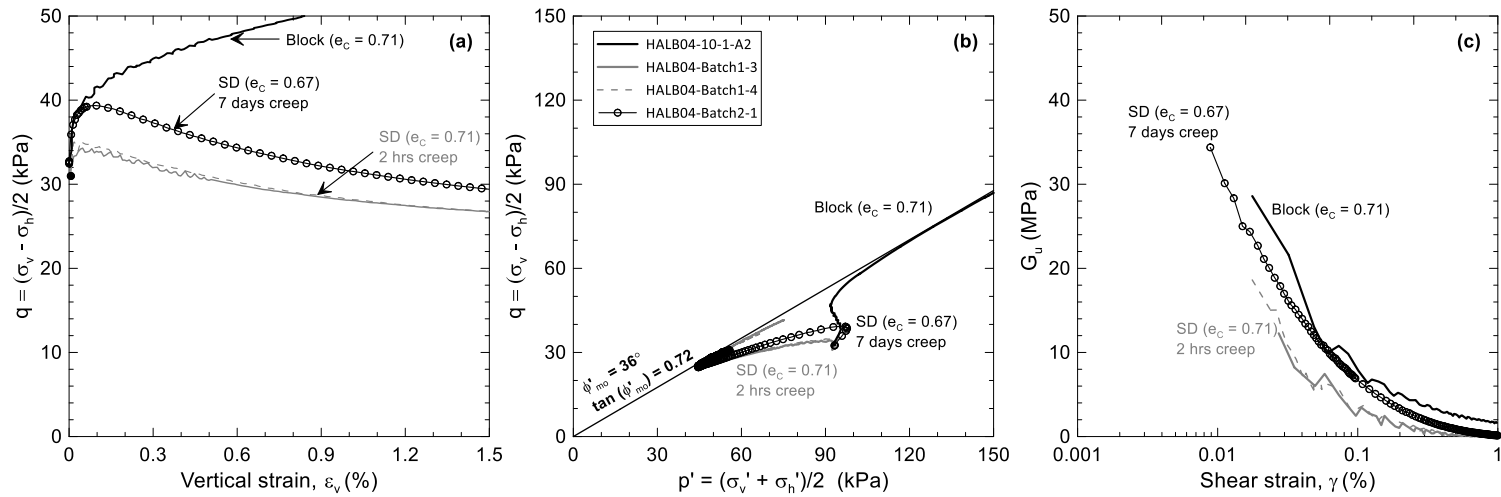


Figure 3.4 "Aging" effect on undrained triaxial compression shear behavior of reconstituted (slurry) Halden silt. (a) Stress - strain, (b) stress - path, and (c) shear modulus reduction with shear strain.

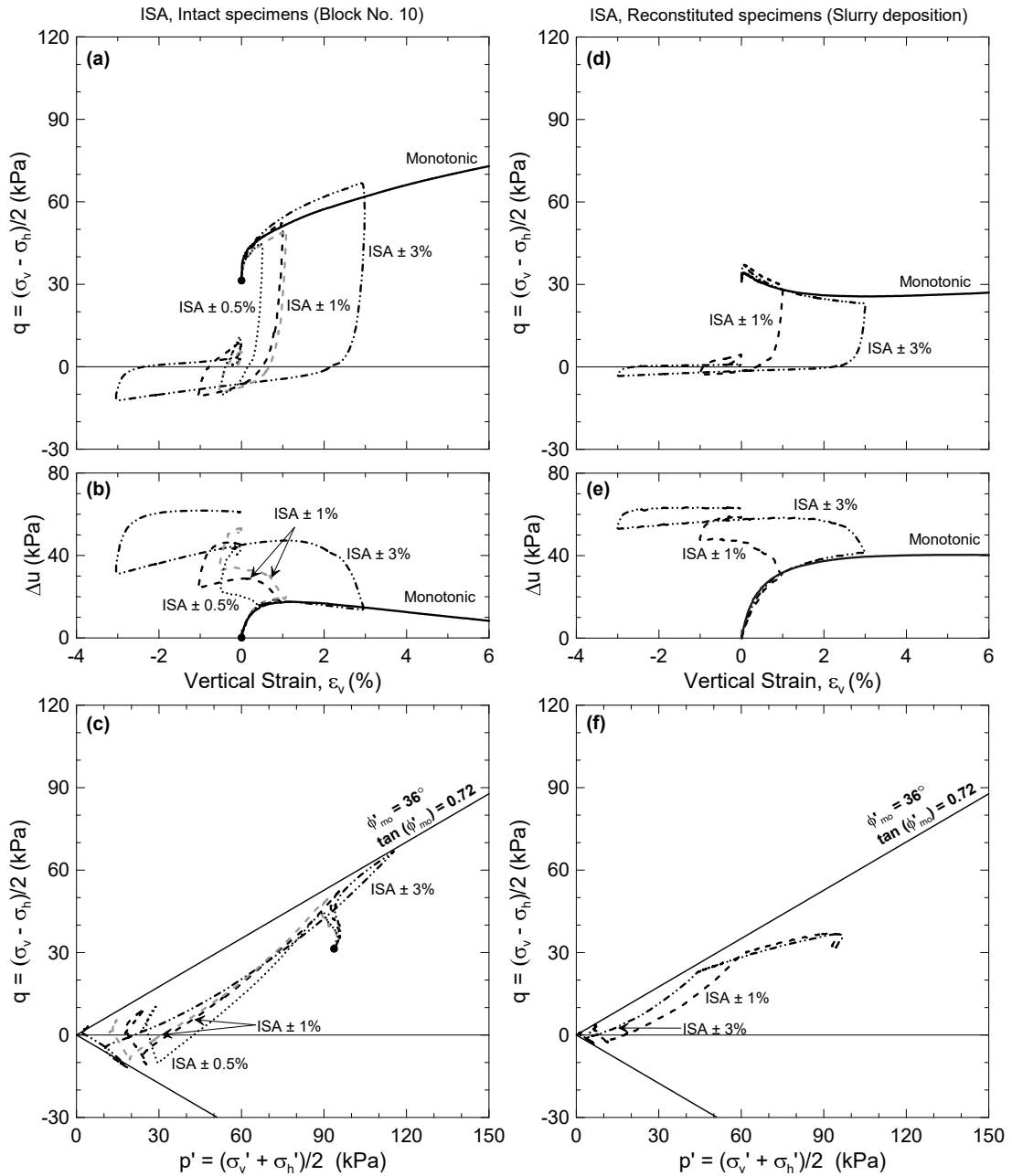


Figure 3.5 ISA strain cycling behavior from triaxial tests on (a to c) block, and (d to f) reconstituted (slurry) Halden silt.

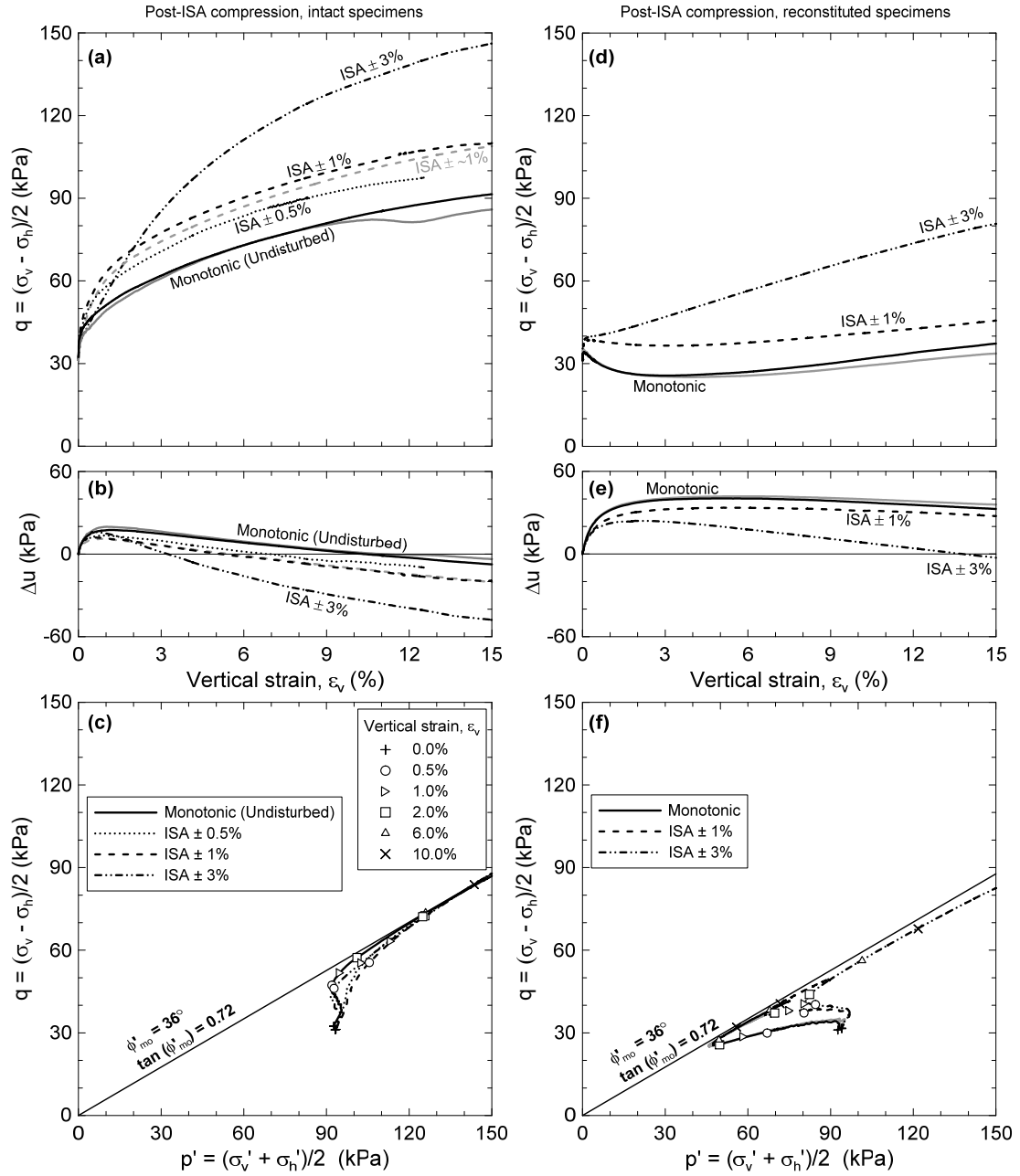


Figure 3.6 Post-ISA undrained shear behavior from triaxial tests on (a to c) block, and (d to f) reconstituted (slurry) Halden silt.

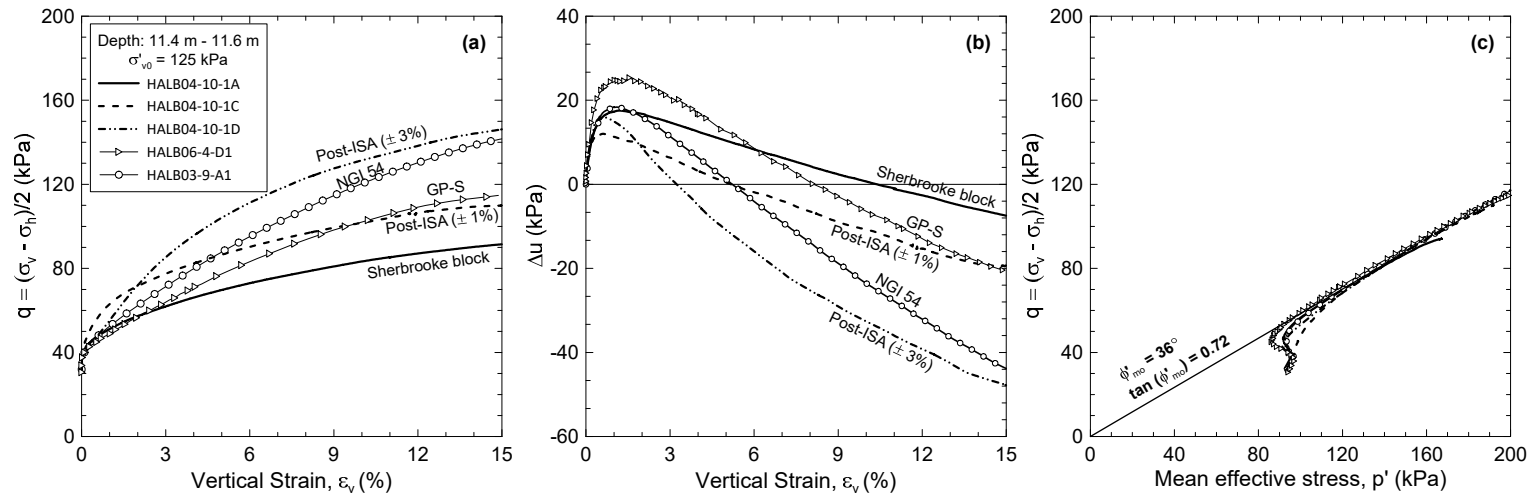


Figure 3.7 Effect of simulated (ISA, Baligh et al., 1987) and true sample disturbance on undrained shear behavior of Halden silt. (a) Stress - strain, (b) pore pressure - strain, and (c) stress - path.

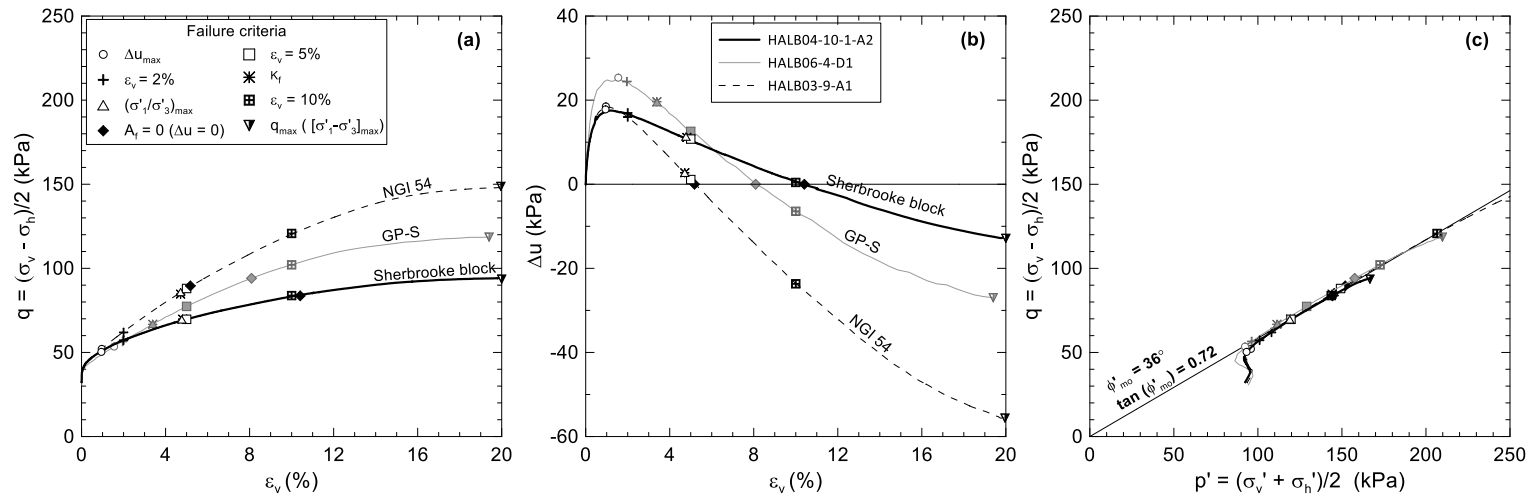


Figure 3.8 Undrained shear strength criteria (Brandon et al.2006) illustrated for CAUC tests on three types of Halden silt samples (NGI 54, GP-S and Sherbrooke block). (a) Stress – strain, (b) pore pressure - strain, and (c) stress - path.

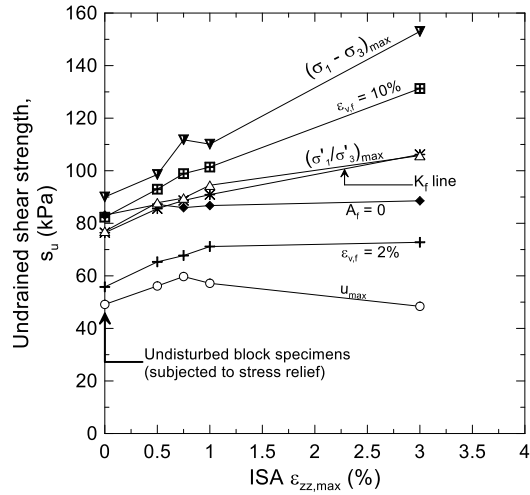


Figure 3.9 Effects of simulated sampling disturbance (ISA, Baligh et al., 1987) on selection of undrained shear strength from CAUC tests on Sherbrooke block samples of Halden silt for various criteria (data in Table 3-2).

CHAPTER 4

EFFECTS OF SAMPLING TECHNIQUES ON MATERIAL BEHAVIOUR AND ENGINEERING PROPERTIES OF LOW-PLASTICITY NATURAL SILT

The National GeoTest Site (NGTS) for silts in Norway was used to assess the effects of sampling techniques on stress-strain behaviour and engineering properties of low-plasticity natural silt. Advanced tests results on specimens collected using the Sherbrooke block and three different tubes samplers are presented creating an important silt behaviour database. Tests include oedometer, triaxial and bender element tests at parallel depth intervals in adjacent boreholes. There are currently no universal quantitative sample quality criteria valid for low-plasticity silts, and as a result, comparison of material behavior using stress-strain characteristics and changes in index properties were used in this study to qualitatively assess sample quality. Advanced test results showed that acceptable and repeatable sample quality or stress-strain behaviour could be obtained using the 72mm piston and GP-S samplers. Sherbrooke block samples, however, showed high variability whereas the 54mm composite samples exhibited obvious signs of disturbed behaviour. Clay-based sample quality criteria, using recompression strain and shear wave velocity, and the oedometer strain energy-based framework for low plasticity soils showed contrasting results and overall these methods yielded misleading quality analysis of the samples in this study.

4.1 Introduction

There is an increasing awareness in the geotechnical community that little guidance exists for quantitative classification of sample quality for silts. The state of the art framework for sample quality assessment of low to medium overconsolidation clays,

using $\Delta e/e_0$ criteria (Lunne et al. 1997), were not developed for silts and an increasing number of studies have confirmed that this approach is inappropriate and presents a misleading assessment of quality for silts (Carroll 2013; Pineda et al. 2013; Carroll and Long 2017; DeJong et al. 2018; Lukas et al. 2019; Blaker and DeGroot In press). A detailed review of previous experience in sampling and the current status of evaluation of sample disturbance for silts was presented by Carroll and Long (2017). They presented laboratory tests from parallel block and piston samples from the Letterkenny, Ireland and Refneveien at Halden, Norway silt sites. Results showed identical specimen responses for Refneveien and similar for Letterkenny indicating that good quality silt samples were attainable with these techniques, where sampling was likely to be undrained. At Skibbereen, Ireland (a site containing a non-plastic silt with less fines and greater potential for drainage during sampling) significant densification of the piston samples occurred which led to stiffer and higher strengths than would be expected in situ for undrained conditions. The Authors concluded that evaluation of sample quality based on engineering behaviour alone was not sufficient and in situ tests, e.g. the Cone Penetration Test (CPTU), should be included for comparison to in situ conditions.

Studies on tube sampler geometry and its association with centreline strains experienced by the soil sample (e.g. Baligh et al. 1987; Clayton and Siddique 1999) have highlighted the importance of a high diameter to wall thickness ratio (D_w/t), small area ratio (AR) and low taper angle to collect high quality samples in clays. Using the Ideal Sampling Approach, ISA (Baligh et al. 1987), centreline tube sample disturbance can be simulated in the laboratory by applying a strain cycle of axial strains (ϵ_a) using a triaxial stress path cell system. Carroll and Long (2017) presented the first results of ISA tests on

block samples of silt from the Letterkenny, Ireland site. Axial strains in the order of $\pm 0.6\%$, representative of the centreline strain caused by thin walled piston tubes, and subsequent reconsolidation to the estimated in situ vertical and horizontal effective stress (σ'_{v0} , σ'_{h0}) resulted in little change to the material behaviour. However, axial strains between 1% and 3%, the latter reflective of the centreline strain induced by a poor geometry composite sampler (Clayton and Siddique 1999), resulted in an increase in undrained shear strength (s_u) and increased secant shear stiffness (G) at a given strain. The stress path plot was flatter and there was a greater tendency for dilative type behaviour with increased strain damage. Conclusions from similar experimental sample disturbance simulations on synthetic specimens of low-plasticity silt-mixtures by Lukas et al. (2019) were decreasing initial pre-peak stiffness, decreasing strain softening response and increasing s_u and strain to failure with increased strain damage. Most recently, Blaker and DeGroot (In press) presented results of strain damage testing on a block sample of silt from the Halden NGTS site at 11.5 m depth. Results showed that increasing the degree of simulated sampling disturbance altered the specimens' undrained shear behaviour, resulting in a significant increase in the tendency for dilative behaviour. Companion triaxial results from Sherbrooke block and NGI 54mm composite piston sampler showed that the stress-strain behaviour and net negative pore pressure development during undrained shear increased at a significantly larger rate for the poor geometry sampler compared to the block sample.

Høeg et al. (2000) and Blaker and DeGroot (In press) found dramatic differences between undisturbed and reconstituted silt specimens; dilative and ductile versus contractive respectively, despite specimens having the same void ratio. Wang and Luna

(2012) tested reconstituted silt specimens and reported initial contraction followed by dilation for normally consolidated (NC) tests. They found a greater initial contractive response for NC specimens compared to overconsolidated specimens. Researchers also found that s_u/σ'_{vc} increased with increased overconsolidation ratio, OCR (Fleming and Duncan 1990; Yasuhara et al. 2003; Page 2004; Izadi 2006; Wang and Luna 2012). Wang and Luna (2012) concluded that clay content and particle shape were important controlling factors for this response, s_u/σ'_{vc} was less affected by OCR for low plasticity index (I_p) silts compared to clays, and OCR did not affect the effective stress friction angle (ϕ') as no memory of stress history was retained. Reconstituted specimens were not used in this study as the in situ soil fabric and stress history at Halden could not be recreated through reconstitution.

In recent years a focus on vertically (v) propagating horizontally polarized (h), shear wave velocity (V_{vh}) measurements on unconfined specimens (V_{vh-0}) to quickly and non-destructively evaluate sample quality has occurred. Studies by Hight and Leroueil (2003), Nash (2003) and Landon et al. (2007) demonstrate the effectiveness of these on-site tests to evaluate sample quality for clays. Donohue and Long (2010) concluded that V_{vh-0} measurements correlated best with traditional assessment of disturbance and presented quantitative sample quality criteria for clay. Viana da Fonseca et al. (2019) presented a quantitative analysis of sample quality based on the normalized shear wave velocity, $V_s^* = V_{vh}/\sqrt{F(e)}$ (Ferreira et al. 2011), where $F(e) = e^{-1.3}$ (Presti et al. 1997) and accounts for changes in void ratio from in situ state to the consolidated state of the specimen in a triaxial cell. Samples of loose sands to silty sands from Benavente, Portugal were collected using two different fixed piston tube samplers, and shear wave

velocity results suggested largely excellent to very good sample quality for these soils and the samplers used. Most recently, DeJong et al. (2018) proposed a framework for evaluating sample quality of intermediate soils using the strain energy-based compression ratio, $C_{rw,i}/C_{cw}$ from constant rate of strain (CRS) consolidation tests on synthetic mixtures of non-plastic silts and clays as well as results from previously published studies. However, all these quantitative sample quality criteria require application to a robust study on silt samples for evaluation of usefulness.

Developments in soil sampling equipment has produced the commercially available Gel Push Static (GP-S) sampler (Tani and Kaneko 2006). Taylor et al. (2012) reported use of the GP-S as promising with initial recovery of very good silty sand samples based on qualitative evaluation of samples at Christchurch, New Zealand. The Authors noted potential for densification of loose sandy silts with $V_s < 150\text{m/s}$, and improvements to design and sampling procedures to avoid this. Kiso-Jiban Consultants (2013) trailed the GP-S and Gel Push Triple (GP-Tr) samplers at Zelazny Most Tailings in Poland. Recovery was reported as good to moderate using the GP-S and the sampler was suggested more effective for sampling very loose, saturated or unsaturated, sand and soft clay. The GP-Tr was found to be more suitable for loose to dense conditions. Stringer et al. (2015) reported very similar cyclic resistance relationships from samples collected using both the Dames & Moore and GP-S samplers for high soil behaviour type index (I_c) material (clayey silts) at Christchurch New Zealand. Comparison of in situ shear wave velocity ($V_{vh,in-situ}$) with measurements of V_{vh} on specimens consolidated to σ'_{v0} ($V_{vh-\sigma'_{v0}}$) showed good agreement for the low I_p silty sand. Huang (2016) recovered silty sand samples using the GP-S at sites in Western and Southern Taiwan and reported

good quality. Similarly, Bray et al. (2017) reported good quality GP-S from Christchurch silty sand. However, all these studies report qualitative sample quality evaluations.

This paper investigates the effects of sampling techniques by way of comparison of 1-D consolidation, undrained and drained triaxial shear behaviour of a natural silt. Soil samples were collected at the national test site for silt at Halden, Norway using four different samplers selected to provide advanced laboratory test specimens in both disturbed and acceptable states. The usefulness of quantitative sample quality criteria, using V_{vh} and the strain energy-based framework, are evaluated for the first time together on this soil type.

4.2 In situ and laboratory test techniques

Soil sampling was conducted below the ground water table using the Sherbrooke block sampler (Lefebvre and Poulin 1979), Geonor K-200 72mm inner diameter (ID) piston sampler, NGI 54mm inner diameter (ID) composite (with plastic liner) piston sampler (referred to hereafter as 54mm(L)) (Andresen and Kolstad 1979) and 71.5 mm ID Japanese GP-S sampler (Tani and Kaneko 2006). Each borehole was dedicated to a single sampler type in order to collect samples at parallel depths with different samplers and all samples were collected using traditional techniques associated with their use in Norway (Andresen and Kolstad 1979; Lefebvre and Poulin 1979; Lacasse et al. 1985; Lunne et al. 1997; Lunne et al. 2006). Further details, definitions and geometries of the different samplers are presented in the supplemental section (Section 4.8). The GP-S technique (Tani and Kaneko 2006; Taylor et al. 2012) required some modifications to set up following initial trials by the Norwegian Geotechnical Institute (NGI) drillers after

which sampling was successful. Drainage conditions during tube sampling were likely to be associated with some degree of partial drainage (Carroll and Paniagua López 2018). In this study it was initially assumed that the Sherbrooke block samples, if carefully collected, transported, cut, trimmed and subjected only to stress relief upon retrieval, could be considered the best representation of in situ soil state and behaviour. Whereas the NGI 54mm composite sampler, with its poor geometry and well documented disturbance effects in clays (Tanaka et al. 1996; Lunne et al. 1997; Long 2006; Lunne et al. 2006; Long and Donohue 2010), was chosen to represent a high degree of sample disturbance. As the 72 mm sampler has been found to obtain silt samples of similar quality as block samples (Carroll and Long 2017), and to induce limited strain damage on clay samples (with centreline axial strains approximately equal to $\epsilon_a = 0.6\%$, as suggested by Clayton and Siddique (1999)), this thin walled piston sampler was chosen to assess its performance in comparison to the assumed high quality (acceptable) block and poor quality 54mm(L) (disturbed) samples.

All tube samples were extruded vertically in the NGI laboratory. Triaxial specimens were mounted on the triaxial pedestal directly after extrusion using the diameter (d) equal to the inside diameter of the sampler, i.e. $d = 54 \text{ mm} - 72 \text{ mm}$, and a height diameter ratio of about 2. Exceptions were two 72 mm sample specimens from 7.6 m and 12.6 m depth tested at University of Massachusetts (UMass) Amherst which had $d = 35 \text{ mm}$. Block sample specimens were generally trimmed to $d = 70 \text{ mm}$ using a height diameter ratio of 2, with the exception of one specimen from 11.5 m depth which had $d = 54 \text{ mm}$ (Blaker and DeGroot In press). Triaxial test specimens were mounted, consolidated and sheared in accordance with NGI standard practice (Berre 1982; Lacasse

et al. 1985) and as detailed by Blaker et al. (2019). Except for one K_0 consolidated undrained triaxial test in compression (CK₀UC), specimens were anisotropically consolidated to the best estimate in situ vertical effective stress ($\sigma'_{vc} = \sigma'_{v0}$) and horizontal effective stress ($\sigma'_{hc} = \sigma'_{h0}$) using an assumed $K_0 = 0.5$ (Blaker et al. 2019). The K_0 consolidated specimen was loaded directly to the best estimate σ'_{v0} and yielded $K_0 = 0.55$ at end of consolidation. It is noted, however, that 1-D consolidation directly to σ'_{v0} have been shown to produce too low values of K_0 for clays (Mesri and Hayat 1993). B values, which were measured at the end of the consolidation phase, were generally $\geq 97\%$ except for three specimens with measured B values of 93%, 96% and 95%. Shearing was strain-controlled at 0.5 – 1.4 %/hr for all K_0 and anisotropically consolidated undrained (CAUC) and drained (CADC) triaxial compression tests. All stress measurements were corrected for membrane resistance and changes in specimen area (Berre 1982).

CRS oedometer tests were conducted as per Sandbækken et al. (1986) using initially dry porous filter stones and a strain rate of about 5.4 %/hr. Specimen areas were primarily 20 cm² to reduce variability and allow better comparison with the 54mm(L) specimens. Exceptions were specimens from the 72mm sampler (borehole HALB01) which were all 35 cm².

Measurements of in situ shear wave velocity ($V_{vh \text{ in-situ}}$) with depth were conducted using seismic CPTUs and one seismic flat dilatometer, SDMT, (Blaker et al. 2019). Interpretation methodologies of $V_{vh \text{ in-situ}}$ at the site are described in the supplemental section (Section 4.8). Bender element tests were carried out on the laboratory triaxial test specimens (Dyvik and Madshus 1985; Dyvik and Olsen 1989) using a vertically propagating (v) horizontally polarized (h) shear wave to estimate velocity (V_{vh}) at the

estimated in situ vertical effective stress using peak to peak to select travel time. Unconfined shear wave velocity (V_{vh-0}) tests were carried out on most sample types except for the 72 mm samples (borehole HALB01). Unconfined specimen height ranged from 30 mm to 70 mm and a combination of peak-to-peak and first-cross-over values of travel time were used to evaluate V_{vh-0} . Signal transmission in remolded silt specimens, with initial water content maintained, was challenging and few values of remolded shear wave velocity ($V_{vh rem}$) on unconfined specimens were obtained. Suction measurements were attempted in the laboratory directly on extruded sample sections. However, results were poor to none, hence no suction data is presented in this study.

4.3 Results

Samples were collected from five separate boreholes from 4.5 m to 14.6 m (Blaker et al. (2019): HALB01 – 72 mm, HALB03 – 54 mm(L), HALB04 – Sherbrooke block, HALB05 and HALB06 – GP-S. The driller's log from borehole HALB04 (supplemental section, Section 4.8) provided an important contribution in the evaluation of block quality. Typical average classification properties include 22 - 30% for water content (w_i), 5 - 10% for I_p , 70 - 80% for silt content and 7 - 12% for clay content (Table 4-1, Figure 4.1). Relative to the other samplers the GP-S shows a trend of higher w_i with depth. It believed that higher w_i is representative of in situ conditions. However, it is not possible to quantify potential absorption of liquid from the gel into the GP-S samples. The liquid limit values of $w_L = 26 - 37\%$ were determined using the fall cone method (ISO 2018) and equivalent values of the Casagrande cup liquid limit were estimated to be in the range of $w_{L,CC} = 21\% - 34\%$ based on DeGroot et al. (2019)

resulting in $I_{p,CC} = 9\% - 1\%$. This classifies the Halden silt as ML according to the Unified Soil Classification System (ASTM 2018), see Figure 4.1(d). For reference, values of the sample quality indicator for clays, $\Delta e/e_0$, from CRS oedometer and triaxial tests on Halden silt specimens are presented with the Lunne et al. (1997) sample quality boundaries in Figures 4.1(e-f). These results will be referenced with respect to sample quality and its application to silts in subsequent sections.

4.3.1 CRS behavior

Figures 2(a-c) present CRS results of tests from three depth intervals; (i) 4.4 - 5.5 m, (ii) 7.0 - 10.4 m, and (iii) 12.7 - 14.6 m. A summary of CRS specimen properties, test results and qualitative sample quality evaluation is presented in the supplemental section, Section 4.8. Relative to the representative water content profile w_i of the CRS specimens (Figure 4.1b) were generally on the lower bound with depth for all sampler types. This may be due to poor quality block samples which will be discussed further with respect to triaxial results in Section 4.3.2. Figure 4.1e shows that $\Delta e/e_0$ plot below 0.07 for all tests, with the poor geometry 54mm(L) sampler generally producing the lowest values and the GP-S sampler giving the highest. The oedometer data generally revealed no distinctive yield or preconsolidation stress (σ'_p) due to the flat nature of the compression curves (Figure 4.2) which confirms the behavior observed during 1-D compression in previous studies on silt (Long 2007; Long et al. 2010; Carroll and Long 2017; Blaker et al. 2019). The 72 mm and Sherbrooke block sample specimens at 4.4 - 5.5 m depth (Figure 4.2a) show similar responses while the 54mm(L) specimens show lower strains for given stresses. The 54 mm(L) tube at this depth suffered additional disturbance due to handling

as the tube was dropped prior to extrusion. In the 7.0 – 10.4 m depth interval (Figure 4.2b) three 54mm(L) specimens were tested and the results showed high repeatability and a similar material response plotting above block and GP-S sample specimens, confirming that poor handling can result in significant additional destructing, straining and or densification of a silt sample irrespective of initial quality. For the 12.5 - 14.6 m depth interval (Figure 4.2c), the CRS results from the block and 54mm(L) sample specimens plot together, with significantly lower vertical strains for any given stress relative to the results from the GP-S sample specimens. This suggests that the block from 14.6 m depth may be disturbed. The behaviour of the triaxial specimen from this block sample during shear (Section 4.3.2) agrees with the CRS response being similar to the disturbed 54mm(L) in this case.

The Janbu (1985) constrained modulus ($M = \Delta\sigma'_a/\Delta\varepsilon_a$) versus effective stress (Figures 2d - 2f) show similar findings to that from the semi-log plots of stress versus strain in that the stiffness of the Halden silt tend to increase with increasing disturbance. This is particularly pronounced for the mishandled and additionally disturbed 54mm(L) CRS specimen at 5.4 m depth, and the disturbed 54mm(L) and block sample specimens from about 14.5 m depth. In these tests, M at any given value of vertical stress, but also the slope of the constrained modulus curves in the normally consolidated stress range (modulus number, m) are higher than the results from the companion tests. In the 7.5 - 10.5 m depth interval the differences in response with sampler type is subtler, suggesting that the dramatic changes in values of M and m , observed for the other depth intervals, may not always occur.

CRS strain energy (Becker et al. 1987) results for the Halden silt are presented in the supplemental section (Section 4.8). The strain energy-based compression ratios, $C_{rv,i}/C_{cv}$ (DeJong et al. 2018) were in the range of 0.16 – 0.6, with the lowest value calculated from the mishandled and additionally disturbed 54mm(L) CRS specimen (Section 4.8). Disturbed specimens of Halden silt generally showed increased stress required to reach similar strains of acceptable quality silt samples.

4.3.2 Triaxial shear behaviour

Figure 4.3 shows normalised shear stress, $(\sigma_a - \sigma_r)/2\sigma'_{ac}$, and pore pressure, $\Delta u/\sigma'_{ac}$, with axial strain and stress-path during undrained triaxial shear in compression for three depth intervals; (i) 5.3m, (ii) 7.5 - 9.5 m, and (iii) 11.4 - 14.5 m. A summary of specimen properties, test results and qualitative sample quality evaluation of the nineteen CAUC tests and one CK₀UC test is presented in the supplemental section, Section 4.8. The majority of $\Delta e/e_0$ values plot below 0.04, with no systematic trend with sampling technique (Figure 4.1f). For all depth intervals the initial material response of the silt specimens upon undrained shear showed a tendency for contractive behaviour up to 0.5% - 2% axial strain for all specimens, independent of sampler type used (Figure 4.3). Thereafter, the behaviour changed to a dilative tendency and the stress paths tracked the failure envelope (K_f line). All tests exhibited effective stress friction angles, assessed at maximum obliquity $(\sigma'_1/\sigma'_3)_{max}$, of $\phi'_{mo} = 35.8^\circ \pm 1.2^\circ$. In the 5.3m depth interval the 54mm(L) sample specimen shows a more pronounced tendency for dilative behavior and a flat stress path compared to the block and 72mm sample specimens, which had a S-shaped stress-path. This has been suggested as indicative of sample disturbance in silts

(Carroll and Long 2017). However, from subsequent depth intervals the stress-paths for acceptable and disturbed samples both show this S-shape (or acceptable samples showing flat stress paths). This suggests that reliance on the initial shape of the stress path alone may be misleading as a generic qualitative sample quality indicator for silts.

At 5.3m depth the water content of the 72mm, Sherbrooke block and 54mm(L) sample specimens were similar ($w_i = 30 - 32\%$) and after consolidation void ratios (e_c) in the range of 0.78 – 0.83 (supplemental section, Section 4.8). Yet, during shear there was an increasing disparity between the different specimens with increasing axial strain. Figures 4.3(a-b) shows that the 72 mm and block sample specimens showed differences in stress – strain, but similar pore pressure development with axial strain, whereas the 54mm(L) sample specimen developed negative pore pressures at a significantly higher rate.

In the 7.5 - 9.5 m depth interval specimens pre-shear properties were 28% to 31% for w_i and 0.74 and 0.81 for e_c (supplemental section, Section 4.8). One 72mm specimen, however, suffered drying during transport from NGI to UMass Amherst and $w_i = 23\%$ was measured prior to testing. The result of this test is noted as "dried" in Figures 4.3(e-h) and the undrained shear behaviour appears to be significantly altered. The three GP-S sample specimens showed excellent repeatability and shear stresses and pore pressures plotted on and close to the 72 mm sample specimen result even though e_c for the former three specimens were higher. These results plotted above the results of the block sample specimen at 8.36 m depth, which was considered acceptable. The block sample specimen from 8.02 m (CK₀UC test), however, showed unexpected shear stress and pore pressure similarities with the companion 54mm(L) sample specimen during undrained shear.

Similarly, the CADC test specimen, also from 8.02 m depth, showed a significantly higher rate of shear stress development, more dilation (negative volumetric strains) and higher ϕ'_{mo} compared to the companion GP-S specimen at the same depth (Figure 4.4). These inconsistencies in block sample response are likely associated with issues during sampling. The driller's log (see supplemental section, Section 4.8) reported three attempts to release the cutting knives at block interval 7.6 - 7.9m depth (i.e. immediately above the 8.02 m block sample). No sample was recovered and, as a result of the repeated and likely extensive strain damage from the sampling attempts above, the laboratory undrained triaxial shear behaviour of the underlying block was altered.

All triaxial specimens in depth interval 11.4 - 14.5 m showed 23% to 31% for w_i and 0.58 and 0.77 for e_c (supplemental section, Section 4.8). The low water contents measured on some of the test specimens may be reflective of sample disturbance effects rather than to soil variability, as the increased sand fraction below 14 m depth (Table 4-1) is likely to have facilitated drainage of water from the soil during sampling. The three block sample specimens show conflicting responses with two of three results (from 12.58m and 14.60 m depth) exhibiting stress-strain and pore pressure similarities with the disturbed 54mm(L) sample specimens (Figures 4.3i to 4.3l). Further examination of sample photos, e.g. Blaker et al. (2019) and the driller's logs (supplemental section, Section 4.8) revealed that the block sample collected from 12.45 m – 12.80 m depth had obvious wedge-like failures at the base (from the retracting cutting knives of the Sherbrooke sampler) thus confirming the hypothesized damaged state suggested by the undrained triaxial test result, regardless of the upper portion of the block appearing visually intact. Similarly, the deepest block (from 14.45m - 14.8 m) is believed to have

experienced disturbance due to sampling difficulties immediately above. Figures 4.3i and 4.3j also show that relative to the block sample specimens from 11.5 m depth (Blaker and DeGroot In press) the two GP-S specimens generally developed similar normalised shear stresses and net negative pore pressures. There was no indication of disturbance induced to this block, based on field observations or sample photos, and the material response in undrained triaxial compression suggests this block to be of acceptable quality. Results reported by Blaker and DeGroot (In press) show that the 54mm(L) sample specimen from the same depth was overly disturbed.

In summary, using the 54mm(L) specimen behaviour to frame expected material response for disturbed specimens, the driller's log and block sample photos the results indicate that the Sherbrooke block sample specimens from 8.02 m, 12.58 m and 14.6 m depth and the two dried 72mm specimens are significantly altered by disturbance. These disturbed specimens all show considerably greater tendency for dilative type behaviour relative to the GP-S, 72 mm and acceptable block sample specimens. The 54mm(L) sample from 14.4m and block sample from 14.6m had very low w_i at about 23.3% and behave similarly to one another. Based on these two factors the samples are suspected to be disturbed.

4.3.3 Shear wave velocity

Figure 4.5a to 4.5e, and supplemental section (Section 4.8), present measured and normalised values of in-situ and laboratory shear wave velocity tests. The representative profile of in situ shear wave velocity, $V_{vh,in-situ\ avg}$, comprising of only reliable measurements is shown in Figure 4.5a. It is used in the normalisation of laboratory V_{vh}

results for analysis of sample quality. From the evaluation of undrained triaxial shear behaviour and observations from CRS results (Sections 4.3.1 to 4.3.2) qualitative specimen quality designations 'disturbed' (grey) or 'acceptable' (black) are assigned to results shown in Figures 4.5b to 4.5e. For the triaxial specimens in Figure 4.5b there is a trend of 10–20% under prediction of $V_{vh-\sigma_{vo}}$ relative to $V_{vh,in-situ\ avg}$ irrespective of quality designation. Donohue (2005) noted that reconsolidation of laboratory test specimens back to in situ stress state provides some repair of sample disturbance in clays, and thus, masking effects of disturbance on $V_{vh-\sigma_{vo}}$ values - which in turn yields an evaluation of sample quality based on $V_{vh-\sigma_{vo}}/V_{vh,in-situ}$ to be misleading. This observation was confirmed by simulated disturbance testing conducted on Halden silt by Blaker and DeGroot (In press) where post-disturbance shear wave velocities were completely recovered upon reconsolidation to pre-disturbance stress conditions. The ratio of $V_{vh-\sigma_{vo}}^*$ to $V_{vh,in-situ}^*$ is presented in Figure 4.5c with sample quality criteria proposed by Ferreira et al. (2011), where the in situ void ratios are calculated based on the representative w_i line (Figure 4.1a) and a unit weight of solid particles (γ_s) of 2.7. The results plot in a different sequence than $V_{vh-\sigma_{vo}}/V_{vh,in-situ}$ (Figure 4.5b) indicating the effect of change in e after reconsolidation. Certain results from specimens considered acceptable plot on the upper end of the scale however some plot together with those from disturbed specimens. This indicates that evaluation of sample quality with this criterion may be misleading based on the number of tests available in this study. Assessment of $V_{vh-\sigma_{vo}}^*$ from bender element tests conducted after strain damage tests at Halden (Blaker and DeGroot In press) showed negligible change in $V_{vh-\sigma_{vo}}^*$ following significant strain damage relative to the intact reference specimen. This suggests that the shear wave may recover from this level of

strain damage or the soil and its' fabric are relatively insensitive to such disturbance effects using this parameter. Assessments of sample quality using the frameworks proposed by Landon et al. (2007) and Donohue and Long (2010) for testing unconfined clay specimens are presented in Figure 4.5d to Figure 4.5e, respectively, with qualitative specimen quality designations 'disturbed' (grey) or 'acceptable' (black) are assigned to the Halden V_{vh} data. V_{vh-0} results from two block sample specimens have no companion triaxial tests for guiding the quality of the blocks but based on an overall evaluation of the direct simple shear (DSS) test behaviour of the same two blocks (DSS tests not included in this paper), indications are that the samples were disturbed. Irrespective of assigned quality, based on consistent trends for material behaviour from triaxial tests and drillers logs, for any individual sample the shear wave sample quality criteria present a misleading and unreliable representation of quality as samples considered acceptable and disturbed plot on top of each other or with assigned quality plotting at the opposite end of the quality scale.

4.4 Discussion

The field work demonstrated that both tube and Sherbrooke block samples could be collected in a low plasticity natural silt. Visual inspection of laboratory specimens or use of different quantitative quality assessment methods for clays or low I_P soils such as $\Delta e/e_0$, strain energy-based recompression ratio or shear wave velocity criteria, did not identify disturbed and acceptable samples in accordance with the qualitative sample quality approach used herein. Low values of recompression volumetric strains and $\Delta e/e_0$ for all sample types, even from one CRS test conducted after dropping the sample tube to

the floor, confirm recent studies that suggest that these consolidation metrics are ineffective indicators of sample quality in silts.

Sherbrooke block sampling, which was initially assumed to provide consistently high quality, proved challenging as the cutting knives did not always release. As noted by Blaker et al. (2019) this may be due to silt size particle accumulation within the equipment, thereby stopping operation of moving equipment parts. Repeated attempts at the same depths typically resulted in subsequent disturbance or loss of sample, and in some cases disturbance to the soil immediately below the sampling interval. Similar observations were also reported during piston sampling by Carroll and Long (2017) at Skibbereen, Ireland, and highlights the importance of a detailed drillers log when tracing the history of a recovered sample. Interestingly, of the nine Sherbrooke block samples collected at Halden (that were opened and tested in the laboratory) six were classified as disturbed to some degree (Section 4.8, Figure 4.8b). This implies that, in contrast to sampling in clays, the Sherbrook block sampler may not always provide high and consistent sample quality in silts. The composition of fines (clay and silt particles) and I_p of the soil may be a contributing factor influencing the level of success of block sampling and its' repeatability. In contrast, Carroll and Long (2017) reported no significant challenges during block and tube sampling of the clayey silt at the Refeneveien site, also located at Halden. Advanced testing of these block and 72 mm sample specimens showed excellent repeatability, demonstrating that from sampling to build in of clayey silt block specimens were successful. Furthermore, sealing, transportation, storage, and handling during opening and subsampling of block samples are potentially associated with greater variability as the soil is unconfined and maintains low values of soil suction, may have

increased potential for drainage and strain damage relative to clays, throughout the process.

Tube sampling at Halden was successful with good recovery. The effects of tube sampling strains on silt are a function of their lower suction, lower plasticity, coarser grain size and increased hydraulic conductivity relative to clays, all leading to increased potential for drainage and densification despite the fact that destructing of soil fabric can occur in both soil types. As a result, sampler geometry and techniques to reduce soil-tube friction are central in reducing tube sampling disturbance effects. With tube sampling the geometry is fixed and sampling is a single attempt over the sample length. Low D_w/t and high AR has been shown to alter the silt behaviour during 1D and triaxial compression. The GP-S sampler used in this study had similar poor geometry to that of the 54mm(L) which contrasts from the thin walled 72mm piston sampler (Section 4.8). However, from the consistency of the advanced test results with the block sample and 72 mm specimen test results at Halden it is considered likely that the polymer gel, inside clearance, and tapered cutting edge of the GP-S sampler reduces the friction, and thus, compensates for its poor overall cutting shoe geometry. Similarly, the 54mm(L) sample specimens showed consistent trends of disturbed behaviour.

By way of soil sampling using different techniques and advanced laboratory tests at parallel depth intervals the effects of disturbance on engineering properties was studied. CRS oedometer test results at Halden showed that both 54mm(L) sample specimens and specimens which suffered from mishandling and additional disturbance were generally stiffer, i.e. they had smaller vertical strains at all stress levels relative to the acceptable block, 72mm and GP-S sample specimens (Figure 4.2). According to

Janbu (1985) silts typically display a gradually increasing constrained modulus with increasing vertical stress, σ'_v , according to $M = 1/m_v = mp_a(\sigma'_v/p_a)^{1-a}$, where m_v = volume compressibility, $\Delta\varepsilon/\Delta\sigma'_v$; p_a = reference stress, 100 kPa; and a = stress exponent, taken as 0.25 – 0.5 for silts, and 0 for clays. The modulus numbers interpreted at Halden plot in the range of 28 to 46 where w_i has a narrow band of 26 - 30% (Figure 4.6a). The 72 mm sample specimen from 4.5 m depth has the highest water content by sample type and fits in the range of m noted above. There is a trend of increasing m with decreasing w which fall under the lower bound of Janbu (1985) and Skúlason (1996) trends for sandy silt, and some results plot below the upper bound for clays presented suggested by Janbu (1985). There is no systematic trend between disturbed and acceptable specimens, suggesting that m is not very sensitive to sampler induced disturbance. However, significant disturbance beyond that induced by a poor-quality sampler, for example disturbance from a sample tube hitting the floor, results in an increase in m . This is also evident in the trend of m with depth (Figure 4.6b) where outliers are easily identified in this uniform deposit. The strain energy-based framework for sample quality (Figure 4.6c) and $\Delta e/e_0$ criteria are applied to CRS results (Figure 4.10) however neither reflect the expected quality as opposing trends in criteria and response are evident. These criteria show that GP-S sample results plot separately from the block and 54mm(L) sample results which tend to plot close to one another irrespective of evaluated quality.

Drained and undrained triaxial shear behaviour (Figures 4.3 and 4.4) demonstrated more clearly than the CRS tests the sensitivity of the Halden silt to disturbance. CAUC test specimens displayed large differences in normalised stress-strain and pore pressure behaviour between different samplers, with the 54mm(L) and disturbed

block sample specimens consistently exhibiting a stronger tendency for dilative behaviour relative to the acceptable quality block, 72 mm and GP-S sample specimens. The disparity had limited effect on the ϕ'_{mo} and mobilized shear stresses at small axial strains but increased with increasing axial strain during testing leading to higher values of interpreted s_u at larger axial strains. Brandon et al. (2006) described six criteria for interpretation of s_u of two natural silts from the Mississippi River Valley, USA. The normalized shear stresses at Halden for three of these criteria: 1) maximum shear induced pore pressure, u_{max} ; 2) state of zero excess shear induced pore pressure at failure $\Delta u_f = 0$, which is equivalent to Skempton's A parameter at failure equal to zero, $A_f = 0$; and 3) an assigned limiting axial strain, $\varepsilon_{a,f}$, are presented in Figure 4.7. There is a trend of near constant normalised undrained shear strength, s_u/σ'_{vc} , with depth for both criterion 1 and 2, resulting in roughly 70% increase in s_u defined at u_{max} to that defined at $A_f = 0$. Due to the tendency for dilative behaviour of the Halden silt, any value of s_u evaluated at vertical strains greater than that associated with $A_f = 0$ will be associated with negative pore pressures. As shown in Figure 4.7a and Figure 4.7b the effects of sample disturbance on the Halden silt, observed in the stress-strain and stress-path development described in the results, are not particularly pronounced for the normalised undrained shear strengths defined at u_{max} and $A_f = 0$. At u_{max} the shear stresses are well below the failure envelope, and thus, not fully mobilized. For $A_f = 0$ all tests essentially have the same normalised undrained shear strength as they were consolidated using $K_0 = 0.5$ and specimens from all depths generally converge onto the same failure envelope defined by the K_f -line at $\phi'_{mo} = 36^\circ$. The conflicting results from different samplers and resulting increase in strength due to sampling disturbance is far more pronounced when the s_u is defined by vertical strains

in the range of 5% to 10% and associated negative pore pressures changes (Figure 4.7c). Using 10% axial strain as strength criteria results in large scatter at each depth interval due to sampler induced disturbance effects. The acceptable specimens form the lower bound of results, with $s_u/\sigma'_{vc} = 0.75 - 0.95$, while the disturbed specimens are scattered with considerably greater strengths, i.e. $s_u/\sigma'_{vc} = 1.1 - 1.8$. The differences should not be underestimated as they can be significant; in the extreme case providing a ratio of upper bound strength, defined by e.g. a disturbed sample at 10% vertical strain, to lower bound strength, defined by e.g. an acceptable quality sample at u_{max} , criterion, of more than 2.5.

4.5 Conclusions

This paper presents an experimental study on laboratory testing of a natural clayey silt from Halden, Norway. Advanced tests results on specimens collected using the Sherbrooke block, NGI 54 mm composite piston, 72 mm piston and Gel-Push samplers are presented creating an important silt behaviour database. A qualitative assessment of sample quality was implemented based on; 1) material response in advanced tests, namely triaxial; 2) comparison of intentionally disturbed specimens from the 54 mm composite piston sampler, and specimens from samplers known to yield high quality in clays, such as Sherbrooke block and 72 mm piston samplers; 3) field observations from drillers logs; and 4) classification data, namely w , as relatively lower w is a likely indication of expelled water during sampling. The definitions of 'acceptable' and 'disturbed' quality were based on evidence from simulated tube sample disturbance (ISA) testing, where strain damaging resulted in increased rate of shear stress development with increased disturbance. Main findings were:

- Lower bound shear strength specimens guided the definition of acceptable samples, which were typically provided by the GP-S and 72mm samplers and a limited number of samples collected using the Sherbrooke block sampler. Upper bound strength specimens guided the definition of disturbed samples, which were consistently provided by the 54mm(L) sampler, and some samples which experienced issues during Sherbrooke block sampling.
- Clay-based frameworks for evaluation of quantitative sample quality were found inappropriate and misleading for the Halden silt, confirming earlier findings on other intermediate soils. Sample quality assessment using the framework based on soil suction was not attempted as suction measurements were not possible on this silt.
- Advanced laboratory tests demonstrated that triaxial results provided good guidance on sample quality, in contrast to CRS results where sampler induced disturbance effects were subtler.
- The qualitative assessment revealed that, as expected, the 54mm (L) sampler produced overly disturbed samples. More interestingly, 6 of the 9 block samples tested in this study had experienced some degree of disturbance, likely a result of sampling issues due to repeated sampling attempts at the same depths or immediately above. This suggests that, although historically known as the gold standard for sampling in soft clays, the Sherbrooke block sampler in this study did not consistently collect high-quality samples with respect to the three other samplers.

- Despite recent experimental strain damage testing on silts demonstrating potentially adverse effects for tube sampling, the 72 mm thin walled piston and GP-S samplers used in this study provided the most consistent and repeatable quality samples. Without these tube samples it was difficult to identify a borderline disturbed block samples from acceptable block samples. These samplers may provide the most reliable and consistent results in silts at present despite possible induced centreline strains in order of 0.6%.
- Overall effects from increased sample disturbance evident from this study included: i) reduction in w_i , ii) lower values of $\Delta e/e_0^*$ in some cases (*opposite bound of quality index, hence misleading); iii) decreasing values of $C_{rw,i}/C_{cw}^*$; and iv) increasing m with increasing degree of disturbance. The modulus number, however, showed relatively low sensitivity.
- Moreover, undrained triaxial tests revealed: i) increasing tendency for dilative behaviour for a disturbed relative to an acceptable specimen; ii) differences in stress-strain and shear induced pore pressure behavior between the different samplers were mostly pronounced after the point of u_{max} ; iii) normalized undrained shear strengths at the u_{max} and $A_f = 0$ criteria provided consistent and near constant values with depth with s_u/σ'_{vc} (at u_{max}) $<$ s_u/σ'_{vc} (at $A_f = 0$); and iv) at high axial strain, e.g., $\varepsilon_{a,f} = 5\% - 10\%$, sample disturbance caused an increased range in normalized s_u .
- While one CADC test displayed an increased drained peak friction angle due to disturbance ($\phi' = 39^\circ$), there was generally limited to no effect of disturbance on ϕ'_{mo} interpreted from CAUC tests ($\phi'_{mo} = 36^\circ$).

- With more experience in block sampling silts more consistent acceptable quality blocks may be achievable as was found at Refneveien, Halden. As silt deposits vary from site to site in composition, namely grain size distribution and I_p , obtaining some disturbed 54mm(L) samples would i) provide a boundary representative of disturbed material behavior, and ii) enhance the understanding of sample disturbance effects for more silt deposits.
- As of now, reliance on a qualitative sample quality approach, as used in this study including consideration of repeatable acceptable quality from 72mm and GP-S samples in silts, provides the best information on evaluation of quality and is recommended for future studies. This is provided sample handling is carried out according to best practice.
- Nonetheless, design criteria plays a role in: i) selection of strengths, ii) consideration of drainage conditions in the design approach, and iii) allowance for dilation as strengths increase considerably with negative pore pressures and disturbance effects enhance this response.

4.6 Data Availability Statement

All data used during the study are available online in accordance with funder data retention policies. Access to data is under Datamap as documented by Doherty et al. (2018) at <http://www.datamap.geocalcs.com/>. Information on access to NGTS sties is available at <http://geotestsite.no/>.

4.7 Acknowledgements

The authors appreciate the contribution from with Shreeya Pandey and Don J. DeGroot at the University of Massachusetts Amherst for CAUC tests carried out there. This work was completed with funding from the Research Council of Norway through project Norwegian GeoTest Sites (NGTS) under Grant No. 245650/F50. NGTS committee members' and NGI colleagues' contributions are gratefully appreciated by the authors for coordination and execution of work culminating in results used in this study. Any opinions, findings, and conclusions or recommendations expressed in this paper are those of the authors and do not necessarily reflect the views of the Research Council of Norway.

4.8 Supplemental section

4.8.1 Sampler geometry

The inside clearance ratio (ICR) quantifies the difference in internal diameter of the sampling tube and the cutting shoe, and $ICR > 0$ reduces the wall friction between soil. However, this difference in internal diameter also causes an elastic expansion of the soil sample due to the stress relief and may cause further sample disturbance. For general practice Hvorslev (1949) suggested an inside clearance ratio of 0.75 to 1.5% for long samplers and 0 to 0.5% for very short samplers, while ASTM (2018) specifies the inside clearance ratio should be 1%, unless otherwise specified; the inside clearance ratio should increase with an increase in soil sample plasticity. ISO (2014) recommends the inside clearance ratio to be preferably below 0.5%. Several authors (Hight and Leroueil 2003;

Ladd and DeGroot 2003; DeGroot and Ladd 2012) have recommend an inside clearance ratio close to zero for soft clay sampling. An outside clearance ratio (OCR) greater than unity facilitates the withdrawal of the sampling tube as an external diameter of the cutting shoe larger than that of the sampling tube reduces friction between the soil and the tube. Nonetheless, inside clearance may in some cases be more desirable than the negative effects of adhesion between soil and inside of sampler (Clayton and Siddique 1999). This is potentially a positive factor for the GP-S together with the lubricating polymer gel to aid friction reduction between soil and tube. Outside clearance increases area ratio (AR) which have been shown to increase strain on a sample. However, 2-3% OCR can be beneficial in clays (Hvorslev 1949). AR is the ratio of annular cross-sectional area of the tube to the area of the sample. Increasing area ratio increases the penetration resistance of the sampler, entrance of excess soil, and the potential of increased sample disturbance. Hvorslev (1949) recommends an AR of less than 10% and ISO (2014) requires AR less than 15% (but allows for AR = 25% if it is demonstrated that the quality class is not affected). ASTM (2018) states that AR should generally be less than 10 to 15% and that larger AR of up to 25 to 30% have been used for stiffer soils to prevent tube buckling. The GP-S sampler has a higher AR than the 54mm(L) and however its effects may be beneficial during sampling as we see consistently acceptable quality GP-S samples at Halden. It also has the lowest $D_{largest}/t$ ratio of all samplers used in this study which would indicate, based on studies of effect of $D_{largest}/t$ ratio, that it would yield disturbed samples. However, the contrary is the case which must be attributed to its' overall geometry and use of gel.

Definition of terms provided in Table 4-2 using Figure 4.8a:

- Inside clearance ratio, ICR (Hvorslev 1949) controls internal friction, principal cause of disturbance.

$$ICR = \left(\frac{D_s - D_i}{D_i} \right) \times 100 \quad (4.1)$$

- Outside clearance ratio, OCR, reduces outside wall friction.

$$OCR = \left(\frac{D_w - D_e}{D_e} \right) \times 100 \quad (4.2)$$

- Outside cutting angle, OCA, and inside cutting angle, ICA, where r is the radius at the associated subscript diameter location:

$$OCA = \tan^{-1} \left(\frac{r_w - r_i}{H_2} \right) \quad (4.3)$$

$$ICA = \tan^{-1} \left(\frac{r_e - r_i}{H_1} \right) \quad (4.4)$$

- Area ratio, AR, quantifies the relationship between volume of displaced soil and sampled soil.

$$AR = \left(\frac{D_w^2 - D_i^2}{D_i^2} \right) \times 100 \quad (4.5)$$

- $D_{largest}/t$ ratio is traditionally referred to as B/t (external diameter to thickness ratio or aspect ratio of a sampler). However, for clarity on evaluation of B and evaluation of t this annotation has been selected, where $t = D_{largest} - D_{smallest}$. This ratio controls overall distortion patterns of the soil around the sampler (Siddique 1990).

$$\frac{D_{largest}}{t} = \left(\frac{D_{largest}}{D_{largest} - D_{smallest}} \right) \quad (4.6)$$

4.8.2 Driller's log from borehole HALB04

Table 4-3 provides details from the Sherbrooke block sampling in borehole HALB04.

4.8.3 CRS specimen data

Table 4-4 provides a tabulated summary of initial and after consolidation test data from CRS oedometer tests at Halden.

4.8.4 CAUC specimen data

Table 4-5 provides a tabulated summary of initial and after consolidation test data from CAUC triaxial test at Halden.

4.8.5 CADC specimen data

Table 4-6 provides a tabulated summary of initial and after consolidation test data from CADC triaxial test at Halden.

4.8.6 V_s analysis of in situ results

NGI developed a set of Python routines to process SCPT data and estimate S -wave velocity profile together with its associated uncertainty as there is no standard

SCPT or SDMT format for service providers to follow for presentation of data or geometry of seismic components of the cone used. Table 4-7 summarizes the seismic cone geometry and the components (vertical Z, horizontal X and Y) available in the recorded data.

Data is imported, processed according to geometry of the set up and plotted for visual quality control from each provider. In order to increase the signal-to-noise ratio, several shots are typically acquired for a given sensor and source position. The resulting traces are subsequently vertically stacked together. This process enhances the coherent signal and tends to reduce the incoherent noise. If coherent noise exists within the data, it would also be enhanced, and stacking would then not be recommended. Some of the acquisition systems such as the Pagani only provide already stacked data. In order to remove some of the undesired noise from the seismic records, one can apply a bandpass filter. As the source and receivers are band-limited, and the soil also acts as a low-pass filter, only a portion of the frequency spectrum contains meaningful information. The two horizontal accelerometers usually have orthogonal orientations. The orientation of the horizontal source at the surface does not necessarily align with one of these two components. Therefore, it might be beneficial to perform a vector summation of the two horizontal components.

To estimate the *S*-wave velocity at depth, one needs to estimate the difference in travel time (*dt*) between the upper and the lower level of accelerometers. Knowing the distance between the two levels, the *S*-wave velocity can then be estimated according to:

$$V_s = d_z / (t_2 - t_1) \quad (4.7)$$

In order to estimate *dt*, one could, e.g. 1) try to pick the first arrival (manually or using first breaking algorithms) for both levels and take the difference, 2) compute the

time lag corresponding to the maximum of the cross - correlation between both levels, 3) compute the phase shift between both levels and convert to dt . NGI have implemented the cross-correlation methods which is the most robust and its uncertainty is derived from the corresponding cross-correlation value.

Table 4–1 Summary of average classification properties at Halden.

Depth m	Soil unit -	w_i %	w_L %	w_P %	I_P -	Sand %	Silt %	Clay %
4.5 – 7	II	30.5	35	21	10.5	20	73	7.6
8.0 – 10	II	29.5	31.6	23	8.6	10	80	9.7
11.0 – 12.0	II	29	28	20	7.7	10	80	9.3
14 – 14.85*	III	22	26	20	5.5	20-25	70-75	7-12

* Unit III is 14 -16 m, classification data acquired up to 14.9 m.

Table 4–2 Summary of dimensions and derived properties of samplers used in this study.

Sampler type	D_e	D_w	D_s	D_i	t	ICR	AR	OCA	$D_{Largest}/t$
-	mm	mm	mm	mm	mm	%	-	°	-
GP – S sampler	90	93	72.1	71.5	10.75	0.8	69	Tapering	8.7
NGI 54 mm composite sampler	65	65	54.3	54	5.5	0.6	45	5	12
Sherbrooke block sampler	250	250	250	250	0.00	0.0	0	-	-
Geonor K200 sampler	76	76	72.1	72.1	1.95	0	11	5	39

Table 4–3 Driller's log from borehole HALB04 (Sherbrooke block sampling) at Halden.

Top m	Bottom m	Ref -	Q ¹⁾ -	Driller's comment -
0.0	3.10			Pre-drilling
3.10	3.45	x		Discarded. Poor quality.
3.45	3.70	1		Ok minus. Part of sample missing.
3.70	4.05	x		Discarded. Poor quality.
4.05	4.40	x		Unsuccessful. One knife did not release.
4.40	4.75	x		Unsuccessful. One knife did not release.
4.75	5.15	2		Ok minus. Silt, some clay.
5.15	5.50	3	A	Ok. Silt clay
5.50	5.85	x		Discarded. Silt, clay
5.85	6.10	4		Ok. Silt, clay
6.10	6.55	x		Discarded. Silt, clay
6.55	6.90	x		Discarded. Silt, clay
6.90	7.25	5	A* No Tx	Silt/clay
7.25	7.60	x		Discarded. Silt, clay
7.60	7.90	x		3 attempts until cutting knives released
7.90	8.25	6	D	Silt/clay
8.25	8.60	5.5	A	Block
8.60	8.95	*		Poor quality. Sample bagged.
8.95	9.30	*		Knives did not release. 2 attempts. Sample bagged.
9.30	9.65	7		Clay, silt
9.65	10.00	*		Sample bagged
10.00	10.35	8	A* No Tx	Block
10.35	10.70	*		Pose
10.70	10.70	x		Sample lost. 2 knives released but no sample collected
11.05	11.40	9		Sample disturbed due to attempts above.
11.40	11.75	10	A	Block
11.75	12.10	*		Bagged
12.10	12.45	11		Block
12.45	12.80	12	D	Block (not noted in log but photo in Blaker et al. (2019) showing injury from cutting knife removal)
13.00	13.10	1m		Mini-block. Knives did not release. 2 attempts with mini-block sampler
13.10	13.40	*		Mini-block. Poor quality/disturbed. Bagged
13.40	13.75	2m	D	Mini block sampler. Only one knife released.
13.75	14.10	3m		Mini-block. OK. Knife not fully released.
14.10				Continue with Sherbrooke Block Sampler Flushed through the interval that the mini block was sampled from
14.10	14.45	*		Poor quality. Bagged
14.45	14.80	13	D	Block
14.80	15.15	14		Block
15.15	15.20	15		Block

Note: ¹⁾ Q = qualitative quality, with A= acceptable, D = disturbed.

Table 4–4 Summary initial and after consolidation data from Halden CRS oedometer test specimens and associated qualitative sample quality assessments.

Test	Sample	z	w_i	γ_t	$e_i^{1)}$	$\varepsilon_{vc}^{2)}$	$\Delta e/e_0$	$Q^{3)}$
-	-	m	%	kN/m ³	-	%	-	-
HALB01-8-B-2	72mm	4.47	34.1	18.96	0.93	1.66	0.035	A
HALB03-3-A-1	54mm(L)	5.42	29.0	19.6	0.78	0.34	0.008	D
HALB03-5-A-1	54mm(L)	7.50	29.3	19.3	0.79	1.10	0.025	D
HALB03-6-B-1	54mm(L)	8.28	27.5	19.7	0.74	1.08	0.025	D
HALB03-8-F-1	54mm(L)	10.33	27.7	19.7	0.75	1.17	0.027	D
HALB03-12-B-1	54mm(L)	14.31	24.5	20.0	0.66	1.63	0.041	D
HALB04-3-1B-1	Block	5.27	30.5	19.5	0.82	1.24	0.027	A
HALB04-5-1	Block	7.03	28.5	19.3	0.77	1.20	0.028	D
HALB04-5.5-C-1	Block	8.40	28.8	19.5	0.77	1.49	0.034	A
HALB04-8-A-1	Block	10.07	26.1	20.0	0.70	1.83	0.044	D
HALB04-13-A-2	Block	14.60	22.2	20.7	0.60	1.55	0.041	D
HALB05-1-B-1	GP-S	9.35	28.5	20.1	0.77	2.99	0.069	A
HALB05-2-D-1	GP-S	12.71	29.4	19.9	0.79	3.01	0.068	A
HALB06-6-C-1	GP-S	13.07	26.6	19.9	0.72	2.88	0.069	A

Note: ¹⁾ e_i = initial void ratio. ²⁾ ε_{vc} = vertical strain at σ'_{v0} . ³⁾ Q = qualitative quality, with A= acceptable, D = disturbed.

Table 4–5 Summary initial and after consolidation data from Halden CAUC test specimens and associated qualitative sample quality assessments.

Test	z	Sample	w_i	γ_i	$e_i^{1)}$	$e_c^{1)}$	$\varepsilon_{vc}^{2)}$	$\varepsilon_{vol}^{2)}$	$\Delta e/e_0$	$\frac{V_{svh-\sigma_{vc}}}{V_{svh-insitu-avg}}^{3)}$	Q ⁴⁾
-	m	-	%	kN/m ³	-	-	%	%	-	-	-
HALB01-9-A-1	5.30	72mm	29.6	19.0	0.80	0.78	0.71	0.86	0.019	0.91	A
HALB01-11-C-1	7.60	72mm	23.2	19.0	0.62	0.62	0.50	0.19	0.005	n/a	D
HALB01-12-B-4	8.60	72mm	28.6	19.1	0.77	0.75	0.81	0.84	0.019	0.84	D
HALB01-14-B-1	12.60	72mm	22.6	19.6	0.61	0.60	0.75	0.40	0.011	n/a	D
HALB03-3-A-1	5.32	54mm(L)	30.0	19.4	0.81	0.80	0.77	0.56	0.012	0.90	D
HALB03-6-A-1	8.46	54mm(L)	28.3	18.8	0.76	0.74	1.02	1.33	0.031	0.81	D
HALB03-9-A-1	11.60	54mm(L)	27.9	19.55	0.75	0.73	0.90	1.08	0.025	n/a	D
HALB03-12-A-1	14.42	54mm(L)	23.4	20.0	0.63	0.59	0.85	2.25	0.058	0.82	D
HALB04-3-A-1	5.28	Block	31.9	18.9	0.86	0.83	0.90	1.63	0.035	0.95	A
HALB04-6-A-2	8.02*	Block	28.0	19.33	0.76	0.75	0.71	0.70	0.016	n/a	D
HALB04-5.5-A-1	8.36	Block	30.1	19.2	0.81	0.79	0.81	1.30	0.029	0.84	A
HALB04-10-1A-2	11.45	Block	28.0	19.42	0.75	0.74	0.72	0.99	0.023	0.86	A
HALB04-12-A-1	12.58	Block	26.6	19.1	0.72	0.70	0.78	1.07	0.026	0.82	D
HALB04-2-A-1	13.55	Block	25.2	19.8	0.68	0.67	0.93	0.64	0.016	0.84	D
HALB04-13-A-1	14.60	Block	23.2	20.1	0.62	0.58	0.81	2.56	0.067	0.83	D
HALB05-1-A-1	9.45	GP-S	30.4	18.7	0.82	0.81	0.63	0.23	0.005	0.82	A
HALB05-2-A-1	12.50	GP-S	30.3	19.6	0.82	0.77	1.21	2.60	0.058	0.82	A
HALB06-3-A-1	8.32	GP-S	30.7	19.7	0.83	0.80	0.89	1.51	0.033	n/a	A
HALB06-4-A-1	9.93	GP-S	29.4	19.7	0.79	0.77	0.97	1.42	0.032	n/a	A
HALB06-4-D-1	11.40	GP-S	28.2	20.34	0.76	0.74	1.11	1.06	0.025	n/a	A

Note: ¹⁾ e_i = initial void ratio, e_c = void ratio after consolidation. ²⁾ ε_{vc} = vertical strain, and ε_{vol} = volumetric strain after consolidation. ³⁾ Shear wave velocity after consolidation, $V_{svh-\sigma_{vc}}$, relative to the average in situ shear wave velocity, $V_{svh-insitu-avg}$. ⁴⁾ Q = qualitative quality, with A= acceptable, D = disturbed. * K_0 consolidated specimen (CK₀UC).

Table 4–6 Summary initial and after consolidation data from Halden CADC test specimens and associated qualitative sample quality assessments.

Test	z	Sample	w_i	γ_i	$e_i^{1)}$	$e_c^{1)}$	$\varepsilon_{vc}^{2)}$	$\varepsilon_{vol}^{2)}$	$\Delta e/e_0$	$\frac{V_{vh-\sigma_{vc}}}{V_{vh-insitu-avg}^{3)}$	Q ⁴⁾
-	m	-	%	kN/m ³	-	-	%	%	-	-	-
HALB04-6-A-1	8.02	Block	27.1	19.2	0.73	0.68	0.57	2.64	0.063	0.91	D
HALB05-1-B-1	9.60	GP-S	30.2	19.3	0.81	0.72	0.93	5.21	0.116	n/a	A
HALB06-3-B-1	8.47	GP-S	29.5	19.7	0.79	0.76	0.91	1.75	0.040	n/a	A
HALB06-6-B-1	12.95	GP-S	27.9	20.0	0.75	0.73	0.96	1.24	0.029	n/a	A

¹⁾ e_i = initial void ratio, e_c = void ratio after consolidation. ²⁾ ε_{vc} = vertical strain, and ε_{vol} = volumetric strain after consolidation. ³⁾ Shear wave velocity after consolidation, $V_{svh-\sigma_{vc}}$, relative to the average in situ shear wave velocity, $V_{svh-insitu-avg}$. ⁴⁾ Q = qualitative quality, with A= acceptable, D = disturbed.

Table 4–7 Seismic cone geometry for the different equipment.

Seismic Cone	$z_0^{1)}$	$d_z^{2)}$	Components
Geotech	0.37 m	1.0 m	XYZ
A.P. Van den Berg	0.50 m	0.5 m	XY
Pagani	0.60 m	0.5 m	Vector sum (X+Y)
Marchetti	0.25 m	0.5 m	XYZ

Note: ¹⁾ z_0 = the distance from the tip to the closest level of sensor. ²⁾ d_z = the distance between the 2 levels of sensors (dz).

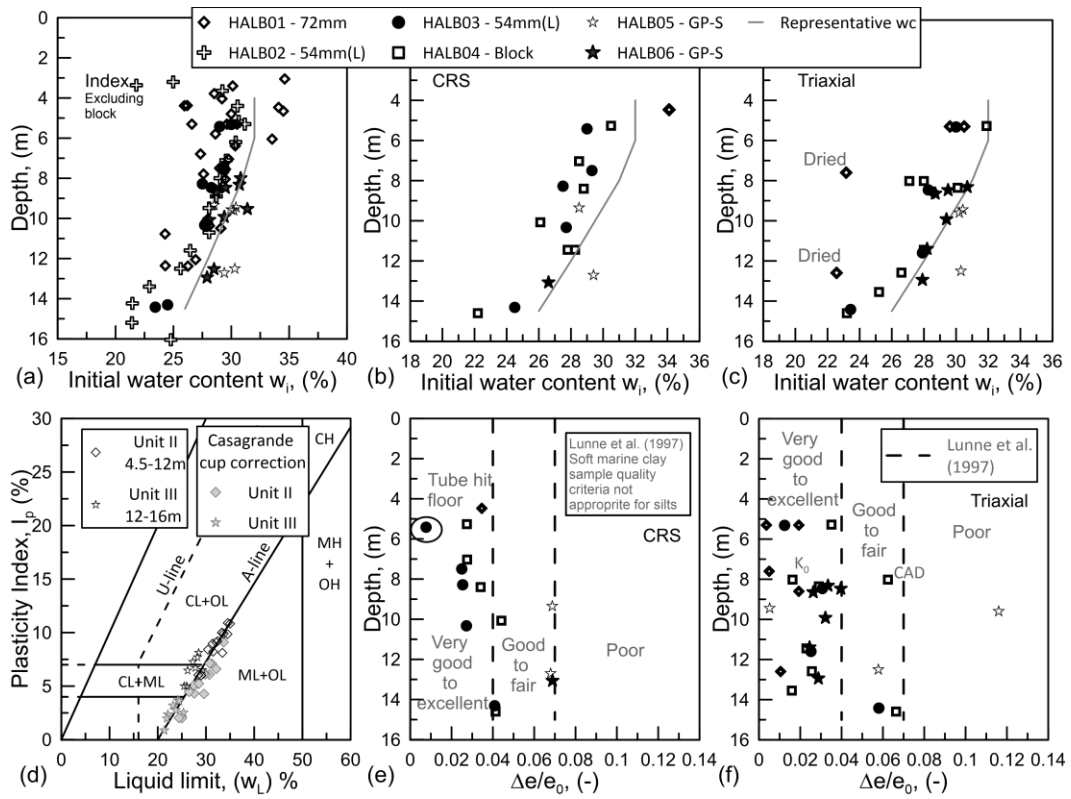


Figure 4.1 Classification properties with depth based on sampler and advanced test type. Halden research site.

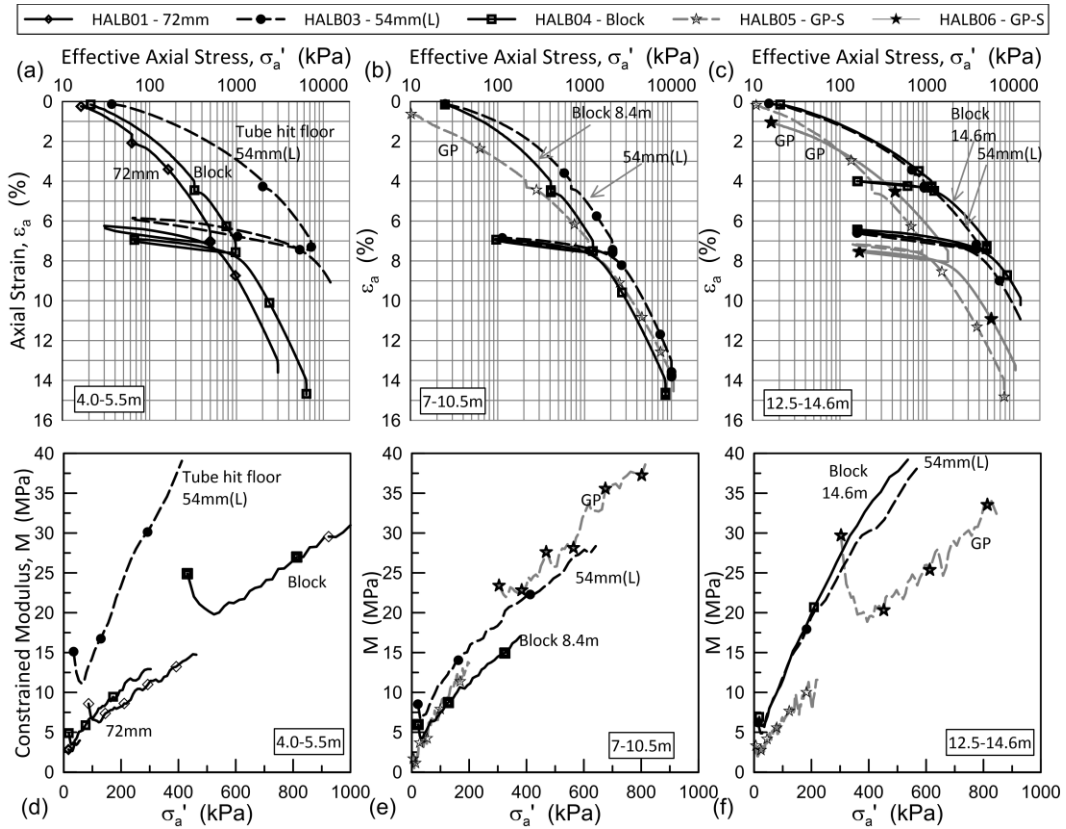


Figure 4.2 1-D consolidation behaviour of Halden silt specimens from different samplers and depth intervals. (a – c) Vertical effective stress with vertical strain, and (d – f) constrained modulus with vertical effective stress.

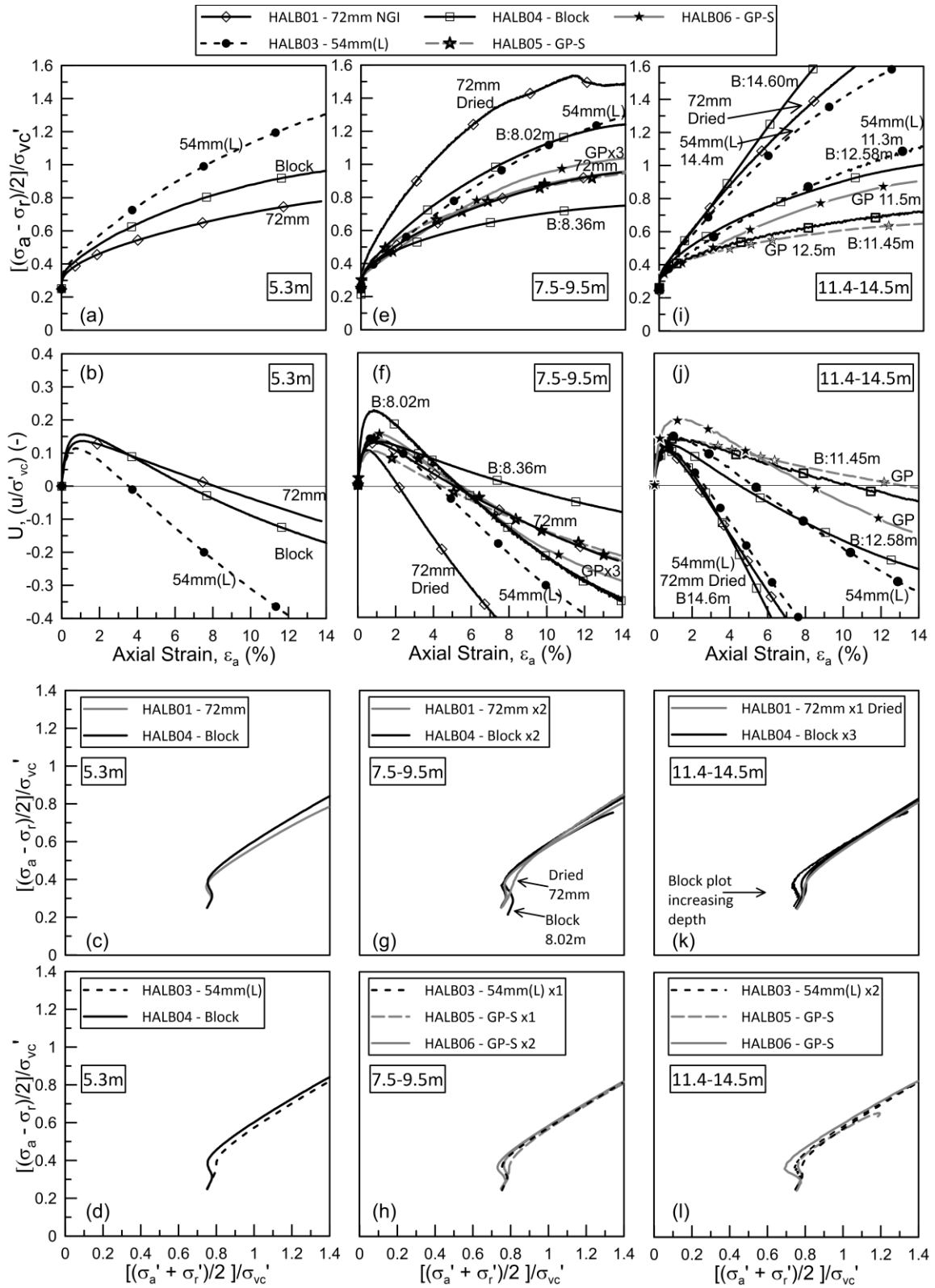


Figure 4.3 Undrained shear behaviour of Halden silt specimens from different samplers and depth intervals (a-d) 5.3m, (e-h) 7.5 - 9.5m and (i-l) 12.6 - 14.5m. Normalised shear stress and pore pressure with strain and stress path.

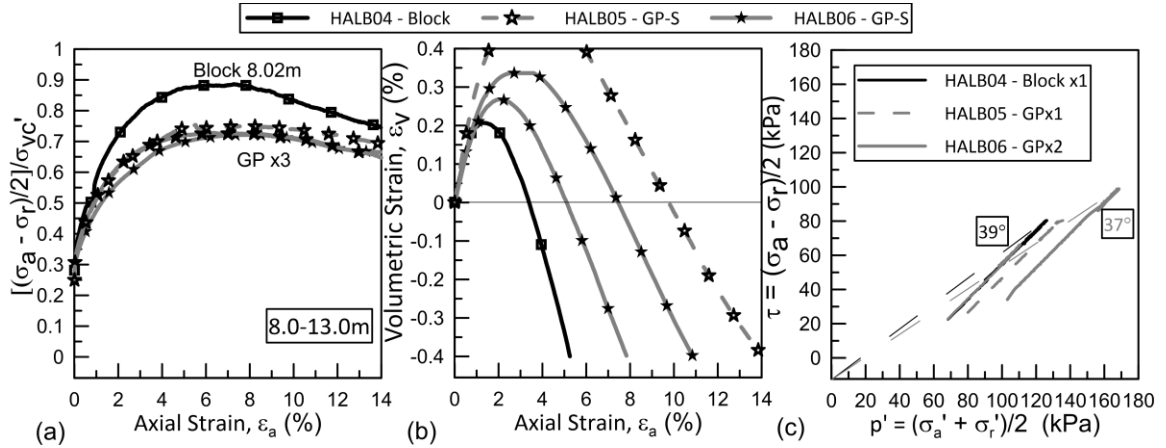


Figure 4.4 Drained shear behaviour of Halden silt specimens from depth interval 8 -13m with (a) normalised shear stress, (b) volumetric strain with axial strain, and (c) normalised stress path.

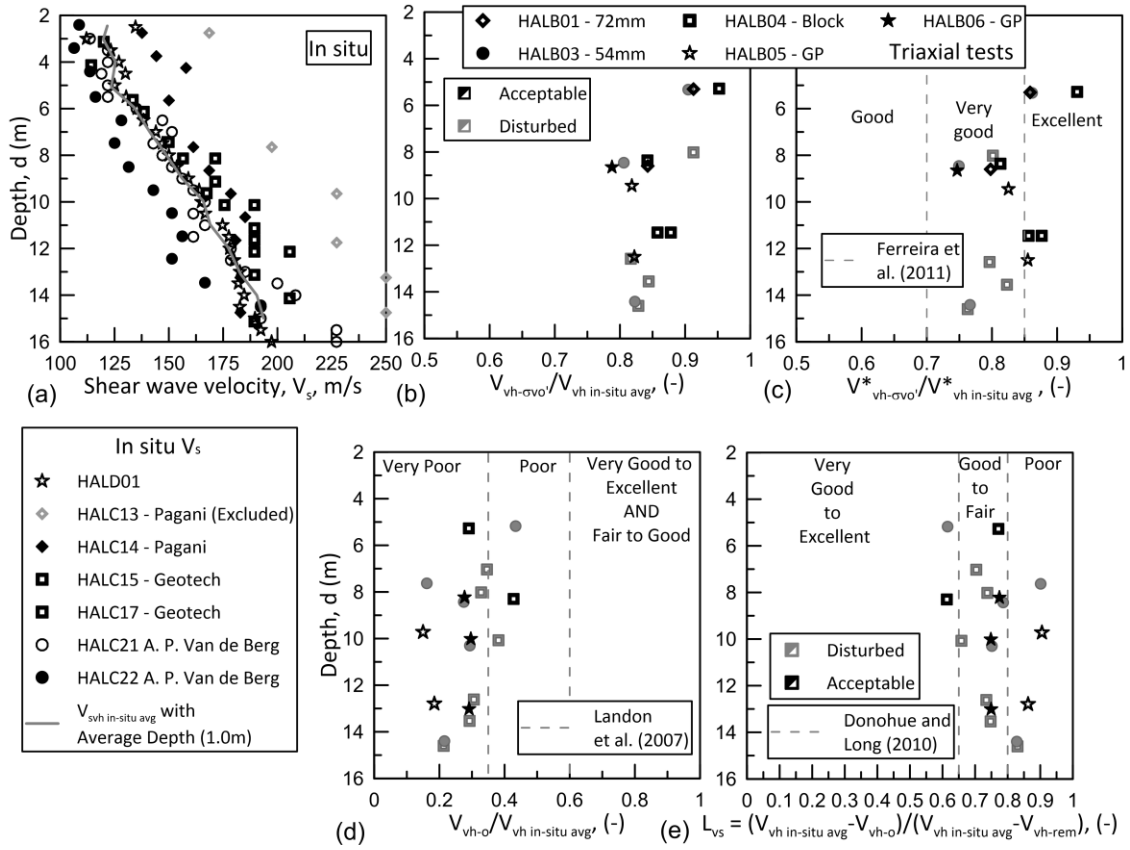


Figure 4.5 Measured and normalized shear wave velocities with depth at Halden, with (a) $V_{vh\ in\ situ}$ with depth, (b) $V_{vh-\sigma_{vo}}/V_{vh\ in\ situ\ avg}$ from triaxial test specimens, (c) $V_{vh-\sigma_{vo}}^*/V_{vh\ in\ situ\ avg}^*$ from triaxial test specimens, and Halden V_s data with sample quality criteria for clays proposed by (d) Landon et al. (2007) and (e) Donohue and Long (2010). With annotation of acceptable or disturbed quality assessment based on material behaviour.

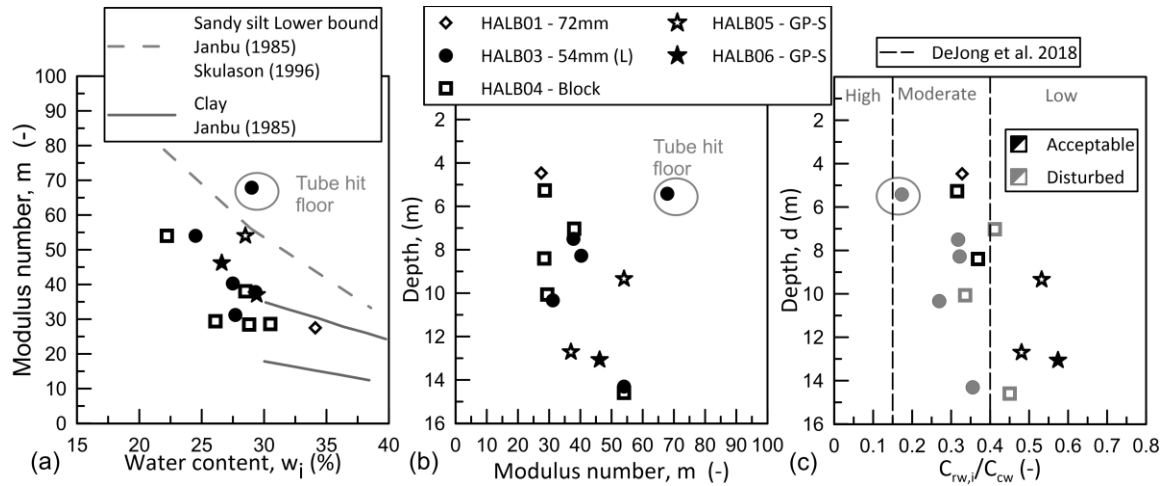


Figure 4.6 Derived CRS oedometer properties of Halden silt specimens from different samplers and depths, with (a) w_i versus m , (b) m versus depth, and (c) C_{rwi}/C_{cw} with depth and sample quality criteria for intermediate soils proposed DeJong et al. (2018).

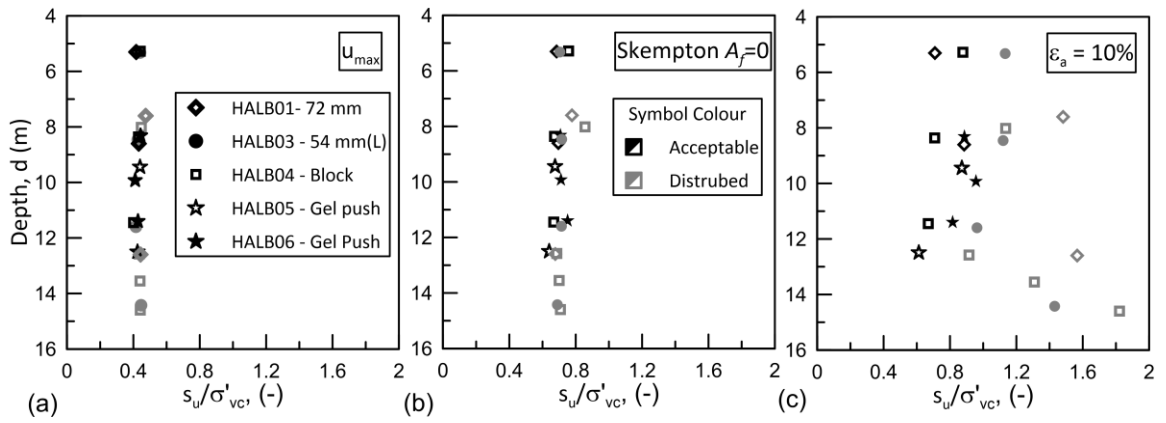


Figure 4.7 Normalised undrained shear strengths from triaxial tests on Halden silt specimens from different samplers at various criteria: (a) u_{max} , (b) Skempton $A_f = 0$ and (c) 10% axial strain.

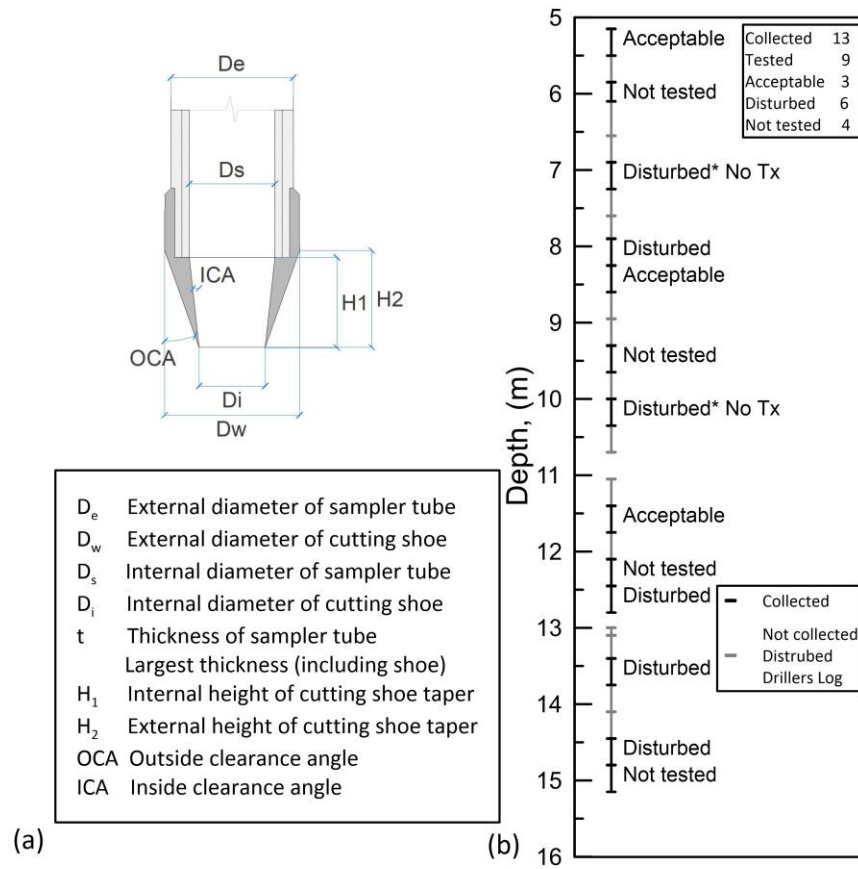


Figure 4.8 (a) Geometry of generic sampler and terms used in sampler geometry equations, and (b) Classification of Sherbrooke block samples of Halden silt from qualitative review.

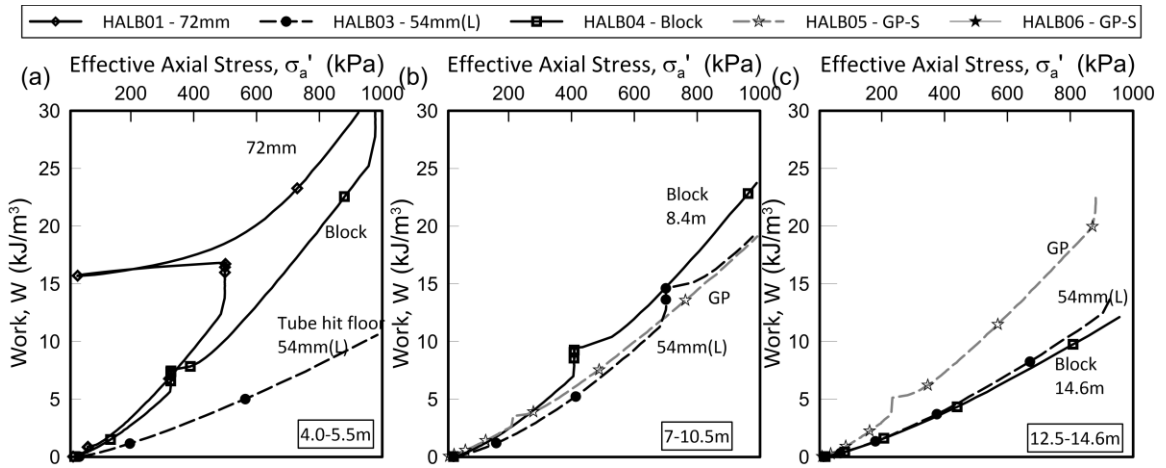


Figure 4.9 Strain energy versus vertical effective stress from CRS oedometer tests on Halden silt specimens from different samplers and depth intervals (a) 4.0 - 5.5m, (b) 7.0 - 10.5m and (c) 12.5 - 14.5m.

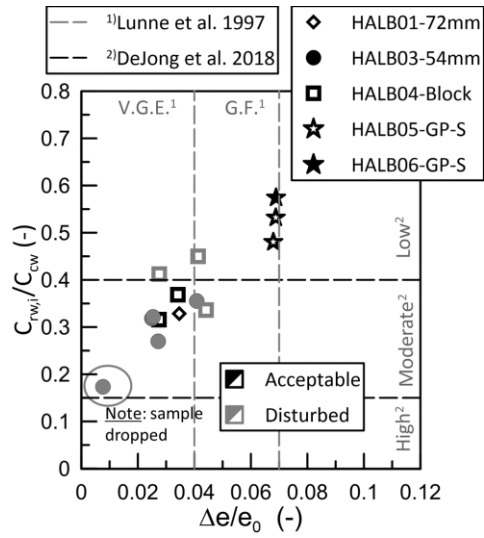


Figure 4.10 Strain energy - based compression ratio, $C_{rv,i}/C_{cw}$, versus $\Delta e/e_0$ from CRS oedometer tests on Halden silt specimens from different samplers.

CHAPTER 5

IN SITU STRENGTH AND STIFFNESS PROPERTIES FROM SCREW PLATE LOAD TESTING IN SILT

The in situ screw plate test was initially developed for estimation of the compressibility of sands and was later adopted for use in clays to estimate undrained shear strength and stiffness properties. There has been limited research on determining the engineering parameters of silts either by in situ or laboratory testing, and recent studies demonstrated the adverse and potentially unsafe effects of sample disturbance on laboratory measurement of these parameters if applied in stability problems. The research presented in this paper investigates the in situ stress-displacement behavior of a clayey silt and an underlying clay unit at Halden, Norway using screw plate load tests. Variations in drainage conditions during testing was investigated by conducting tests at different loading rates and measured data were evaluated using finite element simulations, data from piezocone tests, and data from anisotropically consolidated triaxial compression and direct simple shear tests performed on block samples. Interpreted engineering parameters were derived using several established theoretical frameworks that were developed for plate load tests. All screw plate load tests conducted at Halden demonstrated a strain hardening response that was dependent on the rate of loading. Derived bearing capacities varied significantly depending on the method used to interpret the stress-displacement data. Tests conducted at a rate of 1.3 mm/min were considered to be partially drained or drained whereas tests conducted at 15 mm/min were considered undrained. Bearing capacities estimated from the undrained tests were lower than the companion partially drained or drained tests. Practical recommendations relating laboratory drained and undrained shear strength to estimates of bearing capacity and

vertical displacements of a prototype foundation in silts such as the Halden silt are proposed.

5.1 Introduction

Sampling, in situ and advanced laboratory testing of silt are associated with higher uncertainty and complexity than what is generally encountered during soil investigations on clays. The typically higher hydraulic conductivity (k) of silt relative to most clays may allow drainage or partial drainage to occur during in situ testing and sampling at standard penetration rates, thus resulting in volumetric strains (ϵ_{vol}) in the soil immediately surrounding the penetrometer or sampler. An unknown volumetric expansion or compression caused by drainage during sampling may damage the sample; i.e. drained or partially drained sampling can cause densification of silts with a high void ratio (loose) whereas silts with a low void ratio (dense) is likely to dilate and exhibit an increased void ratio (Hight and Leroueil 2003; Sandven 2003). It is generally recognized that means of increasing sample quality and reducing adverse effects of sample disturbance on engineering properties of clays are achieved by using block samplers or thin walled, large diameter fixed piston samplers with a sharp cutting edge (e.g. Hight and Leroueil 2003; Ladd and DeGroot 2003). However, for silt high quality sampling may be challenging using any type of sampler and no quantitative sample quality frameworks have been suggested for silts, other than the strain energy and compression-based ratios proposed for 1D consolidation tests by DeJong et al. (2018). These criteria, however, are based on synthetic silt mixtures that do not exhibit the fabric and structure of a naturally occurring soil (but also shown to work on clays). Clay - based sample

quality criteria, based on volumetric metrics measured during recompression of a specimen back to the best estimate in situ vertical effective stress, σ'_{v0} (Terzaghi et al. 1996; Lunne et al. 2006), applied to silts have been cautioned by several researchers (Lunne et al. 2006; Long et al. 2010; Carroll and Long 2017).

The effects of sample disturbance on strength and stiffness properties of silts have been observed to be adverse and opposite of those often observed in soft, structured clays (Carroll and Long 2017; Lukas et al. 2019; Blaker and DeGroot In press). The interpretation of advanced laboratory triaxial tests conducted on silt is further complicated by the fact that often the undrained shear strength s_u of a silt exhibiting dilative type behavior is not uniquely defined, and the soil may also exhibit very different behavior in the "intact" and reconstituted states (Høeg et al. 2000; Blaker and DeGroot In press). For stability problems there is limited practical guidance on how to interpret laboratory test results for selection of design drained or undrained strength parameters and how they compare to the values derived from in situ tests. In situ tests, such as the cone penetration test (CPTU), plate load tests (PLT) and the pressuremeter tests (PMT) may provide valuable data of soil resistance with time or displacement without introducing sampling induced disturbance (albeit some disturbance occurs due to equipment installation or stress relief during drilling). The screw plate load test (SPLT) is a variation of the PLT where the plate, conceptually a single flight helical auger, is installed by torsion to target depth, z , (without the need for a pre-augered borehole) and loaded vertically (average stress acting on the plate, q_a) to provoke soil failure or large deformations (s).

This paper presents results from a series of SPLTs conducted at the Norwegian National GeoTest Site for silt in Halden, Norway (Blaker et al. 2019). SPLT load - displacement behavior in the clayey silt and underlying clay units are presented and used to interpret engineering parameters. The measured SPLT bearing capacities with depth are compared with the calculated base unit resistance for an equivalent diameter closed end pile (CEP). Drainage conditions during loading were assessed by comparison of normalized velocities, V , computed from the SPLTs conducted at different rates of loading, v , and finite element (FE) simulations. Preliminary results obtained early in the research were presented by Blaker et al. (2020) and used to plan the follow-up field testing campaign.

5.2 Background and analysis

5.2.1 Previous work

The SPLT was originally developed in Norway for evaluation of in situ deformation characteristics of a loose sand (Kummeneje 1956). These first tests were conducted using a simple screw plate of diameter $D = 294$ mm. The experience gained from these tests in loose sand were influential in the development of Janbu's modulus concept for settlement prediction (Janbu 1963), and in turn, this framework was incorporated in the Norwegian SPLT interpretation theory (Janbu and Senneset 1973). Schmertmann (1970) and Dahlberg (1975) adopted this method to study in situ compressibility of different sands and the influence of preconsolidation stress on the deformability. The Norwegian Geotechnical Institute, NGI (Aas 1983) summarized

results and an interpretation methodology from a series of SPLTs in Norwegian sands. Marsland (1972) used the more conventional PLT in stiff, fissured London clay although the same principles as Marsland were applied to SPLT to back-calculate the large-scale undrained shear strength from the ultimate bearing capacity, q_{ult} , in a number of different clays (Selvadurai et al. 1980; Kay and Avalue 1982; Kay and Parry 1982; Powell and Quarterman 1986; Bergado and Huan 1987; Bergado et al. 1990). Few SPLTs have been conducted in silt: Janbu and Senneset (1973) and Sandven (2003) report incremental loading SPLTs (i.e., fully drained conditions) conducted at a silt site in Stjørdal, Norway for evaluation of in situ compressibility of the deposit.

5.2.2 Bearing capacity

The ultimate bearing capacity from PLT or SPLT stress - displacement data can be assessed using a number of methods, including:

- Relative displacement method – the ultimate bearing stress is taken at a relative displacement, typically 10% of the footing width or pile diameter (Briaud and Jeanjean 1994; Salgado et al. 2011), i.e., $q_{ult} = q_{0.1D}$ for 10% of the screw plate diameter D .
- Tangent intersect method – the ultimate bearing stress corresponds to a distinct change in stress - displacement plot, i.e. intersection of initial and final tangent slopes (Trautmann and Kulhawy 1988), i.e. $q_{ult} = q_{TI}$.
- Hyperbolic method – the ultimate bearing capacity is taken as an extrapolation of the stress - displacement curve to an asymptotic value using a simple hyperbolic model (e.g. Chin 1983; Thomas 1994), i.e. $q_{ult} = q_{HYP}$.

A deeply embedded screw plate may be modeled as being the same as the base of a circular CEP with equivalent diameter and area. The ultimate unit base resistance, $q_{b,ult}$, of a pile tip equivalent to that of the screw plate may be assessed using:

- soil property-based methods, in which $q_{b,ult}$ is estimated from basic design parameters determined in the soil at the pile tip and the classical bearing capacity equation disregarding the minor contribution of the $0.5\gamma'DN_{\gamma}^*$ term, i.e.:

$$q_{b,ult} = N_c^* s_u + N_q^* \sigma'_{v0} \quad (5.1)$$

where $N_c^*, N_q^*, N_{\gamma}^*$ = dimensionless bearing capacity factors for deep foundations, including necessary shape and depth factors; and γ' = effective unit weight of soil (Salgado 2008).

- in situ test-based methods, in which $q_{b,ult}$ is correlated directly with e.g. CPTU cone resistance, q_c , including:
 - Purdue-CPT (Salgado et al. 2011),
 - NGI-05 (Clausen et al. 2005; Karlsrud et al. 2005),
 - ICP-05/MTD-1996 (Jardine and Chow 1996; Jardine et al. 2005), and
 - UWA-05/UWA-13 (Lehane et al. 2005; Lehane et al. 2013).

All of these CPT based design methods are summarized by Han et al. (2017). The NGI-05 and API (1993) procedures recommend using the unconsolidated undrained shear strength, s_{uUU} , in clay which in this paper is assumed to equal the CAUC shear strength, s_{uC} .

5.2.3 Soil parameters from SPLT

In Norway the SPLT interpretation theory for sands was adopted to Janbu's modulus concept (Janbu 1963) where the stress dependent constrained modulus ($M = d\sigma'/d\varepsilon$), or the inverse coefficient of volume compressibility (m_v), is expressed by the modulus number (m), a reference stress, $\sigma_{atm} = 100$ kPa, and a stress exponent, a (typically taken as 0.5 for sand and silt), i.e.:

$$M = m\sigma_{atm} \left(\frac{\sigma'}{\sigma_{atm}} \right)^{1-a} \quad (5.2)$$

where σ' in this paper is taken as the average value over the stress range chosen for calculation of M . The theory assumes that deformations occur in a constrained cylinder beneath the screw plate, under zero radial strain ($\varepsilon_r = 0$), but uses plasticity theory to determine the vertical stress distribution ($\sigma'_{v0} + \Delta\sigma'$) resulting from the load on the plate by equilibrium with the mobilized shear stresses along the cylinder perimeter. Aas (1983), however, suggested that the stress distribution be simply assumed to decrease linearly with depth below the plate with $\Delta\sigma' = 0$ at $z = 2D$. By integration of the vertical strain over the depth of influence, Janbu and Senneset (1973) presented a simplified expression for the modulus number as:

$$m = S \frac{Dq_n}{s_n\sigma_a} \quad (5.3)$$

where S = dimensionless settlement number, which contains the stress dependency of M and the assumptions for the vertical effective stress profile (typically in the range 0.35 – 1.5 for sand and silt with q_n in the range of 50 kPa to 350 kPa); q_n = the net vertical stress on the screw plate, which for the results presented in this paper was assessed from σ'_{v0} to

$q_a = 0.5(q_{TI} + \sigma'_{v0})$; and s_n = the plate displacement at q_n . S may be computed and plotted for different soil types, in situ vertical effective stresses and values of q_n as shown by Janbu and Senneset (1973) and Aas (1983).

Interpretation theories for assessment of the coefficient of horizontal consolidation (c_h) were also developed in the early stages of the screw plate test device. Sandven (2003) describes a procedure where c_h is estimated from time to 90% consolidation (t_{90}), determined graphically from a plot of $t^{0.465}$ versus s , i.e.

$$c_h = 0.335 \frac{R^2}{t_{90}} \quad (5.4)$$

where R = is radius of screw plate (= $0.5D$)

Selvadurai et al. (1980) examined several theoretical models of the SPLT conditions to evaluate the in situ stiffness and shear strength directly from the load versus displacement response of the screw plate. Different approximations to the SPLT conditions were considered by modelling a circular plate in an elastic medium and varying the plate stiffness and contact properties at the soil - plate interface. In clays, if the test is conducted at such a rate that undrained conditions prevail (Poisson's ratio, $\nu = 0.5$) the in situ undrained elastic modulus, E_u may be estimated from:

$$E_u = \lambda \frac{q_n R}{s_n} = \{0.60 \text{ to } 0.75\} \frac{q_n R}{s_n} \quad (5.5)$$

where λ = a factor dependent on the Poisson's ratio and plate-soil bonding. When drained conditions prevail, a Poisson's ratio of $\nu = 0.2$ may be more reasonable. Using the Keer (1975) expression for displacement of a rigid, partially bonded rigid disc the drained elastic modulus, E_d , becomes:

$$E_d = \lambda \frac{q_n R}{s_n} = 0.84 \frac{q_n R}{s_n} \quad (5.6)$$

It should be noted that the constrained and shear modulus (G) can be estimated from the elastic modulus according to the theory of elasticity as:

$$M = \frac{(1 - \nu)E}{(1 + \nu)(1 - 2\nu)} \quad (5.7)$$

and

$$G = \frac{E}{2(1 + \nu)} \quad (5.8)$$

Estimates of in situ shear strength parameters from SPLTs require an assessment of likely drainage regime during loading and the appropriate bearing capacity factors. A prediction of the prevailing drainage conditions can be made by evaluation of in situ tests such as the CPTU using the pore pressure parameter ($B_q = (u_2 - u_0)/(q_t - \sigma_{v0})$), where u_2 and u_0 are the cone shoulder and in situ pore water pressures respectively, and q_t is the cone resistance, q_c , corrected for pore pressure effects. In clays, B_q typically ranges from 0.4 to >1.2 and while $B_q = 0$ is indicative of fully drained conditions, $B_q < 0.4$ has been suggested indicative of partially drained or drained response (Senneset et al. 1989). In silts displaying dilative type behavior during in situ loading, net negative pore pressure changes may develop behind the cone and low values of $B_q (< 0.4)$ may likely occur even for undrained conditions. Alternatively, the normalized penetration velocity of an in situ test has been found useful for evaluation of prevailing drainage conditions:

$$V = \frac{vd}{c_h} \quad (5.9)$$

where v = rate of penetration, and d = penetrometer diameter. $V > 10 - 100$ is typically suggested to be indicative of fully undrained conditions, while fully drained conditions

typically occurs for $V < 0.05 - 0.01$ (Randolph 2004; Kim et al. 2008; DeJong and Randolph 2012). Penetrometer measurements conducted between $V = 0.05 - 10$ may therefore be affected by partial drainage.

In clays, Selvadurai et al. (1980) suggested a range of theoretical bearing capacity factors being:

$$N_c^* = \frac{q_{ult}}{s_u} = \{9.00 \text{ to } 11.35\} \quad (5.10)$$

However, these solutions were based on idealized plasticity and more recent advances in numerical limit analysis (e.g. Martin and Randolph 2001; Salgado et al. 2004) have demonstrated that the value of N_c^* is more likely in the range of 11.0 and 13.7 for deep foundations in clay. The factor for estimation of bearing capacity in granular soils from the effective stress conditions is a function of the effective stress friction angle of the soil, ϕ' , and shows significant variation in the literature, ranging from $N_q^* = 8$ in silt to several hundred for a dense sand (Fellenius 1991).

5.3 Materials and methods

5.3.1 Soil sampling and laboratory testing

Soil samples were collected at the Norwegian National GeoTest Site (NGTS) for silts at Halden, Norway (Blaker et al. 2019) using the Sherbrooke block sampler (Lefebvre and Poulin 1979) in location HALB04; the NGI 54 mm inner diameter (ID) composite piston sampler (Andresen and Kolstad 1979) in location HALB02 and HALB03; the Gel-Push Static (GP-S) sampler (Tani and Kaneko 2006) in location HALB05 and HALB06; and the Gregory Undisturbed Sampler (GUS), a hydraulic fixed

piston sampler, manufactured by Acker Drill Company, PA, USA in location HALB07. The Sherbrooke block samples are considered the best representation of intact soil and were used as the reference laboratory behavior for the Halden silt by Blaker et al. (2019) and Blaker and DeGroot (In press). All locations are presented on the map in Figure 5.1.

Triaxial specimens were prepared by trimming of Sherbrooke block and GUS specimens using the procedures described by Lacasse and Berre (1988) and Ladd and DeGroot (2003). All specimens were anisotropically consolidated to the best estimate σ'_{v0} and horizontal effective stress, σ'_{h0} , using an assumed $K_0 = 0.5$ (Blaker et al. 2019) and stress measurements were corrected for membrane resistance and changes in specimen area (Berre 1982). Anisotropically consolidated triaxial tests were conducted in undrained compression loading (CAUC), extension unloading (CAUE) and drained compression loading (CADC).

5.3.2 Screw plate load testing

Screw plate load tests, representing a circular prototype foundation, were conducted in two rounds and in three boreholes: the first round in boreholes HALSP01 and HALSP02, from 5.3 m to 17.8 m depth; the second round in borehole HALSP04, from 5.3 m to 13.3 m depth. The SPLT equipment consisted of a single helix flight auger with $D = 160$ mm (area, $A = 200$ cm²) and a pitch, $\Delta h = 45$ mm for one auger flight (Figure 5.2). The plate was founded in ductile cast iron (grade EN-GJS-500) by Ulefoss Foundry, Norway based on a model by Strout (1998). The screw plate was positioned directly in front of a custom-made down-hole hydraulic jack and concentric double-rod configuration described by Janbu and Senneset (1973). The outer 42.5 mm outer diameter

(OD) steel rods provided torque during installation and reaction from the jack to the drill tower of the Georigg 607 (Geotech AB, Sweden) drill rig during static loading in compression. A simple load frame was positioned between the outer rod and drill rig, and allowed access to the top of the 27 mm OD center rods. The unloaded center rods provided direct measurement of the plate displacement (i.e. no correction needed for the elastic compression of loaded outer rods) using two Mitutoyo Digimatic ID-C 0.001/50.8 mm deformation indicators mounted on an independent reference beam. An Enerpac P392 hand pump and a 64 MPa GDS high pressure volume controller (Global Digital Systems Ltd, Hampshire, U.K.) provided hydraulic pressure to the closed system through a 400 MPa capacity hydraulic hose connected to the jack. Hydraulic cylinder pressure to plate stress conversions were calibrated in the laboratory using an Interface (Interface Inc., Scottsdale, AZ, USA) load cell.

The screw plate was carefully installed by rotation from ground level to each target depth by the drill rig. The rate of penetration during installation was adjusted to equal the pitch of the screw plate (i.e. about 45 mm per 360° rotation) in order to minimize disturbance to the surrounding soil. The Enerpac pump and GDS volume controller were connected to the hydraulic hose, and the equipment was paused for about 15 min to allow equalization of installation pore pressures near the screw plate. Displacement gauges were zeroed, and constant rate or incremental deformation testing was conducted using the GDS pump. A GDS flow rate of 40 mm³/s – 350 mm³/s was used, providing a loading rate of about $v = 1.3 - 15$ mm/min (0.5 *D*/hour – 5.6 *D*/hour). Readings of cylinder pressure and plate displacement were recorded to a displacement of about $s = 0.2D - 0.3D$. After completion of a test, the oil reservoir was carefully vented

to atmospheric pressure and the hydraulic cylinder, typically fully extended after testing, was reset to its original position using the drill rig. Finally, the pumps were disconnected, and the screw plate advanced to the next test depth.

5.3.3 Finite element modelling

One screw plate load test was simulated using the finite element (FE) program Plaxis 2D 2019 (Brinkgreve et al. 2019) and the two-surface critical state plasticity soil model SANISAND (Simple ANIsotropic SAND) formulation proposed by Dafalias and Manzari (2004). The model is based on the concept of critical state soil mechanics (CSSM) and has been demonstrated to be able to simulate drained and undrained behavior of sand for a wide range of soil densities and stresses (e.g. Jostad et al. In Press). By allowing different bounding and phase transformation surfaces (with inclinations M^b and M^d , respectively) in triaxial compression and extension the stress strain development can follow different stress paths. The SANISAND soil model was calibrated to drained and undrained triaxial compression and extension tests conducted on block samples from the Halden site (Blaker et al. 2019).

A simplified axisymmetric 2-D analysis of a vertical cross section was performed with the screw plate modelled as wished-in-place and ignoring any installation effects. The 2D model of the ground was $5D$ wide \times $6D$ m high and a thin elastic dummy layer with high unit weight simulated the estimated overburden stress. Hydraulic conductivity of the silt units was taken as 10^{-8} m/s based on tests reported by Blaker et al. (2019). The geometry contained 309 15-noded triangular elements with refined mesh around the plate, which was located at a depth of $2D$ (Figure 5.3). The bottom boundary was fixed,

whereas along the vertical boundaries horizontal displacements were fixed and vertical displacements were free.

5.4 Results

The general stratigraphy of the research site at Halden, Norway consisted of a top layer of sand (Unit I) extending to about 5 m depth below grade; two silt units (II and III), separated based on different CPTU, water content and Atterberg limit characteristics; and a lower soft clay unit (IV), starting at about 16 m depth. Bedrock was located at about 21 m depth (Blaker et al. 2019). Sherbrooke block, 54 mm fixed piston, GP-S and GUS samples were collected and SPLTs conducted in the depth interval 5.0 - 18.5 m below grade. Figure 5.4 depicts stratigraphy, classification data and CPTU characteristics. The cone resistance (q_c) in soil unit II was about 1 MPa and similar to that observed in the clay of Unit IV. B_q was generally around 0.1 - 0.3 in the silt units and 0.8 - 1.0 in the deeper clay. The soil behavior type index, I_c (Robertson 2009), generally plot close to 2.95, or immediately above (Silt mixtures - clayey silt to silty clay, or clays – clay to silty clay), which is consistent with the typical soil classification test results (Table 1).

SPLTs in boreholes HALSP01 and HALSP02 were performed at the end of a very dry summer, for which physical measurements and electrical piezometers at the site confirmed the ground water level (GWL) was at its lowest during the year at about 2 m below grade. Tests in HALSP04 were conducted late fall of the following year when the GWL was almost at the ground surface at about 0.25 m depth. This approximately 1.75 m

difference in GWL levels between the two test campaigns represents a σ'_{v0} of about 20 kPa lower for the second round of SPLTs.

5.4.1 Drained and undrained triaxial shear behavior

Volumetric sample quality assessment indices such as normalized void ratio change, $\Delta e/e_0$, (Lunne et al. 1997) and the recompression volumetric strain, ε_{vol} , (Terzaghi et al. 1996) for the CAUC and CAUE silt specimens presented in Figure 5.5 were low and range from 0.014 - 0.035 and 0.6% – 1.6%, respectively (Table 2). However, as noted by Blaker and DeGroot (In press) neither $\Delta e/e_0$ nor ε_{vol} track sample disturbance well for this low plasticity silt unlike that for moderate to low OCR clays. The CAUC clay specimen from 18.6 m depth, collected with the GUS sampler, had $\varepsilon_{vol} = 2.7\%$, corresponding to $\Delta e/e_0 = 0.054$, thus giving it a "good to fair" sample quality rating. During shear, the block sample specimens of Halden silt exhibited an initial contractive type behavior up to 1 - 2% vertical strain but thereafter switched to dilative type behavior and strain hardening response as depicted in Figure 5.5a and b. This behavior is clearly observed in Figure 5.5c which shows the effective stress paths, $q = 0.5 \times (\sigma'_1 - \sigma'_3)$ versus $p' = 0.5 \times (\sigma'_1 + \sigma'_3)$, turn towards and eventually run along the failure envelope (K_f line). All CAU tests, including the extension tests, exhibited an effective stress friction angle at maximum obliquity of $\phi'_{mo} = 35.8^\circ \pm 1.2^\circ$. The phase transformation points (PTP), the point at which the soil transitions from contractive type behavior to dilative type behavior, were located at an angle of approximately $\phi'_{PTP} = 33^\circ$. Due to the strain hardening behavior, interpretation of the undrained shear strength is complex and test results provided no unique (peak) undrained shear strength, $q_f = s_u$.

Table 3 shows how the interpreted undrained shear strengths in the silt units vary with the Brandon et al. (2006) and Blaker and DeGroot (In press) different strength criteria for dilating soils. The shear stress at the maximum pore pressure, u_{max} , typically represents a lower bound s_u value whereas for the $\Delta u = 0$ (Skempton's pore pressure parameter, $A_f = 0$) and at the point of maximum obliquity, $(\sigma'_1/\sigma'_3)_{max}$, criteria the shear stresses are on the failure envelope with values of s_{uC} larger than at the u_{max} criterion. Due to the dilative type behavior of the silt, the undrained shear strength at a limiting value of vertical strain (ε_f) increases with increasing strain and typically is a maximum value at the end of the test, i.e. at $(\sigma'_1 - \sigma'_3)_{max}$. The drained CAD tests confirmed the initial contractive behavior (with initial positive volumetric strain changes, $+\Delta\varepsilon_{vol}$) followed by a change to dilation ($-\Delta\varepsilon_{vol}$) after about 2% vertical strain and with the same effective stress friction angles obtained from the undrained tests (Figure 5.5c).

5.4.2 SANISAND model calibration

The SANISAND numerical soil model was calibrated using a set of drained and undrained triaxial tests in compression and extension performed on silt specimens trimmed from the Sherbrooke block and GP-S samples. Key input parameters and a simplified explanation with best fit model constants are presented in Table 4. Fabric effects are not considered in this paper and the two corresponding model constants are taken as zero ($z_{max} = c_z = 0$). The numerical results of the CAUC and CAUE tests are compared to the experimental laboratory test data in Figure 5.5. SANISAND shows an excellent fit to the measured undrained stress - strain response of the Halden silt in both compression and extension. The initial positive pore pressure and subsequent change to

negative shear induced pore pressure is captured by the model, but the simulations do not display the exact peak pore pressures observed in the laboratory CAUE test. This is also clear from the stress-path plot in Figure 5.5c where the SANISAND soil model does not track the laboratory data all the way down to the lowest mean effective stresses. It was not possible to fit the post-peak softening response of the drained tests.

5.4.3 Screw plate load – displacement behavior

Stress-displacement curves from screw plate tests in silt and clay are presented in Figure 5.6 for three different depth ranges: (a) 5.3 m, (b) 7.3 m to 9.3 m, and (c) 11.3 to 17.8 m, with bearing capacity from the different interpretation methods (q_{TI} , $q_{0.1D}$, $q_{0.15D}$, and q_{HYP}) indicated on each curve. Due to the higher GWL at the time of the second round of SPLT field work the tests from borehole HALSP04 were performed under σ'_{v0} about 20 kPa lower than the tests in HALSP01 and HALSP02 (Table 5). In the following, the normalized average plate stress (q_a/σ'_{v0}) calculated for the individual HALSP04 test results was therefore de-normalized using the value of σ'_{v0} at the time of the first round. Further, certain tests showed evidence of stiction, i.e., friction due to soil adhering to the shaft section immediately behind the screw plate (Powell and Quarterman 1986), preventing plate displacement until the friction was overcome. These stress – displacement curves were corrected accordingly.

The SPLT results from 5.3 m in boreholes HALSP01 and HALSP02 demonstrated repeatability and the silt exhibited strain hardening response analogous to that observed in the triaxial tests at the same depth. However, one stress displacement curve shows evidence of reaching a plateau of about 600 kPa (Figure 5.6a). Using $c_h = c_v$,

= 6.4×10^{-6} m²/s (Blaker et al. 2019) and $v = 1.33$ mm/min the normalized velocities for these tests is estimated as $V = 0.55$, which suggests partially drained behavior. For the second round of tests (in borehole HALSP04) the first test was performed as an incremental load test at 5.3 m to create drained failure conditions in the silt. The close agreement between the three tests, when the HALSP04 result was de-normalized as noted above, and the low value of V collectively suggests that the HALSP01 and HALSP02 load tests were partially drained or near drained.

The four tests conducted between 7.3 to 9.3 m depth were conducted at two different displacement rates: two tests from HALSP04 were performed at a rate of about $v = 15$ mm/min ($V = 5$, for an estimated $c_h = 8.0 \times 10^{-6}$ m²/s) whereas the companion tests from HALSP01 were performed at $v = 1.33$ mm/min ($V = 0.44$). The results show an overall strain hardening response for both embedment depths and loading rates, but with a greater plate stress at a given displacement for the greater embedment depth of 9.3 m versus 7.3 m (Figure 5.6b). The two tests from HALSP04 were stopped early due to loss of reaction from the drill rig but show a somewhat higher initial stiffness with a trend towards a lower rate of stress development than their companion HALSP01 tests, in which q_a continued to increase with increasing displacement.

In the depth range 11.3 m to 17.8 m, six SPLTs were performed, including one in the unit IV silty clay. As shown in Figure 5.6c, all six tests have similar initial stiffness and all show a strain hardening response at larger displacements but at a much lower rate for the silty clay test at 17.8 m depth. Furthermore, this test performed in the silty clay, developed a significantly lower plate stress for $s > 5$ mm than the five tests performed in the overlying silts. The HALSP01 and HALSP02 tests at 11.3 m depth ($v = 1.33$ mm/s

and $V = 0.52$, for an estimated $c_h = 6.8 \times 10^{-6} \text{ m}^2/\text{s}$) are close to each other with some minor differences for $s > 10 \text{ mm}$. The test performed in HALSP04 at this same depth with an increased loading rate ($v = 15 \text{ mm/s}$ and $V = 5.9$) developed a lower plate stress. Likewise for the companion $v = 1.33$ and 15 mm/s tests performed at a depth of 13.3 m , although the difference in plate stress for this pair of tests is much greater. The undrained numerical simulation using SANISAND for the 11.3 m test depth matches both the initial stiffness and the general stress-displacement behavior of the experimental $v = 15 \text{ mm/min}$ SPLTs at this depth, although indications are that refinement of the element mesh (i.e. increasing the number of elements > 309) would further reduce the undrained capacity.

5.4.4 Measured and predicted bearing capacity

Values of estimated bearing capacity vary with soil type, interpretation method and loading rate (Table 5). There is a significant decrease in q_{ult} for all interpretation methods in the clay compared to the silt units as depicted in Figure 5.7. In the silt units the bearing capacity generally increases with increasing depth below grade and with $q_{TI} < q_{0.1D} < q_{HYP}$, as expected from the dilative and strain hardening behavior of the silts measured at large strains in the triaxial tests. Moreover, all tests conducted at $v = 15 \text{ mm/min}$ show lower bearing capacities than the tests with $v = 1.3 \text{ mm/min}$ (HALSP01 and HALSP02), which is hypothesized to be the result of a greater excess positive pore pressures developed beneath the screw plate with increasing loading rate. The FE simulations of the SPLT at 11.3 m depth suggest that the faster loading rate generates a significantly larger elevated positive pore pressure field below the plate with the maximum Δu at 16 mm displacement ($0.1D$) being about 34% higher than that of the

slower rate of loading (Figure 5.8). Note that in the figure positive values of pore pressure ($+\Delta u$) is suction and negative values ($-\Delta u$) are pressure. The dissipation of Δu in the vertical and radial direction is also noteworthy. Using the laboratory measured hydraulic conductivity the SANISAND soil model overestimated the constrained modulus at σ'_{v0} by a factor of about 10 and consequently overpredicted the c_h in the initial simulations. The hydraulic conductivity was therefore decreased by an order of magnitude to reflect this overprediction of M .

Interestingly, for the loading rate of 15 mm/min values of q_{HYP} in the silt units are in close agreement with the cone resistance from CPTUs HALC11, HALC12 and HALC19 whereas at 1.3 mm/min the bearing capacities are significantly higher than q_c (Figure 5.7c). Some researchers have considered the unit base resistance of a pile in sand as proportional to the CPTU cone resistance (e.g. Ghionna et al. 1994) based an assumption that q_c is approximately equal to the limit unit base resistance, q_{bL} (or in the case of SPLT, q_{HYP}) corresponding to the vertical load at which the foundation can no longer mobilize additional resistance. At the standard rate of penetration ($v = 20$ mm/s) CPTUs conducted in the Halden silt have V in the range 95 to 273 (Carroll and Paniagua López 2018) and is likely an undrained response. The corresponding values of q_c and q_{HYP} in this silt implies that significant displacements are required to mobilize the limit bearing capacity of the silt and further strengthens the hypothesis that the $v = 15$ mm/min tests were conducted under undrained conditions in spite of V being estimated to be equal to 5.9.

Predicted bearing capacities in the two silt units using CPT-based methods (e.g. NGI-05, Purdue CPT, UWA-05 and ICP-05 methods) for end bearing of a pile were

generally underestimated relative to the SPLTs conducted at $v = 1.3$ mm/min (Figure 5.7b). The ICP-05 method provides the closest agreement and better predicts the bearing capacity of the $v = 15$ mm/min tests. The underestimation of $q_{0.1D}$ by the CPT-based methods is caused by the low cone resistance measured at the site, partially resulting from an undrained response measured during penetration at the standard CPT rate, and by the fact that these design methods were calibrated to significantly higher values of q_c . The current API standard (API 2014) recommends using CPT based methods in silt, but the earlier API (1993) suggested using a bearing capacity factor $N_q^* = 8 - 12$, which tends to somewhat overestimate $q_{0.1D}$. In the clay unit, $q_{0.1D}$ predictions using q_c (UWA-05 and ICP-05) and $s_{uUU} = s_{uC} = 82.4$ kPa (API 1993, NGI-05 and Purdue CPT) all overestimate the bearing capacity (Figure 5.7b).

5.5 Interpretation of results

5.5.1 Coefficient of horizontal consolidation

The coefficient of horizontal consolidation was computed from the drained SPLT at 5.3 m depth and compared to the values from dissipation tests conducted and reported by Carroll and Paniagua López (2018). For the plate stress increment $q_a = 133$ to $q_a = 278$ kPa (with an average plate stress of 205 kPa) $c_{h,SPLT} = 1.84 \times 10^{-5}$ m²/s (580 m²/year). This is higher than the average results from the dissipation tests conducted at the site ($c_h = 7.44 \times 10^{-6}$), which is believed to be an effect of the larger soil volume involved in the SPLT relative to the dissipation tests, and an order of magnitude higher than the values interpreted from drained SPLTs at Halsen, Norway silt ($w_i = 20\% - 25\%$, clay content 0 -

25%, low plasticity) reported by Sandven (2003). However, $c_{h,SPLT}$ is consistent with the value determined from a horizontally mounted CRS specimen ($c_{h,lab} = 1.42 \times 10^{-5} \text{ m}^2/\text{s}$) trimmed from the Sherbrooke block sample at 8 m depth (Blaker et al. 2019).

5.5.2 Stiffness

Stress-strain, and consequently stiffness, characteristics of a soil depend on stress and strain history (including sampling disturbance and in situ tool installation effects), initial conditions, stress path and stress range over which these characteristics are assessed. It follows that soil stiffness (e.g. M , E_d or E_u) interpreted using different test methods may provide a challenging comparison. However, the importance of soil stiffness in certain design aspects (e.g. design of wind turbines, shallow foundations) and the lack of data in silts and other intermediate soils merit an evaluation. Estimated drained elastic secant moduli from the partially drained or drained SPLTs show that E_d generally increases with depth in the range 7 MPa to 16 MPa (Figure 5.9), with some variation between the three tests conducted at 5.3 m (likely a result of partial drainage in the HALSP01 and HALSP02 tests). E_d from these tests was assessed for a stress range σ'_{v0} to $q_a = 0.5 \times (q_{TI} + \sigma'_{v0})$ using $\lambda = 0.84$. The screw plate results are compared to those derived from the first unload-reload loop of four self-boring pressuremeter (SBP) tests and laboratory oedometer (constant rate of strain, CRS, and incremental loading, IL) tests on the Sherbrooke block sample specimens in the same soil units (Blaker et al. 2019). The average vertical stress over which the SPLT secant moduli were interpreted, i.e. $q_{avg} = 0.5 \times (q_a + \sigma'_{v0}) = 0.25 \times (q_{TI} + 3\sigma'_{v0})$, typically equaled approximately $2\sigma'_{v0}$. Thus, the oedometer tests were interpreted at σ'_{v0} and $2\sigma'_{v0}$ with the resulting M values

converted to E_d using $\nu = 0.2$. The oedometer E_d value at σ'_{v0} are lower than all of the SPLT values, perhaps due to stress relief during sampling and sample extrusion, while the oedometer values determined at $2\sigma'_{v0}$ are closer to that of the SPLT values. The secant unload-reload shear moduli (G_{ur}) from the first loops of the SBP tests were converted to E_d using $\nu = 0.2$ and show that the stiffness obtained from these results are generally higher than that of the SPLT results. It is likely that if a similar unload-reload loops had been performed for the SPLTs the resulting modulus values from such a loop would be higher than those plotted in Figure 5.9.

5.5.3 Shear strength

The back - calculated undrained shear strength in the clay from q_{TI} , $q_{0.1D}$, $q_{0.15D}$ and q_{HYP} gave values of $s_{u,SPLT} = 37$ kPa, 44 kPa, 49 kPa and 62 kPa, respectively (Figure 5.10) when applying a lower bound bearing capacity factor for deep foundations in clay of $N_c^* = 11$ (Salgado et al. 2004). The latter three values of $s_{u,SPLT}$ are associated with relatively large displacements, i.e. $s_f \geq 0.1D$, and will have mobilized a large volume of soil beneath the screw plate. The FE simulations in the silt revealed that at 16 mm vertical displacements the failure mechanism below the screw plate mobilized large shear strains along a wedge extending down to more than one diameter below the embedment depth. $s_{u,SPLT}$ from $q_{0.1D}$, $q_{0.15D}$ and q_{HYP} are therefore considered "average" or "mobilized" undrained shear strengths for the soil at the screw plate embedment depth, thus approximately equivalent to the direct simple shear (DSS) undrained shear strength (s_{uD}) of the same soil. The undrained shear strength of the Halden clay for DSS and CAUE modes of shear can be estimated as $s_{uD} = 57$ kPa and $s_{uE} = 34$ kPa, respectively, based on

the available CAUC test in this soil unit and strength anisotropy factors $s_{uD}/s_{uC} = 0.69$ and $s_{uE}/s_{uC} = 0.42$ reported by Lunne et al. (2006) for similar clays from the Oslo, Norway area. Thus, the undrained shear strengths back-calculated from $q_{0.1D}$, $q_{0.15D}$ and q_{HYP} , with an average value of $s_{u,SPLT} = 52$ kPa, provide good agreement with the laboratory tests and strength anisotropy of the region, and validates both the SPLT stress-displacement results and the equipment as an effective tool for evaluation of undrained shear strength in clay.

Drainage conditions during the SPLTs in the silt units are complex and without pore pressure transducers on the screw plate, quantification of the mobilized excess pore pressures during loading is uncertain. However, as noted above the second round of tests (HALSP04, at 7.3 m depth and below) is considered near undrained and the interpreted undrained shear strengths from these results at q_{TI} ($N_c^* = 11$) show close agreement with laboratory values of s_{uC} and s_{uD} interpreted from block sample specimens at the maximum pore pressure, u_{max} (Figure 5.10a). As with the shear stress at u_{max} in CAUC (Figure 5.5) or constant volume DSS tests on Halden silt the bearing capacity at q_{TI} is associated with a point on the stress-displacement curve where the displacement is relatively small (s_f in the range of $0.02D$ to $0.05D$), and globally, the vertical bearing stresses are not fully mobilized. These results suggest that q_{TI} provides a low estimate bearing capacity for short term loading and can be estimated using the shear stress from undrained triaxial tests interpreted at u_{max} .

However, for the assumption of zero excess pore pressure at failure (i.e. $A_f = 0$) in the same undrained laboratory tests the shear stresses are fully mobilized and on the failure envelope (Figure 5.5). At this point with $A_f = 0$ the undrained strength is

equivalent to the peak drained (CADC) shear strength, q_f . As depicted in Figure 5.10b, these values of s_{uC} generally coincide with: (i) $s_{u,SPLT}$ determined from the undrained SPLTs at $q_{0.15D}$ using $N_c^* = 11$; and (ii) drained shear strengths computed from the partially drained and drained SPLTs at $q_{0.15D}$ (i.e. $q_f = \sigma'_{v0} \times \tan \phi'_{cv} = (q_{0.15D}/N_q^*) \times \tan \phi'_{cv}$, where $N_q^* = 8$ for silt (API 1993) and $\phi'_{cv} =$ constant volume friction angle approximately equal to $\phi'_{PTP} = 33^\circ$). Note that the average back-calculated bearing capacity factor from drained and partially drained tests at $q_{0.15D}$ gives $N_q^* = 7.7$, and caution should be taken not to apply conventional bearing capacity factors proposed for sands as this will: (i) provide significantly higher values for the values of ϕ' measured at Halden (Fellenius 1991) and, (ii) strictly apply only when q_{ult} is taken as the limit bearing capacity, q_{bL} (Salgado 2008). These results suggest that at Halden the $A_f = 0$ provides a meaningful criterion for interpretation of s_u from laboratory undrained shear data where the u_{max} criterion is deemed too conservative for stability evaluations but design is governed by foundation displacements. As noted by Brandon et al. (2006) and Blaker and DeGroot (In press), values of $A_f > 0$ could also be used as a criterion for soils that do not exhibit the same dilative behavior as the Mississippi Valley and Halden silts. Using $A_f = 0$ could also provide a low estimate strength in design where short term, high soil resistance is considered conservative and displacements exceeding $0.15D$ are of limited importance. For these situations the high estimate bearing capacity, or the upper the limit values are of greater importance. The SPLT tests reported in this study show that the hyperbolic interpretation method provides the upper limit undrained capacity (very similar to the CPTU cone resistance), as they are values extrapolated to the asymptotic value of q_{ult} and, as such, q_{HYP} are also generally associated with large displacements $s_f >$

0.15D. At q_{HYP} the back-calculated undrained shear strengths generally seem to correspond to laboratory values of s_{uC} and s_{uD} at large shear strains, e.g. $\gamma_{lim} = \gamma_f = 15\%$ (Figure 5.10c). Due to the dilative nature of the Halden silt, CAUC and constant volume DSS tests give negative shear induced pore pressures at larger shear strains, and subsequently, $A_f < 0$ at this level of shear strain (and beyond) and the interpreted undrained shear strengths are typically higher than at the u_{max} or $A_f \geq 0$ criteria.

In summary, these SPLT results confirm: (i) that reliable values of undrained shear strength can be obtained both in the Halden clay and silt units; (ii) that the u_{max} criterion for interpretation of s_u from undrained triaxial or DSS tests in the silt provide a lower bound strength for short term loading design problems; (iii) the $A_f \geq 0$ interpretation as an effective strength criterion at the Halden site for allowing some dilative type behavior in design but at the same time limiting foundation settlement to $s \leq 0.15D$, and; (iv) if large deformations, i.e. $s > 0.1D - 0.15D$, can be allowed, strength criteria yielding $A_f < 0$ may be used.

5.6 Summary and conclusions

This paper presents an investigation of the stress-displacement behavior and bearing capacity from screw plate load tests in a natural low plasticity silt from Halden, Norway, and engineering parameters interpreted from these results. Drainage conditions during loading were assessed by comparison of normalized velocities computed from the SPLTs conducted at different rates of loading and finite element simulations. An overall strain hardening response was demonstrated for all screw plate test depths. The results suggest that tests conducted at $v = 1.3$ mm/min were partially drained to fully drained

whereas tests conducted at $v = 15$ mm/min were near undrained, although it seems likely that some degree of partial drainage is inevitable unless a very high rate of loading is used. In situ behavior and bearing capacities at Halden were strongly dependent on the rate of loading and the applied interpretation method. Bearing capacities estimated from the undrained tests were lower than the companion partially drained or drained tests. Estimates of q_{TI} and $q_{0.15D}$ from test conducted at $v = 15$ mm/min provided values of $s_{u,SPLT}$ consistent with laboratory s_u interpreted from tests on block sample specimens at the u_{max} and $A_f = 0$ criteria, respectively. At $q_{0.15D}$, the undrained tests also showed values of $s_{u,SPLT}$ generally consistent with the drained strength back-calculated from the drained or partially drained tests and peak shear strengths from laboratory drained triaxial test. For practical applications it is important to evaluate rate of loading in the field and an appropriate limit state to be used in design. From this research using a prototype foundation it appears that the shear strength from laboratory undrained shear tests at the u_{max} criterion may be applied for estimation of a lower bound ultimate bearing capacity for short term loading in stability analyses, with limited associated displacements. Undrained shear strengths from laboratory tests interpreted at some criterion $A_f \geq 0$ provide higher ultimate bearing capacities in design but are also associated with larger foundation displacements - up to perhaps $s \approx 0.15D$. For long term assessments of stability in silts such as that present at Halden, caution should be taken when using CPT-based methods as they in this study tend to underestimate $q_{0.1D}$. Moreover, soil property-based methods using conventional bearing capacity factors proposed for sands with the same friction angle as the Halden silt may significantly overestimate the drained bearing capacity.

5.7 Acknowledgements

This study has primarily been financed by the Norwegian Geotechnical Institute (NGI), the Research Council of Norway (RCN) through project Norwegian GeoTest Sites (NGTS) Grant No. 245650, and Norway-America Association's (NORAM) Graduate Study and Research Scholarship Program. The GUS sampling was conducted with support from the US National Science Foundation (NSF) under Grant Nos. CMMI-1436793 and CMMI-1436617. Any opinions, findings, and conclusions or recommendations expressed in this material are those of the author(s) and do not necessarily reflect the views of the NGI, RCN, NORAM or NSF. The support is gratefully acknowledged.

Table 5–1 Average classification properties of Halden silt and clay (Blaker et al. 2019).

Depth range (m)	Soil unit (-)	Soil type (-)	w_i (%)	$I_p^{1)}$ (%)	Clay content ²⁾ (%)	Fines content ²⁾ (%)
5.0 – 6.0	II	Clayey silt (ML)	30	10	8	73
7.0 – 8.0	II	Clayey silt (ML)	29	9	8	84
9.0 – 10.0	II	Clayey silt (ML)	27	9	10	91
11 – 12.0	II	Clayey silt (ML)	27	6	9	89
13.0 – 14.0	III	Clayey silt (ML)	24	7	9	81
17.0 – 19.0	IV	Silty clay (CL)	33	18	28	87

Note: ¹⁾ I_p = plasticity index (= PI); ²⁾ Clay content = particles < 0.002 mm, fines content = particles < 0.063 mm.

Table 5–2 Summary of classification and consolidation metrics for triaxial tests at Halden research site.

Test (-)	Type (-)	Depth (m)	Sample ¹⁾ (-)	w_i (%)	γ_t (kN/m ³)	$e_i^{2)}$ (-)	$e_c^{2)}$ (-)	$\varepsilon_{vc}^{3)}$ (%)	$\varepsilon_{vol}^{3)}$ (%)	$\Delta e/e_0$ (-)
<i>Undrained</i>										
HALB04-3-A-1	CAUC	5.3	SB	31.9	18.9	0.86	0.83	0.90	1.63	0.035
HALB04-5.5-A-1	CAUC	8.4	SB	30.1	19.2	0.81	0.79	0.81	1.30	0.029
HALB06-3-C-1	CAUE	8.7	GP-S	28.7	19.1	0.80	0.78	0.71	1.15	0.026
HALB04-10-1-A2	CAUC	11.5	SB	28.0	19.4	0.74	0.72	0.72	0.99	0.024
HALB04-10-1-D2	CAUE	11.5	SB	26.8	19.5	0.72	0.71	0.54	0.56	0.014
HALB07-GUS-6-1	CAUC	18.6	GUS	34.5	18.5	0.91	0.96	0.91	2.71	0.054
<i>Drained</i>										
HALB04-6-A-1	CADC	8.0	SB	27.1	19.2	0.73	0.68	0.57	2.64	0.063
HALB05-1-B-1	CADC	9.6	GP-S	30.2	19.3	0.81	0.72	0.93	5.21	0.116
HALB06-3-B-1	CADC	8.5	GP-S	29.5	19.7	0.79	0.76	0.91	1.75	0.040
HALB06-6-B-1	CADC	13.0	GP-S	27.9	20.0	0.75	0.73	0.96	1.24	0.029

Note: ¹⁾ SB = Sherbrooke Block, GP-S = Gel Push sampler, GUS = Gregory Undisturbed Sampler; ²⁾ Void ratio after preparation (e_i) and after consolidation to best estimate in situ stress conditions (e_c); ³⁾ vertical (ε_{vc}) and volumetric (ε_{vol}) strains after consolidation.

Table 5–3 Summary of s_{uC} and s_{uE} at different failure criteria for dilating soils. Undrained triaxial tests at Halden research site.

Test	Type	Depth	$A_f = 0$		$A_f = 0.25$		$(\sigma'_1/\sigma'_3)_{max}$		u_{max}		$\varepsilon_{v,f} = 5.0\%$	$\varepsilon_{v,f} = 10\%$	$(\sigma'_1 - \sigma'_3)_{max}$	
			q_f (kPa)	ε_f (%)	q_f (kPa)	ε_f (%)	q_f (kPa)	ε_f (%)	q_f (kPa)	ε_f (%)	q_f (kPa)	q_f (kPa)	q_f (kPa)	ε_f (%)
HALB04-3-A-1	CAUC	5.3	58.2	6.4	43.0	2.6	51.0	4.4	33.9	1.0	53.2	67.5	75.5	15.5
HALB04-5.5-A-1	CAUC	8.4	70.5	8.0	54.3	2.7	62.6	4.9	45.2	1.1	62.9	74.3	79.1	14.7
HALB06-3-C-1	CAUE	8.7	16.4	-3.5	-	-	29.3	-8.4	11.7	-1.3	20.0	33.8	38.3	-11.7
HALB04-10-1-A2	CAUC	11.5	83.1	11.0	62.3	3.3	76.9	7.2	49.1	1.0	71.5	82.3	91.5	15.0
HALB04-10-1-D2	CAUE	11.5	-	-	-	-	26.1	-7.8	14.6	-1.9	20.2	28.3	28.3	-10.0
HALB07-GUS-6-1	CAUC	18.6	-	-	-	-	-	-	-	-	-	-	82.4	0.8

Table 5–4 Best fit SANISAND input parameters for Halden silt at 11.5 m depth.

Constant	Variable ¹⁾	Value	Comment	
Elasticity	G_0	250	Dimensionless constant for calculation of elastic shear and bulk modulus, G and K , respectively.	
	ν	0.24	Poisson's ratio.	
Critical state	M_C	1.33	Critical state surface inclination (triaxial compression).	
	M_E	0.92	Critical state surface inclination (triaxial extension).	
	c	-	Ratio of M_E and M_C (not used herein).	
	λ_c	0.159	Material constant for definition of the critical state line	
	$e_{0,C}$	0.93	Critical void ratio at $p'_c = (\sigma'_1 - 2\sigma'_3)/3 = 0$ for triaxial compression.	
	$e_{0,E}$	0.93	Critical void ratio at $p'_c = 0$ for triaxial extension.	
Yield surface Plastic modulus	ξ	0.7	Material constant for definition of the critical state line.	
	m	0.05	Constant for definition of the small elastic regime.	
	h_0	4	Dimensionless constant for calculation of plastic hardening modulus, H .	
	c_h	1.34	Dimensionless constant for calculation of plastic hardening modulus, H .	
	n^b_C	1.6	Dimensionless constant for calculation of the bounding surface with inclination M^b (triaxial compression).	
	n^b_E	1.6	Dimensionless constant for calculation of the bounding surface with inclination M^b (triaxial extension).	
	Dilatancy	A_0	0.026	Dimensionless constant for calculation of dilatancy.
		n^d_C	0.4	Dimensionless constant for calculation of the phase transformation surface with inclination M^d (triaxial compression).
		n^d_E	0.4	Dimensionless constant for calculation of the phase transformation surface with inclination M^d (triaxial extension).
	Fabric - dilatancy tensor	z_{max}	0	Maximum value of fabric – dilatancy internal variable z .
c_z		0	Constant controlling the pace of evolution of z .	

Note: ¹⁾ See Dafalias and Manzari (2004) for details on the formulation of the SANISAND model.

Table 5–5 Measured and predicted bearing capacities from SPLTs at Halden research site.

Test	Depth	σ'_{v0}	u_0	Rate of displacement	Average CPTU q_c	$q_{0.1D}$	$q_{0.15D}$	q_{TI}	q_{HYP}	NGI-05 ¹⁾	ICP-05	UWA-05	Purdue CPT ¹⁾	API (1993)
(-)	(m)	(kPa)	(kPa)	(mm/min.)	(kPa)	(kPa)	(kPa)	(kPa)	(kPa)	(kPa)	(kPa)	(kPa)	(kPa)	(kPa)
HALSP01-1	5.3	71.7	29.0	1.33	758	516 ²⁾	600	364	580	370	511	455	406	574
HALSP02-1	5.3	71.7	29.0	1.33	758	503	556	349	715	370	511	455	406	574
HALSP04-1	5.3	50.4	50.3	Staged	758	459	539	376	799	370	511	455	406	574
HALSP01-2	7.3	91.1	47.6	1.33	909	646	750	451	1258	444	613	546	487	729
HALSP04-2	7.3	91.1	47.6	15.0	909	559	640 ²⁾	390	817	444	613	546	487	729
HALSP01-3	9.3	110.5	66.2	1.33	892	768	875	584	1395	435	601	535	478	884
HALSP04-3	9.3	110.5	66.2	15.0	892	638 ²⁾	741	437	831	435	601	535	478	884
HALSP01-4	11.3	130.4	84.3	1.33	978	810	923	634	1461	477	660	587	524	1043
HALSP02-2	11.3	130.4	84.3	1.33	978	842	962	660	1535	477	660	587	524	1043
HALSP04-4	11.3	108.7	106.0	15.0	978	769	862	572	1088	477	660	587	524	1043
HALSP01-5	13.3	151.8	102.1	1.33	1092	937	1071	711	1759	532	736	655	585	1214
HALSP04-5	13.3	130.4	123.5	15.0	1092	721	783	573	1186	532	736	655	585	1214
HALSP02-3	17.8	211.8	132.1	1.33	809	487	539	410	682	742 ³⁾	647	647	906 ³⁾	742 ³⁾

Note: ¹⁾ Using $D_r = 80\%$ in the silt, based on $e_{min} = 0,60$ and $e_{max} = 1,55$. ²⁾ Estimated from linear extrapolation. ³⁾ Using $s_{u,UU}$, in this case assumed equal to $s_{uC} = 82,4$ kPa.

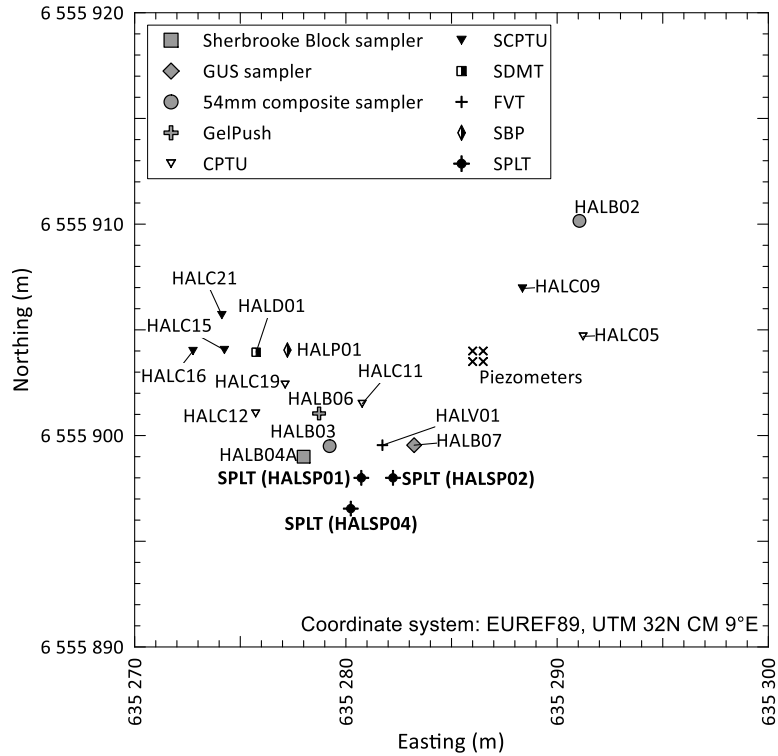


Figure 5.1 Halden research site layout. Investigated locations include electrical piezometers, cone penetration testing, field vane testing, self-boring pressuremeter testing, soil sampling and screw plate load testing.

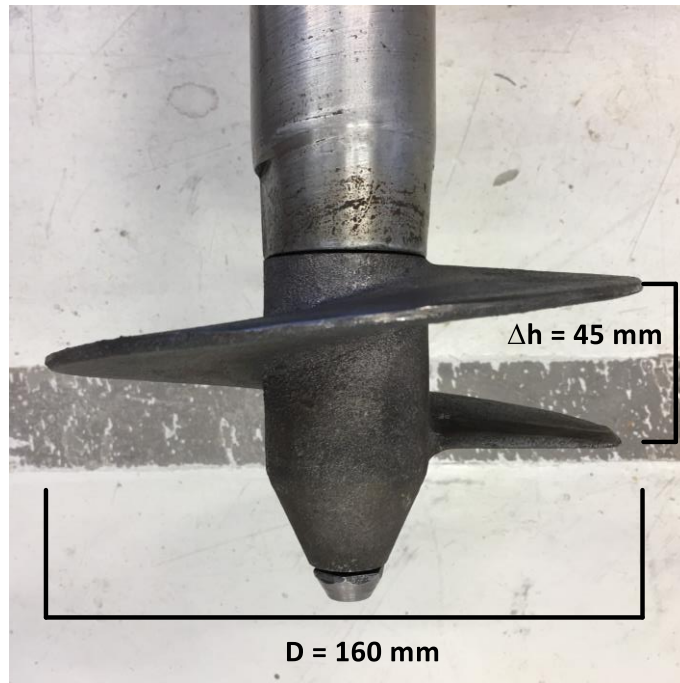


Figure 5.2 The screw plate load test (SPLT) equipment.

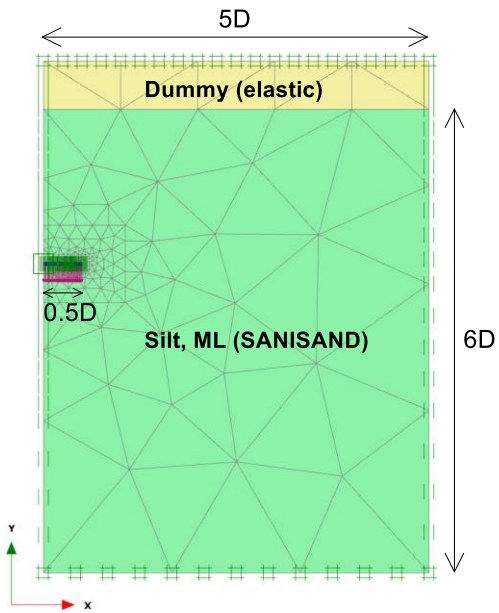


Figure 5.3 Simplified 2D axisymmetric Plaxis model of SPLTs using 309 15-noded triangular elements with refined mesh around the screw plate.

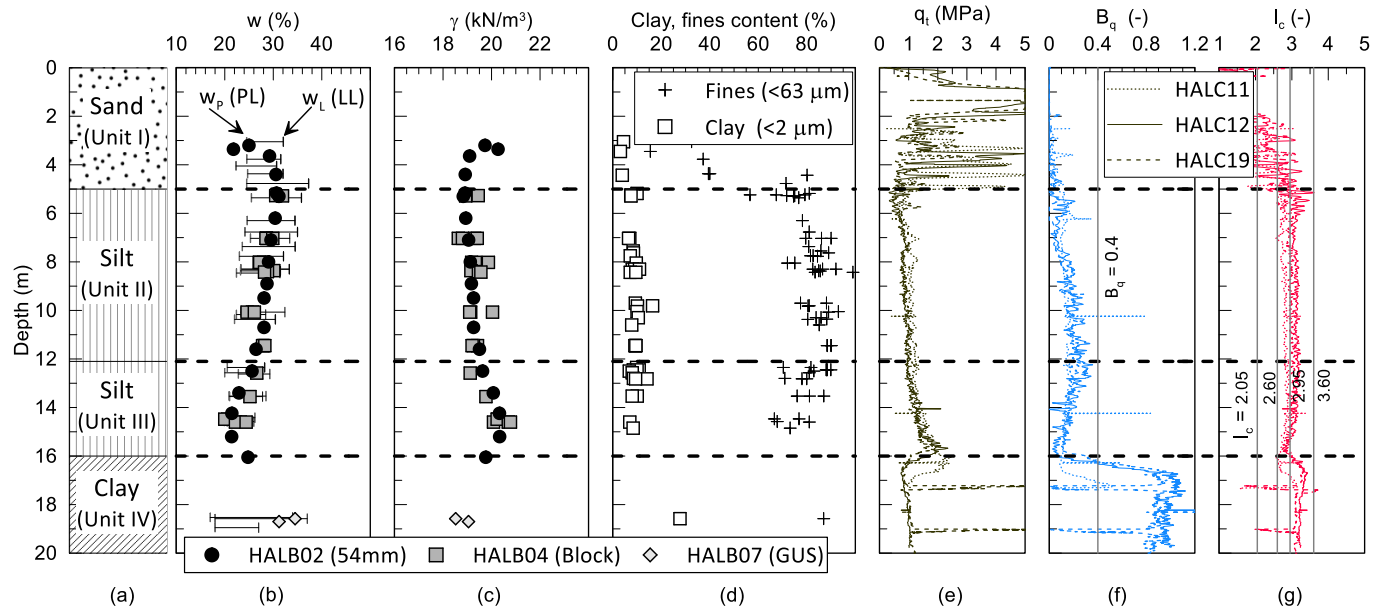


Figure 5.4 Classification and CPTU parameters with depth at the Halden research site: (a) soil units; (b) water content and Atterberg limits; (c) total unit weight; (d) percentage clay (< 0.002 mm) and fines (< 0.063 mm) particles; (e) CPTU corrected cone resistance; (f) pore pressure ratio, and; (g) soil behavior type index.

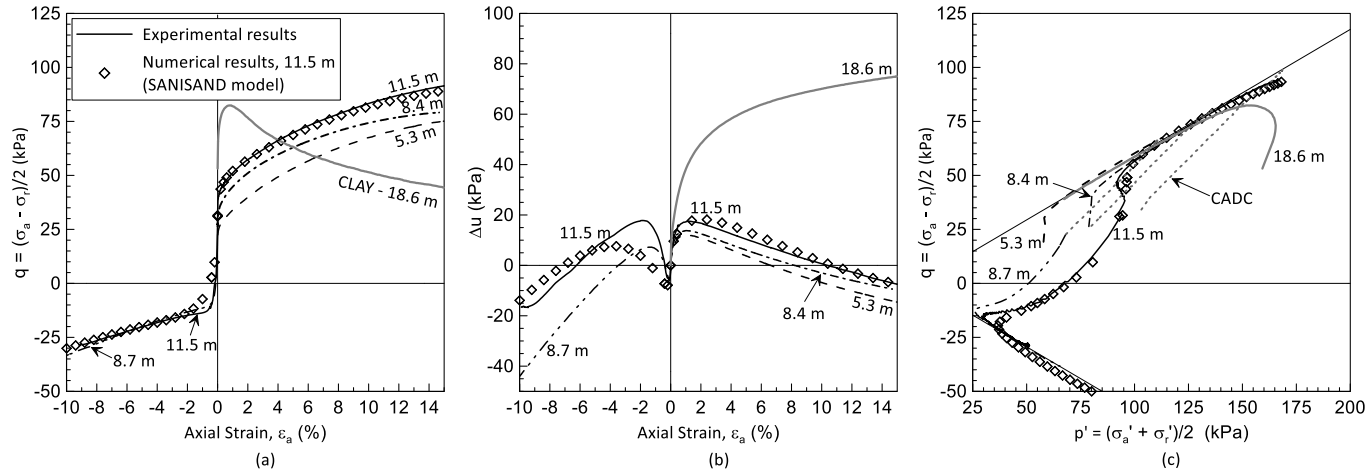


Figure 5.5 Undrained and drained triaxial test (CAUC, CAUE and CADC) results at Halden research site. (a) Shear stress and (b) excess pore pressure versus vertical strain, and (c) stress – path. Results from the SANISAND numerical model calibration for 11.5 m depth are plotted with experimental data.

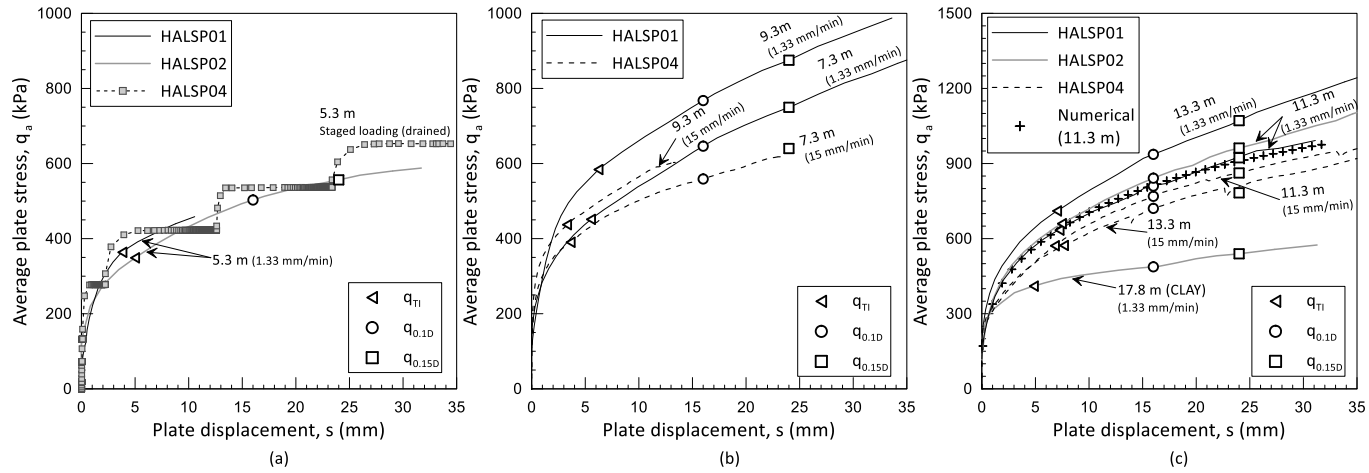


Figure 5.6 Screw plate load test results from (a) 5.3 m, (b) 7.3 m to 9.3 m, and (c) 11.3 m to 17.8 m depth, with values of interpreted bearing capacities q_{Tl} , $q_{0.1D}$, and $q_{0.15D}$ indicated on each curve. q_{HYP} were extrapolated from the stress – displacement results to the asymptotic value.

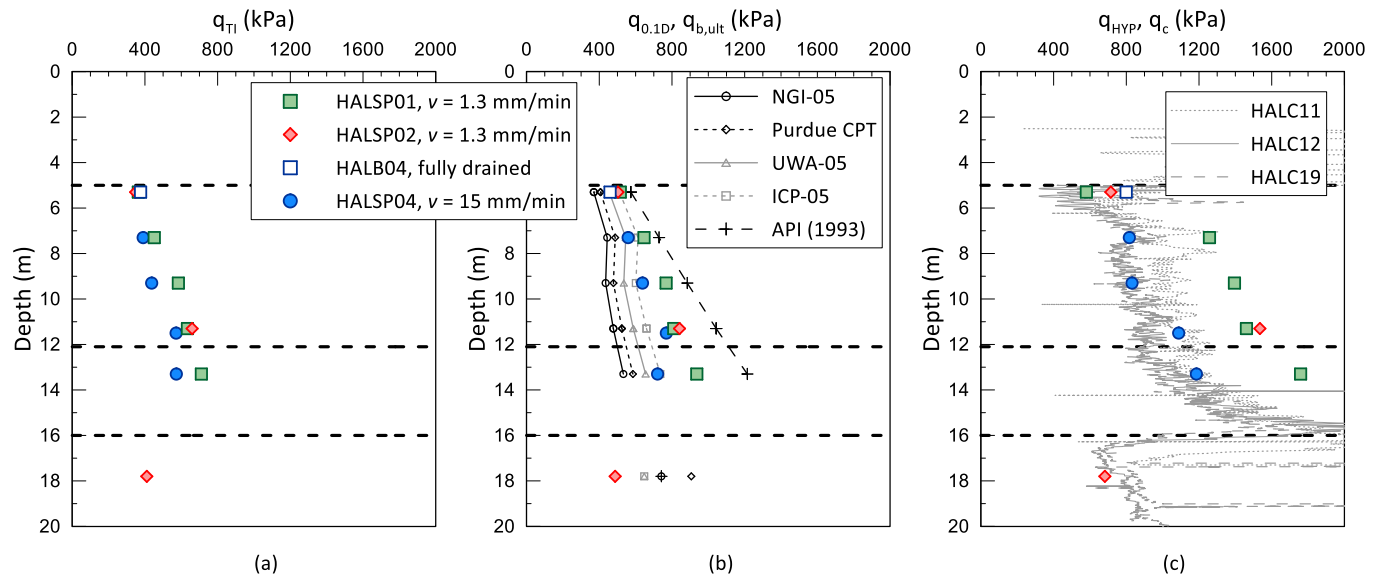


Figure 5.7 Interpreted bearing capacities, q_{ult} , with depth from the (a) tangent intersect (q_{Ti}), (b) 0.1D ($q_{0.1D}$), and (c) hyperbolic (q_{HYP}) methods.

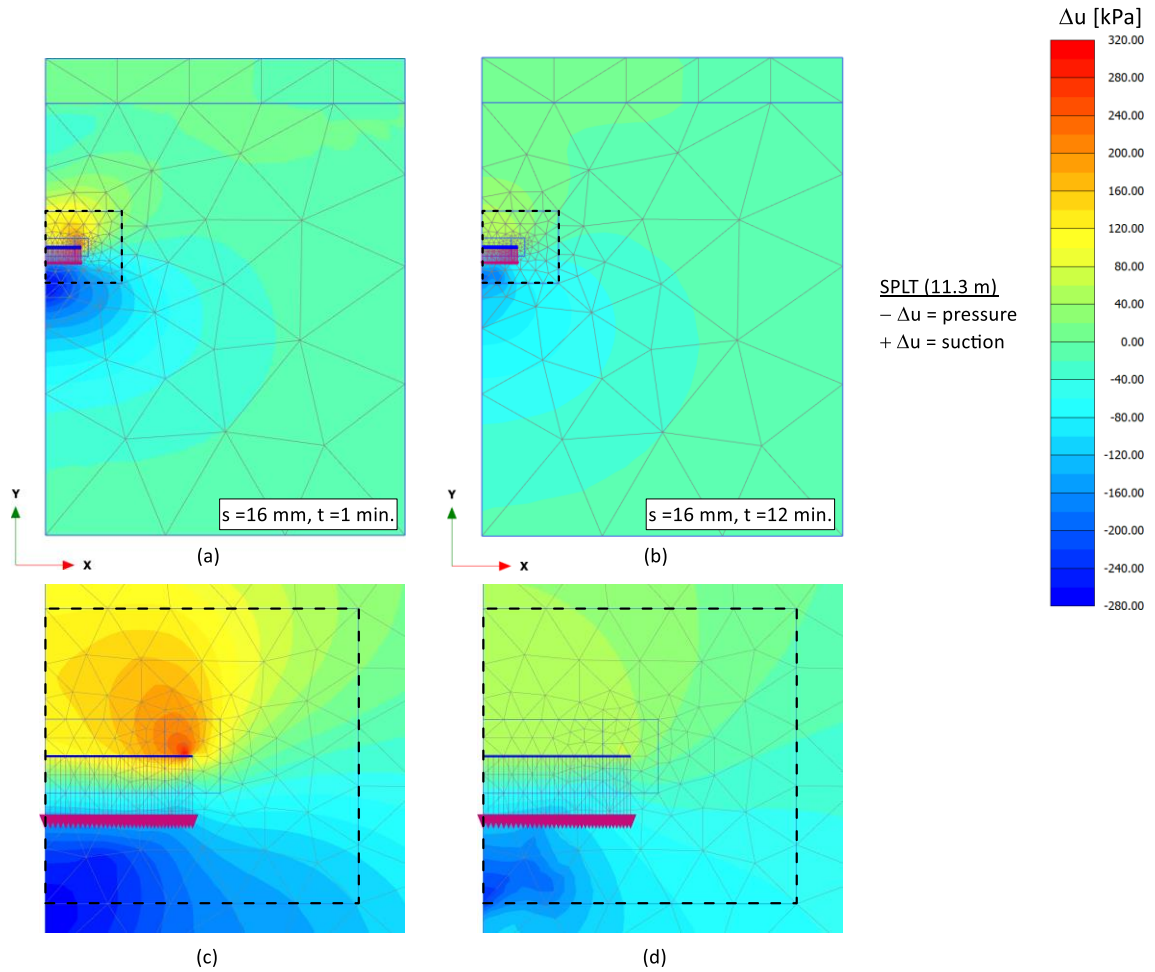


Figure 5.8 Numerical simulation of SPLTs from 11.3 m depth using the SANISAND soil model. Development of excess pore pressures, Δu , at 16 mm vertical displacement in (a) $t = 1$ min ($v = 16$ mm/min), and (c) $t = 12$ min ($v = 1.3$ mm/min), with (c-d) showing zoomed view of the refined mesh around the plate.

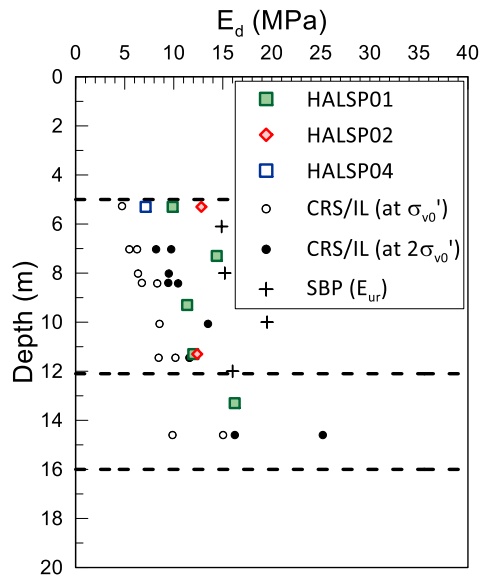


Figure 5.9 Drained elastic modulus, E_d , interpreted from SPLTs, laboratory oedometer (CRS and IL) tests and self-boring pressuremeter tests.

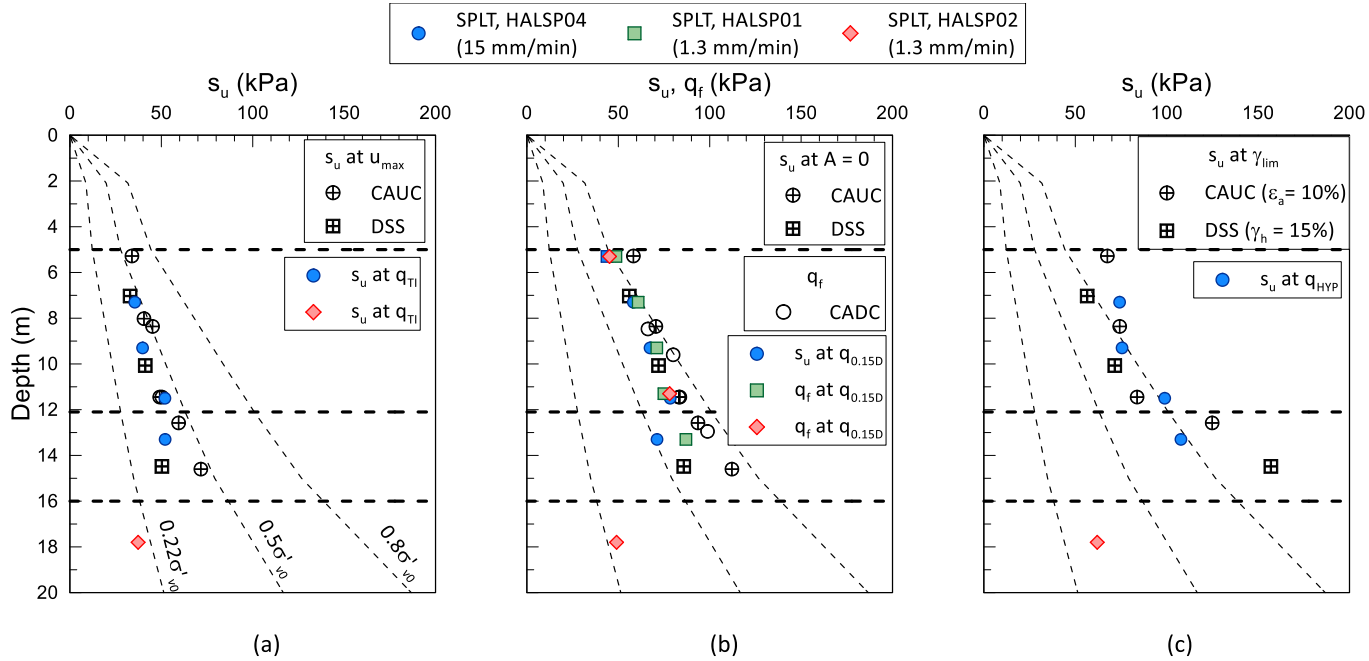


Figure 5.10 I Interpreted soil strength parameters from SPLTs compared to laboratory triaxial and DSS tests, with: (a) Undrained shear strength from q_{TI} relative to s_{uC} and s_{uD} interpreted at the u_{max} criterion; (b) Undrained and drained shear strength from $q_{0.15D}$ relative to s_{uC} and s_{uD} interpreted at the $A_f = 0$ criterion, and q_f from drained triaxial compression tests; and (c) Undrained shear strength from q_{HYP} relative to s_{uC} and s_{uD} interpreted at the $\gamma_{lim} = \gamma_f = 15\%$ criterion.

CHAPTER 6

SUMMARY AND CONCLUSIONS

The main objectives of this dissertation were to provide a new and extensive data set of engineering properties of a natural silt, complementing the limited number of studies on this soil type relative to that of clays and sands; improve the understanding of the importance of high quality sampling and potentially adverse effects of poor quality samples on soil behavior and engineering parameters; and provide some practical recommendations on the selection of shear strength for use in design based on high quality laboratory tests and field loading experiments. The objectives were met through the research discussed in chapters 2 through 5 which presented the results and interpretation of an extensive field, laboratory and numerical testing program. A brief overview of the main conclusions from this work are summarized below.

Chapter 2 provided an overview of the Halden, Norway research site with a geological background; stratigraphy; in situ characteristics from cone penetrometer, dilatometer, self-boring pressuremeter testing; and laboratory tests. Advanced oedometer, undrained triaxial and direct simple shear tests revealed several challenges and limitations, including: (i) Clay-based sample quality assessment methods may not necessarily apply to the low plasticity Halden silt and there is no established universal framework to quantify the degree of sample disturbance in silt. (ii) Interpretation of the stress history based on both oedometer test results and clay-based correlations to CPTU cone resistance were considered problematic and unreliable as they were in conflict the geological history in the area. Geology, and evidence of normally consolidated stress conditions in the lower clay, were suggested indicative of a near normally consolidated stress state of the silt as well. (iii) Undrained shear strengths, as interpreted from e.g. field

vane tests, were consistent with the CPTU interpretations using $N_{kt} = 18$ but plotted significantly lower than the results from undrained triaxial tests on block samples interpreted at large strain. CAUC tests exhibited dilative type behavior and provided no unique (peak) undrained shear strength. As a result, different strength criteria provided different results. Despite certain interpretation challenges the paper presented an important data set to assist in the interpretation and assessment of similar silts, and provided some guidance on important geotechnical properties for projects where limited site specific design parameters are available.

Chapter 3 presented a laboratory investigation of the undrained shear behavior of a natural low plasticity silt from Halden, Norway in the intact, disturbed and reconstituted states. The sample quality recompression metrics, demonstrated that neither the normalized change in recompression void ratio or volumetric strain, nor shear wave velocity track sample disturbance well for the investigated low plasticity silt unlike that for moderate to low OCR clays. Relative to the intact reference Sherbrooke block sample specimens varying degree of simulated sample disturbance, and subsequent reconsolidation to the best estimate in situ effective stress conditions, resulted in an increasingly pronounced dilative type behavior during conventional undrained triaxial shear, and a general increase in undrained shear strength. Moreover, block sample specimens subjected to simulated tube sampling disturbance also exhibited similar stress-strain behavior as that measured in conventional CAUC tests conducted on specimens from two types of fixed piston tube samplers. Practical suggestions for selection of undrained shear strength for intact low plasticity silts that exhibit dilative behavior such as the Halden silt were proposed.

Chapter 4 investigated the effects of sampling techniques on soil behavior and engineering properties of the Halden silt. The paper defined 'acceptable' and 'disturbed' quality based on experiences made from simulated sample disturbance tests at Halden and other silts reported in literature, and comparisons made between suites of companion tests conducted on specimens from four different sampler types. Results of advanced tests demonstrated that acceptable and repeatable sample quality or stress-strain behavior could be obtained using the 72 mm and Gel-push fixed piston samplers whereas specimens from the 54 mm composite fixed piston sampler showed obvious signs of significant disturbance. Although considered the gold standard for sampling in soft clays, the Sherbrooke block sampler provided specimens that displayed both acceptable and disturbed type behavior. Overall effects from increased sample disturbance included: (i) reduction in initial water content; (ii) decreasing values of normalized change in recompression void ratio and strain energy-based compression ratio with increasing disturbance; (iii) somewhat increased modulus number with increasing disturbance, although m showed relatively low sensitivity; (iv) increasing tendency for dilative behavior with increasing sample disturbance.

Chapter 5 presented an investigation of the stress-displacement behavior and bearing capacity from screw plate load tests in the natural low plasticity silt at Halden and engineering parameters interpreted from these results. All screw plate load tests demonstrated a strain hardening response that was dependent on the rate of loading. Derived bearing capacities varied significantly depending on the method used to interpret the stress-displacement data. Bearing capacities estimated from the undrained tests were lower than the companion partially drained or drained tests. Practical recommendations

relating laboratory drained and undrained shear strength to estimates of bearing capacity and vertical displacements of a prototype foundation in silts such as the Halden silt were proposed.

APPENDIX A
CONFERENCE PUBLICATION

Characterisation of Halden silt

Ø. Blaker, R. Carroll, J.-S. L'Heureux
Norwegian Geotechnical Institute, Oslo & Trondheim, Norway

M. Klug
Geological Survey of Norway, Trondheim, Norway

ABSTRACT: NGI recently established a research site on a natural silt deposit to accommodate some of the challenges related to intermediate soils. This study briefly summarises the geological history and the preliminary geotechnical characteristics of the Halden silt deposit. The stratigraphy at the site consists of four main units. Two structureless silt units sit between a 4.5 m thick layer of sand and a 6 m thick deposit of clay. Soil behaviour type charts classify the silt deposit as transitional soils/silts to low I_p clays. Classification tests indicate that these soils are low plasticity silts with very similar mineralogical content. The results presented will form a useful reference to engineers working on similar intermediate soils worldwide.

1 INTRODUCTION

Intermediate silty soils are still considered challenging materials in geotechnical engineering, and limited information in on the engineering properties and how these relate to the geological background is available. This is primarily due to uncertainty in material behaviour, difficulties associated with sampling undisturbed material and the interpretation of *in situ* and laboratory test data. There is a need to provide guidance to practicing geotechnical engineers regarding characterization of silty material. To this aim, the Norwegian Geotechnical Institute (NGI) recently established a research site on a natural silt deposit.

The Halden Research Site is located in south-eastern Norway, approximately 120 km south of Oslo (Fig. 1). Here the marine silt deposit is up to 10 m thick and uniform in nature. Over the last two years a series of geophysical, geological and geotechnical investigations have been carried out in the field and in the laboratory to characterize the natural silt deposit. This information will provide a basis for understanding the main factors controlling the engineering properties.

The purpose of this study is to present preliminary results summarizing the geological history and the geotechnical characteristics of the silt deposit at the Halden Research Site. The results presented will form a useful reference to engineers working on similar intermediate soils worldwide. Due to restrictions on the length of this study, we focus on the most significant properties.

2 GEOLOGICAL SETTING

The Halden Research Site is a recreational park area surrounded by hills, minor ravines and landslide scars. The site elevation is about 29 m above sea level and it slopes gently to the SW/W. Deposits at the site consists of marine and fjord marine sediments that emerged from the sea following a fall in relative sea level in the Oslofjord region during the last c. 11 000 years. During the post-glacial period, the depositional environment mainly led to hemipelagic deposition in a fjord marine environment. Due to the steady isostatic uplift in the Holocene and the fact that the sediments deposited continuously during a single period of submergence (Kenney, 1964), the soils in the study area are expected to be essentially normally consolidated except for some surface weathering, desiccation or in the vicinity of slide scars.

3 FIELD AND LABORATORY METHODS

3.1 *Field tests*

Several investigation methods are combined to provide information on the natural silt deposit and facilitate the understanding of the geotechnical behaviour and its link to the geological history. At present, geotechnical site investigation methods include Electrical Resistivity Tomography (ERT), several Total Pressure Soundings (TPS), Cone Penetration Tests with pore pressure measurements (CPTU), Seismic



Figure 1. Location of Halden Research Site.

Cone Penetration Testing (SCPT), Resistivity Cone Penetration Testing (RCPT), dissipation tests (Paniagua et al. 2016) and soil sampling. The latter was performed using two different Geonor thin walled stationary piston samplers; the K-100 54 mm composite sampler with zero inside clearance ratio (ICR) and a 10° cutting edge and the K-200 sampler modified to 72 mm inside diameter, ICR = 0 and a 5° cutting edge.

3.2 Laboratory tests

The samples were sent to the NGI and Geological Survey of Norway (NGU) laboratories in Oslo and Trondheim, respectively, for soil identification, classification, and assessment of index properties and advanced testing. Laboratory tests include; (i) Grain size distribution analyses by wet sieving (NSF, 1990), falling drop method (Moum, 1965) and hydrometer method (BSI, 1990); (ii) water content and Atterberg limits; (iii) unit weight of solid particles; (iv) mineralogical analyses using X-ray diffraction (XRD) and Scanning Electron Microscopy (SEM); (v) CAUC triaxial tests and (vi) constant rate of strain oedometer tests (CRS); (vii) geological and sedimentological analysis of the sediment using X-ray imaging and Multi-Sensor Core Logging techniques (magnetic susceptibility and gamma density) on 54 mm whole core samples. Whole core Gamma density (i.e. wet bulk density) and magnetic susceptibility (MS) were measured using the GEOTEK Standard Multi-Sensor Core Logger (MSCL-S) at 0.5 cm resolution with 5 s exposure/measurement time, see Figure 2. Total carbon (TC) and total organic carbon (TOC) measurements were performed on 7 samples.

4 SOIL CHARACTERISATION

4.1 Stratigraphy

The stratigraphy at the site is divided into four main units based on laboratory and *in situ* testing results, see Figure 2. It consist of c. 4.5 m of silty sand (Unit I) above c. 11 m of silt (Units IIA, IIB and III) and the final clay unit (Unit IV). Groundwater level was measured from an *in situ* stand pipe to be 2.5 m below ground level.

X-ray analyses show that both the Units II and III are structureless to mottled. Bioturbation has likely destroyed most of the primary sedimentary features. Such structureless sediments are common in fjord-marine environments subjected to hemipelagic sedimentation and seafloor biological activity (Hansen et al. 2010). In contrast, the Unit IV shows some weak laminations and the occasional presence of drop stones (sand/gravel particles) interpreted as ice rafted debris (IRD).

4.2 Water content and Atterberg limits

Natural water content (w) in Unit II generally falls between 28% and 31%. In Unit III the water content decreases with depth from about 27% at 12 m depth to about 21% at 15 m with an average value of 24%. The liquid limit (w_L) in Unit II varies between 31% and 37%, while in Unit III w_L is about 28%. Plastic limit (w_p) values are between 22% and 25% in the upper 11 m while below $w_p = 20\% - 22\%$. This gives plasticity indices (I_p) between 8% - 13% for Unit II. The average I_p is 10 % between 4.5 m and 10.5 m. The plasticity data for Units I and IIa fall on and below the A-line while Unit IIb and III data points are on and above the A-line, respectively (see Fig. 3). The average I_p of Unit I and III (12 – 13 m depth) is 7.5% and 8%, respectively. Based on the data in Figure 3 the Unified Soil Classification System (USCS) classifies the soils as silty clay with sand to lean clay with sand.

4.3 Total unit weight and magnetic susceptibility

The total unit weight (γ_t), both estimated from whole core gamma density measurements and that based on water content, are presented in Figure 2. Total unit weight in Unit II generally falls between 18.9 kN/m³ and 19.2 kN/m³. In Unit III the total unit weight increase with depth from about 19.5 kN/m³ at 12 m to about 20.5 kN/m³ at 15 m, with an average value of 19.9 kN/m³.

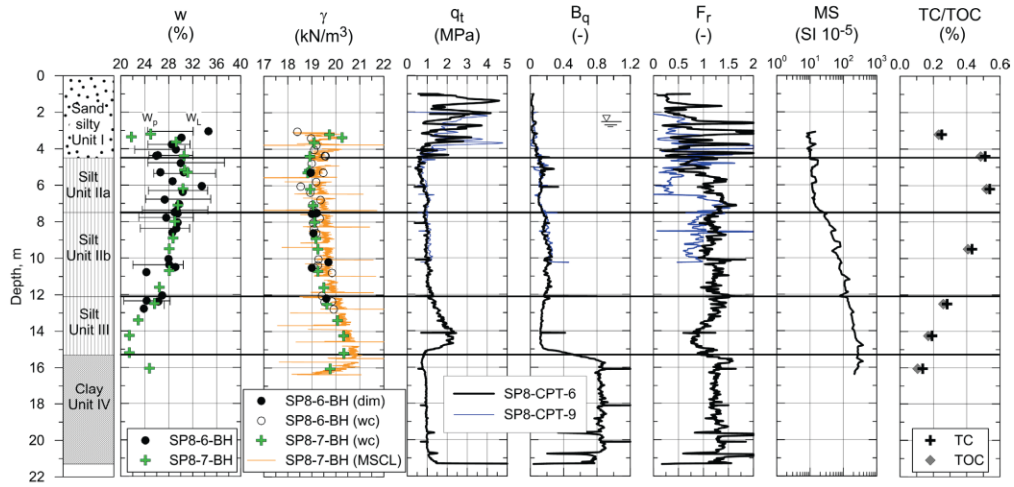


Figure 2. Basic parameters for Halden Research Site, corrected cone resistance, q_t , normalised pore pressure, B_q , normalised friction, F_r , versus depth from CPTU, magnetic susceptibility from MSCL, and TC/TOC. Whole core Gamma density (i.e. wet bulk density) is shown in yellow on the total unit weight log.

Results from MSCL-S show an increase in wet bulk density (or total unit weight) in Unit II. The trend is similar to that obtained from laboratory results based on direct measurements and from water content. However, the wet bulk density values from the MSCL-S are slightly higher than those from direct measurement or values based on water content analysis (Fig. 2). This may be due to whole core measurements where wet bulk density measurements integrate the entire sample thickness. The MS results show constant values in the first c. 2 m of Unit II and thereafter a linear increase with depth until culminating at the upper boundary of Unit IV.

4.4 Grain size distribution

Figure 4 presents typical grain size distributions for the silt in Units II and III. All results are from the falling drop method (Moum, 1963). However, there is a trend of lower clay content based on the hydrometer method and the clay content determined by this method varies between 4% and 8% in Units II and III.

4.5 Carbon content and mineralogy

In Unit II the average Total Carbon (TC) was measured to 0.486% with a range from 0.432% - 0.539%. In Unit III the average TC is 0.238%, ranging from 0.193% - 0.282%. Meanwhile the Total Organic Carbon (TOC) in Unit II average is 0.464% while the average is lower in Unit III at a value of 0.215%.

Table 1 presents the result of XRD analyses performed on soil from Unit II and III. They reveal very similar mineralogical content for the silt Units II and

III. Both units contain similar amounts of quartz, plagioclase, mica (muscovite and possibly illite), chlorite and amphibole. A Scanning Electron Microscope (SEM) image of a specimen from 6.4 m depth is presented in Figure 5.

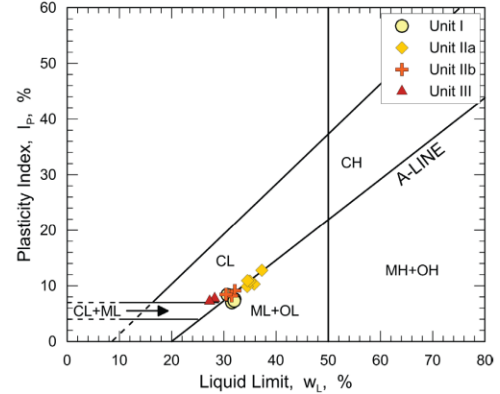


Figure 3. Plasticity chart, Unit I to III.

Table 1. Results from XRD analyses on silt Units IIa and IIb.

Depth (Unit) m	Q* %	K-F* %	P* %	M/I* %	C* %	A* %	P* %
6.2 (Unit IIa)	41	12	30	8	3	6	trace
9.5 (Unit IIb)	40	13	29	8	4	6	trace
13.4 (Unit III)	44	12	30	7	2	5	trace

* Q – Quartz, K-F – Potassium Feldspar, P – Plagioclase, M/I – Muscovite/Illite, A – Amphibole, P – Pyrite

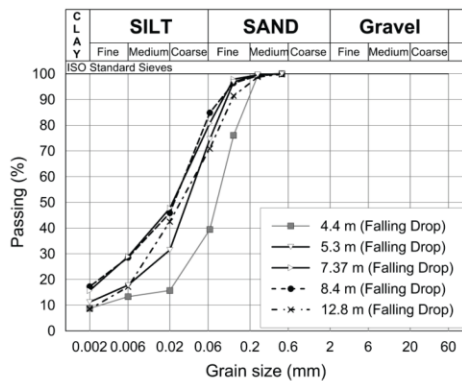


Figure 4. Typical grain size distribution curves, Unit II and III.

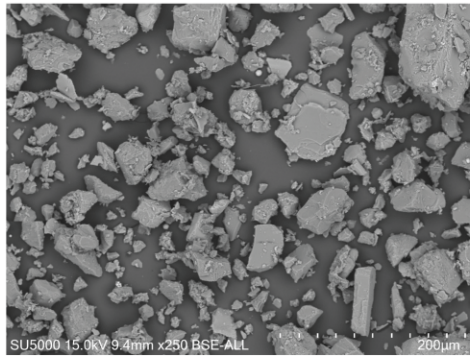


Figure 5. SEM image of a silt specimen from 6.4 m depth.

5 CONE PENETRATION TESTING

5.1 Corrected cone resistance and pore pressure

The corrected cone resistance (q_t) from CPTU tests, SP8-CPT-6 and SP8-CPT-9, are presented in Figure 2. The higher cone resistance in Unit I compared to the other units reflects the silty sand extending to about 4.5 m depth. Unit II has a uniform cone resistance throughout with q_t in the order of 1.0 MPa. In Unit III q_t increases from 1 MPa to 2.0 MPa between 12 m to 14.5 m before reducing to 1.0 MPa in the clay Unit IV. Pore pressure, u_2 , is not presented but increases steadily with depth to approximately 380 kPa at 14 m depth. There is a clear change in rate of increase in u_2 from 15 m to 17 m which coincides with the upper boundary of Unit IV. Below 17 m u_2 increases steadily with depth.

5.2 Soil behaviour type and soil classification charts

Figure 6 presents the traditional SBT chart from Robertson (1990) combined with the more recent classification chart from Schneider et al. (2008).

This system is based on Q_t and B_q and using Schneider et al. (2008) lines. Depth bias is known to occur when using soil classification charts if q_{net} and Δu_2 are not normalised, especially for sites with changes in OCR with depth. In this case only normalised charts are used for analysis. Unit I is classed as transitional. Unit IIa and IIb are classified as Transitional soil changing to Silts and low I_r (rigidity index) clays with depth. Unit III falls on the border between Transitional soils and Silts and low I_r clays before the deeper Clay Unit IV is identified. The Robertson (1990) classification chart, see Figure 6, indicates that Unit I is a Silt mixture with some transition into Sand mixture and Sands. Using this chart, Unit IIa, IIb and III are all Clays (clay to silty clay) with some transition into the Silt mixtures. Unit IV also a Clay (clay to silty clay) plots on the far right of the figure.

The Schneider et al. (2008) classification chart in Figure 7 presents a slightly different classification for the soil units as Units IIa and IIb both fall in Silts and low I_r clays classification and do not cross into the Transitional soils area. The classification for Unit III is Silts and low I_r clays before the deeper Clays / Sensitive Clays. Overall this Q_t - $\Delta u_2/\sigma'_{v0}$ chart from Schneider et al. (2008) shows a clear classification of Silts and low I_r clays. It is also notable that Unit IIa and IIb are grouped separately within this classification. Unit I is a distinctively different material and clearly falls in the transitional soils classification in contrast to Unit II.

6 ENGINEERING PROPERTIES

Two CAUC tests were performed on 72 mm specimens from Units IIa and IIb, from 5.3 m and 8.6 m depth, respectively. Both specimens were consolidated to a best estimate vertical effective stress σ'_{v0} using K_0 of 0.5. The change in $\Delta e/e_0$ during sample consolidation was less than 0.02 for both specimens. Sample quality is therefore qualified as very good to excellent for and OCR of 1 - 2 according to Lunne et al. (1997). However it is noted that this criteria was developed for marine clays and might not be applicable to intermediate soils. The normalised shear stress with strain behaviour showed a steady increase in shear stress for both samples. At 10% axial strain the samples had normalised shear stress in the region of $\tau_t/\sigma'_{v0} = 0.7 - 0.9$. The normalised pore pressure reached a peak in the region of $\Delta u_2/\sigma'_{v0} = 0.14$ before 1% strain and the test specimens dilated strongly. The stress paths showed a clear 'S' shaped response before dilation. The samples had clay contents of 11% and 17% determined by the falling drop method. The silt content was approximately 65% and I_p was less than 10% for both samples. At peak pore pressure the normalised shear stress is in the range of 0.4 - 0.45. The measured response from

the tube samples is thought to be representative of good quality silt samples considering the corresponding index data.

7 DISCUSSION

Initially the silt deposit at the Halden Resesarch Site showed to be very homogenous. No layering was observed and the sediment proved to be structureless even with X-ray imaging. However, combining the data obtained from *in situ* testing, classification testing and the Multi Sensor Core Logger one can observe two distinct silt units. Units II and III differ slightly in terms of water content, total unit weight and magnetic susceptibility. This correlates also with an increase in corrected cone penetration resistance from 12 m. Reasons for this gradual change are not fully understood, but one possibility is that such subtle changes are linked to variation in organic matter as observed in both units. This interpretation is corroborated by other studies of geotechnical properties of marine sediments which showed to be altered to varying degrees by subtle changes in organic content (e.g. Keller 1982, Booth & Dahl 1986). Organic matter absorbs water and causes clay-sized particles to aggregate forming an open fabric. This causes an increase in water content and plasticity, and a decrease in the total unit weight. Since the mineralogical contents of both Units II and III are almost identical, the changes in magnetic susceptibility and gamma density obtained from MSCL-S could be linked to the observed patterns of organic matter and water contents (c.f. St-Onge et al. 2007).

The variations between the different SBT charts highlight the importance of cross checking CPTU interpretation of soil classification or behaviour type with index data. Falling drop grain size data for Unit IIa and IIb show average clay content of 13.4% and Unit III lower at 9% clay content. There is evidence that clay contents may be lower based on hydrometer results. For example, in Units IIa and IIb the clay content is in the range of 7.8% and 3% to 7% in Unit III. Clay contents at the lower bounds are questionable as Atterberg limits were measured on the material in Unit III. The plasticity index data for Unit IIa and IIb agrees well with the clustered results in the soil classification charts as Unit IIa is just on and below the A-line and has a higher I_p while Unit IIb plots on the A-line and has a lower I_p . Unit I, a transitional soil plots just below the A-line and has a low I_p which agrees well with the classification charts for both Robertson (1990) and Schneider et al. (2008). The soil classification based on CPTU results in Units IIa and IIb plot in a similar region of the Q-B_q chart (Schneider et al. 2008) as CPTU data from a silt site, Halsen, in Northern Norway tested by Sandven (2003).

A very limited program of advanced tests are carried out on the Halden silt. However, the normalised shear stress τ_f/σ_{v0}' interpreted at peak pore pressure in the CAUC tests are in the range of 0.4 to 0.45. This is slightly below the ratios presented by Brandon et al. (2006) for Yazoo and LMVD silt, but within the range reported by Long (2007) for the estuarine Sligo silt.

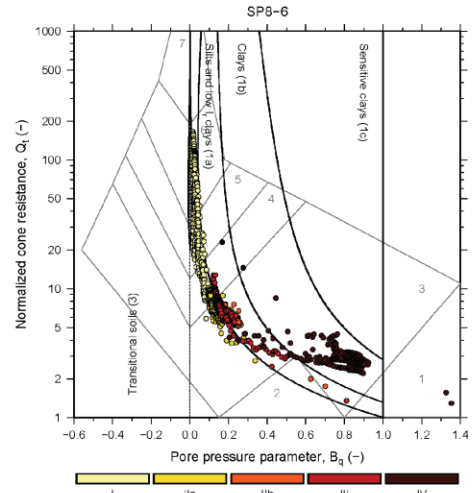


Figure 6. Robertson (1990) soil behaviour type chart for SP8-CPT-6.

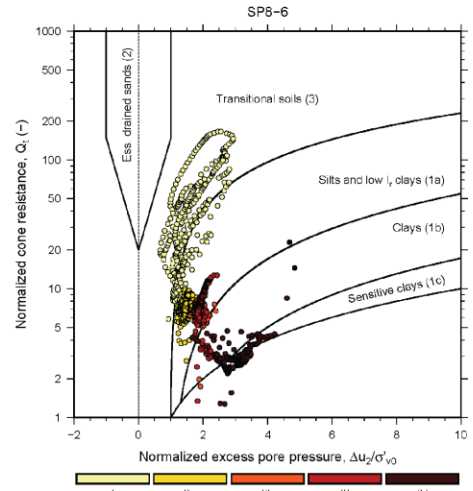


Figure 7. Schneider et al. (2008) soil behaviour type chart for SP8-CPT-6.

8 CONCLUSIONS

This study has detailed some characteristics and engineering properties of the Halden silt, a 11 m thick deposit of fjord marine silt in south-eastern Norway. NGI recently established a research site on this deposit to accommodate some of the challenges related to intermediate soils. A variety of *in situ* and laboratory tests have been performed to investigate its properties. Some preliminary conclusions are:

(i) The silt is considered normally consolidated and is of low plasticity, with a clay content between 8% – 18%.

(ii) Similar mineralogical content of the silt layers, Units II and III, is found. The soil consists mainly of quartz, K-feldspar and plagioclase, with 7% - 8% muscovite/illite.

(iii) Corrected cone resistance from CPTU in Unit II and III shows a 1 MPa to 2 MPa response, while pore pressures are positive and steadily increasing with depth down to the clay layer.

(iv) Patterns of water content, unit weight, magnetic susceptibility and cone penetration resistance could be attributed to subtle changes in organic content. Reasons for these gradual change are not fully understood and will need further studies.

(v) Various SBT charts classify the soils as transitional soils or silts to low I_r clays. The Schneider et al. (2008) $Q_1-\Delta u_2/\sigma_{v0}'$ chart shows a clear classification of Unit II-IV as silts and low I_r clays, and separates Unit IIa and IIb from each other.

(vi) The variation between the different SBT charts highlights the importance of cross checking CPTU interpretation of soil classification or behaviour type with laboratory index data.

(vii) CAUC tests on 72 mm silt specimens from Unit II indicate a normalised shear stress at failure the region of $\tau_f'/\sigma_{v0}' = 0.4 - 0.9$, depending on the failure criteria selected.

The results contribute to the developing global knowledge of properties and behaviour characteristics of intermediate soils. Further studies are planned at this site to better understand factors controlling the mechanical response of intermediate soils.

9 ACKNOWLEDGEMENT

This work is funded by the Norwegian Research Council (NRC) through the strategic research project SP8 – GEODIP at NGI. The contributions from other colleagues at NGI and Geological Survey of Norway are also highly appreciated.

REFERENCES

- Booth, J.S. and Dahl A.G. 1986. A note on the relationships between organic matter and some geotechnical properties of a marine sediment. *Marine Geotechnolgy* 6(3): 281–297.
- Brandon, T. L., Rose, A. T. & Duncan, M. J. 2006. Drained and undrained strength interpretation for low-plasticity silts. *Journal of Geotechnical and Geoenvironmental Engineering* 132(2): 250-257.
- BSI (1990). British Standard methods of test for soils for civil engineering purposes: Part 2 Classification tests. *BS1377*, British Standards Institution, London.
- Keller, G. H. 1982. Organic matter and the geotechnical properties of submarine sediments. *Geo-Marine Letters* 2(3): 191–198.
- Kenney, T.C. 1964. Sea-level movements and the geological histories of the post-glacial marine soils at Boston, Nicolet, Ottawa and Oslo. *Géotechnique* 14(3): 203–230.
- Long, M. 2007. Engineering characterization of estuarine silts. *Quarterly Journal of Engineering Geology and Hydrogeology* 40(2): 147-161.
- Lunne, T., Berre, T. and Strandvik, S. 1997. Sample disturbance in soft low plastic Norwegian clay. M. Almeida (Ed.), *Recent Developments in Soil and Pavement Mechanics*, Balkema, Rotterdam, pp. 81–102.
- NSF 1990. Geotechnical testing. Laboratory methods. Grainsize analysis of soil samples. *NS 8005:1990*. NSF, Oslo.
- Moum, J. 1965. Falling drop used for grain-size analysis of fine grained materials. *Sedimentology* 5(4): 343–347.
- Paniagua-López, P., Carroll, R., Blaker, Ø., L'Heureux, J.-S., Nordal, S. 2016. Monotonic and dilatatory excess pore water dissipations in silt following CPTU at variable penetration rate, Int. conf. on Geotech. and Geophys. Site Char., Gold Coast, Australia, 5-9. September, 2016.
- Robertson, P. K. 1990. Soil classification using the cone penetration test. *Canadian Geotechnical Journal* 27(1): 151–158.
- Sandven, R. 2003. Geotechnical properties of a natural silt deposit obtained from field and laboratory tests. In Tan, T.S., Phoon, K.K., Hight, D.W. & Leroueil, S. (ed.) *Characterization and engineering properties of natural soils; Proc. Int. Workshop*, NUS Singapore, 2-4 December, 2002, Balkema, Rotterdam, 2, 1121-1148.
- Schneider, J. A., Randolph, M. F., Mayne, P. W. & Ramsey, N. R. 2008. Analysis of factors influencing soil classification using normalized piezocone tip resistance and pore pressure parameters. *Journal of Geotechnical and Geoenvironmental Engineering* 134(11): 1569–1586.
- St-Onge G., Mulder T., Francus P., & Long B. 2007. Chapter Two; Continuous Physical Properties of Cored Marine Sediments. *Developments in Marine Geology*, Elsevier: 63–98.
- Sorensen, R. (1979). Late Weichselian deglaciation in the Oslo fjord area, South Norway. *Boreas* 8: 241–246.

APPENDIX B
CONFERENCE PUBLICATION

Evaluation of bearing capacity and in situ shear strength using the screw plate load test in clay and silt

Ø. Blaker

Norwegian Geotechnical Institute, Oslo, Norway, oyvind.blaker@ngi.no

D. J. DeGroot

University of Massachusetts, Amherst, MA, USA, degroot@umass.edu

J. T. DeJong

University of California, Davis, CA, USA, jdejong@ucdavis.edu

ABSTRACT: Recent studies show that silts are sensitive to sampling disturbance, and that the effects of sampling can be adverse and opposite of those typically observed for clays. Silts often exhibit a tendency for dilative behavior upon undrained triaxial shear. As a result, the interpreted shear strength is highly dependent on which failure criterion is selected but there is limited guidance or consensus on what criterion represents the relevant in situ shear strength for design applications. To this end, in situ Screw Plate Load Tests (SPLT) have been conducted at Halden, Norway, to investigate the bearing capacity and behavior of the silt and clay deposits under field loading, and uncertainties associated with undrained/draind/partially-draind conditions. Normalized penetration velocity indicates that the SPLTs were likely partially-draind in the silt unit and undraind in the clay unit. This information was used to back-calculate estimates of the in situ strengths for comparison with laboratory tests conducted on undisturbed specimens from both soil units.

Keywords: silt; clay; triaxial test; screw plate load test; bearing capacity.

1. Introduction

An increasing number of geotechnical projects involving silt has sparked a series of research efforts to better understand the fundamentals of this intermediate soil, the effects of sampling disturbance and uncertainties associated with undraind/draind/partially-draind conditions. For sands and clays, deformation and strength parameters can be evaluated in situ through well-established correlations with measured or derived parameters from cone penetration tests with pore pressure measurements (CPTU), dilatometer tests (DMT), self-boring pressuremeter tests (SBP), or back-calculated and interpreted from plate load tests (PLT). The CPTU, for example, can be used to estimate undraind shear strength (s_u), effective stress friction angle (ϕ'), constrained modulus (M) and small strain shear modulus (G_{max}) of a soil with depth, and to estimate axial pile capacity (Q_{ult}) from the cone resistance (q_c).

Methods for interpretation of laboratory and in situ tests in silt have not seen the same developments or conclusive research as for clays and sands, and there are still large uncertainties associated with in situ behavior and appropriate geotechnical parameters for practical engineering design in this soil type. Partial drainage effects may have a significant effect on sample quality, the interpreted soil behavior type and soil properties from in situ and laboratory testing. For example, results from "twitch" testing at variable penetration rates have demonstrated how CPTU measurements change with normalized penetration velocity (V), expressed as:

$$V = vD/c_h \quad (1)$$

where v = rate of penetration; D = penetrometer diameter; and c_h = coefficient of horizontal consolidation. $V > 10 - 100$ have been suggested to be indicative of fully undraind conditions, while fully draind conditions typically occurs for $V < 0.05 - 0.01$ [1-3]. Penetrometer measurements conducted under $V = 0.05 - 10$ may therefore be affected by partial drainage.

Furthermore, recent studies demonstrated that silts are particularly sensitive to sampling disturbance, and that the effects of tube sampling on engineering properties can be adverse and opposite of those typically observed for clays [4]. Tube samples of silt often exhibit a tendency for dilative behavior and strain hardening upon undraind triaxial shear in compression and, as a result, the undraind shear strength of this material cannot be readily interpreted at the conventional peak shear stress as for soft structured clays [4-8]. The shear strength of the material depends on the criterion selected for interpretation and there is limited guidance or consensus on what criterion most accurately represents the relevant in situ shear strength for design.

As sampling of silt has traditionally been considered challenging, and quantitative assessment of sample quality using clay-based criteria is highly questionable in this soil type, in situ loading tests were considered attractive for evaluation of bearing capacity and shear strength. Marsland [9] used PLT data to back-calculate undraind shear strength of stiff, fissured London clay, showing that the large-scale undraind shear strength was significantly lower than that measured in small undraind triaxial compression test (CAUC) specimens. A variation of the PLT, the SPLT uses a single flight helical screw to advance from ground level without the need for a pre-augered borehole, thus retaining the overburden stress [10]. This configuration was adopted and used to evaluate compressibility of different sands and the influence of

preconsolidation stress on sand deformability by Schmertmann [11] and Dahlberg [12], respectively. The device has also been successfully used in a number of different clays [13-17], but only a few results have been conducted in silt. Janbu and Senneset [18] and Sandven [19] report incremental loading SPLTs (i.e., fully drained conditions) conducted at a silt site in Stjørdal, Norway for evaluation of in situ compressibility of the deposit.

This paper presents results of three SPLTs conducted at the National GeoTest Site for silt in Halden, Norway. It investigates load-deformation behavior in the clayey silt and underlying clay units, interpretation of engineering parameters and compares the measured bearing capacities with calculated base unit resistance for an equivalent diameter closed end pile.

2. Methods

2.1. Sampling

Soil samples were collected at the Halden, Norway research site [8] using the Sherbrooke block sampler [20] in location HALB04, the NGI 54 mm inner diameter (ID) composite piston sampler [21] in location HALB03 and the Gregory Undisturbed Sampler (GUS), a hydraulic fixed piston sampler, manufactured by Acker Drill Company, PA, USA in location HALB07. All locations are presented on the map in Figure 1.

2.2. Field equipment

The screw plate equipment consisted of a single helix flight auger (Figure 2) with $D = 160$ mm (Area, $A = 200$ cm²) and a 45 mm pitch. The plate was founded in ductile cast iron (EN-GJS-500) by Ulefoss Foundry, Norway based on a model by Strout [22]. The screw plate was positioned directly in front of a custom-made down-hole hydraulic jack and double-rod configuration described by Janbu and Senneset [18]. The outer 42.5 mm outer diameter (OD) steel rods provided torque during installation and reaction from the jack to the drill tower of the Georigg 607 (Geotech AB, Sweden) drill rig during static loading. A simple load frame was positioned between the outer rod and drill rig and allowed access to the top of the 27 mm OD center rods. The unloaded center rods provided direct measurement of the plate displacement using two Mitutoyo Digimatic ID-C 0.001/50.8 mm deformation indicators mounted on an independent reference beam. An Enerpac P392 hand pump and a 64 MPa GDS high pressure volume controller provided hydraulic pressure to the closed system through a 400 MPa capacity hydraulic hose connected to the jack positioned directly behind the screw plate. Hydraulic cylinder pressure to plate stress (q_p) conversions were calibrated in the laboratory using an Interface (Interface Inc., Scottsdale, AZ, USA) 250 kN load cell.

The screw plate was carefully installed by rotation from ground level to target depth (z) by the drill rig. The rate of penetration during installation was adjusted to equal the pitch of the screw plate (i.e. about 45 mm per 360° rotation) in order to minimize disturbance to the surrounding soil. The Enerpac pump and GDS volume controller were connected to the hydraulic hose, the plate

pressure was set equal to the in situ vertical effective stress and the equipment was allowed to rest for about 15 min to allow equalization of installation pore pressures near the screw plate. Displacement gauges were zeroed, and continuous rate of deformation testing was conducted using the GDS pump. A GDS flow rate of about 40 mm³/s was typically used, providing a displacement rate of about 1.33 mm/min (0.5D/hr). Readings of cylinder pressure and plate displacement (s) at fixed time intervals (t) were recorded to a displacement of about $s = 0.2D$. After completion of a test, the reference beam and deformation indicators were dismantled, and the system carefully vented to atmospheric pressure. The oil reservoir was vented and the hydraulic cylinder, typically fully extended after testing, was reset to its original position using the drill rig. Finally, the pumps were disconnected, and the screw plate advanced to the next test depth.

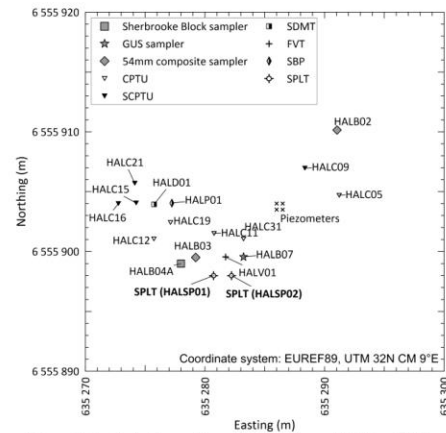


Figure 1. In situ testing and sampling locations at Halden. SPLTs were conducted in HALSP01 and HALSP02.

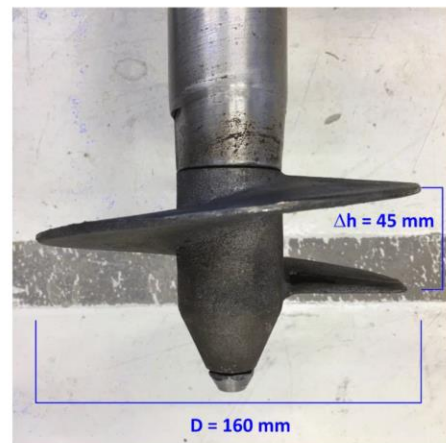


Figure 2. Screw plate with diameter $D = 160$ mm and pitch of 45 mm used at the Halden GeoTest Site.

2.3. Triaxial testing

Triaxial specimens were prepared by trimming of Sherbrooke block and GUS specimens using the procedures described by Lacasse and Berre [23] and Ladd and DeGroot [24]. During back pressure saturation the test specimens were first subjected to an isotropic stress (cell pressure) equal to the estimated value of the initial negative pore pressure (suction) within the specimen. The porous filter stones were initially dry. At the initial isotropic stress, de-aired water was flushed through the porous stones and any tendency for volume change was prevented by adjusting the cell pressure until a stable condition was reached. Following this stage, backpressure was applied and all B values, which were measured at the end of the consolidation phase, were $\geq 97\%$. All specimens were anisotropically consolidated to the best estimate in situ vertical effective stress, σ'_{v0} and horizontal effective stress σ'_{h0} using an assumed $K_0 = 0.5$ [8]. All specimens were allowed to creep for 12 to 24 hours prior to undrained shear testing performed at a strain rate of 0.5 – 1.4 %/hr. The total radial stress was kept constant while the total axial stress was increased in compression (CAUC). All stress measurements were corrected for membrane resistance and changes in specimen area [25].

2.4. Analysis

2.4.1. Ultimate bearing capacity from SPLT

Three methods were used to assess the ultimate bearing capacity, q_{ult} from the SPLT stress-displacement curves:

- 0.1B method – ultimate bearing stress limited by a relative displacement, typically 10% of the footing width or pile diameter, B [26, 27]. In this case, 10% of the screw plate diameter, D , i.e. $q_{ult} = q_{0.1D}$.
- Tangent intersect – bearing stress corresponding to a distinct change in plate displacement, i.e. intersection of initial and final tangent slope of stress - settlement plot [28], i.e. $q_{ult} = q_{TI}$.
- Curve fitting – ultimate bearing capacity extrapolated using an exponential curve intersecting the bearing stress, q_x and q_y at $0.015D$ and $0.02D$, respectively [15], i.e. $q_{ult} = q_{KP}$.

Other methods are available, e.g. the Log-Log method [29], but were considered inappropriate for the interpretation of the load tests described in this paper. For all methods listed above the displacement at failure (s_f) were taken as the displacement corresponding to q_{ult} .

2.4.2. Pile ultimate unit base resistance

A deeply embedded screw plate ($z/D > 33$) may be compared to the base of a circular closed end pile (CEP) with equivalent diameter and area. The ultimate base resistance of a pile is expressed as [30]:

$$Q_{b,ult} = q_{b,ult}A_b \quad (2)$$

where $q_{b,ult}$ = the ultimate unit base resistance and A_b = area of the pile base. The ultimate unit base resistance of a pile tip equivalent to that of the screw plate ($D = 160$ mm) was assessed using a number of methods, including:

- the classical bearing capacity equation (disregarding the $0.5\gamma'DN'_y$ term due to its small relative contribution), i.e.:

$$q_{b,ult} = N_c^*s_u + N_q^*\sigma'_{v0} \quad (3)$$

where N_c^* , N_q^* , N_γ^* = dimensionless bearing capacity factors for deep foundations, including necessary shape and depth factors; s_u = undrained shear strength; and γ' = effective unit weight of soil [31-33].

- CPTU-based methods, including:
 - Purdue-CPT [27],
 - NGI-05 [34, 35],
 - ICP-05/MTD-1996 [36, 37], and
 - UWA-05/UWA-13 [38, 39].

All CPTU-based design methods are summarized by Han, et al. [40].

2.4.3. Shear strength

Undrained shear strength from CAUC tests on clay specimens were assessed at peak shear stress, i.e. $s_{uC} = 0.5(\sigma_1 - \sigma_3)_{max}$. For silt specimens displaying dilative type behavior during undrained shear, and thus, no peak shear stress, s_{uC} was evaluated using the following strength criteria [41]:

- maximum deviator stress, $(\sigma_1 - \sigma_3)_{max}$;
- an assigned limiting vertical strain, ε_{vf} ;
- state of zero excess shear induced pore pressure at failure $\Delta u_f = 0$, which is equivalent to Skempton's A parameter at failure equal to zero, $A_f = 0$;
- point at which the effective stress path first reaches the failure envelope, defined by the K_f line;
- maximum obliquity, $(\sigma'_1/\sigma'_3)_{max}$;
- maximum shear induced pore pressure, u_{max} .

Undrained shear strength assessed from the screw plate load tests were back-calculated using:

$$s_u = q_{ult}/N_c^* \quad (4)$$

3. Test program and site description

Three SPLTs were performed, one at a depth of 11.3 m in borehole HALSP01, and one each at 11.3 and 17.8 m depths in borehole HALSP02 (Figure 2) at the Norwegian GeoTest Site (NGTS) for silt. The site is located in Halden, Norway, approximately 120 km south of Oslo and has been well characterized [see 8] by combining the

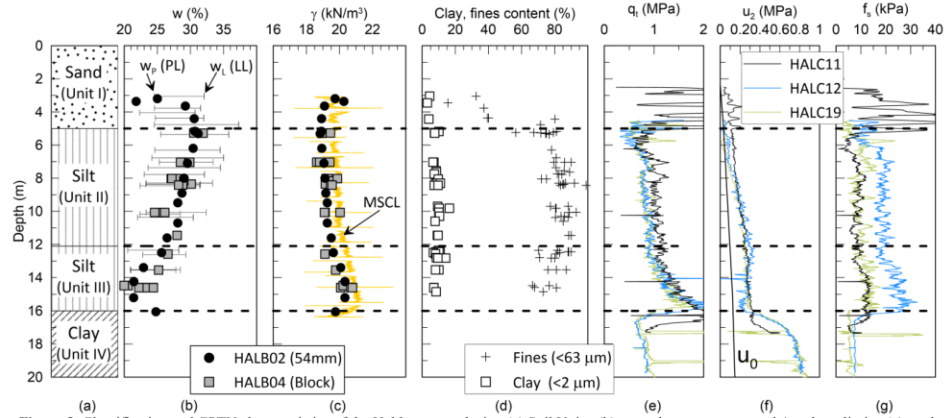


Figure 3. Classification and CPTU characteristics of the Halden research site; (a) Soil Units, (b) natural water content and Atterberg limits, (c) total unit weight, and (d) clay particle and fines content, (e) corrected cone resistance, q_c , (f) pore pressure, u_2 , and (g) sleeve friction, f_s . Modified from Blaker, et al. [8].

results of a number of geological, geophysical and geotechnical site investigation tools; including sampling, CPTU, CPTU pore pressure dissipation tests and field vane tests (FVT).

A silty, clayey sand constitutes the top soil (Unit I) and extends down to about 4.5 to 5 m depth. The geologically normally consolidated clayey silt below (Units II and III) extend down to about 15 to 16 m depth, with soil behavior type index (I_c) generally plotting between 2.6 and 2.95. Normalized cone resistance (Q_n) and pore pressure ratio (B_p) in these soil units are generally in the order of 7.5 and 0.1 – 0.3, respectively. The silt is uniform and structureless to mottled, with primary bedding and laminations almost absent due to bioturbation. Both Units II and III contain similar amounts of quartz (40%), plagioclase (30%), feldspar (12%), clay minerals and mafic minerals (amphibole). Clay minerals are illite and chlorite, and the presence of expanding clay minerals are low or absent. Unit IV, a low to medium strength clay has a slightly laminated structure, with occasional shell fragments and drop stones. Q_n and B_p are generally in the order of 4 and 0.8 – 1.0, respectively. Depth to bedrock dips sharply from the northeast to southwest but is typically identified at 21 m depth in the southern part of the site. Table 1 and Figure 3 summarizes typical soil properties and CPTU characteristics of the silt at 11.3 m and clay at 17.8 m depth.

Table 1. Typical soil properties at Halden Research site, 11.3 m and 17.8 m depth.

z	w	e_i ¹⁾	w_L ²⁾	I_p	Fines ₃₎	Clay ₃₎	c_{v0} ⁴⁾
[m]	[m]	[-]	[%]	[%]	[%]	[%]	[m ² /yr]
11.5	27	0.73	23	1	89	9	221
18.6	34	0.96	27	9	87	28	10

¹⁾ e_i = initial void ratio. Note also $e_{max} = 1.51$ and $e_{min} = 0.60$, giving an estimated relative density, $D_r = 86\%$ for $z = 11.3$ m;
²⁾ Liquid limit determined by the Casagrande cup;
³⁾ Fines < 0.063 mm, clay < 0.002 mm;
⁴⁾ Coefficient of vertical consolidation at σ'_{vs} .

4. Results

4.1. Triaxial testing

The CAUC clay specimen from 18.6 m depth had a volumetric recompression strain of $\epsilon_{vol} = 2.7\%$, corresponding to $\Delta e/e_0 = 0.054$, thus giving it a "good to fair" sample quality rating [42]. During shear the specimen showed a peak shear stress and exhibited strain softening thereafter. The undrained shear strength indicated from this test was $s_{uc} = 82$ kPa at a vertical strain of $\epsilon_{vf} = 0.8\%$. The pore pressure at peak shear stress was 35 kPa corresponding to a Skempton's pore pressure parameter $A_f = 0.59$ at failure (Figure 4). Interestingly, the effective stress path tags the failure envelope defined by the K_f line of the CAUC tests conducted in the silt units, indicated by the maximum obliquity friction angle $\phi'_{mo} = 35.8^\circ$ [8].

The CAUC silt specimen from 8.4 m, 11.5 m and 12.6 m depth [8] had recompression metrics of $\epsilon_{vol} = 1.3\%$, 1.0% and 1.1% for volumetric strain and $\Delta e/e_0 = 0.029$, 0.023 and 0.026, respectively. By the clay-based sample quality framework these low values of $\Delta e/e_0$ would rate the specimens as "good to excellent" sample quality [42, 43]. However, the clay-based sample quality criteria have been shown to be misleading for low plasticity silts [4, 44]. Figure 4 shows that, except for the initial contractive type behavior, the specimens develop net negative pore pressure changes, and thus, show a strong tendency towards dilative behavior. The test results show a distinct initial S-shape behavior in stress-path space, particularly for the specimens sampled at 8.4 m and 11.5 m depth. Phase transformation points (PTP), i.e., the point at which the soil transitions from contractive type behavior to dilative type behavior, are located at an angle of approximately $\phi'_{PTP} = 33^\circ$. The stress-path results generally track the K_f line at a maximum obliquity friction angle $\phi'_{mo} = 35.8^\circ$ [8] to the end of the test. Due to this strain hardening behavior interpretation of the undrained shear strength from these CAUC tests is complex and the

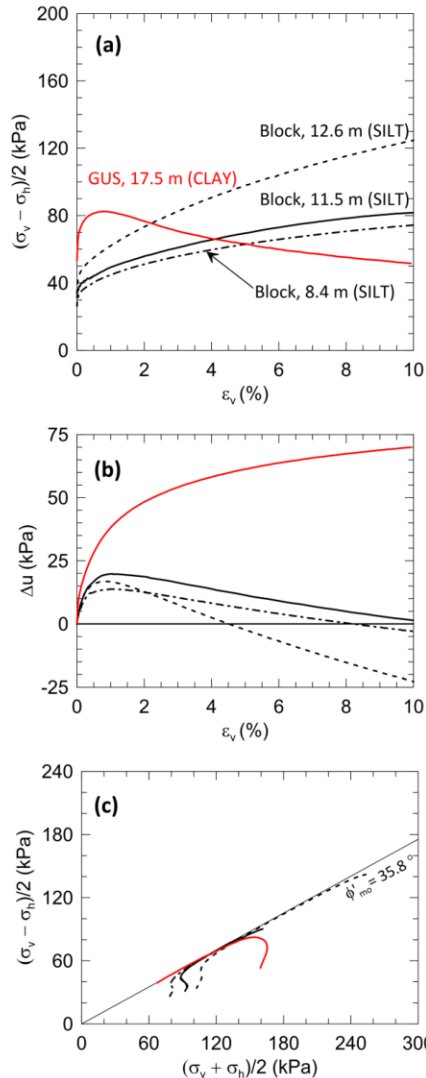


Figure 4. Undrained triaxial test results (CAUC) from the Halden clay and silt units.

results provide no unique (peak) undrained shear strength. Undrained shear strength evaluated at different criteria [41] are presented in Table 2.

4.2. Screw plate load testing

4.2.1. Load-displacement behavior

Typical stress - displacement curves from the silt (11.3 m) and clay (17.8 m) tests are presented in Figure 5. The SPLT results from the clay shows a distinct change in displacement around $q_p = 400$ kPa and relatively large

displacements for small changes in load thereafter. The results of the two silt tests show more gradual increase in deformation with load. The tests exhibit a significantly more pronounced strain-hardening relative to the clay test - similar to the triaxial test results described above. There is reasonable agreement between the two tests conducted at 11.3 m depth in boreholes HALSP01 and HALSP02, although some variability is evident. All tests were stopped at a displacement corresponding to about $0.2D$.

Although traditionally calculated for CPTU twitch tests [1], an assessment of normalized penetration velocity gives $V = 10$ for the SPLT in the clay unit (assuming $c_h = c_{vh}$, Table 1) indicating that undrained conditions prevailed, as expected. From the load tests in the silt unit, the normalized penetration velocity is about $V = 0.5$, and thus, suggests partially drained conditions during loading. These conditions cause complex pore pressure fields surrounding the screw plate, with large gradients in the vertical direction. Locally near the plate the soil shear resistance is fully mobilized and likely developed negative pore pressure changes combined with some dilation due to partial drainage. Whereas at some distance below the plate (and radially), soil elements may have experienced positive pore pressure changes combined with some contraction due to the increase in compression stresses being greater than the mobilized shear stresses (resulting in the soil remaining well below the failure envelope). Globally, however, the load-displacement behavior of the silt tests suggests a dilative type of behavior, with stresses acting on the screw plate increasing at a significantly larger rate relative to the test in clay.

4.2.2. Bearing capacity

Ultimate bearing capacities from the SPLTs were assessed using three different criteria as detailed above and illustrated for each individual SPLT on Figure 5. The bearing capacity interpreted at a displacement equal to 10% of the plate diameter, gave consistently higher values, i.e. $q_{0.1D} > q_{TI}, q_{KP}$, relative to the other two criteria. The tangent intersect and Kay and Parry [15] interpretation methods gave similar values of q_{ult} in both the silt and clay units (Table 3).

4.2.3. Undrained shear strength

The back-calculated undrained shear strength in the clay from $q_{0.1D}$, q_{TI} and q_{KP} (Eq. (4)) gave values of $s_u = 54$ kPa, 46 kPa and 47 kPa, respectively (Table 2) when applying a bearing capacity factor of $N_c^* = 9$. These values are considered "average" or "mobilized" undrained shear strengths for the soil at the screw plate embedment depth, thus approximately equivalent to the direct simple shear (DSS) undrained shear strength (s_{uD}) of the same soil. The DSS and CAUE undrained shear strengths of the Halden clay can be estimated as $s_{uD} = 57$ kPa and $s_{uE} = 34$ kPa, respectively, based on the strength anisotropy factors $s_{uD}/s_{uC} = 0.69$ and $s_{uE}/s_{uC} = 0.42$ reported by Lunne, et al. [42] for similar clays from the Oslo, Norway area. Thus, the undrained shear strength back-calculated from $q_{0.1D}$ provides excellent agreement (within 5%) with the laboratory test and strength anisotropy of the region,

Table 2. Apparent and measured undrained shear strength from screw plate load tests, field vane and triaxial tests at Halden.

Type	z [m]	11.3 – 11.5	17.8 – 18.5
		(silt)	(clay)
[-]		[kPa]	
<i>Laboratory CAUC</i>			
$s_{u,C}[(\sigma_1 - \sigma_3)_{max}]$		94	82
$s_{u,C}(u_{max})$		50	-
$s_{u,C}(e_f = 2\%)$		57	-
$s_{u,C}(A_f = 0)$		84	-
$s_{u,C}[(\sigma_1/\sigma_2)_{max}]$		70	-
$s_{u,C}(K_f)$		70	-
$s_{u,C}(e_f = 10\%)$		84	-
<i>In situ tests</i>			
$s_{u,TI}$		72 ¹⁾	46
$s_{u,0.1D}$		92 ¹⁾	54
$s_{u,KP}$		64 ¹⁾	47
$s_{u,FVT}$		45	41
$s_{u,SHP}$		51	-

Note: ¹⁾ Average of two tests

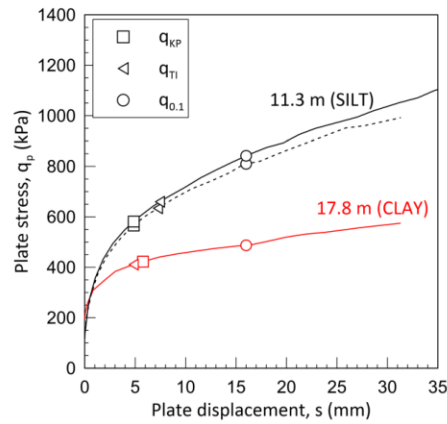


Figure 5. Typical stress-displacement curves from screw plate load tests in the silt (11.3 m) and clay (17.8 m) units at Halden. Ultimate bearing stress assessed using the 0.1D, ($q_{0.1D}$), tangent intersect (q_{TI}) and Kay and Parry (q_{KP}) methods.

Table 3. Bearing capacity interpreted from screw plate load tests at 11.3 m and 17.8 m depth.

Borehole	Depth	TI	0.1D	KP
[-]	[m]	[kPa]	[kPa]	[kPa]
HALSP01	11.3	634	810	566
HALSP02	11.3	660	842	581
HALSP02	17.8	410	487	422

and validates both the SPLT stress-displacement results and the equipment as an effective tool for evaluation of undrained shear strength in soft clay. FVT results at the same depth [8] resulted in $s_{u,FVT} = 41$ kPa (i.e. $s_{u,FVT}/s_{u,C} = 0.5$), and thus show better agreement with the back-calculated undrained shear strength using q_{TI} .

Drainage conditions during the SPLTs in the silt unit are complex and uncertain, but as noted above the tests

were likely partially drained ($V = 0.5$). However, back-calculation of in situ strength parameters using conventional methods requires an assumption of the prevailing conditions as either drained or undrained during loading. By assuming undrained conditions s_u of the silt was back-calculated using Eq. (4). Table 2 presents the results from these back-calculations, in terms of average $s_{u,TI}$, $s_{u,0.1D}$ and $s_{u,KP}$ representing the undrained shear strength calculated from q_{TI} , $q_{0.1D}$ and q_{KP} , respectively. Interestingly, the TI and KP results (72 kPa and 64 kPa) show agreement with the CAUC test at the same depth level for $s_{u,C}$ interpreted using the shear stress at the K_f line and at maximum obliquity criteria (70 kPa). It is hypothesized that the SPLT tests in the silt do generate negative pore pressures changes, and that the TI (\approx KP) failure criteria represent the point at which the soil elements involved in the global failure mechanism below the plate start becoming fully mobilized. Furthermore, the undrained shear strengths back-calculated from $q_{0.1D}$ ($s_{u,0.1D} = 92$ kPa) show similarities with the undrained strength interpreted at $(\sigma_1 - \sigma_3)_{max}$ of the companion CAUC test ($s_{u,C} = 94$ kPa). This implies that the shear stress obtained from CAUC tests on silt block sample specimens at large strains can be used to reliably estimate the bearing capacity at 0.1D for short term loading and that the strain hardening effect can be relied upon. This, however, requires high quality samples with minimum of sample disturbance from sampling, transportation and handling. Recent studies have shown that effects of disturbance on silt samples can have opposite effects of that often seen for structured clays, i.e., larger interpreted strength and stiffness properties with increasing disturbance [4, 44].

4.2.4. Effective stress friction angle

For back-calculation of the effective stress friction angle of the silt using conventional methods drained conditions are required. By assuming fully drained conditions during SPLT loading ϕ' were estimated using the stress-displacement curve and Eq. (3). The largest uncertainty in this back-calculation is the bearing capacity factor, N_q^* , which varies significantly in the literature [45, 46] (Figure 6). The bearing capacity factor computed from the SPLTs at 11.3 m depth are failure criteria dependent, but range between $N_q^* = 4.3$ and 6.5, resulting in corresponding values of $\phi' = 12^\circ - 24^\circ$ using the curves in Figure 6. Effective stress friction angles in this range are considered unrealistically low compared to results from triaxial tests conducted specimens of Halden silt and other international silts reported in literature [7, 19, 41, 47-49]. This implies that the SPLTs were not fully drained during loading, i.e. partial drainage prevailed as suggested by $V = 0.5$, and that the measured bearing capacities cannot be used to reliably back-calculate the friction angle. The bearing capacity factor appear highly uncertain in silts. Helical Anchors Inc. [50] suggests $N_q^* = 28$ for compression loading of a helical pile in a cohesionless soil and hence with an effective stress friction angle of $\phi'_{mo} = 35.8^\circ$, overestimates the ultimate bearing capacity (unfactored) of the screw plate load tests at 11.3 m depth by factors of 3.5 to 5.5. Using the constant volume friction angle (approximately equal to ϕ'_{FVT}) of $\phi'_{cv} = 33^\circ$ reduces the corresponding value of N_q^* to about 19.

The Canadian foundation engineering manual [33] presents typical bearing capacity factors for deep foundations in silt as 10 – 30 (cast-in-place piles) and 20 – 40 (driven piles), and as a result, also overpredicts q_{ult} . For offshore piles in cohesionless soils API RP2A [31] suggests N_q^* in the range of 8 – 12 for medium dense to dense silts, giving better agreement with the SPLT bearing capacity results. However, predictions of axial capacity of piles driven into cohesionless soil using API RP2A have been noted to be inaccurate [36, 51] and more recent guidelines [e.g. 52] recommend CPTU-based methods to assess bearing capacity in these soils.

5. Measured and calculated capacity

Figure 7 presents the measured SPLT bearing capacity at $s = 0.1D$ displacement ($q_{0.1D}$) plotted with ultimate unit base resistance ($q_{b,ult}$) of an equivalent diameter closed end pile using clay methods at 17.8 m depth and cohesionless soil (sand) methods for the silt at 11.3 m depth. In the clay the measured SPLT result shows excellent agreement with the calculated bearing capacity using $N_q^* = 9$ and a DSS undrained shear strength, $s_{u,D}$, as noted in Section 4.2.3 above. The API RP2A and NGI-05 methods use the unconsolidated undrained shear strength ($s_{u(U)}$), in this case assumed equal to $s_{u(C)}$, and appear to overestimate the capacity by about 50%. The ICP/MTD-1996 and UWA-13 methods (using corrected cone resistance, q_c) also overestimate the capacity in the clay, by a factor of 1.33. Helical Anchors Inc. [50] do not state what undrained shear strength to use for design but for illustration purposes $s_{u,D}$ was used in Figure 7 for calculation of $q_{b,ult}$. CGS [33] suggests the minimum undrained shear strength (i.e., $s_{u(E)}$) for capacity assessment, and as a result $q_{b,ult}$ is underestimated relative to $q_{0.1D}$. In summary, the best agreement with the measured bearing capacity of the SPLT at $0.1D$ in the Halden clay was obtained by using $s_{u,D}$ and a bearing capacity factor equal to 9.

Relative to the measured values of $q_{0.1D}$, the classic drained bearing capacity equation for deep foundations in cohesionless soil typically over estimates the unit base resistance at Halden by a factor of up to 4.5, but the values of $q_{b,ult}$ are highly dependent on the selected bearing capacity factor, N_q^* . For example, API RP2A using $N_q^* = 8$ shows fair agreement with the measured values from the SPLTs. The CPTU-based methods all underestimate the unit base resistance at 10% vertical displacement. It should be noted, however, that these methods were developed for sands with significantly higher cone resistances and that CPTU q_c at 11.3 m depth at Halden were measured using the conventional penetration rate of 20 mm/s, giving normalized velocities of about $V = 180$ [53], i.e., fully undrained conditions. Furthermore, relative density (D_r) derived from q_c and estimated effective horizontal stresses, σ_h [54], were developed for clean sands. D_r estimates at Halden (80% - 86%) were based on measured initial void ratios (e_i) of seven triaxial specimens trimmed from a block sample collected at 11.5m depth and maximum and minimum void ratios measured on air dried silt from the same block sample (Table 1). Values of q_c and D_r used in the CPTU-based methods for calculation of $q_{b,ult}$ are therefore somewhat uncertain.

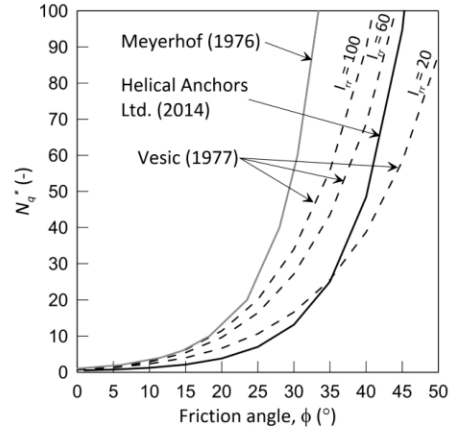


Figure 6. Bearing capacity factors, N_q^* for deep foundations in cohesionless soil as function of effective stress friction angle.

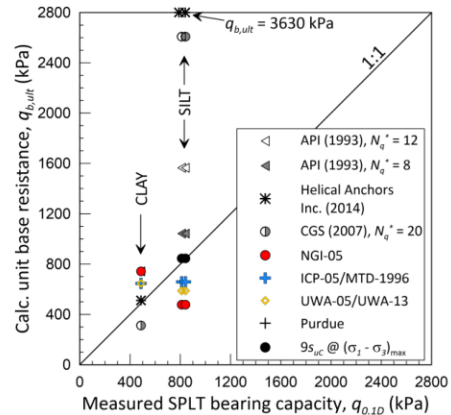


Figure 7. Measured SPLT bearing capacity ($q_{0.1D}$) versus calculated base unit resistance of an equivalent closed end pile ($q_{b,ult}$).

6. Summary and conclusions

The screw plate load test (SPLT) was considered an attractive tool for investigation of the in situ soil behavior of the silt deposit at Halden, Norway described by Blaker, et al. [8], which displays dilative type behavior during undrained shear in the laboratory CAUC tests and a maximum obliquity friction angle of $\phi'_{mo} = 35.8^\circ$. One test was conducted in the clay unit below 16 m depth and two companion tests were performed in the silt at 11.3 m depth. The main findings were:

- The SPLT in the clay were conducted with a normalized velocity of about $V = 10$, indicating undrained conditions during loading. The soil displayed a distinct break in the stress - displacement curve during loading.
- Interpretation of the clay test confirmed (within 5%) the theoretical bearing capacity estimated using the direct simple shear (DSS) undrained shear strength of the same soil, thus validating the

stress-displacement curve and the equipment as an effective tool for evaluation of undrained shear strength in soft clay.

- The two SPLTs performed in silt showed good repeatability and a normalized velocity of about 0.5. Normalized velocities in the range $10 > V > 0.05$ have been suggested to be indicative of partially drained conditions. Thus, the rate of loading used at Halden likely caused complex pore pressure fields surrounding the screw plate.
- Both silt tests displayed a significantly more pronounced strain-hardening behavior relative to the clay SPLT. This behavior confirmed the observations from the stress-strain and stress-path development during undrained triaxial shearing (CAUC) of the block sample from the same depth.
- Due to the strain hardening effect the bearing capacities at a displacement equal to $0.1D$ gave consistently higher values relative to the tangent intersect and Kay and Parry [15] methods.
- It is suggested that the SPLT generated negative pore pressure changes in the silt immediately below the plate, and that q_{ult} for the tangent intersect criteria represents the start of a fully mobilized shear stress state below the screw plate, equivalent to the K_f and maximum obliquity failure criteria used for assessment of s_v from CAUC tests.
- The negative shear induced pore pressures and undrained shear strength at large strains observed from CAUC testing on the silt block sample can likely be relied upon for short term loading in the field. For extrapolation to other silt sites one must ensure high quality samples for laboratory testing and that the effects of disturbance on the engineering design parameter are properly evaluated.
- Fully drained bearing capacities were likely not measured during the SPLTs at Halden. The bearing capacity factor is a function of effective stress friction angle and, as a result Eq. (3) typically over predict q_{ult} at Halden. Similarly, as an effect of the undrained response and relatively low values of cone resistance the CPTU-based methods for estimation of q_{ult} under predict the bearing capacity.

Acknowledgements

This study has primarily been financed by the Norwegian Geotechnical Institute (NGI) and the Research Council of Norway (RCN) under Grant No. 245650. The field vane tests were conducted with support from the US National Science Foundation (NSF) under Grant Nos. CMMI-1436793 and CMMI-1436617. Any opinions, findings, and conclusions or recommendations expressed in this material are those of the author(s) and do not necessarily reflect the views of NGI, RCN or NSF. This support is gratefully acknowledged.

References

- [1] Randolph, M.F., "Characterization of Soft Sediments for Offshore Applications", in Geotechnical and Geophysical Site Characterization, A. Viana da Fonseca and P.W. Mayne, (eds.). 2004, Millpress: Rotterdam, The Netherlands. p. 209–232.

- [2] DeJong, J.T. and M. Randolph, "Influence of Partial Consolidation during Cone Penetration on Estimated Soil Behavior Type and Pore Pressure Dissipation Measurements". *Journal of Geotechnical and Geoenvironmental Engineering*, 2012, **138**(7): p. 777-788. [https://doi.org/10.1061/\(ASCE\)GT.1943-5606.0000646](https://doi.org/10.1061/(ASCE)GT.1943-5606.0000646).
- [3] Kim, K., M. Prezzi, R. Salgado, and W. Lee, "Effect of Penetration Rate on Cone Penetration Resistance in Saturated Clayey Soils". *Journal of Geotechnical and Geoenvironmental Engineering*, 2008, **134**(8): p. 1142-1153. [https://doi.org/10.1061/\(ASCE\)1090-0241\(2008\)134:8\(1142\)](https://doi.org/10.1061/(ASCE)1090-0241(2008)134:8(1142)).
- [4] Carroll, R. and M. Long, "Sample Disturbance Effects in Silt". *Journal of Geotechnical and Geoenvironmental Engineering*, 2017, **143**(9): p. 04017061. [https://doi.org/10.1061/\(ASCE\)GT.1943-5606.0001749](https://doi.org/10.1061/(ASCE)GT.1943-5606.0001749).
- [5] Fleming, L.N. and J.M. Duncan, "Stress-Deformation Characteristics of Alaskan Silt". *Journal of Geotechnical Engineering*, 1990, **116**(3): p. 377-393. [https://doi.org/10.1061/\(asce\)0733-9410\(1990\)116:3\(377\)](https://doi.org/10.1061/(asce)0733-9410(1990)116:3(377)).
- [6] Hoeg, K., R. Dyvik, and G. Sandbakken, "Strength of undisturbed versus reconstituted silt and silty sand specimens". *Journal of Geotechnical and Geoenvironmental Engineering*, 2000, **126**(7): p. 606-617. [https://doi.org/10.1061/\(asce\)1090-0241\(2000\)126:7\(606\)](https://doi.org/10.1061/(asce)1090-0241(2000)126:7(606)).
- [7] Long, M., G. Gudjonsson, S. Donohue, and K. Hagberg, "Engineering characterisation of Norwegian glaciomarine silt". *Engineering Geology*, 2010, **110**(3): p. 51-65. <https://doi.org/10.1016/j.enggeo.2009.11.002>.
- [8] Blaker, O., R. Carroll, P. Paniagua, D.J. DeGroot, and J.-S. L'Heureux, "Halden research site: geotechnical characterization of a post glacial silt". *AIMS Geosciences*, 2019, **5**(2): p. 184-234. <https://doi.org/10.3934/geosci.2019.2.184>.
- [9] Marsland, A., "Clays subjected to in situ plate tests". *Ground Engineering*, 1972, **5**(6): p. 24-31.
- [10] Kummeneje, O., "Fundamentering av oljetank i Drammen (Foundation of an oil tank in Drammen)". Norwegian Geotechnical Institute Publication (In [Norwegian]), 1956. **12**: p. 1-6.
- [11] Schmertmann, J.H., "Static Cone to Compute Static Settlement over Sand". *Journal of the Soil Mechanics and Foundations Division, ASCE*, 1970, **96**(SM3): p. 1011-1043.
- [12] Dahlberg, R., "Settlement characteristics of preconsolidated natural sands: In-situ screw-plate, pressuremeter and penetration tests". 1975, National Swedish Institute for Building Research: Stockholm, Sweden. p. 315.
- [13] Bergado, D. and N. Huan, "Undrained Deformability and Strength Characteristics of Soft Bangkok Clay By the Screw Plate Test". *Geotechnical Testing Journal*, 1987, **10**(3): p. 113-122. <https://doi.org/10.1520/GTJ10943J>.
- [14] Bergado, D.T., K.C. Chong, P.A.M. Daria, and M.C. Alfaro, "Deformability and consolidation characteristics of soft Bangkok clay using screw plate tests". *Canadian Geotechnical Journal*, 1990, **27**(5): p. 531-545. <https://doi.org/10.1139/t90-069>.
- [15] Kay, J.N. and R.H.G. Parry, "Screw plate tests in a stiff clay". *Ground Engineering*, 1982, **15**(6): p. 22-27.
- [16] Selvadurai, A.P.S., G.E. Bauer, and T.J. Nicholas, "Screw plate testing of a soft clay". *Canadian Geotechnical Journal*, 1980, **17**(4): p. 465-472. <https://doi.org/10.1139/t80-055>.
- [17] Kay, J.N. and D.L. Avasle, "Application of Screw Plate to Stiff Clays". *Journal of the Geotechnical Engineering Division, ASCE*, 1982, **108**(GT1): p. 145-154.
- [18] Janbu, N. and K. Senneset, "Field compresometer - principles and applications", in Eighth International Conference on Soil Mechanics and Foundation Engineering, N.A. TsytovichN and S. Chetyrkin, (eds.). 1973. p. 191-198.
- [19] Sandven, R., "Geotechnical properties of a natural silt deposit obtained from field and laboratory tests", in Characterisation and Engineering Properties of Natural Soils, T.S. Tan, et al., (eds.). 2003, A.A. Balkema: Lisse. p. 1121–1148.
- [20] Lefebvre, G. and C. Poulin, "A new method of sampling in sensitive clay". *Canadian Geotechnical Journal*, 1979, **16**(1): p. 226-233. <https://doi.org/10.1139/t79-019>.
- [21] Andresen, A. and P. Kolstad, "The NGI 54-mm samplers for undisturbed sampling of clays and representative sampling of coarser materials", in Proc., Int. Symp. of Soil Sampling, State of the Art on Current Practice of Soil Sampling, 1979, Japanese Society of Soil Mechanics and Foundation Engineering: Tokyo, Japan. p. 13-21.

- [22] Strout, J.M., "Evaluation of the field compressometer test in sand", Ph.D., The Norwegian University of Science and Technology, 1998.
- [23] Lacasse, S. and T. Berre, "State-of-the-Art: Triaxial testing methods for soils", in *Advanced Triaxial Testing of Soil and Rock*, ASTM STP 977, R. Donaghe, R. Chaney, and M. M. Silver, (eds.), 1988, ASTM International: West Conshohocken, PA, p. 264-289.
- [24] Ladd, C.C. and D.J. DeGroot, "Recommended practice for soft ground site characterization: Arthur Casagrande lecture", in *Proc., 12th Panamerican Conf. on Soil Mech. and Geotech. Eng.*, P.J. Culligan, H.H. Einstein, and A.J. Whittle, (eds.), 2003, Verlag Glückauf: Essen, Germany, p. 1-55.
- [25] Berre, T., "Triaxial Testing at the Norwegian Geotechnical Institute", *Geotechnical Testing Journal*, 1982, **5**(1/2): p. 3-17 <https://doi.org/10.1520/GTJ10794J>.
- [26] Briaud, J.-L. and P. Jeanjean, "Load settlement curve method for spread footings on sand", in *Vertical and Horizontal Deformations of Foundations and Embankments*, GSP 40, A.T. Yeung and G.Y. Félio, (eds.), 1994, ASCE: New York, NY, p. 1774-1804.
- [27] Salgado, R., S.I. Woo, and D. Kim, "Development of Load and Resistance Factor Design for Ultimate and Serviceability Limit States of Transportation Structure Foundations", 2011, Joint Transportation Research Program, Indiana Department of Transportation and Purdue University: West Lafayette, IN, USA.
- [28] Trautmann, C.H. and F.H. Kulhawy, "Uplift Load-Displacement Behavior of Spread Foundations", *Journal of Geotechnical Engineering*, 1988, **114**(2): p. 168-184 [https://doi.org/10.1061/\(ASCE\)0733-9410\(1988\)114:2\(168\)](https://doi.org/10.1061/(ASCE)0733-9410(1988)114:2(168)).
- [29] De Beer, E.E., "Experimental Determination of the Shape Factors and the Bearing Capacity Factors of Sand", *Géotechnique*, 1970, **20**(4): p. 387-411 <https://doi.org/10.1680/geot.1970.20.4.387>.
- [30] Salgado, R., "The Engineering of Foundations", 2008, Boston, MA, USA: McGraw Hill.
- [31] API, "Recommended practice for planning, designing and constructing fixed offshore platforms – working stress design. API RP 2A-WSD, 20th Edition", 1993, American Petroleum Institute: Washington, DC, USA.
- [32] Bowles, J.E., "Foundation Analysis and Design", 1996, New York: McGraw-Hill.
- [33] CGS, "Canadian Foundation Engineering Manual, 4th edition", 2007, Canadian Geotechnical Society: Richmond, B.C., Canada.
- [34] Clausen, C.J.F., P.M. Aas, and K. Karlsrud, "Bearing Capacity of Driven Piles in Sand, the NGI Approach", in *Proc. of the 1st Int. Symp. on Frontiers in Offshore Geotech.*, S. Gourvenec and M. Cassidy, (eds.), 2005, Taylor & Francis: London, p. 677-682.
- [35] Karlsrud, K., C.J.F. Clausen, and P.M. Aas, "Bearing Capacity of Driven Piles in Clay, the NGI Approach", in *Proc. of the 1st Int. Symp. on Frontiers in Offshore Geotech.*, S. Gourvenec and M. Cassidy, (eds.), 2005, Taylor & Francis: London, p. 775-782.
- [36] Jardine, R.J. and F.C. Chow, "New Design Methods for Offshore Piles", MTD Publication. Vol. 96/103, 1996, London: Marine Technology Directorate, 48.
- [37] Jardine, R.J., F.C. Chow, R. Overy, and J. Standing, "ICP Design Methods for Driven Piles in Sand and Clay", 2005, London: Thomas Telford Publishing.
- [38] Lehan, B.M., J.A. Schneider, and X. Xu, "The UWA-05 Method for Prediction of Axial Capacity of Driven Piles in Sand", in *Proc. of the 1st Int. Symp. on Frontiers in Offshore Geotech.*, S. Gourvenec and M. Cassidy, (eds.), 2005, Taylor & Francis: London, p. 683-689.
- [39] Lehan, B.M., Y. Li, and R. Williams, "Shaft Capacity of Displacement Piles in Clay Using the Cone Penetration Test", *Journal of Geotechnical and Geoenvironmental Engineering*, 2013, **139**(2): p. 253-266 [https://doi.org/10.1061/\(ASCE\)GT.1943-5606.0000749](https://doi.org/10.1061/(ASCE)GT.1943-5606.0000749).
- [40] Han, F., M. Prezzi, R. Salgado, and M. Zaheer, "Axial Resistance of Closed-Ended Steel-Pipe Piles Driven in Multilayered Soil", *Journal of Geotechnical and Geoenvironmental Engineering*, 2017, **143**(3): p. 04016102 [https://doi.org/10.1061/\(ASCE\)GT.1943-5606.0001589](https://doi.org/10.1061/(ASCE)GT.1943-5606.0001589).
- [41] Brandon, T.L., A.T. Rose, and J.M. Duncan, "Drained and undrained strength interpretation for low-plasticity silts", *Journal of Geotechnical and Geoenvironmental Engineering*, 2006, **132**(2): p. 250-257 [https://doi.org/10.1016/\(asce\)1090-0241\(2006\)132:2\(250\)](https://doi.org/10.1016/(asce)1090-0241(2006)132:2(250)).
- [42] Lunne, T., T. Berre, K.H. Andersen, S. Strandvik, and M. Sjørsen, "Effects of sample disturbance and consolidation procedures on measured shear strength of soft marine Norwegian clays", *Canadian Geotechnical Journal*, 2006, **43**(7): p. 726-750 <https://doi.org/10.1139/t06-040>.
- [43] Lunne, T., P.K. Robertson, and J.J.M. Powell, "Cone penetration testing in geotechnical practice", 1997, London: Blackie Academic & Professional.
- [44] Lukas, W.G., D.J. DeGroot, J.T. DeJong, C.P. Krage, and G. Zhang, "Undrained Shear Behavior of Low-Plasticity Intermediate Soils Subjected to Simulated Tube-Sampling Disturbance", *Journal of Geotechnical and Geoenvironmental Engineering*, 2019, **145**(1): p. 04018098 [https://doi.org/10.1061/\(ASCE\)GT.1943-5606.0001967](https://doi.org/10.1061/(ASCE)GT.1943-5606.0001967).
- [45] Meyerhof, G.G., "Bearing Capacity and Settlement of Pile Foundations", *Journal of the Geotechnical Engineering Division, ASCE*, 1976, **102**(GT3): p. 195-228.
- [46] Vesic, A.S., "Design of pile foundations", 1977, National Cooperative Highway Research Program Synthesis of Highway Practice No. 42: Washington, D.C., USA.
- [47] Cola, S. and P. Simonini, "Mechanical behavior of silty soils of the Venice lagoon as a function of their grading characteristics", *Canadian Geotechnical Journal*, 2002, **39**(4): p. 879-893 <https://doi.org/10.1139/t02-037>.
- [48] Nocilla, A., M.R. Coop, and F. Colleselli, "The mechanics of an Italian silt: an example of 'transitional' behaviour", *Géotechnique*, 2006, **56**(4): p. 261-271 <https://doi.org/10.1680/geot.2006.56.4.261>.
- [49] Long, M., "Engineering characterization of estuarine silts", *Quarterly Journal of Engineering Geology and Hydrogeology*, 2007, **40**: p. 147-161 <https://doi.org/10.1144/1470-9236/05-061>.
- [50] Helical Anchors Inc., "Engineering Design Manual, Rev 02", 2014, Helical Anchors, Inc.: Minneapolis, MN, USA.
- [51] Randolph, M.F., R. Dolwin, and R. Beck, "Design of driven piles in sand", *Géotechnique*, 1994, **44**(3): p. 427-448 <https://doi.org/10.1680/geot.1994.44.3.427>.
- [52] API, "Geotechnical and Foundation Design Considerations. ANSI/API Recommended Practice 2GEO 1st edition, April 2011. ISO 19901-4:2003 (Modified), Petroleum and natural gas industries - Specific requirements for offshore structures, Part 4 - Geotechnical and foundation design considerations", 2011, American Petroleum Institute: Washington, DC, USA.
- [53] Carroll, R. and A.P. Paniagua López, "Variable rate of penetration and dissipation test results in a natural silty soil", in *Cone Penetration Testing 2018: Proc. of the 4th Int. Symp. on Cone Penetration Testing*, M.A. Hicks, F. Pisanò, and J. Peuchen, (eds.), 2018, CRC Press: London.
- [54] Jamiolkowski, M., D.C.F.L. Presti, and M. Manassero, "Evaluation of Relative Density and Shear Strength of Sands from CPT and DMT", in *Geotechnical Special Publication No. 119: Soil Behavior and Soft Ground Construction*, J.T. Germaine, T.C. Sheahan, and R.V. Whitman, (eds.), 2003, American Society of Civil Engineers: Reston, VA, p. 201-238.

REFERENCES

- Aas, G. (1983). "Geotekniske dimensjoneringsparametre: Tolkning av skruplateforsøk (Geotechnical design parameters: Interpretation of screw plate tests) [In Norwegian]." Norwegian Geotechnical Institute, Oslo, 16.
- Andersen, K. H., and Schjetne, K. (2013). "Database of Friction Angles of Sand and Consolidation Characteristics of Sand, Silt, and Clay." *J. Geotech. Geoenviron. Eng.*, 139(7), 1140-1155.
- Andresen, A., and Kolstad, P. (1979). "The NGI 54-mm samplers for undisturbed sampling of clays and representative sampling of coarser materials." *Proc., Int. Symp. of Soil Sampling, State of the Art on Current Practice of Soil Sampling*, Japanese Society of Soil Mechanics and Foundation Engineering, Tokyo, Japan, 13-21.
- API (1993). "Recommended practice for planning, designing and constructing fixed offshore platforms – working stress design. API RP 2A-WSD, 20th Edition." American Petroleum Institute, Washington, DC, USA.
- API (2014). "Planning, Designing and Constructing Fixed Offshore Platforms – Working Stress Design. API Recommended Practice 2A-WSD, 22nd Edition, November 2014." American Petroleum Institute, Washington, DC, USA.
- Arroyo, M., Pineda, J. A., Sau, N., Devincenzi, M., and Pérez, N. (2015). "Sample quality examination in silty soils." *Geotechnical engineering for infrastructure and development : proceedings of the XVI European Conference on Soil Mechanics and Geotechnical Engineering*, M. G. Winter, D. M. Smith, P. J. L. Eldred, and D. G. Toll, eds., ICE Publishing, London, 2873–2878.
- ASTM (2015). "Standard Test Method for Consolidated Undrained Direct Simple Shear Testing of Fine Grain Soils (ASTM D6528-17)." ASTM International, West Conshohocken, PA.
- ASTM (2017). "Standard Practice for Classification of Soils for Engineering Purposes (Unified Soil Classification System)." *ASTM D2487-17*, ASTM International, West Conshohocken, PA.
- ASTM (2018). *Annual Book of Standards*, American Society for Testing and Materials, Soil and Rock, West Conshohocken, Pennsylvania, USA.
- ASTM (2018). *Annual Book of Standards*, American Society for Testing and Materials, Soil and Rock, West Conshohocken, Pennsylvania, USA.
- Aubeny, C. P., Whittle, A. J., and Ladd, C. C. (2000). "Effects of Disturbance on Undrained Strengths Interpreted from Pressuremeter Tests." *J. Geotech. Geoenviron. Eng.*, 126(12), 1133-1144.

- Baligh, M. M. (1985). "Strain Path Method." *J. Geotech. Eng.*, 111(9), 1108-1136.
- Baligh, M. M., Azzouz, A. S., and Chin, C. T. (1987). "Disturbances Due to "Ideal" Tube Sampling." *J. Geotech. Eng.*, 113(7), 739-757.
- Becker, D. E., Crooks, J. H. A., Been, K., and Jefferies, M. G. (1987). "Work as a criterion for determining in situ and yield stresses in clays." *Can. Geotech. J.*, 24(4), 549-564.
- Bergado, D., and Huan, N. (1987). "Undrained Deformability and Strength Characteristics of Soft Bangkok Clay By the Screw Plate Test." *Geotech. Test. J.*, 10(3), 113-122.
- Bergado, D. T., Chong, K. C., Daria, P. A. M., and Alfaro, M. C. (1990). "Deformability and consolidation characteristics of soft Bangkok clay using screw plate tests." *Can. Geotech. J.*, 27(5), 531-545.
- Berre, T. (1982). "Triaxial Testing at the Norwegian Geotechnical Institute." *Geotech. Test. J.*, 5(1/2), 3-17.
- Berre, T. (2013). "Test fill on soft plastic marine clay at Onsøy, Norway." *Can. Geotech. J.*, 51(1), 30-50.
- Berre, T., Lunne, T., Andersen, K. H., Strandvik, S., and Sjursen, M. (2007). "Potential improvements of design parameters by taking block samples of soft marine Norwegian clays." *Can. Geotech. J.*, 44(6), 698-716.
- Bjerrum, L., and Andersen, K. H. (1972). "In-situ measurements of lateral pressures in clay." *European Conference on Soil Mechanics and Foundation Engineering, 5. Madrid 1972. Proceedings*, Sociedad Española de Mecánica del Suelo y Cimentaciones, Madrid.
- Bjerrum, L., and Landva, A. (1966). "Direct Simple-Shear Tests on a Norwegian Quick Clay." *Géotechnique*, 16(1), 1-20.
- Blaker, Ø., Carroll, R., Paniagua, P., DeGroot, D. J., and L'Heureux, J.-S. (2019). "Halden research site: geotechnical characterization of a post glacial silt." *AIMS Geosciences*, 5(2), 184-234.
- Blaker, Ø., and DeGroot, D. J. (In press). "Intact, disturbed and reconstituted undrained shear behavior of low plasticity natural silt." *J. Geotech. Geoenviron. Eng.*
- Blaker, Ø., DeGroot, D. J., and DeJong, J. T. (2020). "Evaluation of bearing capacity and in situ shear strength using the screw plate load test in clay and silt." *Geotechnical and Geophysical Site Characterisation 6: the 6th International Conference*, Budapest, Hungary.

- Blight, G. E. (1968). "A Note on Field Vane Testing of Silty Soils." *Can. Geotech. J.*, 5(3), 142-149.
- Börjesson, L. (1981). "Shear strength of inorganic silty soils." *Proc., 10th Int. Conf. on Soil Mech. and Found. Eng.*, A.A. Balkema, Rotterdam, 567-572.
- Bradshaw, A. S., and Baxter, C. D. P. (2007). "Sample Preparation of Silts for Liquefaction Testing." *Geotech. Test. J.*, 30(4), 324-332.
- Brandon, T. L., Rose, A. T., and Duncan, J. M. (2006). "Drained and undrained strength interpretation for low-plasticity silts." *J. Geotech. Geoenviron. Eng.*, 132(2), 250-257.
- Bray, J. D., Markham, C. S., and Cubrinovski, M. (2017). "Liquefaction assessments at shallow foundation building sites in the Central Business District of Christchurch, New Zealand." *Soil Dynamics and Earthquake Engineering*, 92, 153-164.
- Bray, J. D., and Sancio, R. B. (2006). "Assessment of the Liquefaction Susceptibility of Fine-Grained Soils." *J. Geotech. Geoenviron. Eng.*, 132(9), 1165-1177.
- Bray, J. D., Sancio, R. B., Durgunoglu, T., Onalp, A., Youd, T. L., Stewart, J. P., Seed, R. B., Cetin, O. K., Bol, E., Baturay, M. B., Christensen, C., and Karadayilar, T. (2004). "Subsurface Characterization at Ground Failure Sites in Adapazari, Turkey." *J. Geotech. Geoenviron. Eng.*, 130(7), 673-685.
- Briaud, J.-L., and Gibbens, R. (1999). "Behavior of Five Large Spread Footings in Sand." *J. Geotech. Geoenviron. Eng.*, 125(9), 787-796.
- Briaud, J.-L., and Jeanjean, P. (1994). "Load settlement curve method for spread footings on sand." *Vertical and Horizontal Deformations of Foundations and Embankments, GSP 40*, A. T. Yeung, and G. Y. Félio, eds., ASCE, New York, NY, 1774-1804.
- Brinkgreve, R. B. J., Kumarswamy, S., Swolfs, W. M., Zampich, L., and Ragi Manoj, N. 2019. *Plaxis 2D Version 2019* Plaxis bv., The Netherlands.
- Carroll, R. (2013). "The Engineering Behaviour of Irish Silts." PhD thesis, University College Dublin, Dublin.
- Carroll, R., and Long, M. (2017). "Sample Disturbance Effects in Silt." *J. Geotech. Geoenviron. Eng.*, 143(9), 04017061.
- Carroll, R., and Paniagua López, A. P. (2018). "Variable rate of penetration and dissipation test results in a natural silty soil." *Cone Penetration Testing 2018: Proc. of the 4th Int. Symp. on Cone Penetration Testing*, M. A. Hicks, F. Pisanò, and J. Peuchen, eds., CRC Press, London.

- Casagrande, A. (1936). "The determination of the preconsolidation load and its practical significance." *Proc., 1st Int. Conf. SMFE*, Graduate school of engineering, Harvard University, Cambridge, 60-64.
- Chandler, R. J. (1988). "The In-Situ Measurement of the Undrained Shear Strength of Clays Using the Field Vane." *Vane Shear Strength Testing in Soils: Field and Laboratory Studies, STP 1014*, A. F. Richards, ed., ASTM International, West Conshohocken, PA, 13-32.
- Chin, F. K. (1983). "Bilateral Plate Bearing Tests." *International Symposium on In Situ Testing in Soil and Rock, Proc.*, International Association of Engineering Geology, Paris, France, 37- 41.
- Clausen, C. J. F. (2003). "BEAST. A computer program for limit equilibrium analysis by method of slices. Report 8302-2. Rev. 4, 24 April. 2003."
- Clausen, C. J. F., Aas, P. M., and Karlsrud, K. (2005). "Bearing Capacity of Driven Piles in Sand, the NGI Approach." *Proc. of the 1st Int. Symp. on Frontiers in Offshore Geotech.*, S. Gourvenec, and M. Cassidy, eds., Taylor & Francis, London, 677-682.
- Clayton, C. R. I., Hight, D. W., and Hopper, R. J. (1992). "Progressive destructuring of Bothkennar clay. implications for sampling and reconsolidation procedures." *Géotechnique*, 42(2), 219-239.
- Clayton, C. R. I., and Siddique, A. (1999). "Tube sampling disturbance—forgotten truths and new perspectives." *Proceedings of the Institution of Civil Engineers - Geotechnical Engineering*, 137(3), 127-135.
- Clayton, C. R. I., Siddique, A., and Hopper, R. J. (1998). "Effects of sampler design on tube sampling disturbance—numerical and analytical investigations." *Géotechnique*, 48(6), 847-867.
- Cola, S., and Simonini, P. (2002). "Mechanical behavior of silty soils of the Venice lagoon as a function of their grading characteristics." *Can. Geotech. J.*, 39(4), 879–893.
- Dafalias, Y. F., and Manzari, M. T. (2004). "Simple Plasticity Sand Model Accounting for Fabric Change Effects." *Journal of Engineering Mechanics*, 130(6), 622-634.
- Dahlberg, R. (1975). "Settlement characteristics of preconsolidated natural sands: In-situ screw-plate, pressuremeter and penetration tests." National Swedish Institute for Building Research, Stockholm, Sweden, 315.
- DeGroot, D. J., and Ladd, C. C. (2012). "Site Characterization for Cohesive Soil Deposits Using Combined In Situ and Laboratory Testing." *Geotechnical Engineering State of the Art and Practice: Keynote Lectures from GeoCongress 2012, GSP226*, K. Rollins, and D. Zekkos, eds., ASCE, 565-607.

- DeGroot, D. J., Lunne, T., Ghanekar, R., Knudsen, S., Jones, C. D., and Yetginer-Tjelta, T. I. (2019). "Engineering properties of low to medium overconsolidation ratio offshore clays." *AIMS Geosciences*, 5(3), 535-567.
- DeGroot, D. J., and Lutenecker, A. J. (2003). "Geology and engineering properties of Connecticut Valley Varved Clay." *Characterisation and Engineering Properties of Natural Soils*, T. S. Tan, K. K. Phoon, D. W. Hight, and S. Leroueil, eds., A.A. Balkema, Lisse, 695-724.
- DeJong, J. T., Jaeger, R. A., Boulanger, R. W., Randolph, M. F., and Wahl, D. A. J. (2013). "Variable penetration rate cone testing for characterization of intermediate soils." *Geotechnical and Geophysical Site Characterization 4*, R. Q. Coutinho, and P. W. Mayne, eds., Taylor & Francis, Boca Raton, FL, 25-42.
- DeJong, J. T., Krage, C. P., Albin, B. M., and DeGroot, D. J. (2018). "Work-Based Framework for Sample Quality Evaluation of Low Plasticity Soils." *J. Geotech. Geoenviron. Eng.*, 144(10), 04018074.
- DeJong, J. T., and Randolph, M. (2012). "Influence of Partial Consolidation during Cone Penetration on Estimated Soil Behavior Type and Pore Pressure Dissipation Measurements." *J. Geotech. Geoenviron. Eng.*, 138(7), 777-788.
- Doherty, J. P., Gourvenec, S., Gaone, F. M., Pineda, J. A., Kelly, R., O'Loughlin, C. D., Cassidy, M. J., and Sloan, S. W. (2018). "A novel web based application for storing, managing and sharing geotechnical data, illustrated using the national soft soil field testing facility in Ballina, Australia." *Computers and Geotechnics*, 93, 3-8.
- Donohue, S. (2005). "Assessment of sample disturbance in soft clay using shear wave velocity and suction measurements." Ph.D., University College Dublin, Dublin.
- Donohue, S., and Long, M. (2010). "Assessment of sample quality in soft clay using shear wave velocity and suction measurements." *Géotechnique*, 60(11), 883-889.
- Dyvik, R., and Madshus, C. (1985). "Lab Measurements of Gmax Using Bender Elements." *Advances in the Art of Testing Soils under Cyclic Conditions*, V. Khosla, ed., ASCE, New York, 186-196.
- Dyvik, R., and Olsen, T. S. (1989). "Gmax measured in oedometer and DSS tests using bender elements." *Proceedings of the 12th International Conference on Soil Mechanics and Foundation Engineering, Rio de Janeiro, 13-18 August 1989*, A.A. Balkema, Rotterdam, 39-42.
- Emdal, A., Gylland, A., Amundsen, H. A., Kåsin, K., and Long, M. (2016). "Mini-block sampler." *Can. Geotech. J.*, 53(8), 1235-1245.
- Fellenius, B. H. (1991). "Pile Foundations." *Foundation Engineering Handbook*, H.-Y. Fang, ed., Springer, Boston, MA.

- Ferreira, C., Fonseca, A. N. T., Oacute, Nio Viana, D. A., and Nash, D. F. T. (2011). "Shear wave velocities for sample quality assessment on a residual soil." *Soils Found.*, 51(4), 683-692.
- Fleming, L. N., and Duncan, J. M. (1990). "Stress-Deformation Characteristics of Alaskan Silt." *J. Geotech. Eng.*, 116(3), 377-393.
- Ghionna, V. N., Jamiolkowski, M., Pedroni, S., and Salgado, R. (1994). "The Tip Displacement of Drilled Shafts in Sands." *Vertical and Horizontal Deformations of Foundations and Embankments, GSP 40*, A. T. Yeung, and G. Y. Félio, eds., ASCE, New York, NY.
- Gibson, R. E., and Anderson, W. F. (1961). "In situ measurement of soil properties with the pressuremeter " *Civil Engineering and Public Works Review*, 56(658), 615-618.
- Han, F., Prezzi, M., Salgado, R., and Zaheer, M. (2017). "Axial Resistance of Closed-Ended Steel-Pipe Piles Driven in Multilayered Soil." *J. Geotech. Geoenviron. Eng.*, 143(3), 04016102.
- Hansen, L., L'heureux, J. S., and Longva, O. (2011). "Turbiditic, clay-rich event beds in fjord-marine deposits caused by landslides in emerging clay deposits – palaeoenvironmental interpretation and role for submarine mass-wasting." *Sedimentology*, 58(4), 890-915.
- Hight, D. W., Böese, R., Butcher, A. P., Clayton, C. R. I., and Smith, P. R. (1992). "Disturbance of the Bothkennar clay prior to laboratory testing." *Géotechnique*, 42(2), 199-217.
- Hight, D. W., Bond, A. J., and Legge, J. D. (1992). "Characterization of the Bothkennar clay: an overview." *Géotechnique*, 42(2), 303-347.
- Hight, D. W., and Leroueil, S. (2003). "Characterisation of soils for engineering purposes." *Characterisation and Engineering Properties of Natural Soils*, T. S. Tan, K. K. Phoon, D. W. Hight, and S. Leroueil, eds., A.A. Balkema, Lisse, 255-360.
- Høeg, K., Dyvik, R., and Sandbækken, G. (2000). "Strength of undisturbed versus reconstituted silt and silty sand specimens." *J. Geotech. Geoenviron. Eng.*, 126(7), 606-617.
- Huang, A. B. (2016). "The Seventh James K. Mitchell Lecture: Characterization of silt/sand soils." *Geotechnical and Geophysical Site Characterisation 5: Proceedings of the Fifth International Conference*, B. M. Lehane, H. E. Acosta-Martínez, and R. Kelly, eds., Australian Geomechanics Society, Sydney, Australia, 1-18.

- Huang, A. B., Tai, Y. Y., Lee, W. F., and Ishihara, K. (2008). "Sampling and field characterization of the silty sand in Central and Southern Taiwan." *Geotechnical and Geophysical Site Characterization*, A. B. Huang, and P. W. Mayne, eds., Taylor & Francis, Leiden, 1457-1463.
- Hvorslev, M. J. (1949). "Subsurface exploration and sampling of soils for civil engineering purposes." A. S. o. C. Engineers, ed., University of Michigan, Vickburg, Mississippi, 521.
- ISO (1994). "Soil quality." *Determination of the specific electrical conductivity (ISO 11265)*, International Organization for Standardization, Geneva, Switzerland.
- ISO (2002). "Geotechnical investigation and testing - Identification and classification of soil." *Part 1: Identification and description (ISO 14688-1)*, International Organization for Standardization, Geneva, Switzerland.
- ISO (2004). "Geotechnical investigation and testing - Laboratory testing of soil." *Part 11: Determination of permeability by constant and falling head (ISO/TS 17892-11)*, International Organization for Standardization, Geneva, Switzerland.
- ISO (2012). "Geotechnical investigation and testing - Field testing." *Part 5: Flexible dilatometer test (ISO 22476-5:2012)*, International Organization for Standardization, Geneva, Switzerland.
- ISO (2012). "Geotechnical investigation and testing - Field testing." *Part 1: Electrical cone and piezocone penetration test (ISO 22476-1:2012)*, International Organization for Standardization, Geneva, Switzerland.
- ISO (2014). "Geotechnical investigation and testing - Laboratory testing of soil." *Part 2: Determination of bulk density (ISO 17892-2)*, International Organization for Standardization., Geneva, Switzerland.
- ISO (2014). "Geotechnical investigation and testing - Laboratory testing of soil." *Part 1: Determination of water content (ISO 17892-1)*, International Organization for Standardization, Geneva, Switzerland.
- ISO (2014). "Petroleum and natural gas industries — Specific requirements for offshore structures." *Part 8: Marine soil investigations*, International Organization for Standardization, Geneva, Switzerland.
- ISO (2015). "Geotechnical investigation and testing - Laboratory testing of soil." *Part 3: Determination of particle density (ISO 17892-3)*, International Organization for Standardization, Geneva, Switzerland.
- ISO (2016). "ISO (2015) Geotechnical investigation and testing - Laboratory testing of soil." *Part 4: Determination of particle size distribution (ISO 17892-4)*, International Organization for Standardization, Geneva, Switzerland.

- ISO (2017). "Geotechnical investigation and testing - Field testing - Part 11: Flat dilatometer test (ISO 22476-11:2017)." International Organization for Standardization, Geneva, Switzerland.
- ISO (2017). "Geotechnical investigation and testing - Laboratory testing of soil." *Part 5: Incremental loading oedometer test (ISO 17892-5)*. , International Organization for Standardization., Geneva, Switzerland.
- ISO (2018). "Geotechnical investigation and testing - Laboratory testing of soil." *Part 12: Determination of liquid and plastic limits (ISO 17892-12)*, International Organization for Standardization, Geneva, Switzerland.
- ISO (2018). "Geotechnical investigation and testing - Laboratory testing of soil." *Part 9: Consolidated triaxial compression tests on water saturated soils (ISO 17892-9)*, International Organization for Standardization, Geneva, Switzerland.
- Izadi, A. M. (2006). "Behavior of undrained monotonically loaded low plasticity silt under triaxial compression." M.S., University of Missouri-Rolla.
- Jamiolkowski, M., Presti, D. C. F. L., and Manassero, M. (2003). "Evaluation of Relative Density and Shear Strength of Sands from CPT and DMT." *Geotechnical Special Publication No. 119: Soil Behavior and Soft Ground Construction*, J. T. Germaine, T. C. Sheahan, and R. V. Whitman, eds., American Society of Civil Engineers, Reston, VA, 201-238.
- Janbu, N. (1963). "Soil compressibility as determined by oedometer and triaxial tests." *Proc., 4th European Soil Mech. and Found. Eng.*, ECSMFE, Wiesbaden, Germany, 19-25.
- Janbu, N. (1985). "Soil models in offshore engineering." *Géotechnique*, 35(3), 241-281.
- Janbu, N., and Senneset, K. (1973). "Field compressometer - principles and applications." *Eighth International Conference on Soil Mechanics and Foundation Engineering*, N. A. TsytovichN, and S. Chetyrkin, eds., 191-198.
- Janbu, N., and Senneset, K. (1974). "Effective stress interpretation of in-situ static penetration tests." *Proceedings of the European Symposium on Penetration Testing, ESOPT, Stockholm, June 5-7, 1974*, National Swedish Building Research, Stockholm, 181-193.
- Jardine, R. J., and Chow, F. C. (1996). *New Design Methods for Offshore Piles*, Marine Technology Directorate, London.
- Jardine, R. J., Chow, F. C., Overy, R., and Standing, J. (2005). *ICP Design Methods for Driven Piles in Sand and Clay*, Thomas Telford Publishing, London.

- Jostad, H. P., Dahl, B., Page, P., Sivasithamparam, N., and Sturm, H. (In Press). "Evaluation of soil models for improved design of offshore wind turbine foundations in dense sand." *Géotechnique*, 1-37.
- Karlsrud, K., Clausen, C. J. F., and Aas, P. M. (2005). "Bearing Capacity of Driven Piles in Clay, the NGI Approach." *Proc. of the 1st Int. Symp. on Frontiers in Offshore Geotech.*, S. Gourvenec, and M. Cassidy, eds., Taylor & Francis, London, 775-782.
- Kay, J. N., and Avalue, D. L. (1982). "Application of Screw Plate to Stiff Clays." *J. Geotech. Eng. Div.*, 108(GT1), 145-154.
- Kay, J. N., and Parry, R. H. G. (1982). "Screw plate tests in a stiff clay." *Ground Engineering*, 15(6), 22-27.
- Keer, L. M. (1975). "Mixed boundary value problems for a penny-shaped cut." *Journal of Elasticity*, 5(2), 89-98.
- Kelly, R. B., Pineda, J. A., Bates, L., Suwal, L. P., and Fitzallen, A. (2017). "Site characterisation for the Ballina field testing facility." *Géotechnique*, 67(4), 279-300.
- Kenney, T. C. (1964). "Sea-Level Movements and the Geologic Histories of the Post-Glacial Marine Soils at Boston, Nicolet, Ottawa and Oslo." *Géotechnique*, 14(3), 203-230.
- Kim, K., Prezzi, M., Salgado, R., and Lee, W. (2008). "Effect of Penetration Rate on Cone Penetration Resistance in Saturated Clayey Soils." *J. Geotech. Geoenviron. Eng.*, 134(8), 1142-1153.
- Kiso-Jiban Consultants (2013). "Performance of test sampling on the undisturbed sediments samples by 'Gel-Push' sampler on extractive waste neutralization facility Zelazny Mosy in Tailings Management Division." 1-78.
- Klemsdal, T. (2002). "Landformene i Østfold [In Norwegian]." *Natur i Østfold*, 21(1/2), 7-31.
- Kulhawy, F. H., and Mayne, P. W. (1990). "Manual on Estimating Soil Properties for Foundation Design. Report EL-6800." Electric Power Research Institute. Palo Alto, CA.
- Kummeneje, O. (1956). "Fundamentering av oljetank i Drammen (Foundation of an oil tank in Drammen)." *Norwegian Geotechnical Institute Publication (In [Norwegian])*, 12, 1-6.
- La Rochelle, P., and Lefebvre, G. (1971). "Sampling disturbance in Champlain clays." *Sampling of Soil and Rock, STP 483*, B. B. Gordon, and C. B. Crawford, eds., ASTM International, West Conshohocken, PA, 143-163.

- Lacasse, S., and Berre, T. (1988). "State-of-the-Art: Triaxial testing methods for soils." *Advanced Triaxial Testing of Soil and Rock, ASTM STP 977*, R. Donaghe, R. Chaney, and M. M. Silver, eds., ASTM International, West Conshohocken, PA, 264-289.
- Lacasse, S., Berre, T., and Lefebvre, G. (1985). "Block sampling of sensitive clay." *Proc., 11th Int. Conf. on Soil Mech. and Found. Eng.*, A.A. Balkema, Rotterdam, 887-892.
- Ladd, C. C., and DeGroot, D. J. (2003). "Recommended practice for soft ground site characterization: Arthur Casagrande lecture." *Proc., 12th Panamerican Conf. on Soil Mech. and Geotech. Eng.*, P. J. Culligan, H. H. Einstein, and A. J. Whittle, eds., Verlag Glückauf, Essen, Germany, 1-55.
- Ladd, C. C., Weaver, J. S., Germaine, J. T., and Sauls, D. P. (1985). "Strength-Deformation Properties of Arctic Silt." *Civil Engineering in the Arctic Offshore: Conference Arctic '85, San Francisco, CA, March 25-27, 1985*, F. Lawrence Bennett, Jerry L. Machemehl, and N. D. W. Thelen, eds., American Society of Civil Engineers, New York, 820-829.
- Ladd, R. (1978). "Preparing Test Specimens Using Undercompaction." *Geotech. Test. J.*, 1(1), 16-23.
- Landon, M. M., DeGroot, D. J., and Sheahan, T. C. (2007). "Nondestructive Sample Quality Assessment of a Soft Clay Using Shear Wave Velocity." *J. Geotech. Geoenviron. Eng.*, 133(4), 424-432.
- LaRochelle, P., Sarrailh, J., Tavenas, F., Roy, M., and Leroueil, S. (1981). "Causes of sampling disturbance and design of a new sampler for sensitive soils." *Can. Geotech. J.*, 18(1), 52-66.
- Larsson, R. (1997). "Investigations and load tests in silty soils. Results from a series of investigations in silty soils in Sweden. Report 54." Swedish Geotechnical Institute, SGI, Linköping, 257.
- Lefebvre, G., and Poulin, C. (1979). "A new method of sampling in sensitive clay." *Can. Geotech. J.*, 16(1), 226-233.
- Lehane, B. M., Li, Y., and Williams, R. (2013). "Shaft Capacity of Displacement Piles in Clay Using the Cone Penetration Test." *J. Geotech. Geoenviron. Eng.*, 139(2), 253-266.
- Lehane, B. M., Schneider, J. A., and Xu, X. (2005). "The UWA-05 Method for Prediction of Axial Capacity of Driven Piles in Sand." *Proc. of the 1st Int. Symp. on Frontiers in Offshore Geotech.*, S. Gourvenec, and M. Cassidy, eds., Taylor & Francis, London, 683-689.

- Long, M. (2006). "Sample disturbance effects on medium plasticity clay/silt." *Proceedings of the Institution of Civil Engineers - Geotechnical Engineering*, 159(2), 99-111.
- Long, M. (2007). "Engineering characterization of estuarine silts." *Q. J. Eng. Geol. Hydrogeol.*, 40, 147-161.
- Long, M., and Donohue, S. (2010). "Characterization of Norwegian marine clays with combined shear wave velocity and piezocone cone penetration test (CPTU) data." *Can. Geotech. J.*, 47, 709-718.
- Long, M., Gudjonsson, G., Donohue, S., and Hagberg, K. (2010). "Engineering characterisation of Norwegian glaciomarine silt." *Eng. Geology*, 110(3), 51-65.
- Low, H. E., Maynard, M. L., Randolph, M. F., and DeGroot, D. J. (2011). "Geotechnical characterisation and engineering properties of Burswood clay." *Géotechnique*, 61(7), 575-591.
- Lukas, W. G., DeGroot, D. J., DeJong, J. T., Krage, C. P., and Zhang, G. (2019). "Undrained Shear Behavior of Low-Plasticity Intermediate Soils Subjected to Simulated Tube-Sampling Disturbance." *J. Geotech. Geoenviron. Eng.*, 145(1), 04018098.
- Lunne, T., Berre, T., Andersen, K. H., Strandvik, S., and Sjørnsen, M. (2006). "Effects of sample disturbance and consolidation procedures on measured shear strength of soft marine Norwegian clays." *Can. Geotech. J.*, 43(7), 726-750.
- Lunne, T., Berre, T., and Strandvik, S. (1997). "Sample disturbance effects in soft low plastic Norwegian clay." *Proc., Int. Symp. Recent Develop. in Soil and Pavement Mech.*, M. Almeida, ed., A.A. Balkema, Rotterdam, 81-102.
- Lunne, T., Long, M., and Forsberg, C. F. (2003). "Characterization and engineering properties of Onsøy clay." *Characterisation and Engineering Properties of Natural Soils*, T. S. Tan, K. K. Phoon, D. W. Hight, and S. Leroueil, eds., A.A. Balkema, Lisse, 395-427.
- Lunne, T., Robertson, P. K., and Powell, J. J. M. (1997). *Cone penetration testing in geotechnical practice*, Blackie Academic & Professional, London.
- Lunne, T., Strandvik, S. O., Kåsin, K., L'heureux, J. S., Haugen, E., Uruci, E., Veldhuijzen, A., Carlson, M., and Kassner, M. (2018). "Effect of cone penetrometer type on CPTU results at a soft clay test site in Norway." *Cone Penetration Testing 2018*, M. A. Hicks, F. Pisanò, and J. Peuchen, eds., CRC Press, Leiden, 417-422.
- Lutenegger, A. J., and Miller, G. A. (1994). "Uplift Capacity of Small-Diameter Drilled Shafts from In Situ Tests." *J. Geotech. Eng.*, 120(8), 1362-1380.

- Marchetti, S. (1980). "In Situ Tests by Flat Dilatometer." *J. Geotech. Eng. Div.*, 106(GT3), 299-321.
- Marchetti, S., Monaco, P., Totani, G., and Calabrese, M. (2006). "The Flat Dilatometer Test (DMT) in soil investigations A Report by the ISSMGE Committee TC16." *Proceedings from the Second International Conference on the Flat Dilatometer, Washington, D.C., April 2-5, 2006*, R. A. Failmezger, and J. B. Anderson, eds., In-Situ Soil Testing, Lancaster, VA.
- Marsland, A. (1972). "Clays subjected to in situ plate tests." *Ground Engineering*, 5(6), 24-31.
- Marsland, A., and Randolph, M. F. (1977). "Comparisons of the results from pressuremeter tests and large in situ plate tests in London Clay." *Géotechnique*, 27(2), 217-243.
- Martin, C. M., and Randolph, M. F. (2001). "Applications of the Lower and Upper Bound Theorems of Plasticity to Collapse of Circular Foundations." *Proceedings of 10th International Conference on Computer Methods and Advances in Geomechanics*, C. S. Desai, ed., A.A Balkema, Rotterdam, 1417–1428.
- Martins, F. B., Bressani, L. A., Coop, M. R., and Bica, A. V. D. (2001). "Some aspects of the compressibility behaviour of a clayey sand." *Can. Geotech. J.*, 38(6), 1177-1186.
- Mayne, P. W. (2007). *Cone Penetration Testing: A Synthesis of Highway Practice*. NCHRP Synthesis 368, Transportation Research Board, Washington, D.C.
- Mayne, P. W., and Rix, G. J. (1995). "Correlations between shear wave velocity and cone tip resistance in natural clays." *Soils Found.*, 35(2), 107-110.
- Mesri, G., Feng, T. W., and Benak, J. M. (1990). "Postdensification Penetration Resistance of Clean Sands." *J. Geotech. Eng.*, 116(7), 1095-1115.
- Mesri, G., and Hayat, T. M. (1993). "The coefficient of earth pressure at rest." *Can. Geotech. J.*, 30(4), 647-666.
- Mitchell, J. K., and Soga, K. (2005). *Fundamentals of soil behavior*, John Wiley & Sons, Inc., Hoboken, N.J.
- Mori, K., and Sakai, K. (2016). "The GP sampler: a new innovation in core sampling." *Proc., 5th Int. Conf. Geotech. and Geophys. Site Char.*, B. M. Lehane, H. E. Acosta-Martínez, and R. Kelly, eds., Australian Geomechanics Society, Sydney, Australia, 99-124.
- Moum, J. (1965). "Falling drop used for grain-size analysis of fine-grained materials." *Sedimentology*, 5(4), 343-347.

- Nash, D. F. T. (2003). "The use of bender elements in the assessment of sample disturbance." *Presentation to seminar on sample disturbance* Dublin.
- Nocilla, A., Coop, M. R., and Colleselli, F. (2006). "The mechanics of an Italian silt: an example of 'transitional' behaviour." *Géotechnique*, 56(4), 261-271.
- Norwegian Geotechnical Institute (2002). "Early Soil Investigations for Fast Track Projects: Assessment of Soil Design Parameters from Index Measurements in Clays. Summary Report/Manual 521553-3." Norwegian Geotechnical Institute, Oslo.
- Norwegian Geotechnical Society (1989). *Melding 4: Veiledning for utførelse av vinge boring. Rev. 1 [in Norwegian]*, Norwegian Geotechnical Society (NGF), Oslo, Norway.
- Norwegian Geotechnical Society (1989). *Melding 7: Veiledning for utførelse av dreietrykksondering. Rev.1 [in Norwegian]*, Norwegian Geotechnical Society (NGF), Oslo, Norway.
- Norwegian Geotechnical Society (2010). *Melding 5: Veiledning for utførelse av trykksondering. Rev. 3 [in Norwegian]*, Norwegian Geotechnical Society (NGF), Oslo, Norway.
- Norwegian Geotechnical Society (2011). *Melding 2: Veiledning for symboler og definisjoner i geoteknikk - Identifisering og klassifisering av jord. Rev. 2 [In Norwegian]*, Norwegian Geotechnical Society (NGF), Oslo, Norway.
- Norwegian Geotechnical Society (2013). *Melding 11: Veiledning for prøvetaking [In Norwegian]*, Norwegian Geotechnical Society (NGF), Oslo, Norway.
- Norwegian Geotechnical Society (2017). *Melding 6: Veiledning for måling av grunnvannsstand og poretrykk. Rev. 2 [In Norwegian]* Norwegian Geotechnical Society (NGF), Oslo, Norway.
- NS (1988). "Geotechnical testing - Laboratory methods." *Determination of undrained shear strength by fall-cone testing (NS 8015)*, Standards Norway, Oslo, Norway.
- NS (1993). "Geotechnical testing - Laboratory methods." *Determination of one-dimensional consolidation properties by oedometer testing - Method using continuous loading (NS 8018)*, Standards Norway, Oslo, Norway.
- Olsen, L., and Sørensen, E. (1993). "Halden 1913 II, Quaternary map, 1:50.000, with descriptions (in Norwegian)." Geological Survey of Norway, Trondheim.
- Ostendorf, D. W., DeGroot, D. J., Shelburne, W. M., and Mitchell, T. J. (2004). "Hydraulic head in a clayey sand till over multiple timescales." *Can. Geotech. J.*, 41(1), 89-105.

- Pacheco Silva, F. (1970). "A new graphical construction for determination of the pre-consolidation stress of a soil sample." *Proceedings of the 4th Brazilian Conference on Soil Mechanics and Foundation Engineering, Rio de Janeiro, Brazil*, 225-232.
- Page, M. J. (2004). "Sample disturbance and strength of silts." M.S., University of Rhode Island.
- Palmer, A. C. (1972). "Undrained plane-strain expansion of a cylindrical cavity in clay: a simple interpretation of the pressuremeter test." *Géotechnique*, 22(3), 451-457.
- Pettijohn, F. J. (1949). *Sedimentary Rocks*, Harper and Row., New York.
- Pineda, J. A., Arroyo, M., Sau, N., and Gens, A. (2013). "Testing block samples from silty deposits." *Geotechnical and Geophysical Site Characterization 4, Proc. of the International Conference*, R. Q. Coutinho, and P. W. Mayne, eds., CRC Press, London, 1815-1823.
- Pineda, J. A., Suwal, L. P., Kelly, R. B., Bates, L., and Sloan, S. W. (2016). "Characterisation of Ballina clay." *Géotechnique*, 66(7), 556-577.
- Powell, J. J. M., and Quarterman, R. S. T. (1986). "Evaluating the screw plate test in stiff clay soils in the U.K." *Proceedings of a Special Geomechanics Symposium on Interpretation of Field Testing for Design Parameters*, Institution of Engineers Australia, Adelaide, Australia, 128-133.
- Presti, D. C. F. L., Jamiolkowski, M., Pallara, O., Cavallaro, A., and Pedroni, S. (1997). "Shear modulus and damping of soils." *Géotechnique*, 47(3), 603-617.
- Randolph, M. F. (2004). "Characterization of Soft Sediments for Offshore Applications." *Geotechnical and Geophysical Site Characterization*, A. Viana da Fonseca, and P. W. Mayne, eds., Millpress, Rotterdam, The Netherlands, 209-232.
- Ricceri, G., and Butterfield, R. (1974). "An analysis of compressibility data from a deep borehole in Venice." *Géotechnique*, 24(2), 175-192.
- Rix, G. J., and Stoke, K. H. (1991). "Correlation of Initial Tangent Modulus and Cone Resistance." *Calibration Chamber Testing: Proceedings of the First International Symposium (ISOCCTI), Potsdam, NY, USA, 28-29 June, 1991*, A. B. Huang, ed., Elsevier, 351-362.
- Robertson, P. K. (1990). "Soil classification using the cone penetration test." *Can. Geotech. J.*, 27(1), 151-158.
- Robertson, P. K. (2009). "Interpretation of cone penetration tests - a unified approach." *Can. Geotech. J.*, 46(11), 1337-1355.

- Robertson, P. K., and Campanella, R. G. (1983). "Interpretation of cone penetration tests. Part I: Sand." *Can. Geotech. J.*, 20(4), 734-745.
- Rosenqvist, I. T. (1975). "Origin and Mineralogy Glacial and Interglacial Clays of Southern Norway." *Clays and Clay Minerals*, 23(2), 153-159.
- Salgado, R. (2008). *The Engineering of Foundations*, McGraw Hill, Boston, MA, USA.
- Salgado, R., Lyamin, A. V., Sloan, S. W., and Yu, H. S. (2004). "Two- and three-dimensional bearing capacity of foundations in clay." *Géotechnique*, 54(5), 297-306.
- Salgado, R., Woo, S. I., and Kim, D. (2011). "Development of Load and Resistance Factor Design for Ultimate and Serviceability Limit States of Transportation Structure Foundations." Joint Transportation Research Program, Indiana Department of Transportation and Purdue University, West Lafayette, IN, USA.
- Sandbækken, G., Berre, T., and Lacasse, S. (1986). "Oedometer Testing at The Norwegian Geotechnical Institute." *Consolidation of soils: testing and evaluation, STP 892*, R. N. Yong, and F. C. Townsend, eds., American Society for Testing and Materials, 329-353.
- Sandven, R. (2003). "Geotechnical properties of a natural silt deposit obtained from field and laboratory tests." *Characterisation and Engineering Properties of Natural Soils*, T. S. Tan, K. K. Phoon, D. W. Hight, and S. Leroueil, eds., A.A. Balkema, Lisse, 1121-1148.
- Santagata, M., Sinfield, J. V., and Germaine, J. T. (2006). "Laboratory Simulation of Field Sampling: Comparison With Ideal Sampling and Field Data." *J. Geotech. Geoenviron. Eng.*, 132(3), 351-362.
- Santagata, M. C., and Germaine, J. T. (2002). "Sampling Disturbance Effects in Normally Consolidated Clays." *J. Geotech. Geoenviron. Eng.*, 128(12), 997-1006.
- Sau, N., Arroyo, M., Pérez, N., and Pineda, J. A. (2014). "Using CAT to obtain density maps in Sherbrooke specimens of silty soils." *Geomechanics from micro to macro: proceedings of the TC105 ISSMGE International Symposium on Geomechanics from Micro to Macro, Cambridge, UK, 1-3 September 2014*, K. Soga, K. Kumar, G. Biscontin, and M. Kuo, eds., CRC Press, Leiden, Netherlands, 1153-1158.
- Schmertmann, J. H. (1970). "Static Cone to Compute Static Settlement over Sand." *Journal of the Soil Mechanics and Foundations Division, ASCE*, 96(SM3), 1011-1043.
- Schmertmann, J. H. (1991). "The Mechanical Aging of Soils." *J. Geotech. Eng.*, 117(9), 1288-1330.

- Selvadurai, A. P. S., Bauer, G. E., and Nicholas, T. J. (1980). "Screw plate testing of a soft clay." *Can. Geotech. J.*, 17(4), 465-472.
- Senneset, K., Sandven, R., and Janbu, N. (1989). "Evaluation of soil parameters from piezocone tests." *Transportation Research Record*, 1235, 24-37.
- Senneset, K., Sandven, R., Lunne, T., By, T., and Amundsen, T. (1988). "Piezocone tests in silty soils." *Penetration testing, 1988: proceedings of the First International Symposium on Penetration Testing, ISOPT-1, Orlando, 20-24 March 1988*, J. de Ruiter, ed., A.A. Balkema, Rotterdam, The Netherlands, 863-870.
- Siddique, A. (1990). "A numerical and experimental study of sampling disturbance." Ph.D., University of Surrey.
- Skúlason, J. "Settlement investigation on Icelandic silt." *Proc., Proceedings of the 12th Nordic Geotechnical Meeting. NGM-96*, Icelandic Geotechnical Society, Reykjavik, Iceland, 435-441.
- Skúlason, J. (1996). "Settlement investigation on Icelandic silt." *Interplay between geotechnics and environment : XII Nordic Geotechnical Conference, NGM-96, Reykjavik, 1996*, S. Erlingsson, and H. Sigursteinsson, eds., Jardtæknifélag Islands, Reykjavik, 435-441.
- Solberg, I.-L., Rønning, J. S., Dalsegg, E., Hansen, L., Rokoengen, K., and Sandven, R. (2008). "Resistivity measurements as a tool for outlining quick-clay extent and valley-fill stratigraphy: a feasibility study from Buvika, central Norway." *Can. Geotech. J.*, 45(2), 210-225.
- Solberg, I. L., Hansen, L., Rønning, J. S., Haugen, E. D., Dalsegg, E., and Tønnesen, J. F. (2012). "Combined geophysical and geotechnical approach to ground investigations and hazard zonation of a quick clay area, mid Norway." *Bulletin of Engineering Geology and the Environment*, 71(1), 119-133.
- Solhjell, E., Strandvik, S. O., Carroll, R., and Håland, G. (2017). "Johan Sverdrup—Assessment of soil material behaviour and strength properties for the shallow silt layer." *Proc., 8th Int. Conf. Offshore Site Invest. and Geotech.*, SUT, London, 1275-1282.
- Sørensen, R. (1979). "Late Weichselian deglaciation in the Oslofjord area, south Norway." *Boreas*, 8(2), 241-246.
- Sørensen, R. (1999). "En 14C datert og dendrokronologisk kalibrert strandforskyvningskurve for søndre Østfold, Sørøst-Norge [In Norwegian]." *Museumslandskap: artikkelsamling til Kerstin Griffin på 60-årsdagen*, L. Selsing, and G. Lillehammer, eds., Arkeologisk museum i Stavanger, Stavanger, 59-70.
- Stark, T. D., Ebeling, R. M., and Vettel, J. J. (1994). "Hyperbolic Stress-Strain Parameters for Silts." *J. Geotech. Eng.*, 120(2), 420-441.

- Stringer, M., Taylor, M. L., and Cubrinovski, M. (2015). "Advanced Soil Sampling of Silty Sands in Christchurch (Research Report 2015-06 Civil & Natural Resources Engineering)." Department of Civil and Natural Resources Engineering, University of Canterbury, New Zealand.
- Strout, J. M. (1998). "Evaluation of the field compressometer test in sand." Ph.D., The Norwegian University of Science and Technology, Trondheim, Norway.
- Sully, J. P., Robertson, P. K., Campanella, R. G., and Woeller, D. J. (1999). "An approach to evaluation of field CPTU dissipation data in overconsolidated fine-grained soils." *Can. Geotech. J.*, 36(2), 369-381.
- Tanaka, H., Sharma, P., Tsuchida, T., and Tanaka, M. (1996). "Comparative study on sample quality using several types of samplers." *Soils Found.*, 36(2), 57-68.
- Tani, K., and Kaneko, S. (2006). "Undisturbed sampling method using thick water-soluble polymer solution." *Tsuchi-to-Kiso*, 54(4), 145-148 [In Japanese].
- Taylor, D. W. (1948). *Fundamentals of soil mechanics*, J. Wiley, New York.
- Taylor, M. L., Cubrinovski, M., and Haycock, I. (2012). "Application of new 'Gel-push' sampling procedure to obtain high quality laboratory test data for advanced geotechnical analyses." *NZSEE Annual Conference*, New Zealand Society for Earthquake Engineering, Christchurch, New Zealand.
- Terzaghi, K., Peck, R. B., and Mesri, G. (1996). *Soil Mechanics in Engineering Practice*, John Wiley and Sons, New York.
- Thomas, D. (1994). "Spread Footing Prediction Event at the National Geotechnical Experimentation Site on the Texas A&M University Riverside Campus." *Predicted and measured behavior of five spread footings on sand*, GSP 41, J.-L. Briaud, and R. M. Gibbens, eds., ASCE, New York, NY, 149-152.
- Trautmann, C. H., and Kulhawy, F. H. (1988). "Uplift Load-Displacement Behavior of Spread Foundations." *J. Geotech. Eng.*, 114(2), 168-184.
- Vaid, Y. P., Sivathayalan, S., and Stedman, D. (1999). "Influence of specimen-reconstituting method on the undrained response of sand." *Geotech. Test. J.*, 22(3), 187-195.
- Vesterberg, B., Bertilsson, R., and Löfroth, H. (2017). "Photographic feature: Monitoring of negative porewater pressure in silt slopes." *Q. J. Eng. Geol. Hydrogeol.*, 50(3), 245-248.
- Viana da Fonseca, A., Ferreira, C., Molina-Gómez, F., and Ramos, C. (2019). "Collection of high-quality samples in liquefiable soils using new sampling techniques." *XVII European Conference on Soil Mechanics and Geotechnical Engineering* -

Reykjavík, Iceland, H. Sigursteinsson, S. Erlingsson, and N. Bessason, eds., ISSMGE, Reykjavik, Iceland.

- Wang, J. L., Vivatrat, V., and Rusher, J. R. (1982). "Geotechnical properties of Alaskan OCS silts." *Proc., 14th annual Offshore Tech. Conf.*, OTC, Dallas, TX, 415-420.
- Wang, S., and Luna, R. (2012). "Monotonic Behavior of Mississippi River Valley Silt in Triaxial Compression." *J. Geotech. Geoenviron. Eng.*, 138(4), 516-525.
- Wang, S., Luna, R., and Stephenson, R. W. (2011). "A Slurry Consolidation Approach to Reconstitute Low-Plasticity Silt Specimens for Laboratory Triaxial Testing." *Geotech. Test. J.*, 34(4), 288-296.
- Wang, Z., Gelius, L.-J., and Kong, F.-N. (2009). "Simultaneous core sample measurements of elastic properties and resistivity at reservoir conditions employing a modified triaxial cell – a feasibility study." *Geophysical Prospecting*, 57(6), 1009-1026.
- Westerberg, B., Bertilsson, R., Prästings, A., Müller, R., and Bengtsson, P.-E. (2014). "Publication 9: Negativa portryck och stabilitet i siltslänter." Statens Geotekniska Institut, SGI [in Swedish, with summary in English], Linköping.
- Wood, F. M., Yamamuro, J. A., and Lade, P. V. (2008). "Effect of depositional method on the undrained response of silty sand." *Can. Geotech. J.*, 45(11), 1525-1537.
- Wroth, C. P. (1984). "The interpretation of in situ soil tests." *Géotechnique*, 34(4), 449-489.
- Yasuhara, K., Murakami, S., Song, B.-W., Yokokawa, S., and Hyde, A. F. L. (2003). "Postcyclic Degradation of Strength and Stiffness for Low Plasticity Silt." *J. Geotech. Geoenviron. Eng.*, 129(8), 756-769.